Syracuse University

SURFACE

Dissertations - ALL   **SURFACE**

June 2017

Design, Material and Surgical Assembly Effects on Fretting Corrosion Behavior of Modular Tapers in Orthopedic Implants

David Pierre
Syracuse University

Follow this and additional works at: https://surface.syr.edu/etd

Part of the Engineering Commons

Recommended Citation

Abstract

Mechanically assisted crevice corrosion (MACC) has become a significant problem in the orthopedic device industry, particularly in modular devices with metal-on-metal (MoM) tapered interfaces. Oxide film abrasion, leading to fretting corrosion in the presence of a crevice, accelerates the corrosion process and in some instances may lead to failure of the implant. Failure is defined as the need for revision surgery. The basic processes of oxide film abrasion and repassivation, and the associated effects (chemical, transport, mechanical and electrical) of these processes have been well described and studied over time.

Despite these advancements, there is much that is still not well understood about modular taper performance and the role of design, materials, surgical techniques and biological factors, and their effects on MACC performance. For example, the load-displacement behavior of taper junctions during seating, the effect of seating load magnitude, rate of loading and loading orientation, and the role of taper contamination on seating mechanics, pull-off mechanics and MACC behavior remain to be well understood. In addition, few studies have been carried out to improve the understanding of the relationship between MACC, local tissue reaction, taper design and material combination.

Thus, with continued concerns surrounding fretting corrosion and MACC of modular taper junctions there is a continuing need to develop appropriate in vitro tests to evaluate the roles of specific design, material and surgical techniques. These concepts are complex, interdependent and need to be clearly understood for effective design of, and surgical practice using modular taper junctions. Therefore, the goals of this dissertation are to systematically assess the effects of seating mechanics in terms of load magnitude, load rate and load orientation, contamination, taper design and material combination on the MACC behavior of head-neck taper

junctions and taper locking stability (pull-off behavior) for commercially-used total hip replacements. The information provided from these studies offers a more detailed understanding of the interactions that arise between taper design and material combination based on surgical techniques and taper contamination in reference to taper fretting motions and corrosion.

Preliminary testing consisted of a novel test protocol in which the seating (load-displacement) behavior and taper pull-off load were monitored in 12/14 Ti6Al4V/CoCrMo modular taper junctions. The seating behavior for four load magnitudes, three load orientations and five contamination groups was reported. The results showed an increase in seating load magnitude increased seating displacement, work of seating and the taper pull-off load while an increase in load orientation (to 20°) had no significant effect. Taper contamination testing presented findings which suggest the inclusion of lipids into the junction resulted in increased taper stability. The presence of contaminants increased seating displacement and work of seating compared to a control (dry) taper.

Fretting corrosion testing incorporated identical taper testing conditions (load magnitude, orientation and contamination) and underwent incremental cyclic fretting corrosion testing. The goal was to investigate the effects of taper seating conditions on fretting motions and fretting corrosion. The outcome of testing highlighted the significant effects of taper seating conditions on each sample group. In the seating load magnitude groups, a correlation between subsidence and current at the end of testing was reported. An increased seating load orientation reduced micromotion throughout testing and the average onset load but had no effect on subsidence, current at the end of testing or taper pull-off. And the introduction of lipid contaminants into the taper junction reduced fretting corrosion currents.

Lastly, the effects of taper geometry (C taper vs. V40 taper) and material combination (Ti-6Al-4V/CoCrMo vs. TMZF (Ti-Mo-Zr-Fe)/CoCrMo) as well as load rate and compliance were investigated using novel methodologies. The findings from these studies showed changes in the taper geometry affected the stiffness of the construct, fretting motions and the fretting corrosion performance while material combination had no significant effect. In terms of load rate and compliance, the study presented evidence to suggest load rate and system compliance had no significant effect on work of seating or taper locking stability.

Design, Material and Surgical Assembly Effects on Fretting Corrosion Behavior of Modular Tapers in Orthopedic Implants

By

David Pierre

B.S. Bioengineering, Worcester Polytechnic Institute, Worcester, MA, 2012

B.S. Mechanical Engineering, Worcester Polytechnic Institute, Worcester, MA, 2012

Dissertation

Submitted in partial fulfillment of the requirements for the degree of

Doctor of Philosophy in Bioengineering.

Syracuse University

May 2017

Acknowledgement

I would like to thank my advisor, Dr. Jeremy L. Gilbert, without his overwhelming patience and understanding this work would not be possible. He saw a young and ambitious student out of undergrad and took the time to educate and mentor him. He should me that teaching and research is as rewarding as you want it to be. And for that and many other lessons I will forever be grateful.

I would like to thank my mother and father who never let me give up and never gave up on me. The journey all the way up to this moment was not an easy one nor was it one I took alone. With their guidance and love I was able to overcome challenges I had never faced. They inspired me to keep my faith and even when I stumbled they reminded me that God was with me.

To my remaining family and friends, I would also like to thank you for keeping me sane. There were a lot of nights where I was ready to pack it up and head back home but you remind me that you'd disown me if I did. You all knew exactly what to say and when to say it and without you I would have never reached this milestone.

Lastly, I want to say thank you to all my lab mates and the employees at Syracuse University who also helped me.

Table of Contents

Table of Figures

xvii

Chapter 1 – Introduction

Background & Significance

Beginning in the mid-to-late 1980's, orthopedic implant designs have incorporated modularity, where components are assembled intraoperatively by means of a self-locking conical taper junction and have since become state of the art in hip implant design. The modular element of these designs characteristically consists of a conical tapered interface about the neck region of the implant between a metallic alloy and an opposing surface (an alloy or ceramic component). Modularity provides an optimal combination of varying sizes, biomaterials and designs to better restore anatomy and function of the joint for patient specificity. The function also provides a means for surgeons, during initial implantation or revision surgery, to combine elements of an implant to best meet patient needs and deliver successful outcomes. Bostrom et al. and Kurtz et al. predict the annual demand for total hip replacements will increase to about 572,000 replacements in the U.S., an increase upwards of 170%, by year 2030 [1, 2].

However, over time it has become more evident that numerous factors play crucial roles in the overall performance of these tapers. Since their inception in the 1980's and more recently in the 2000's until the present day, modular implants have been linked to mechanically assisted crevice corrosion (MACC) [3-6] in the junction and adverse local tissue reaction (ALTR) [7, 8], in some cases raising the level of metal ions in blood and urine. MACC results from a combination of factors such as mechanical loading, cyclic motion about the interface (measured on a micron scale) and penetration of fluid into the taper junction (Fig. 1).

Mechanically Assisted (Crevice) Corrosion

Materials Surface Structure and Chemistry
Oxide, metal substrate (H, E, ef, ys, etc.)

Electrical Impedance and Transport Phenomena
Resistance and capacitance of oxide, solution, crevices, ionic transport

Mechanically Assisted Corrosion

Bulk Mechanics
Bending, Shear, Compression Plasticity, Flexural Rigidity (EI)

Solution Chemistry
crevices, **pH, ROS**, complexes, protein adsorption, tribochemistry

Surface Mechanics: Wear, Asperity contact stresses, friction, adhesion, abrasion Interfacial structure and mechanics

Electrochemistry: Voltage and Currents
Oxidation (ions, oxide repassivation)
Reduction (Oxygen, ROS, proteins, others)
Semiconducting oxides, high-field oxide growth

Biological Interactions (Affects and Effects)
Inflammation, immunity, allergy, infection
(ROS, enzymes, etc.) Reduction-driven cell apoptosis
Ion and particle toxicity (ALTR/ pseudotumors)

Complex, non-linear, coupled set of interacting processes

Fig. 1: Diagram outlining factors which may affect Mechanically Assisted Crevice Corrosion (MACC) in modular taper junctions [9].

Taper Mechanics

Modular tapers (Fig. 2), often referred to as self-locking conical tapers, incorporate specific design elements (diameters (D_1 and D_2), material composition, length (L), taper angle (α), etc.) which may affect the mechanical behavior of an orthopedic taper during loading.
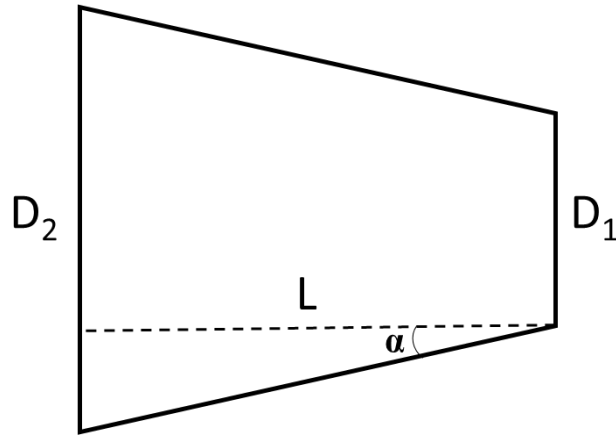
Fig. 2: Male self-locking conical taper.

Taper Assembly

Taper assembly, which clinically is performed by applying an axial load (typically by impaction) to the femoral head to engage the male and female portions of the taper has been defined as a critical factor in taper mechanics and fretting corrosion [10]. Literature published in the Journal of Orthopedic Research found samples impacted at higher loads were less susceptible to fretting corrosion in both head-neck samples comprised of CoCrMo/CoCrMo and CoCrMo/Ti-6Al-4V than those assembled under lower loads [11]. Haschke et al. established larger taper angle differences between the male and female taper exhibited lower relative motion during assembly than those with smaller differences in bi-modular implants [12].
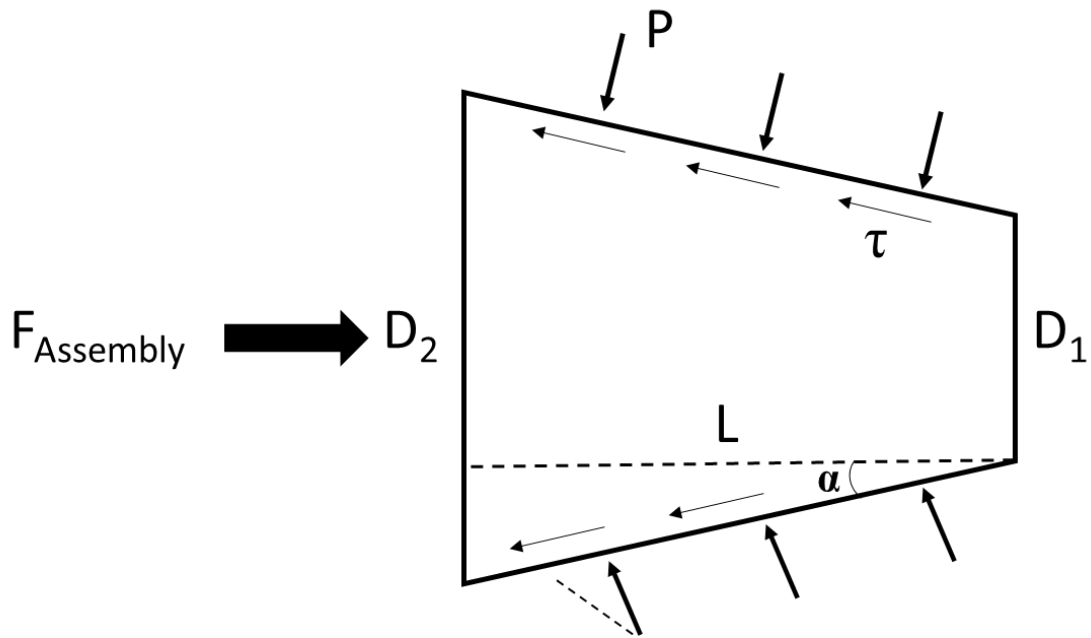
Fig. 3: Force of assembly/seating assembly diagram illustrating the pressures and shear stress acting on and along the taper during loading.

Seating force ($F_{Assembly}$), is the force applied to the trunnion during taper assembly. When $F_{Assembly}$ is removed from the system the taper trunnion is engaged (locked) by a balance of pressure (P) applied to the male trunnion by the female bore and shear stress (τ) applied along the area of the taper (A) (the secondary diameter (D_2) minus the primary diameter (D_1) divided by length of the taper (L). The taper angle is determined from the taper geometry, where Tan (α) is the secondary angle. Shear stress is dependent upon the coefficient of friction (μ) and pressure, P (Fig. 3). The relationship between assembly load, pressure, coefficient of friction and taper angle is summarized in the following equation, where α is the taper angle:

$$F_{Assembly} = P^{max} A(\sin \alpha + \mu \cos \alpha) \quad \text{(Eqn. 1)}$$

Eqn. 1 does not incorporate the influence of off-axis taper assembly which may alter the line of action of the force applied to the construct. Frisch et al. reported the findings of off-axis taper assembly in bi-modular implants, stating an increase in the angle of orientation from 0°

4

(axial) to 15° in the anterior direction decreased the stability of the construct [13]. Stability was defined as the disassembly force determined from tensile testing.

Post assembly, the taper surfaces remain locked only if the locking frictional stresses developed during assembly are not exceed by the axial component of the pressures developed during loading. If $P\sin\alpha < \tau^{max}\cos\alpha$ the taper remains locked but if $P\sin\alpha > \tau^{max}\cos\alpha$ the taper begins to dislodge. Note the difference between τ, the actual shear stress present, and τ^{max}, the shear stress developed before slip can occur.
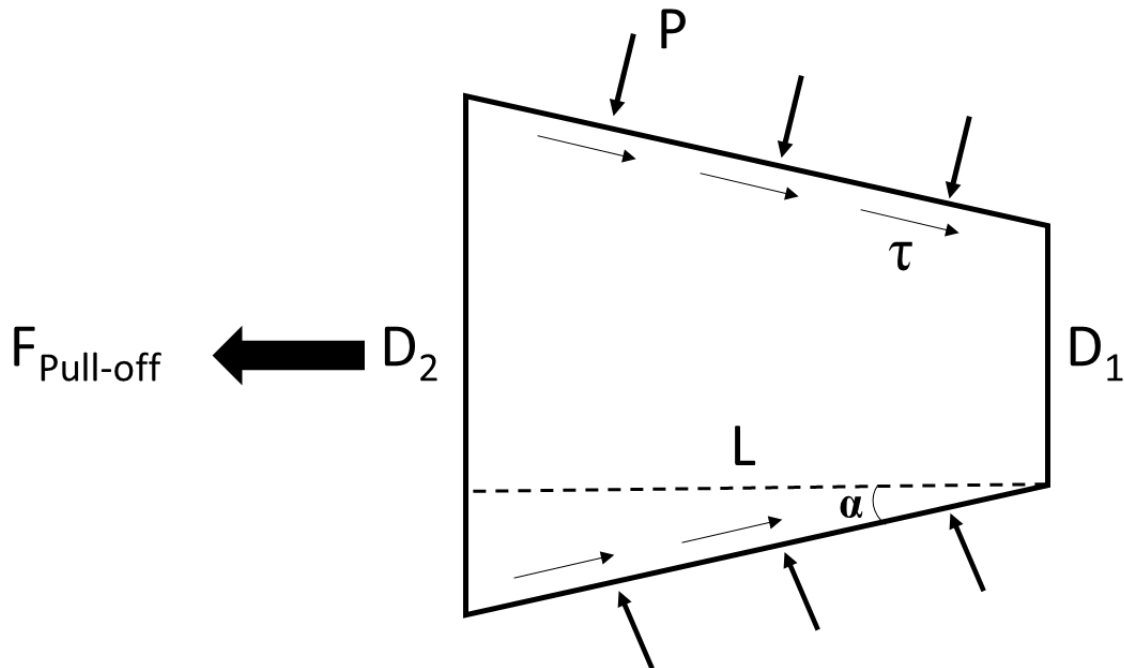
Fig. 4: Force of disassembly/pull-off load diagram.

The disassembly force ($F_{Pull-off}$) relationship is similar to the force of assembly relationship, aside from a sign change due the direction of force (Fig. 4):

$$F_{Pull-off} = P^{max} A(-\sin\alpha + \mu\cos\alpha) \qquad \text{(Eqn. 2)}$$

where, to overcome the taper locking mechanisms, the shear stress must be reversed and opposite to the force applied to the system, hence the negative component. One can create a ratio of force of disassembly to force of assembly:

$$\frac{F_{Pull-off}}{F_{Assembly}} = \frac{(-\sin\alpha + \mu\cos\alpha)}{(\sin\alpha + \mu\cos\alpha)} \qquad \text{(Eqn. 3)}$$

This ratio is dependent upon the taper angle, geometrical specifications such as the diameters, the length of the trunnion and the coefficient of friction which is determined by material combination and taper surface characteristics (roughness, microtopography, etc.). If one were to input typical values for taper half-angle, 2.67° and a coefficient of friction of 0.2, this yields a ratio of 0.62. This ratio allows one to hypothesize a higher assembly force will lead to greater locking pressures and shear stress at the taper junction. A byproduct of those increased variables will yield a greater disassembly force.

Area of Contact

The nominal area of taper engagement, the area of the male taper which may make contact with female taper is defined by the equation

$$A_{nom} = 2\pi r * L \qquad \text{(Eqn. 4)}$$

Where r is the average of D_2 and D_1 divided by two and L is the length of the taper. The nominal area should not be mistaken for the true area of contact between the male and female portions of the junction which is dictated by the asperity contact points. Modular taper surfaces are comprised of various asperities, byproducts of machining techniques or imperfections, which project from the surface of the male taper making contact with the female taper (see Fig. 5).
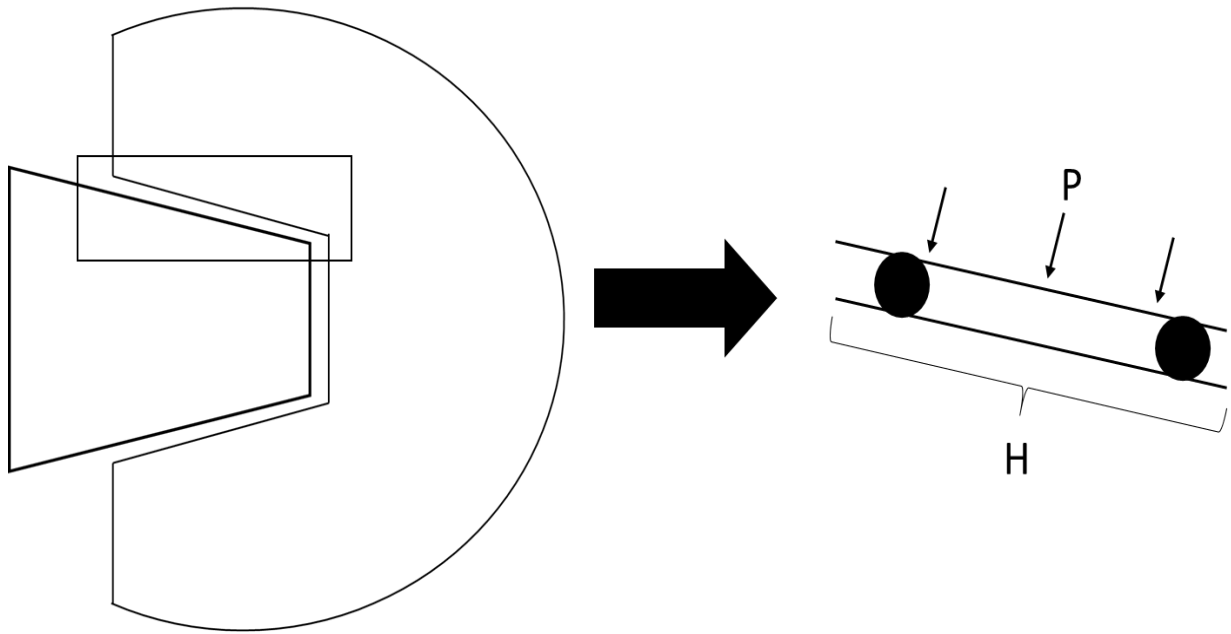
Fig. 5: Area of contact diagram (black dots represent asperity contact points between taper surfaces).

From surface contact mechanics theory, the true area of contact (A_c) is directly affected by the hardness of the material (H) and the assembly force (see below, Eqn. 4).

$$A_c = \frac{P*A}{H} = \frac{F_{Assembly}}{H(\sin\alpha + \mu\cos\alpha)} \qquad \text{(Eqn. 5)}$$

Inputting typical values into the equation, an assembly force of 4000 N on a metal taper angled at 2.67° with a hardness of 2 GPa and coefficient of friction of 0.2, the area of contact is approximately 8 mm^2, 2% of the nominal area of a typical taper junction. This means that the remaining area is not in contact. In a published study by Witt et al., the nominal area of the male taper was lightly covered in a gold coating before seating the head at various assembly loads. The results of the study showed a linear increase in the area of contact with an increase in force of assembly. The study also stated the actual area of contact at loads as high as 8000 N did not

exceed 20% of the nominal area [14]. Based on the A_c equation, one can conclude that if the pressures at the junction increase due to the force of assembly then the area of contact will thereby increase.

The above calculations ignore elastic deformation due to loading which may increase the surface area. The introduction of taper surface modifications, such as machined microtopographies will not significantly alter the true area of contact. A reduction in the area of contact increases the nominal area in which no contact is made which in turn leads to larger crevices between the taper surfaces. Larger crevices allow for greater amounts of liquid flow during cyclic motion. The ideas presented in this section are opposite of what Haschke and Lavernia et al. detail in articles which pertain to the effects of contaminants on modular taper junctions [15, 16]. Both findings assert the introduction of contaminants to the junction decrease taper stability, weaken torsional resistance and altered the motion of the head.

Fretting Motion

The mechanical process referred to as the fretting motion is the process in which contact points between the two surfaces slide at a small amplitude relative to one another due to a cyclic load. In a system where the stem-neck junction remains fixed, the head-neck taper junction is subjected to large bending moments and shear stresses during cyclic loading, which result in both elastic and plastic displacement of the head relative to the neck (Fig. 6).
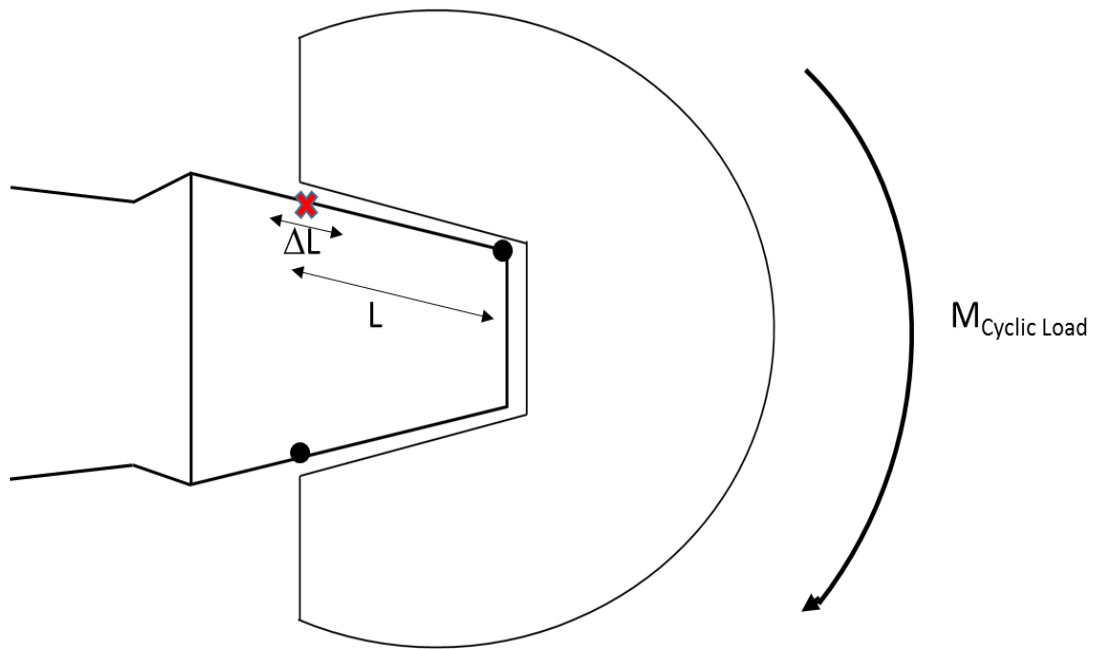
Fig. 6: Diagram of the bending moment about the taper interface (x - represents point of micromotion, black dots represent fixed contact points).

In the above example, throughout cyclic loading the stresses (σ) are assumed to be applied about the fixed contact points (represented by the black dots in the figure above) while no load is applied to the other regions of the taper (**x**). During loading there is a bending moment, $M_{Cyclic\ Load}$, about the contact points as well. Fretting motions are assumed to not occur at the contact points but motion will occur along the length of the taper. Using the strain (ε) equation and Hooke's Law one can determine the change in length (ΔL)/micromotion of the interface at a point.

$$\varepsilon = \frac{\Delta L}{L} \text{ and } \varepsilon = \frac{\sigma}{E} \qquad \text{(Eqn. 6 \&7)}$$

Manipulating the two equations (Eqn. 6 & 7) the change in length can be determined. The coefficient of stress can be equated to the bending moment about the z-axis (M_z) multiplied by the radius (r) divided by the second moment of area (I).

$$\Delta L = \frac{L * M_z * r}{E * I} \qquad \text{(Eqn. 8)}$$

Note the denominator of the equation, E*I, signifies the flexural rigidity of material. Flexural rigidity is defined as the ability of a material to resist bending under an applied load. An increase in modulus will increase the flexural rigidity of a system and decrease the change in length. The change in length is dependent upon the length of the taper, the head offset which may alter the bending moment, contact points, the modulus of the material and the load which affect the applied stress. Eqn. 8 is simplified analysis with L as a constant which causes the ΔL to be the same along the taper. A constant L value will yield an over-approximation of ΔL. However, in Eqn. 9 the integral allows one to solve for ΔL in terms of L.

$$\Delta L = \int_0^L \varepsilon(x) \, \delta L \qquad \text{(Eqn. 9)}$$
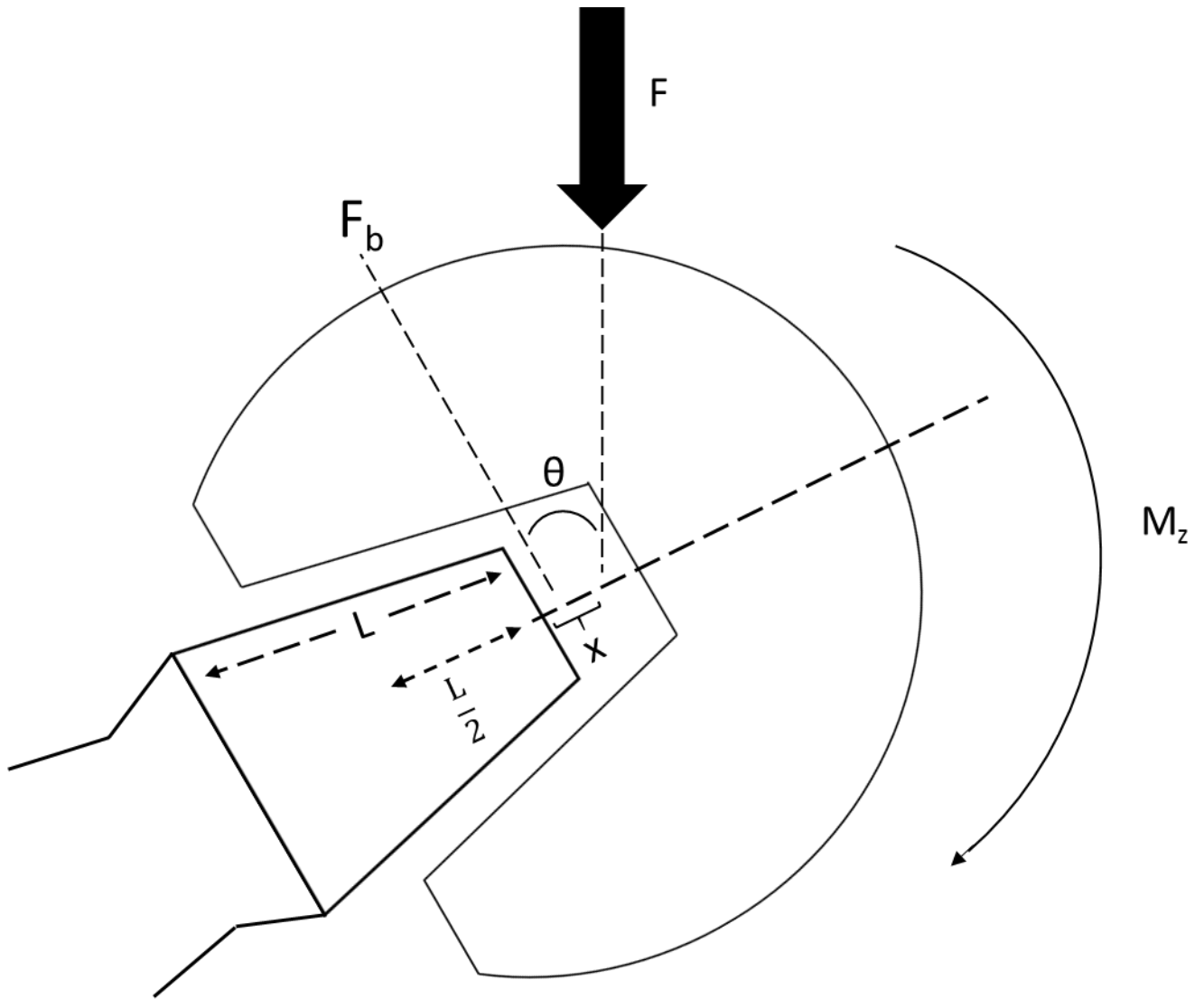
Fig. 7: Bending diagram which arises due to an off-axis cyclic load being applied to the system.

Solving for ΔL in Fig. 7 using Eqn. 9 with typical values of a titanium taper, I is $\frac{\pi r^4}{4}$,

where r is 6.5 mm, E is 110 GPa, the moment in the z direction is equivalent to $F_b(x + L)$ where

L is 10mm and F_b is defined as the force, F, multiplied by $\cos(\theta)$, 3000 N and x is the offset (+5

mm).

$$\Delta L = \int_0^L \varepsilon(x)\, \delta L = \int_0^L K(x + L)\, \delta L = K\left(xL + \frac{L^2}{2}\right)$$

K is $\dfrac{F_b * r}{E * \pi \dfrac{r^4}{4}}$ and the chosen integrated length was $\dfrac{L}{2}$. The calculated change in length

(ΔL) value is approximately 19 µm which is comparable to what is recorded in retrieval studies

[3, 4, 17, 18]. The value is roughly 52% larger than a CoCr sample with a modulus of 230 GPa.

This simplified calculation doesn't incorporate the change in force based on patient physiology

or activity as well as rotational forces acting upon the system.

Fretting Motion to Fretting Corrosion

The result of these mechanically assisted fretting motions will result in fretting about the

interface. Thus, mechanically assisted crevice corrosion is comprised of fretting motions and

abrasion of the thin passive oxide film at the surface of the metals. Throughout cyclic loading,

passivated metals undergo an abrasion-repassivation cycle where the thin oxide layer film on the

surface of the metal was abraded due to the contact of the two surfaces but instantaneously

passivated after contact (Fig. 8).
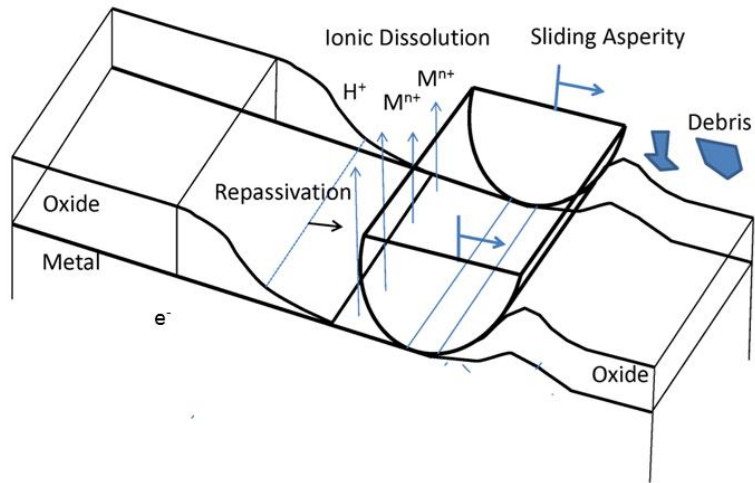
Fig. 8: Oxide film abrasion done by sliding asperity with instantaneous repassivation [19].

The process of corrosion and repassivation is known as an oxidation and reduction reaction. During oxidation the metal atoms release electrons into the metal as they oxidize, before the electrons are subsequently taken by reduction reactions [20, 21]. While repeatedly undergoing the oxidation-repassivation process, the implant sees a drop in potential due to the released free electrons which begin to accumulate on the implant surface. This drop in potential has been correlated to clotting of blood and other cellular behavior [22, 23].

An asperity-asperity scratch test done by Swaminathan et al. related the mechanical abrasion of the oxide film and the measured fretting corrosion current which are dependent upon the material and mechanical and electrochemical properties of the system [24]. The oxide film repassivation rate can be equated to the abrasion rate at slow speeds. As a result, the researchers

13

formulated a simplified equation where repassivation is dependent on the rate of abrasion of the film.

$$I_{film} = 2\frac{\rho n F A}{M_w \Delta} m(E - E_{onset})\frac{d\delta}{dt} \qquad \text{(Eqn. 10)}$$

where ρ is the oxide film density (dependent upon the voltage of the system), n is the charge per cation, F is Faraday's constant (95,000 C/mol), M_w is the molecular weight of the oxide, A is the nominal area of the trunnion, m is the anodization rate for the oxide growth (typically 1.8-2 ηm/V for Ti and CoCr), E is the voltage across the interface, E_{onset} is the onset potential (below this potential there is no oxide film growth), Δ is the average asperity-asperity distance and lastly $\frac{d\delta}{dt}$ is the sliding speed of the mechanical abrasion. Δ incorporates mechanical factors at the junction such as surface properties (i.e. surface roughness, hardness, microtopography, etc.) and contact area load-dependence, which deems an increased load will result in an increased true contact area. Asperity-asperity contact points between the junction may shift throughout the lifetime of the taper due to cyclic loading and potential wear which may alter the mechanics. The simplified equation (Eqn. 10) ignores the effects of solution chemistry on oxide film growth rate and density.

Failure Modes

Biological Interactions.

Potential failure modes related to MACC include fracture of implant components, release of MACC byproducts (metal ions, reactive oxygen intermediates and wear debris) or degradation of adjacent bone and adverse local tissue reactions (ALTR) or pseudotumor formation in surrounding tissue [25-33]. Pseudotumors, which are not to be confused with cancer, are defined as soft tissue reactions in proximity to corroding orthopedic implant devices. These so-called

14

pseudotumors may or may not consist of cysts filled with fluids. Some patients suffering from implant corrosion also report groin pain as well as other clinical complications [34, 35]. Though the head-neck alloy combinations (CoCrMo/CoCrMo, CoCrMo/Ti-6Al-4V, Ti-6Al-4V/ Ti-6Al-4V, 316L/316L, etc.) used for modular joint replacements are corrosion resistant, retrieval analyses of orthopedic implants have shown that all combinations of metal-on-metal (MoM) devices exhibit levels of MACC throughout the industry [17, 36-41]. Wide assortments of design parameters, surgical factors and material combinations have been theorized as the factors, which lead to adverse local tissue reactions (ALTR). However, as yet, there are no clear causal links established.

Recently, Gilbert et al. speculated about the ability of inflammatory reactions to potentially induce or accelerate corrosion, and result in a biological and metallurgical positive feedback process [42]. Some of the observed damage in the retrieval samples has since been attributed to electrocautery but has not ruled out the biological potential for enhanced corrosion [43]. Other studies have shown a broad link between implant corrosion and biological responses but the two phenomena are highly complex and need to be better understood before attempting to pinpoint implant-based criteria for ALTR [44-52]. Modular tapers have numerous design and biomaterial elements within each construct, which can be modified according to the surgeon and/or manufacturers preference.

Design and Material Combination.

Studies performed by researchers such as Langton et al., and Higgs et al. speculated taper design including head offset, surface roughness and taper geometry caused failure of implants [25, 53]. In commercial devices, routinely used designs such as 11/13 and 12/14 tapers widely vary between manufacturers. Studies have shown some manufacturers have a tendency to

machine threaded grooves along the taper while others ground the surface into a smooth finish [54].

Literature states taper junctions with low modulus and flexural rigidity may lead to increased levels of corrosion compared to metals with higher flexural rigidity [55, 56]. Those studies correlate fretting motion with taper contact angle, trunnion length and material properties. Non-standardization of taper design and material combinations have been known to alter the modulus and flexural rigidity of a component [57].

Surgical Factors.

Recent studies have presented the influence of assembly load and material combination on taper stability, suggesting an increase in assembly load between the femoral components will lead to increased stability and less motion between the interface during loading [10, 46]. Studies have also highlighted the possibility of taper junction exposure to organic and inorganic particles during intraoperative assembly. Contaminants may alter the seating mechanics and locking stability of the taper junction. According to studies done by Weisse et al. and Jauch et al., contamination about the interface reduced the interlocking ability of the taper and thus stability [46, 58]. As shown in the taper mechanics section, taper locking stability, defined by the pull-off load, is dependent on the seating load and taper surface conditions (i.e. surface roughness, dimensions and material); taper conditions can vary between manufacturer and surgeon [9, 25, 53, 59, 60].

One question in the scientific community is what influence system compliance (patient dependent) and assembly load rate (clinician dependent) have on taper seating performance? A constant practice in the studies referenced in this dissertation was to fix the taper sample to a rigid support which allowed for less variation in compiled results. A desirable yet clinically

irrelevant assumption, which may alter the loading force during assembly. Clinically, implantation in a patient occurs with the device surrounded by damping material such as fat, muscle and bone which may absorb and alter the assembly load. The influence of compliance has been shown to affect the load mechanics, rebound and stiffness of a construct [61, 62].

Surgical load rate incorporates aspects of inertial force applied during assembly as well as construct stiffness factors which are dependent upon the assembly load, material combination and taper design. During impaction assembly the change in force over time (impulse) is relatively short. Within the two-part system (femoral neck and femoral head), if there is a high stiffness or inertia, which is caused by the impulse, the effect of load rate will be negated. The concept is further discussed in Chapter 4.3.1.

Patient Factors.

It is commonly thought that with increased seating loads, greater contact between surfaces will result in greater resistance to the processes of MACC [10, 46, 63]. These studies assert larger impaction assembly forces increase taper stability and reduce fretting corrosion during cyclic testing. However, it unclear if this is the case, or if the seating load needed to eliminate fretting corrosion can be reached in a clinical setting. Since elastic deformations may result in fretting motions at the interface, even the most well-seated taper may still be susceptible to fretting corrosion processes. In addition, the true contact area within a modular taper junction, based on hard-on-hard asperity interactions, states only a small fraction of the nominal contact area is available. Thus true contact area will depend on the assembly force, but again, it is unknown how the MACC processes will be altered by the increase in true contact area. An inconsistency in assembly technique can alter the impaction assembly force, seating load

orientation, seating displacement, contact area between the head and neck as well as several other factors, which may affect overall taper performance [10, 47, 60, 64-66].

Despite the multitude of studies on taper assembly and overall performance, researchers have failed to report the influence of three surgical factors, seating load magnitude, orientation and contamination on seating mechanics and fretting corrosion. Despite the growing number of total joint replacements and modular implants, little is known about the relationship between these surgical, design and material combination parameters and their effect on the associated biological responses and clinical need for revision. Failure of implants (the need for revision) is also not fully understood.

Hence, the goal of this dissertation is to provide a better understanding of what affect surgical assembly, taper design and implant component material combination have on initial taper stability and initial mechanically assisted crevice corrosion. In addition, a goal of this work is to explore the taper assembly mechanics and fretting corrosion behavior of tapers with known solid and liquid contaminants. The in vitro studies presented are an effort to bridge a gap in understanding of the mechanical factors associated with surgical assembly and the processes of MACC.

Overall Goals

Goal 1: Seating Mechanics – Identify the effects of surgical assembly variables such as assembly load orientation, load magnitude and contamination on measured seating mechanics (load vs. displacement behavior) and taper stability defined by the pull-off load.

Specific Aim 1: Effects of Load Magnitude and Load Orientation on Seating Mechanics in Modular Taper Junctions – Part 1: 12/14 modular couponed samples were axially assembled at

18

various seating load magnitudes. Throughout loading, the seating load-displacement behavior was captured.

Part 2: 12/14 modular couponed samples were assembled at various seating load orientations from 0° to 20°. The load-displacement relationship was monitored throughout testing. The goals of this study were to assess the effects of seating load magnitude and load orientation on load-displacement mechanics and correlate these mechanics taper stability as measured by pull-off load.

Specific Aim 2: Effects of Taper Junction Contamination on Seating Mechanics in Modular Taper Junctions – Using similar 12/14 couponed implant samples and taper surfaces coated with various contaminants (dry, wet, fat and bone chip), each sample will be seated axially at 4000 N while capturing the seating mechanics and taper pull-off load. Retrieval studies have touched upon the negative effects of bone and fat particles found in the taper junction but provide a limited understanding of what role each contaminant plays on seating mechanics and how that in turn alters the overall taper locking stability [46, 67].

Hypothesis: Studies performed by Jauch et al. have touched upon the influence of assembly conditions on ICFC response but did not consider concepts such as assembly load orientation, varied load magnitude and load rate [46]. These variables differ throughout in-vitro studies as well as in surgical practice. With a higher assembly load magnitude the head will be seated further onto the neck with greater locking pressures, which will reduce subsequent subsidence, micromotion and fretting corrosion during testing [68].

Assembly load orientation will also influence the initial seating displacement of the head on the neck. Axial orientation will allow for greater locking and improved mechanical

performance of the taper. The more off-axis the load the lower the seating displacement and pull-off will be.

Taper junction contamination, which can arise during surgery, will reduce the locking ability of the two components and will prevent the head from completely seating on the neck. Thus reducing the pull-off load due the heads inability to seat firmly on the neck. The contamination will also make the junction area a more adverse region leading to local tissue response and/or pitting corrosion of the metals. The introduction of liquid and solid contaminants into the junction area will increase the likelihood of debris collection leading to poor seating mechanics and a lower pull-off load due to the compromised nature of frictional characteristics about the interface defined in the aforementioned taper mechanics section [15, 46, 48].

Goal 2: Incremental Cyclic Fretting Corrosion Testing – Building on Goal 1, Goals 2 will determine the effects of surgical parameters and design variables such as assembly load orientation, magnitude and contamination as well as taper design and material combination on measured seating mechanics (load vs. displacement behavior), ICFC response and pull-off load.

Specific Aim 1: Effects of Seating Load Magnitude on Incremental Cyclic Fretting Corrosion in 12/14 Modular Taper Junctions – 12/14 modular couponed samples were axially assembled at various seating load magnitudes. Throughout cyclic load the fretting behavior (motion and current results) was captured. The goals of this study were to assess the effects of seating load magnitude on load-displacement mechanics and correlate these mechanics taper stability pre and post ICFC testing.

Specific Aim 2: Effects of Seating Load Orientation on Incremental Cyclic Fretting Corrosion in 12/14 Modular Taper Junctions – 12/14 modular couponed samples were

assembled at various seating load orientations before undergoing ICFC testing. Throughout testing the fretting behavior was monitored. The goals of this study were to assess the effects of seating load orientation on load-displacement mechanics and correlate these mechanics taper stability pre and post ICFC testing.

Specific Aim 3: Effects of Taper Contamination on Incremental Cyclic Fretting Corrosion and Taper Stability in 12/14 Modular Taper Junctions – Contaminated 12/14 taper junctions were seated axially at 4000 N while capturing the seating mechanics and monitored during cyclic loading; post cyclic loading the samples underwent pull-off testing. Data from each group was compiled and compared to assess taper performance of contaminated junctions verse a dry control group.

Specific Aim 4: Incremental Cyclic Fretting Corrosion of Head-Neck Tapers in Hip Implants: Comparison of C vs. V40 tapers, and TMZF vs. Ti-6Al-4V under anatomic (off-axis) seating conditions – Study and compare the effects of alloy type (Ti-6Al-4V vs. Ti-Mo-Zr-Fe, (TMZF)) and taper design under anatomic (off axis) seating conditions on Incremental Cyclic Fretting Corrosion (ICFC) response. Dividing the samples into three groups based on alloy type, taper design and geometry, each group was compared using a bench-top test method. The test method, detailed in the experimental design section, allowed for comparisons of seating mechanics, fretting corrosion results, micromotion and subsidence during testing.

Specific Aim 5: Impaction of Ti-6Al-4V/CoCr 12/14 Tapers in Modular Hip Implants: Determining the effects of impaction load on head-neck taper performance using an incremental cyclic fretting corrosion test – Ti-6Al-4V/CoCr 12/14 tapers were axially assembled using an impaction seating method (2500 kN/s). Post seating, samples were oriented at 35º before undergoing ICFC testing. The motivation behind the study was to determine the

effects of impaction assembly (high rate assembly loading) on micromotion, subsidence and fretting corrosion currents.

Hypothesis: Varying assembly factors such as load magnitude and orientation will alter taper performance during ICFC testing. The hypothesis is increasing load magnitude will not only increase taper stability but reduce fretting motions which cause fretting current reactions. However, the increase in load orientation will prove opposite, reducing taper stability and increasing fretting micromotion and subsidence. An increase in fretting motion will increase fretting current.

In terms of taper junction contamination, the incorporation of contaminants will increase micromotion, subsidence and fretting corrosion throughout testing. As previously stated, material debris lodged in the taper junction will reduce the seating ability, decreasing the amount of force needed to induce micromotion[46]. Higher amounts of micromotion will result in higher fretting responses and a lower pull-off load. Fat contamination within the junction will also reduce the frictional characteristics of the taper and increase the fretting response [15, 48].

Specific Aim 5 discusses taper design and material combination. Two different commercially available tapers (C and V40, Stryker Orthopaedics) have different engagement lengths, taper angles and taper diameters. Based on taper mechanics, these parameters may affect the locking of the junction and alter the fretting corrosion response of the taper during cyclic testing.

TMZF, a newer β-phase titanium alloy, with a yield strength of 800-900 MPa and modulus as low as 74 GPa allows for greater flexibility than Ti-6Al-4V, which has a modulus of 110 GPa. The hypothesis for this goal was the use of a more flexible alloy will lead to a more

aggressive response in fretting corrosion behavior compared to Ti-6Al-4V due to a decreased flexural rigidity [57].

Taper combination was compared after testing. The two tapers vary in engagement length (length of taper region), design dimensions (length of the short (D1) and long (D2) diameter region) and taper half-angle (the contact angle). V40 tapers have an engagement length of 10.03 mm, design dimensions of 11.21/12.80 mm (D1/D2≈11/13) and a taper half-angle of 2°48' while C tapers have an engagement length of 10.20-10.27 mm, design dimensions of 12.38/13.62 mm (D1/D2≈12/14) and a taper angle of 2°46' [69-71].

Goal 3: Load Rate and System Compliance – Determine the effects of load rate and system compliance on modular taper seating behavior and stability.

Specific Aim 1: The Effect Load Rate and System Compliance on Seating Mechanics and Taper Stability – Ti6-Al-4V/CoCrMo 12/14 tapers were assembled axially, throughout testing samples were assembled at varying load rates, load magnitudes and the system compliance was altered. The purpose of the study was to present a test method in which the effects of system compliance, load rate and load magnitude on taper stability were studied. Also seating displacement was captured using a novel high speed camera method.

Hypothesis: The load rate will not have a significant effect on taper performance. The higher load rate may cause plastic deformation of the trunnion/taper junction, which will increase the seating displacement but will not alter the locking mechanism based on scientific principles discussed earlier in this chapter. The increase in system compliance will also be negligible due to the high impulse of assembly during testing which will render the pliable surface ineffective.

Dissertation Structure

The overall framework of this dissertation is outlined in the diagram in Fig. 1 with a major focus on bulk and surface mechanics. The chapters and subsections are intended to provide a more thorough understanding of these mechanisms and their effect on modular taper junctions. This dissertation is comprised of a number of chapters divided into two major sections, Seating Mechanics and Incremental Cyclic Fretting Corrosion Testing.

Seating Mechanics.

Goal 1 Subsection 1 begins by introducing a novel seating mechanism test method on couponed test samples. The samples were assembled at specific load magnitudes and orientations then pulled apart in a tensile test to assess to taper locking stability. Seating mechanics (load-displacement behavior) and taper stability were compared to evaluate taper performance.

Subsection 2 explores the effects of taper contamination on the seating behavior in modular implants and taper locking stability. The results from the section begin to reveal a new possible coating system which may improve taper seating and stability.

Incremental Cyclic Fretting Corrosion Testing.

Goal 2 Subsection 1 delves into the effects of seating load magnitude on fretting motions and current during incremental cyclic fretting corrosion testing. The effects of increased load magnitude on micromotion, subsidence and fretting currents were compared. Taper stability post-ICFC testing was also evaluated.

Subsection 2, similar to subsection 1 compares the effects of increased seating load orientation. The same parameters were used to measure taper performance.

Subsection 3 revisits the effects of contamination on taper performance. Testing includes incremental cyclic fretting corrosion testing post seating and taper locking stability testing. The results from testing were used to assess taper performance. The results, like that of chapter 3 reveal an interesting conclusion.

Subsection 4 introduces taper design and material combinational differences to the ICFC benchtop test method and the accompanying results from the comparison test of two alloy and geometrical combinations.

Subsection 5 details the effects of impaction assembly on modular interfaces. Implants were axially impacted at three different load groups before undergoing ICFC testing with a three sensor displacement measurement system. Taper performance (micromotion, subsidence and fretting corrosion results) were compared in post-testing analysis.

Goal 3 Subsection 1 finalizes the laboratory experimentation portion of the dissertation, detailing the effects of load rate, load magnitude and system compliance on seating displacement and taper compliance. The chapter also details the capturing of seating displacement with a novel method.

Section 4.0.2 differs from the previous subsections with a detailed explanation of a Visual Basic program used to aid in visual analysis of experimental data.

Chapters 4, 5 and 6 discuss the overall dissertation discussion, conclusions and future work chapters respectively. The discussions, conclusions and future work are based on the work presented in the preceding sections presented in this dissertation.

Chapter 2 – Methods and Materials

Testing methodology in the identified subsections, 2.1 and 2.2 as well as 2.3-2.8, follow similar test protocols. As such, the details of these methods will be described below to minimize redundancy in subsequent section. The sections will be defined as Seating Mechanics (sections 2.1 & 2.2) and Incremental Cyclic Fretting Corrosion Testing (sections 2.3-2.8).

2.1 – Goal 1: Seating Mechanics Methods

Specimen mounting and seating displacement measurement. Before loading samples were positioned directly under the load applicator. Off-axis samples were mounted into an angled fixture which allowed the load to be applied at the predetermined angles (Fig. 9).
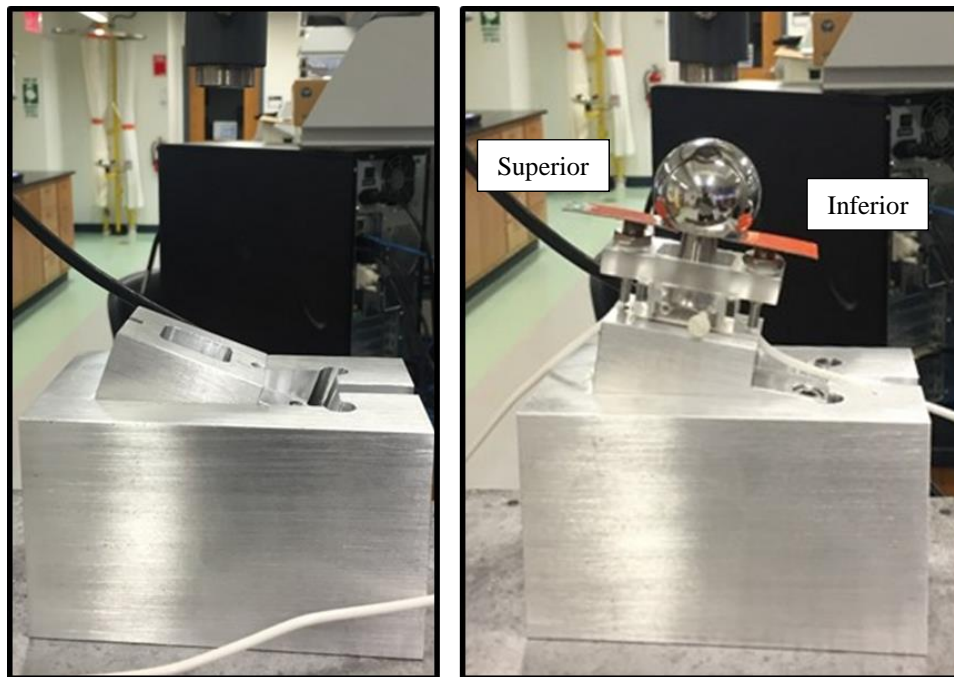
Fig. 9: Seating load orientation fixture oriented at 20°. Fixture securely holds couponed trunnion with DVRTs fixed to the superior and inferior portions of the stem under the load applicator.

Seating displacement was captured using two non-contact eddy current sensors with a range of 1 mm mounted to the superior (DVRT 1) and inferior (DVRT 2) portions of the stem (Micro-Epsilon). Sensors were threaded into an acrylic holder (see Fig. 10) targeting aluminum

plates fixed to the head. Displacement and load were captured by a modified LabView

acquisition program at a rate of 100 points/s.
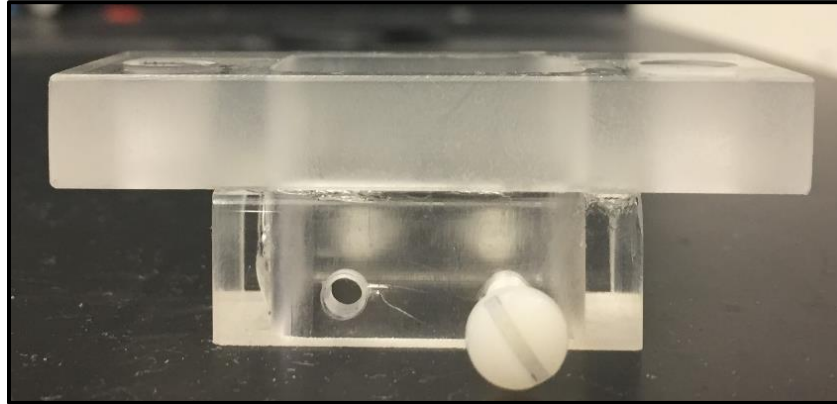
Fig. 10: Image of sensor fixture which held sensors fixed to the superior and inferior portion of the sample stem. Nylon screws were used to rigidly fix the holder to the sample.

Test protocol. Before testing the male and female taper junctions were cleaned with ethanol to

remove particulates from the surfaces. Samples were then tested to the predetermined seating

load magnitude, orientation and contamination specifications. Loads were applied with a

servohydraulic test frame at a rate of 200 N/s and held at the peak load for 5 s before unloading

(Instron).

Pull-off. Post seating, tensile pull-off loads were applied at a rate of 5 mm/min (MTS858, MTS

Systems Corporation, Minnesota) until the taper interlock was overcome. The load at separation

was recorded.

Statistical Analysis. Statistical analysis was performed using an ANOVA test with post-hoc

Tukey analysis to determine differences. A P-value of less than 0.05 as considered significant.

Data analysis. Acquired displacement data was captured from a set initial load to the fully

unloaded condition. The initial load was dependent on the study. The reported seating

displacement is the difference between the rigid final displacement, the displacement recorded at

unload, and the rigid initial displacement, the displacement recorded at the initial load. For

example, if a sample is initially loaded to 50 N and the corresponding displacement measured is 30 μm, the final displacement will be the displacement at the end of testing minus this initial 30 μm. This was done to eliminate any variability in the seating measurement that may arise from an inconsistent initial position. Final displacements were taken at unload due to the elastic nature of the system while a load was applied. Initializing the data to a set initial load gave each study a consistent starting point.

The work of seating, which is the area under the load-displacement plot of seating, was calculated using the following area under the curve equation for rigid seating load-displacement data:

$$W = \sum_{i=0}^{n} \left(\frac{F_{i+1} + F_i}{2}\right) * (D_{i+1} - D_i) \qquad (\text{Eqn. } 11)$$

F is the load applied, i is the indicial point (which is summed over n points) and D is displacement. Work calculations for the superior and inferior sensors used an initial load value and the corresponding displacement value up to the peak load and then unloading and their corresponding displacement values.

2.1.1 – Effects of Seating Load Magnitude and Load Orientation on Seating Mechanics in Modular Taper Junctions

Implant design. Ti-6Al-4V 12/14 trunnion taper test coupons, coupled with CoCrMo heads, were seated axially (0°) at four seating load (n=5): 1000, 2000, 4000 and 8000 N using a quasistatic seating method.

Three load orientation groups were tested at 4000 N: 0°, 10° and 20°.

Specimen mounting and displacement measurement system. Samples were mounted under the load applicator and were seated and analyzed as defined in the aforementioned Seating Mechanics section. The data was initialized with a 50 N initial load.

2.1.2 – Effects of Taper Junction Contamination on Seating Mechanics and Pull-off Loads in 12/14 Tapers

Implant design. Ti-6Al-4V 12/14 tapers with CoCrMo heads were axially seated to 4000 N. Samples were divided into five test groups (n=5): dry (control), wet, liquid porcine lipids/fat, solid lipids/fat and bone chip. Wet trunnions were immersed in a 10% fetal bovine serum and phosphate buffered saline solution. Liquid lipid trunnions were thinly coated in lipids rendered from porcine fat, while solid lipid contaminants approximately 3 mm x 3 mm were directly placed on the male superior portion of the trunnion. Lastly, bone chip models approximately 45-50 µm in thickness and about 2 mm x 2 mm across were positioned on the male trunnion in a superior location at approximately the mid-point of the taper length.

Specimen mounting and displacement measurement system. Samples were positioned directly under the load applicator (Fig. 11) and sensors were fixed as defined in the Seating Mechanics section.
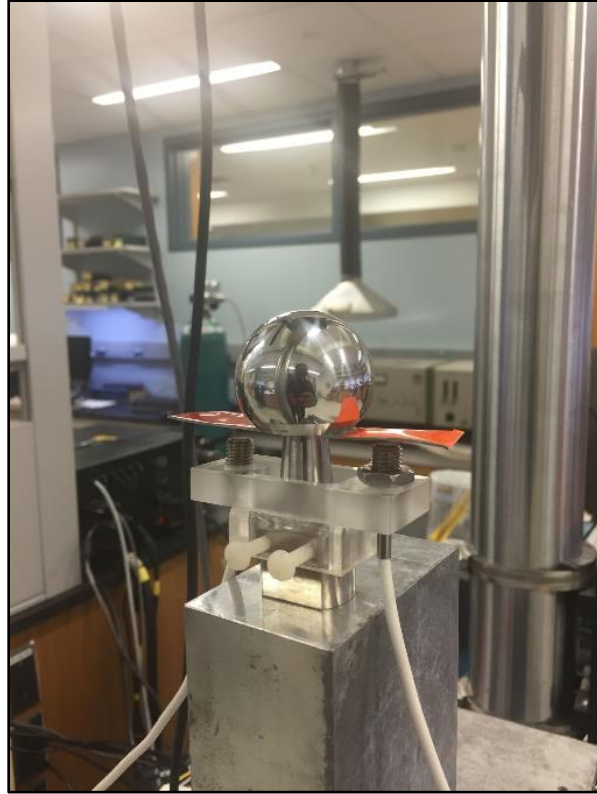
Fig. 11: Contaminated sample under load applicator with sensors fixed to the superior and inferior portion of the neck targeting the head.

Test protocol. The test protocol followed the guidelines defined in the seating mechanics section. However, solid contaminants were placed on the superior portion of the male taper. Reported seating displacements were defined as the distance traveled from 100 N to unload in order to normalize the results.

Statistical analysis was performed using an ANOVA test ($P<0.05$).

2.2 – Goal 2: Incremental Cyclic Fretting Corrosion Testing

Micromotion measurement system. Motion about the junction was sensed using submersible non-contact eddy current sensors. The high-resolution sensors provided a measurement range of 1 mm with a 0.5 µm resolution. A specially designed fixture was used to mount two (specific aims 2.1-2.4) to three (specific aim 2.5) non-contact eddy current sensors to the stem of the

implant while an aluminum plate was mounted to the head component, seen in section 2.2.4.

Sensors were inverted and fixed to the head in sections 2.2.1-3 and 2.2.5. Sensor fixture

components and their evolution in design throughout the course of this dissertation are further

discussed in the discussion section.

In the two DVRT sensor setup the sensors were fixed to the superior and inferior portion

of each sample. The three DVRT sensor setup mounted the sensors to the head and was used to

collect motion data such as pistoning (in z-axis along the length of the taper) and rocking (about

the x-axis, or in the medial-lateral plane; and the y-axis, or the anterior-posterior plane) about the

head-neck taper junction during loading (Fig. 12). Each sensor was offset from one another by

120 degrees. DVRT 3 was fixed to the medial region, while DVRTs 1 and 2 were fixed to the

anterior-lateral and posterior-lateral regions of the head, respectively.
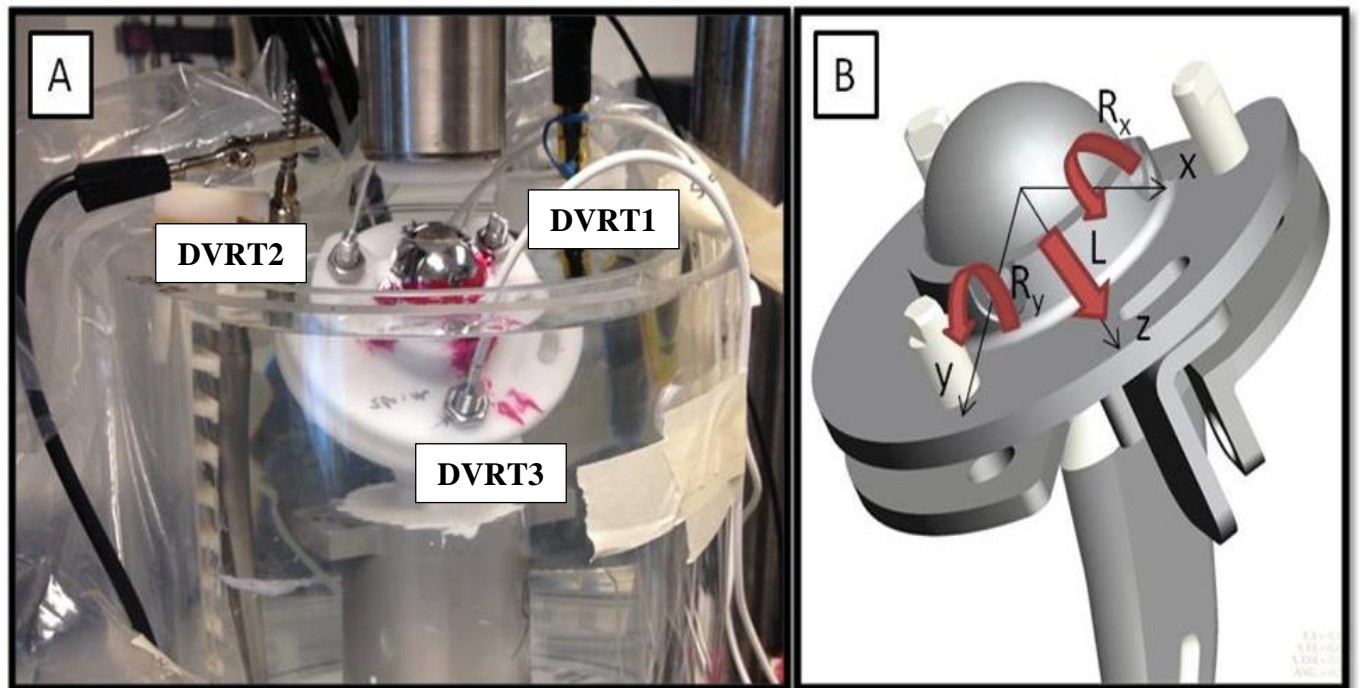
Fig. 12: a) DVRTs mounted to the anterior-lateral (DVRT1), posterior-lateral (DVRT2) and medial (DVRT3) region of a sample. b) Motion sensing schematic of 3 DVRT system.

Off-axis cyclic loading of the head influenced the motions recorded by the sensors, the motions were comprised of both elastic deformation-based motions (i.e., motions between sensor and target arising from the displacements resulting from elastic deformation), and rigid-body motions. Figure 13 shows the loading schematic for a sample loaded 35° off-axis which allows bending about the neck during loading.
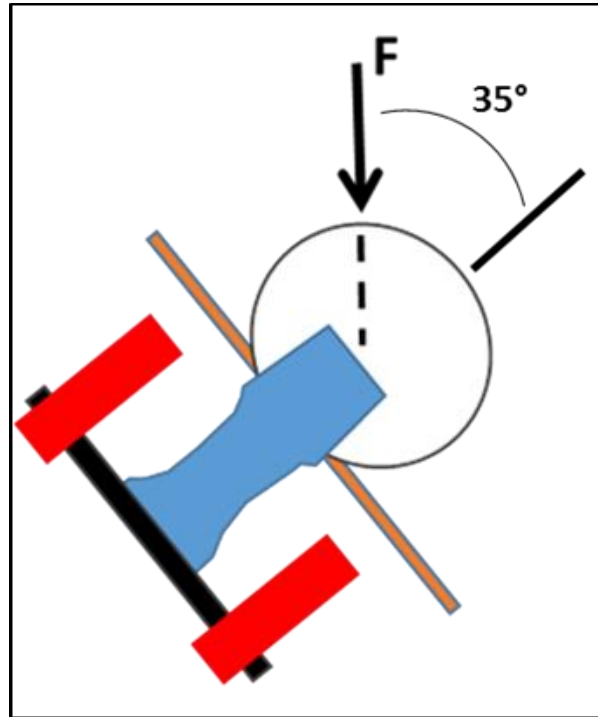
Fig. 13: Implant loading schematic with force (F) 35° from neck axis.

Test protocol. The test protocol was broken into four steps; 1) Seating of the head on to the stem, 2) Incremental cyclic load-corrosion-micromotion measurement, 3) Post-test static calibration and 4) Post-test analysis of seating, motion, corrosion currents and determination of elastic and rigid body motions.

Seating & work of seating. The seating of the head on the stem was performed systematically and monitored with the displacement sensors. The stem was placed into the servohydraulic test frame (Instron or MTS) and the head-neck taper was assembled under predetermined conditions (i.e. dry, wet, contaminated, at a specific assembly load magnitude and orientation). The line of

action of the seating force was also dependent upon the predetermined seating conditions. During cyclic testing the load was 35º from the neck axis. This was to simulate a 45° stem-neck angle and a 10° retroversion of the stem from the vertical.

During seating the eddy current sensors recorded the relative displacement of the femoral head onto the neck. The work of seating was calculated as described before and seating displacements were calculated as described above.

Incremental cyclic loading-corrosion-micromotion testing. The cyclic load testing procedure previously described by Gilbert et al. was modified to concurrently subject the implants to incremental cyclic loading while immersed in PBS and held at a fixed potential of -50 mV (Ag/AgCl) using a potentiostate and carbon graphite counter electrode [5]. The cyclic load increased from 100 N to 1000 N in 100 N increments every three minutes. The load then increased by 200 N increments from 1000 N to 4000 N at three minute intervals. During the change in load magnitude, the samples were held fixed within 10% of the previous load for approximately 20 s before the load was ramped to the next cyclic load level and cyclic testing resumed. This intermittent pause in loading assisted in tracking the motion measurements and the corrosion behavior by allowing a short-pause recovery of the signals.

During testing several parameters were captured synchronously with two separate programs. In the first program, the load, actuator displacement and corrosion currents were captured by the default Instron program (Wavematrix^{TM}). The second program, written in LabView^{TM}, was used to capture the micromotions sensed by the two displacement sensors, as well as the load and the fretting currents (captured from the potentiostat).

Post-test static stiffness calibration. As previously stated, the motions sensed by the displacement sensors were comprised of both elastic-based displacement and rigid body motion. It is possible to account for both contributions of motion by determining the stiffness of the implant construct for each sensor in the loading orientation used. To determine the stiffness of the construct several static loads from 10 to 3000 N were applied to each sample. By measuring the load versus static displacement plots and performing a linear regression of the resulting data, the stiffness (the slope of the linear regression) of the construct for each sensor was calculated.

Post-test Analysis. The resultant files from each test included: 1. Seating file (data on load and DVRT motion for both sensors during seating), 2. Incremental Cyclic Loading test (two files), 3. Stiffness Calibration files.

Post-test pull-off load. A tensile pull-off load was applied (5 mm/min) until the taper junction failed and the head-neck disassembled. Pull-off testing not done in sections 2.2.4 and 2.2.5.

Statistical Analysis. An ANOVA test (P<0.05) was used for statistical comparisons between groups.

2.2.1 – Effects of Seating Load Magnitude on Incremental Cyclic Fretting Corrosion in 12/14 Modular Taper Junctions

Implant design. Ti-6Al-4V 12/14 tapers and CoCrMo heads were axially seated at four load levels (n=5): 1000, 2000, 4000 and 8000 N. Trunnion samples were fabricated with production-like 12/14 taper characteristics and had a 4-inch-long stem and threaded hole at the base to affix to the test base.

Load application and displacement measurement system. Samples were positioned directly under the load applicator during seating. Displacement was captured using two non-contact eddy

current sensors with a range of 1 mm mounted to the superior and inferior portions of the head (Micro-Epsilon). Sensors targeted aluminum plates fixed to the stem (Fig. 14a). Displacement, load and current were captured by a modified LabView acquisition program at a rate of 100 points/s.
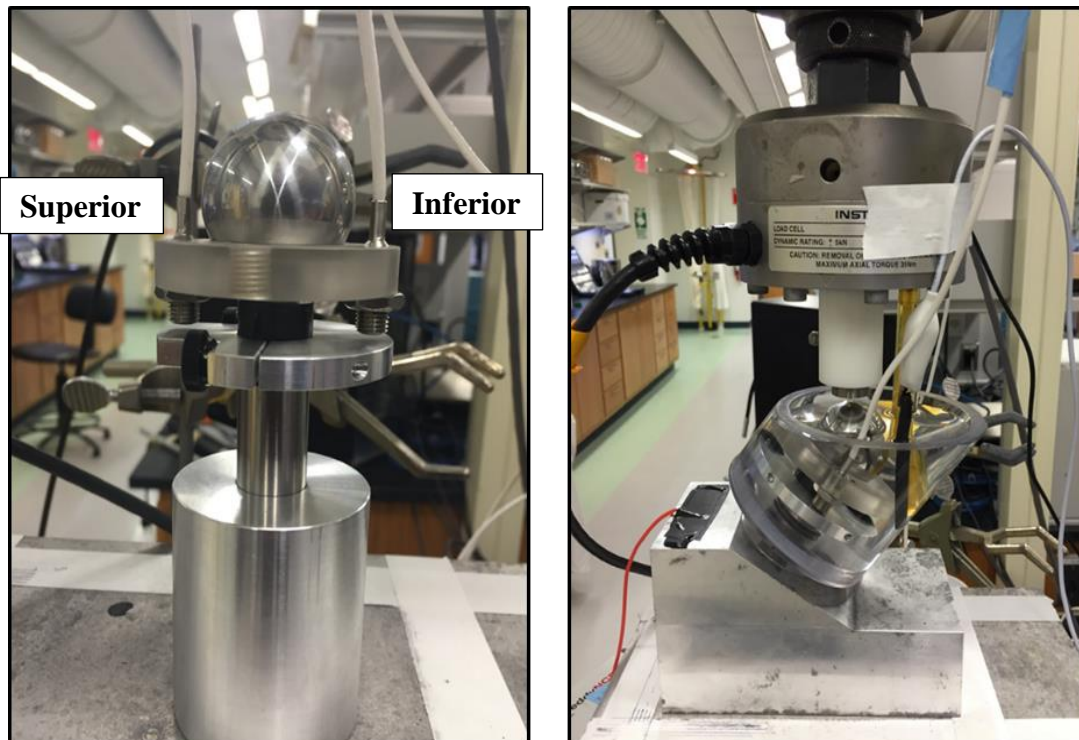
Fig. 14: a) Test sample with sensors fixed to the superior and inferior portion of the head targeting the aluminum plate fixed to the stem. b) Image of a sample awaiting testing in the test fixture filled with PBS.

Test protocol. Testing was broken into four steps: 1) seating, 2) cyclic testing, 3) static calibration and 4) pull-off testing. Taper junctions were cleaned with ethanol to remove particulates from the surfaces and allowed to dry before seating.

All seating, incremental cyclic fretting corrosion and static calibration testing was done as defined in Incremental Cyclic Fretting Corrosion section. ICFC testing was done in the potting fixture in image Fig. 14b.

Post-test pull-off load. A tensile pull-off load was applied (5 mm/min) until taper locking failed and the head-neck junction was disassembled. The peak force of distraction was captured and

used as the pull-off force. The pull-off loads captured post-cyclic testing were compared to the pull-off loads captured Section 2.1.

Data analysis. All data reported consisted solely of rigid body motion. Statistical analysis was performed using a one-way ANOVA test ($P<0.05$).

2.2.2 – Effects of Seating Load Orientation on Incremental Cyclic Fretting Corrosion in 12/14 Modular Taper Junctions

Implant design. Ti6Al4V 12/14 tapers and CoCrMo heads were seated to 4000 N at three load orientations (n=5): 0°, 10° and 20°. Samples were fashioned with a 4-inch-long stem and threaded hole at the base. Before seating, samples were placed in orientation fixture and positioned directly under the load applicator (Fig. 15).
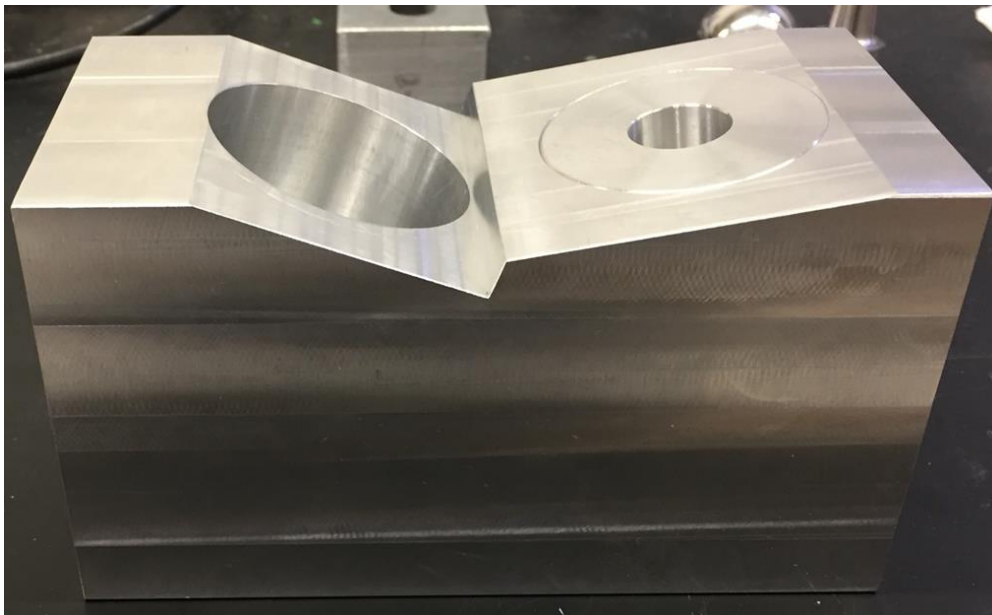
Fig. 15: Seating load orientation fixture used to fix the sample at either 10° or 20°.

Test protocol. Seating, ICFC and static calibration testing was done as previously described in the Incremental Cyclic Fretting Corrosion section.

36

Pull-off load. A tensile load at a rate of 5 mm/min was applied to overcome the interlocking forces and separate the head from the neck.

Statistical Analysis. Statistical analysis was performed using ANOVA test (P<0.05).

2.2.3 – Effects of Taper Junction Contamination on Incremental Cyclic Fretting Corrosion and Pull-off Loads in Modular 12/14 Tapers

Implant design and contamination. Ti6Al4V 12/14 tapers and CoCrMo heads were axially seated to 4000 N in five contamination groups (n=5): dry, wet, liquid porcine lipids (liquid fat), solid lipids (solid fat) and bone chip. Trunnions were thinly coated in liquid lipids, while solid lipid trunnions had the contaminant placed on the male superior portion of the trunnion. Wet trunnions were immersed in a 10% fetal bovine serum and phosphate buffered saline solution. Lastly, bone chip models were approximately 45-50 µm in thickness and 2x2 mm across and positioned on the male superior portion.

Test protocol. Seating, ICFC and static calibration testing was done as previously described in the Incremental Cyclic Fretting Corrosion section.

Post-test pull-off load. A tensile pull-off load was applied (5 mm/min) until the taper junction failed and the head-neck disassembled.

Statistical Analysis. An ANOVA test (P<0.05) was used for statistical comparisons between groups.

2.2.4 – Incremental Cyclic Fretting Corrosion of Head-Neck Tapers in Hip implants: Comparison of C vs. V40 tapers, and TMZF vs. Ti-6Al-4V under anatomic (off axis) seating conditions

Implant designs. Group 1) was comprised of Accolade II with V40 Taper and Low Friction Ion Treatment (LFIT) Anatomic head (Ti-6Al-4V/CoCr). Group 2) was Secure Fit with C Taper and LFIT Anatomic head (Ti-6Al-4V/CoCr). Group 3) was Accolade TMZF with V40 Taper and LFIT Anatomic head (TiMoZrFe/CoCr). Table 1 further details the differences in taper geometry. (Stryker Orthopaedics, Mahwah, NJ) (Fig. 16a).

Taper Type	Diameter (D1/D2) (mm)	Trunnion Length (mm)	Nominal Taper Angle (°)
C Taper	12/14	10.2-10.27	2°46'
V40 Taper	11/13	10.03	2°48'

Table 1: Taper geometry table highlighting the differences in the V40 and C taper used in this study.

Specimen mounting. The femoral stems were mounted in an acrylic base (Lang Dental) with the stem oriented 10-degrees valgus to the vertical. Polypropylene chambers were fixed about the stem with silicone to serve as an environment chamber. Phosphate buffered saline (PBS, at room temperature) was added to the chamber immersing the taper junction. Two non-contact eddy current sensors (Micro-Epsilon eddyNCDT 3010) were mounted to the stem while an electrically isolated aluminum target plate was mounted to the head (Fig. 16b).
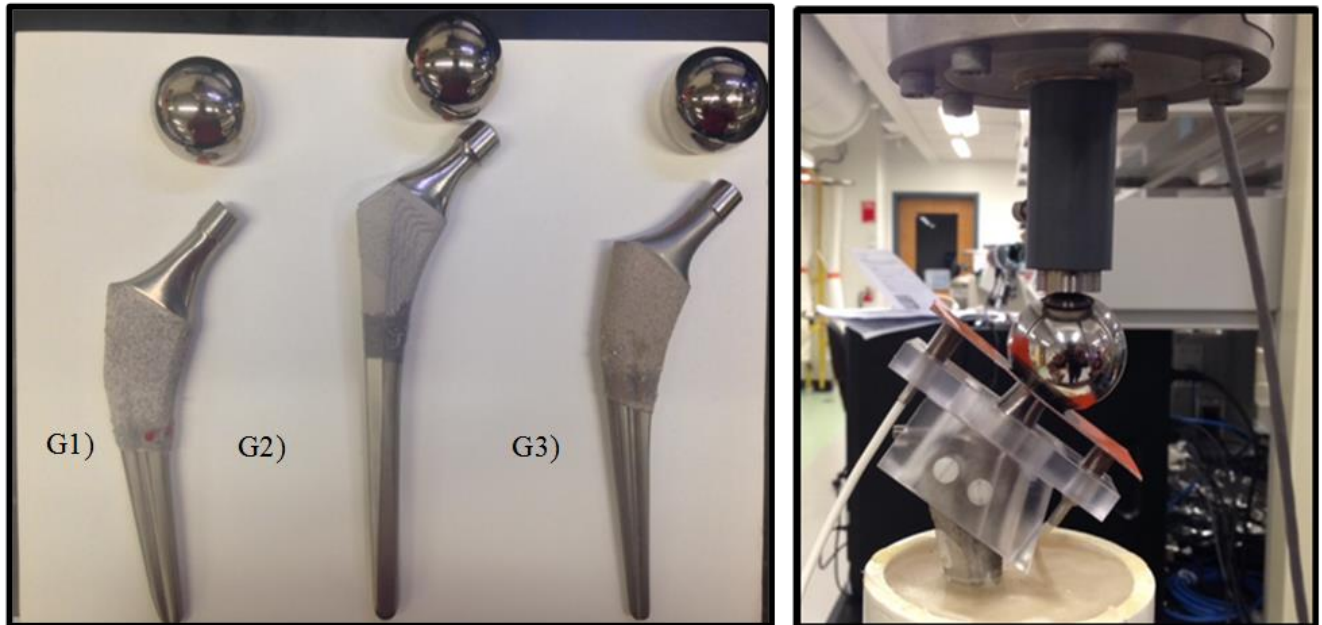
Fig. 16: (a) Image of samples used throughout testing. (b) Ti64/CoCr C taper sample undergoing seating with displacement fixtures mounted to the stem.

Specimen Testing. Seating, incremental cyclic fretting corrosion and static calibration testing of the samples in this study were done as defined in Incremental Cyclic Fretting Corrosion section. Seating data was normalized at 100 N to create a uniform starting position for all samples tested.

Statistical Analysis. Analytical analysis was done using One-way ANOVA testing ($P<0.05$).

2.2.5 – Impaction of Ti-6Al-4V/CoCr 12/14 Tapers in Modular Hip Implants: Determining the effects of impaction load on head-neck taper performance using an incremental cyclic fretting corrosion test

Implant designs. Ti6Al4V 12/14 tapers (Stryker C taper) coupled with CoCrMo heads were impacted at three different assembly loads (n=5): G1) 0.05 kN (hand-assembled), G2) 6 kN and G3) 14 kN. In the hand-assembled group the heads were placed on the necks manually at a presumed force of 0.05 kN. Prior to testing the taper regions were passivated in compliance with

American Society for Testing and Materials (ASTM) standards [72]. Head-neck taper junctions were wetted with phosphate buffered saline prior to seating.

Impaction. Instron Dynatup 9250 G (Instron Corporation) was used to apply the impact seating load. Using a specially designed fixture the samples were oriented axially at 90^0 during impaction (Fig. 17). Seating displacement was not captured due to high rate of impaction.
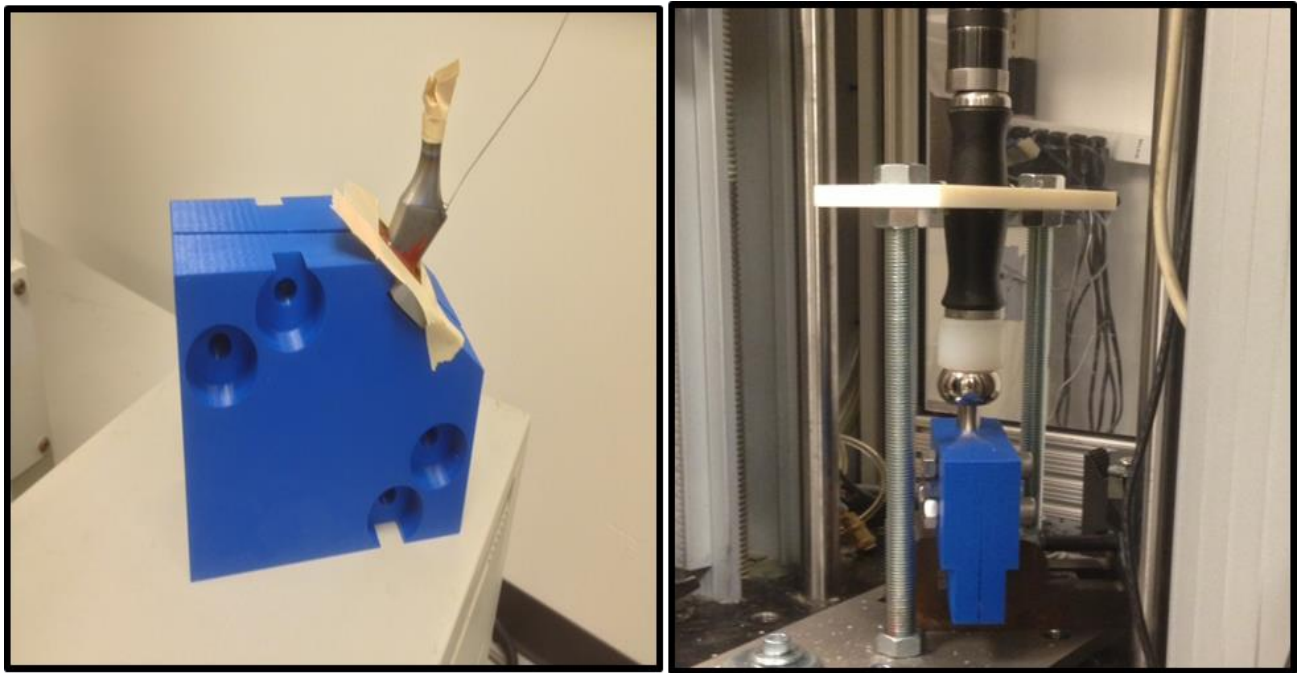
Fig. 17: 90º orientation fixture used during impaction.

Testing setup. Post seating, the femoral stems were mounted in a non-conductive ceramic epoxy (ITW Devcon) at 10^0 valgus/9^0 flexion and allowed to cure for 24 h. The potted stems were then fixed in an environmental chamber in which phosphate buffered saline (PBS, Room T) was placed just above the level of the taper junction, immersing the taper.

Test protocol. Testing consisted of; 1) Impact seating of the head, 2) Incremental cyclic loading and corrosion-micromotion measurement, 3) Post-test static calibration and 4) Post-test analysis of incremental testing. Incremental cyclic fretting corrosion and static calibration testing was identitical to previous studies.

Seating of head. Taper seating in this study differed from seating in the previous ICFC studies and is defined as such. Impact seating of the samples was done using the Instron Dynatup 9250 G. Samples were oriented axially at 90^0 (neck axis parallel to the force vector) allowing the impactor to vertically descend. Each sample was impacted three times at the same load. The impactor of the drop tower was allowed to come to a complete rest before being reset.

Post-test analysis. The resultant files from each test include: 1. Incremental Cyclic Loading test data, 2. Corrosion data and 3. Stiffness Calibration files. From these files the rigid fretting motions (micromotion and subsidence) about the sensors and currents (onset load and current at 4000 N) were used to make comparisons between the groups.

One-way ANOVA testing was used to determine significant differences (P<0.05).

2.3 – Goal 3: Load Rate and System Compliance

Testing done in Goal 3 was done with a novel high-speed camera measurement system which allowed displacement measurement during impaction testing.

2.3.1 – The Effect of Load Rate and System Compliance on Seating Mechanics and Taper Stability

Test samples. Testing was performed on 12/14 Ti6Al4V trunnions with 36mm + 5mm CoCrMo heads, the approximate taper angle was 5º40'. Taper angle standardization was ensured through a coordinate measurement machine (CMM, Wenzel Präzision), which allowed precise pairing of trunnion and head samples. Surface roughness characterization was also performed using a while light interferometer (ZYGO Corp.). Test samples were selected to limit variation in trunnion surface roughness and taper angle mismatch between trunnion and head. Non-contact parts of the samples were spray painted with flat white and black spray paint to create a speckled pattern for

41

imaging purposes (Fig. 18). Taper junctions were then cleaned with isopropanol and allowed to

completely dry.

Fig. 18: Test sample spray painted with speckle paint. Specks were used during displacement analysis.

Testing. Sample group combinations were divided into multiple groups to analyze the effects of

compliance, load rate, and peak force (n=3) on seating mechanics and taper locking stability:

- Compliance:
  - Non-compliant (NC): the trunnions were clamped down to a stainless steel base (Fig. 19a).
  - Compliant (C): the trunnions were clamped down to a stainless steel base with a 40 durometer rubber mat underneath a steel plate (Fig. 19b).

- Load Rate:
  - Impaction test (I): non-compliant ≈ 2500 kN/s, compliant ≈ 25 kN/s
  - Static test (S): ramped up at 300 N/s and unloaded at 500 N/s

- Peak Load:

Peak Load	Load Rate (Impaction/Static)	Compliance (Non-compliant/Compliant)	Notes:
2 kN	I and S	NC/C	Load could not be achieved on NC impaction test
3.5 kN	I and S	NC/C	
6 kN	I and S	NC/C	
10.1 kN	I and S	NC/C	Load could not be achieved on C impaction test
23.5 kN	I and S	NC	Load could not be achieved with compliant test setup
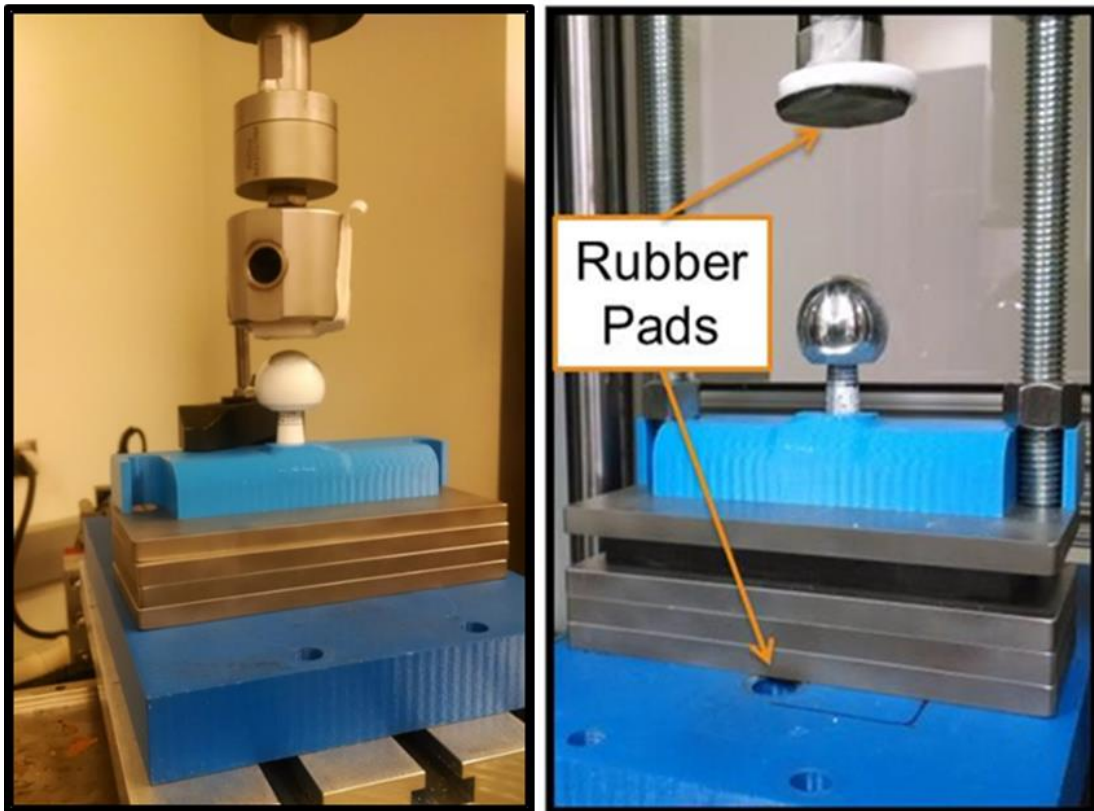
Fig. 19: a) Non-compliant static sample before loading. b) Compliant impaction sample prior to impaction.

Assembled samples were axially preloaded to 10 N then seated to one of the predetermined peak loads on one of the compliant setups. All samples were carefully placed directly under the load applicator to reduce the chances of a non-axial load being applied; a ¼" polyethylene piece was attached to contact surface of the load applicators.

Static loads were applied at a rate of 300 N/s with a servohydraulic test frame (MTS 858, MTS Corp.); the peak load was held for 3 s before being removed. Non-compliant impaction loading was done at an approximate load rate of 2500 kN/s and was reduced in the compliant setup to approximately load rate of 25 kN/s by adjusting the thickness of the rubber mat. The samples were only impacted once; the load applicator was not allowed to bounce.

Displacement during testing was recorded with a high-speed camera (MotinXtra NX8-S2, DEL Imaging Sytems). The system had a max resolution of 1600 x 1200 pixels with a max recording rate of 4,000 fps at max resolution and a pixel accuracy of approximately 8.6 µm. During testing, the camera system was positioned 350 mm away from the samples. The parameters for the camera were as follows: frame rate (100 fps Static, 8000 fps Impaction), f-stop (32 Static, 22 Impaction), region of interest (896x552 Static, 288x552 Impaction) and light exposure time (400 µs Static, 123 µs Impaction). The camera system recorded data before the load applicator was applied until the load was completely removed from the sample. Data from the camera was saved and calibrated for displacement tracking of points along the head and trunnion during playback.

Post-test pull-off testing. Post-seating the samples were disassembled at a tensile rate of 15 mm/min (Instron 5582, Instron Corp.), the load-displacement values were record.

Statistical analysis. ANOVA testing ($P<0.05$) was used to determine significant differences between rigid seating displacement, seating energy and pull-off load.

Chapter 3 – Results

3.1 – Goal 1

The analyzed data was broken into two categories for seating load magnitude and load orientation.

3.1.1 – Load Magnitude and Orientation Analysis and Results

Load Magnitude Analysis.

Seating displacement. Fig. 20a illustrates the load and displacement versus time relationship during the seating test. The displacement increased with the load overtime until the peak load was reached (4000 N in this case) and held for 5 s before unloading. The maximum displacement was achieved at maximum load and upon unloading the sample experienced an elastic rebound before settling at its final displacement.

Seating load-displacement behavior at different seating loads showed a consistent characteristic behavior. During seating, displacements rose somewhat parabolically until reaching the peak load, the unload portion of the graph reflects the elastic rebound as the load is removed leaving subsequent rigid motion. The corresponding load-displacement plots from the seating load magnitude experiment are shown in Fig. 20b. It is interesting to note that the shape of the seating curves overlay one another indicating a consistent and reproducible seating behavior for these tapers. In each loading case, the unloading portion of the plots appear to be

parallel indicating that the elastic rebound during unload is consistent between samples as well.

The y-intercept of the unloading curves reflects the final seating displacement (Fig. 20b).
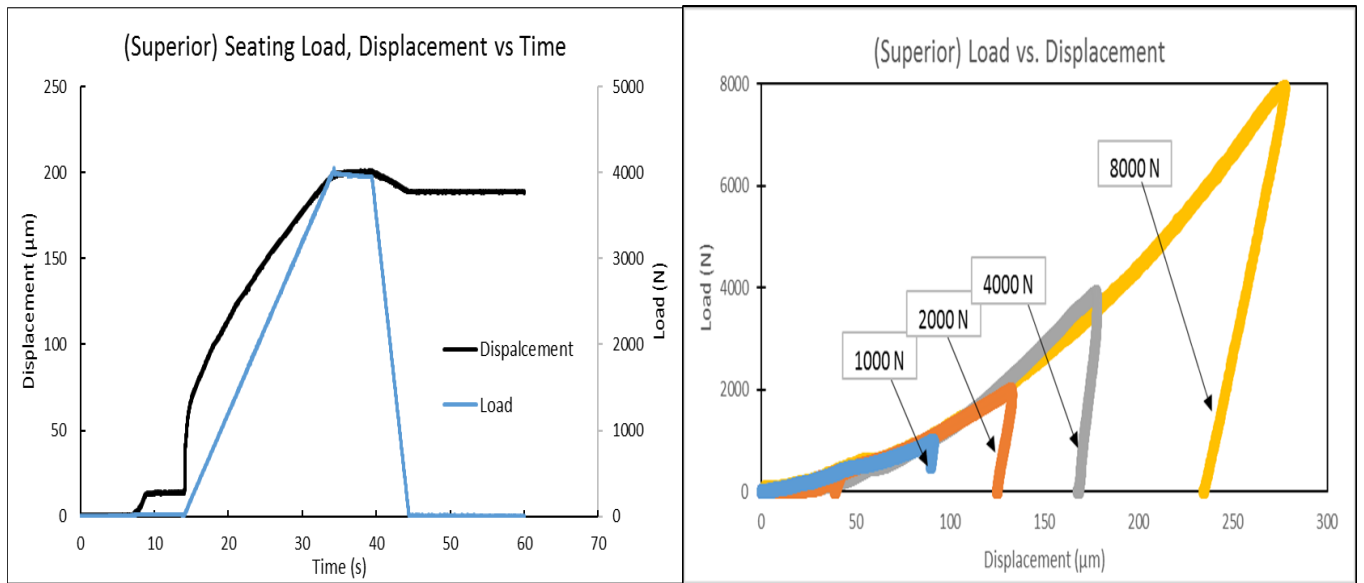
Fig. 20: (a) Superimposed seating load, displacement vs. time plot example of load magnitude sample (4000 N sample). (b) Average seating load-displacement plots for the range of loads.

Load Magnitude Results.

Seating displacement. The average final seating displacement for the superior and inferior

sensors show an approximately linear increase of maximum seating displacement with seating

load for both sensors. Each group was statistically different (Fig. 21) ($P<0.05$).
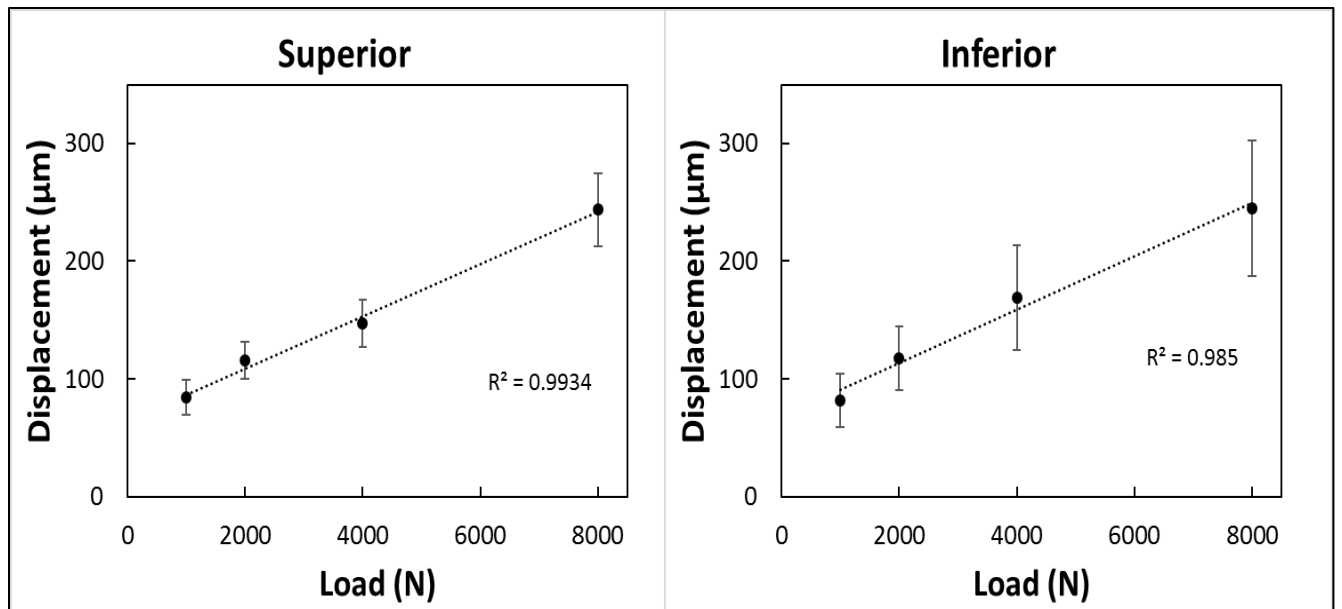
Fig. 21: Average seating displacement vs. load. Each load magnitude was statistically different (P<0.05).

Note from 0 N to 1000 N the displacement goes from 0 to approximately 80 µm. Beyond 1000 N the displacement increases in a less steep progression suggesting a large amount of seating happens at the lower loads.

Work of seating. The average work of seating values show a parabolic increase with an increase in seating load magnitude for both sensors (Fig. 22) (P<0.05). The average work of seating was approximately 0.2 to 0.25 J at 4000 N seating load.
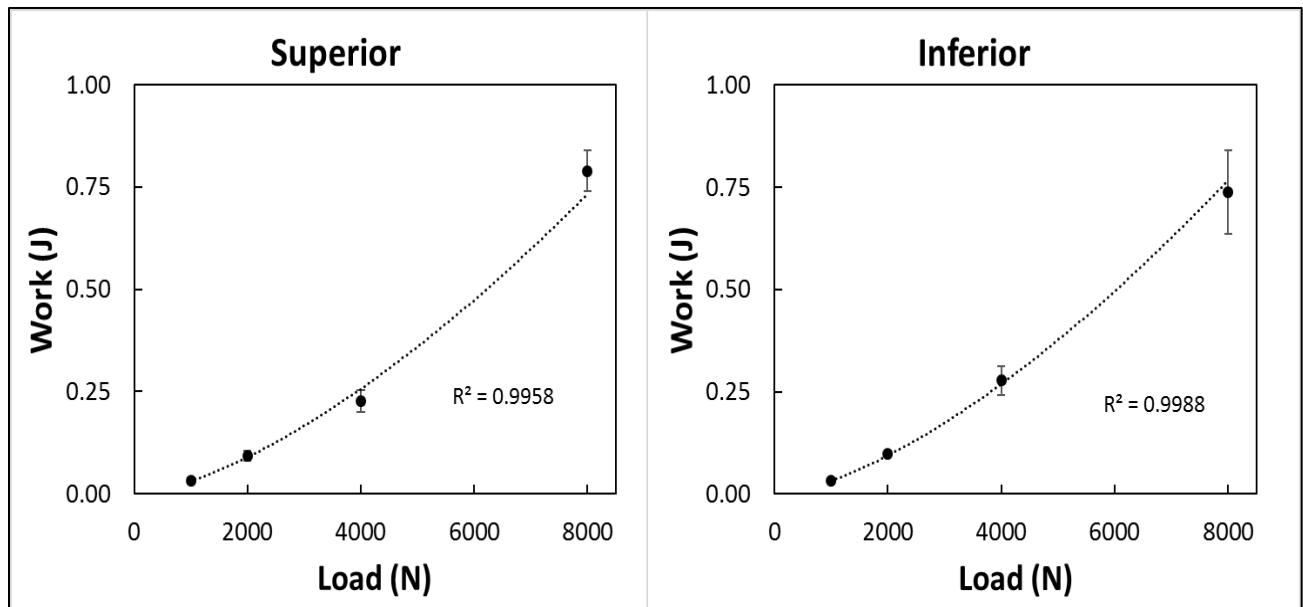
Fig. 22: Average work of seating vs. load. All loads were statistically different from one another (P<0.05)

Pull-off load. The pull-off loads increased linearly with an increase in seating load; all groups were significantly different (Fig. 23) (P<0.05). The pull-off loads were approximately 44% of the seating loads for the test groups.
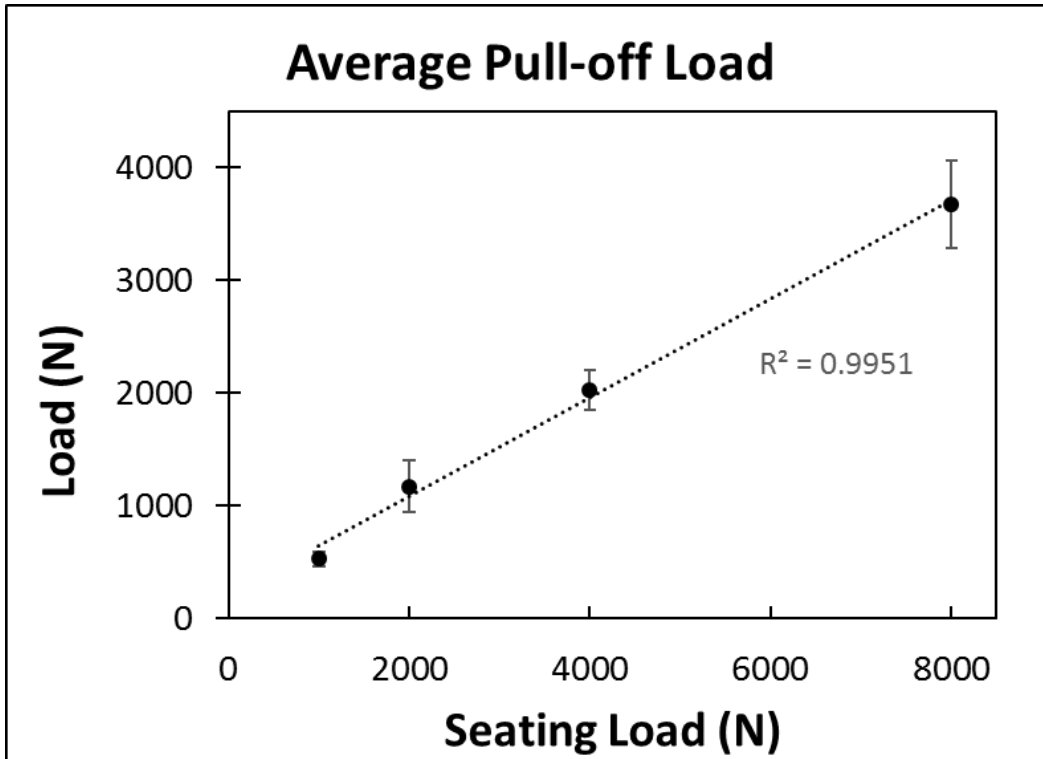
Fig. 23: Average pull-off load for range of loads. Each group was statistically different (P<0.05) The pull-off load was approximately 44% of the seating load.

Load Orientation Analysis.

Displacement of off-axis samples was comprised of both rigid motion as well as elastic motion (associated with the compression and bending of the component in conjunction with such load orientations). A stiffness-correction method removed the elastic motion recorded [59]. All calculations were done using the rigid motion.

Seating displacement. With an increased angle in the seating load orientation, the bending of the neck and elastic motion also increased. Fig. 24, illustrates the trend in elastic bending in the seating load-displacement of the raw data as the seating load orientation increased to 20°. As the off-axis orientation increased, more bending deformation was present in the displacement measurements as the superior side showed elastic-bending displaements that were opposite of the seating direction, while the elastic bending displacements inferiorly were in the same direction as the seating displacements.

49
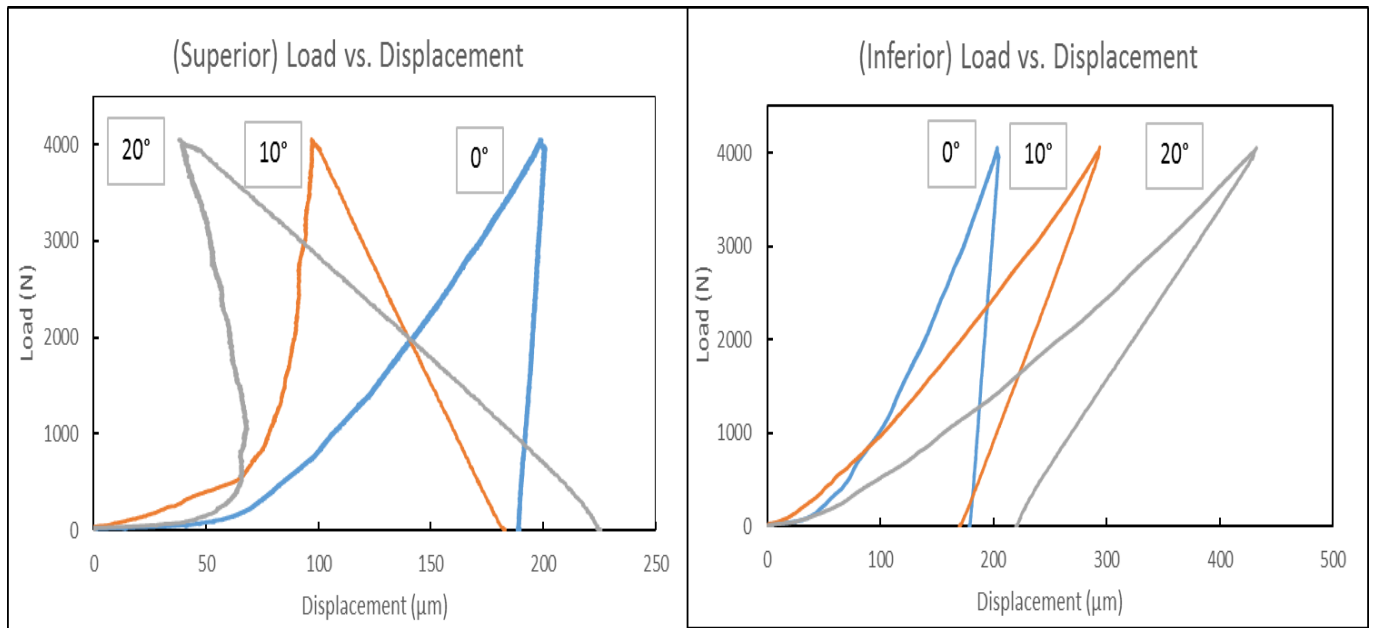
Fig. 24: Load vs. displacement graphs showing the elastic bending nature of off-axis load samples compared to axially loaded samples.

Load Orientation Results.

Seating displacement. The results of testing showed despite the increase in load orientation

there was no statistical difference in average seating displacement between orientation groups,

with an average displacement of 150-190 µm (Fig. 25a).
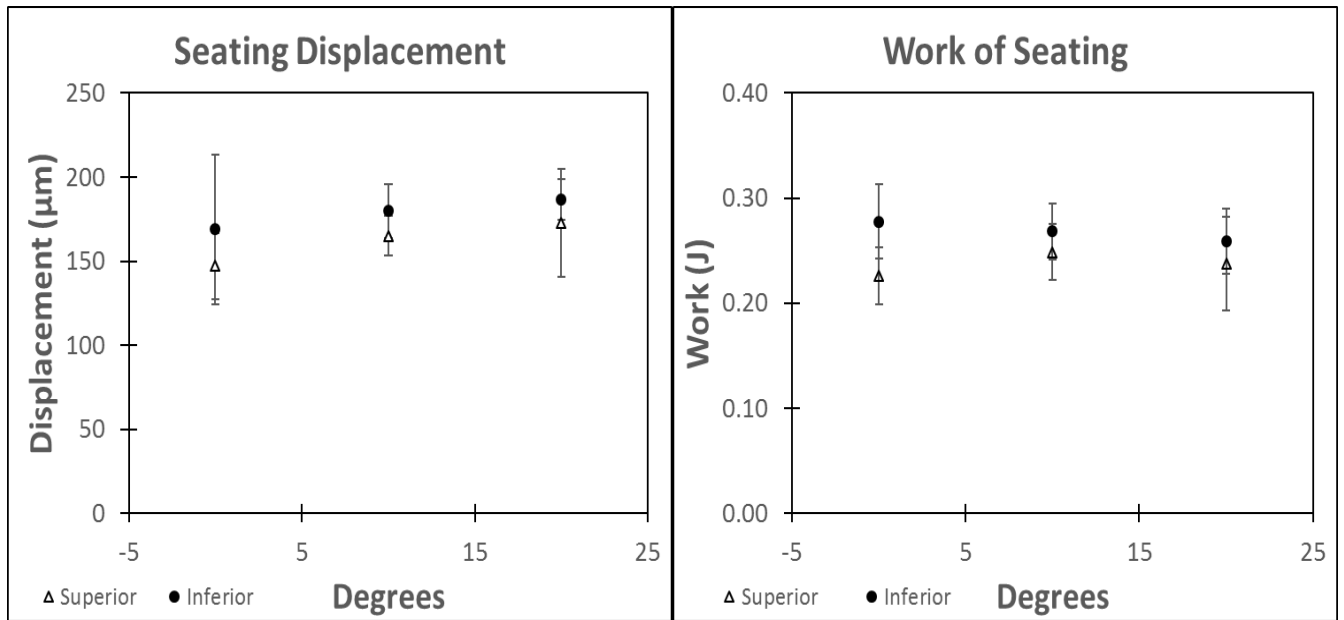
Fig. 25: Average a) seating displacement and b) work of seating per group. All groups were statistically similar.

Work of seating & Pull-off load. There was no statistical difference in work of seating (Fig. 25b) or pull-off load between the orientation groups (Fig. 26).
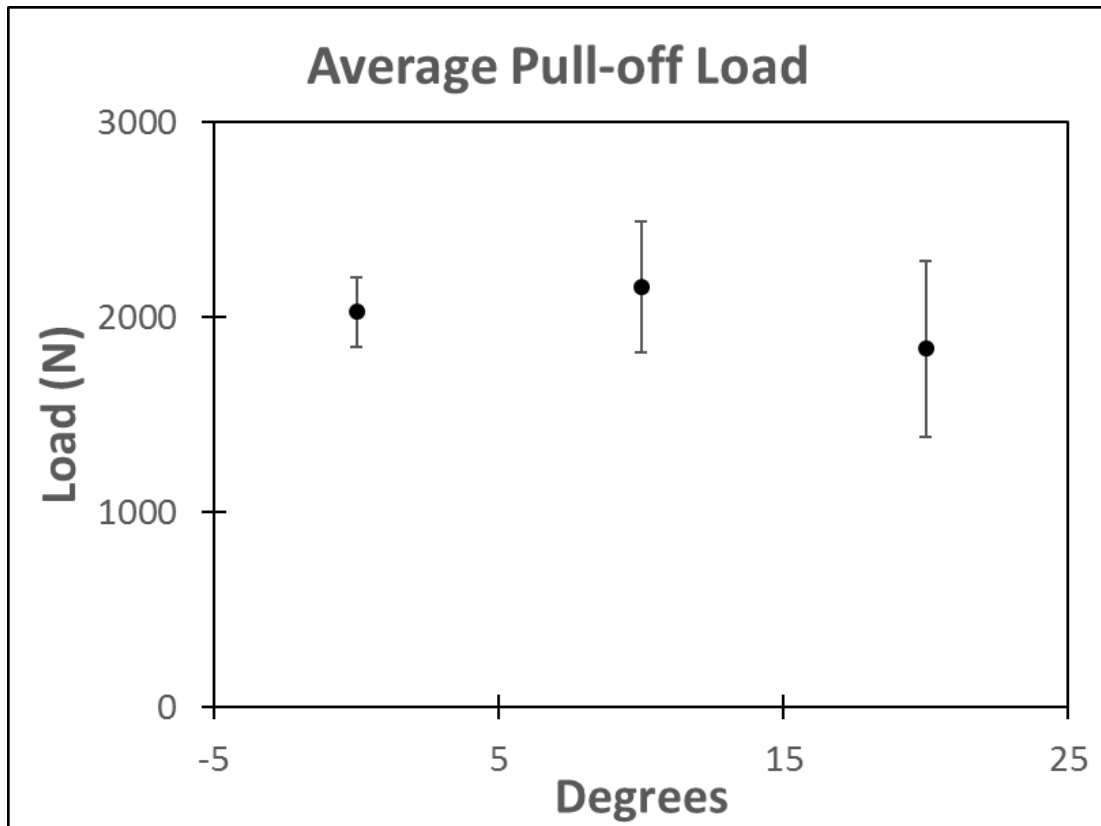
Fig. 26: Average pull-off load of test samples. Groups were not statistically different.

3.1.2 – Taper Contamination Analysis and Results

Data Analysis.

Seating displacement. The seating load-displacement vs. time graph shown in Fig. 27a depicts the relationship between the seating load and relative displacement of the head onto the neck in a dry assembled control sample. As the load increased to the peak load (4000 N) the peak displacement was achieved (approximately 200 μm).

In these studies, seating displacement of the head was defined as the difference between the final displacement point and the initial displacement point. The initial point of contact, where the load begins to increase (and displacement is set to zero), is an arbitrary location on the taper surface that depends on the presence or absence of contamination among other factors. Thus, the

displacement at peak load reflects the distance the head travels on the trunnion to reach its maximum load condition. Examples of these seating load-displacement plots are shown in Fig. 27a, the initial displacement points were normalized at 100 N. The average displacement plot for each contamination group was shifted over to align the plots by the peak load (4000 N). In doing so the unload behavior/compliance of each group could be better understood (Fig. 27b). Fig. 27c displays the average unload of each group. The superior sensor, the portion of the trunnion where the solid contaminants were placed, recorded a similar unload behavior for the dry, wet and liquid fat groups meaning the compliances were similar. The solid fat and bone chip groups exhibit a similar unload while differing from the remaining groups. Note the slope of the unload portion for the solid contaminants was less steep in the superior and more steep in the inferior, while the remaining groups recorded similar behavior. Meaning the introduction of solid contaminants to the specific portion of the taper junction significantly altered the taper compliance behavior.
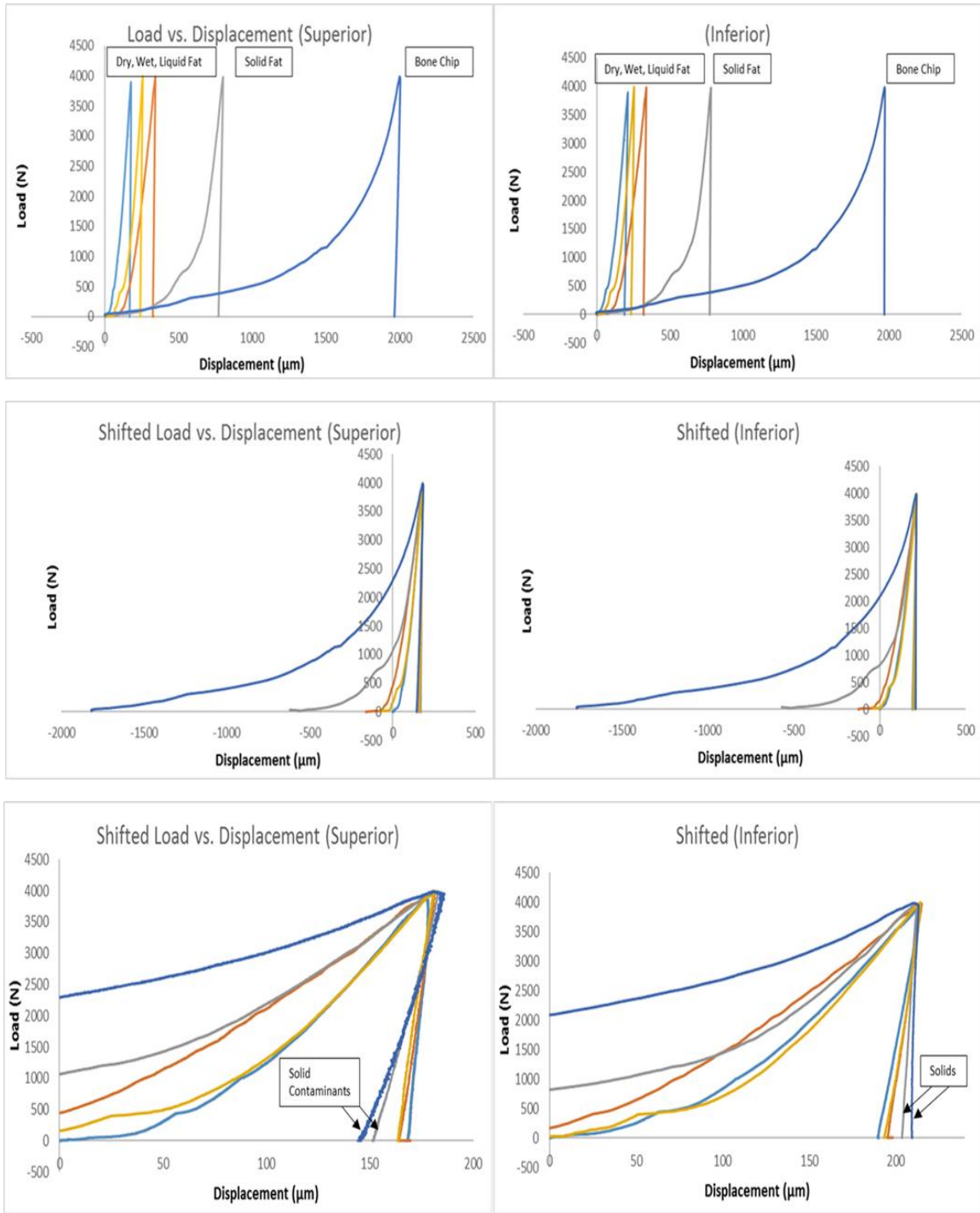
Fig. 27: a) Average seating load-displacement behavior of each test group. b) The graphs in (a) were then shifted to align each group by the peak load. c) The shifted plots in (b) were zoomed in to highlight the unload/compliance behavior of each sample group. Note the solid contaminants displayed a canting behavior with a less steep compliance in the superior compared to the inferior. The remaining groups (dry, wet and liquid fat) were tightly grouped with similar compliance behavior.

54

The solid groups now point toward a less compliant construct than the remaining three test groups. It should also be noted that the liquid fat and solid fat loading curves start out differently, but then become similar at higher loads. This is likely due to the liquefaction of the solid fat at high loads. The wet and dry loading curves appear very similar in these plots.

The compiled data and interesting findings on the effects of seating mechanics are detailed in the following subsections.

Seating displacement. Summarized seating displacement data shows there was a statistically significant difference in the seating displacement for all groups (Fig. 28). The dry group had the lowest displacement ($P<0.05$) while the displacement was greatest in the solid contaminants group (solid lipid and bone chip). The inferior displacement was not different between the dry and wet groups (see Fig. 28).
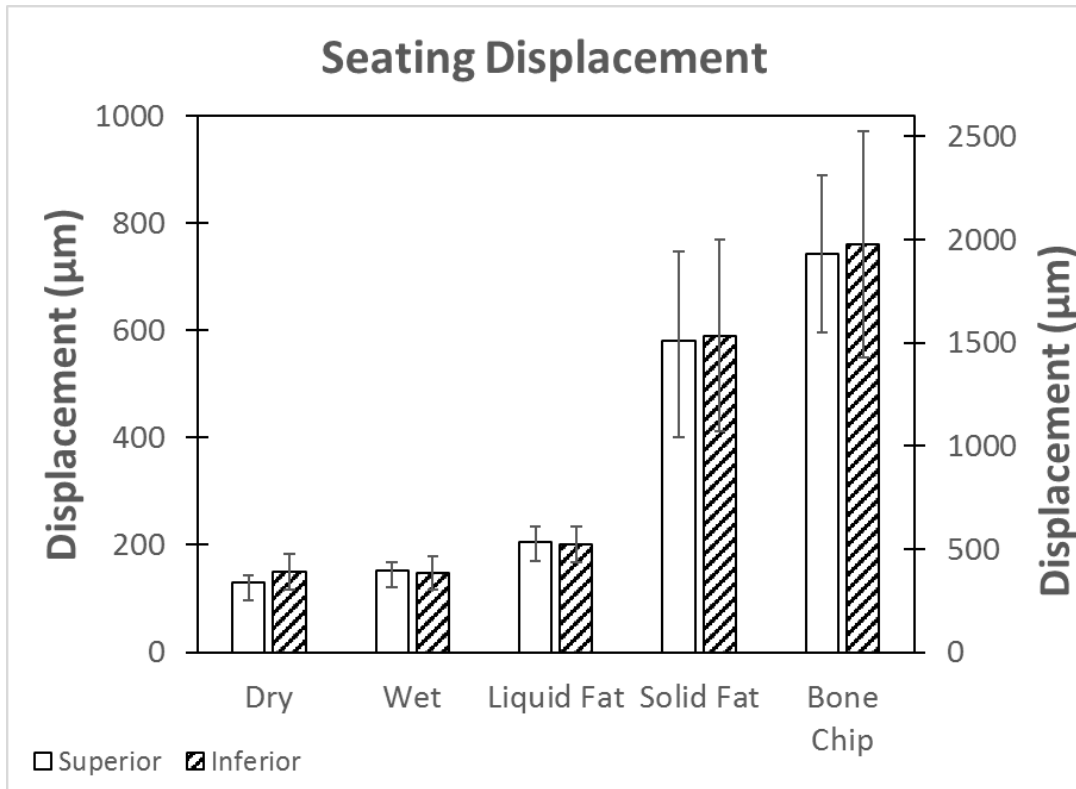
Fig. 28: Average seating displacement per group (n=5). Each group was statistically different with the lowest displacement in the dry group and the greatest in the bone chip group (P<0.05).

Work of Seating. The work of seating (Fig. 29) was highest for the bone chip contamination group, followed by the solid and liquid fat groups (P<0.05). There was no difference between the dry and wet groups. The work to seat a taper with a bone chip was about 4 to 5 times the work to seat a clean and dry taper.
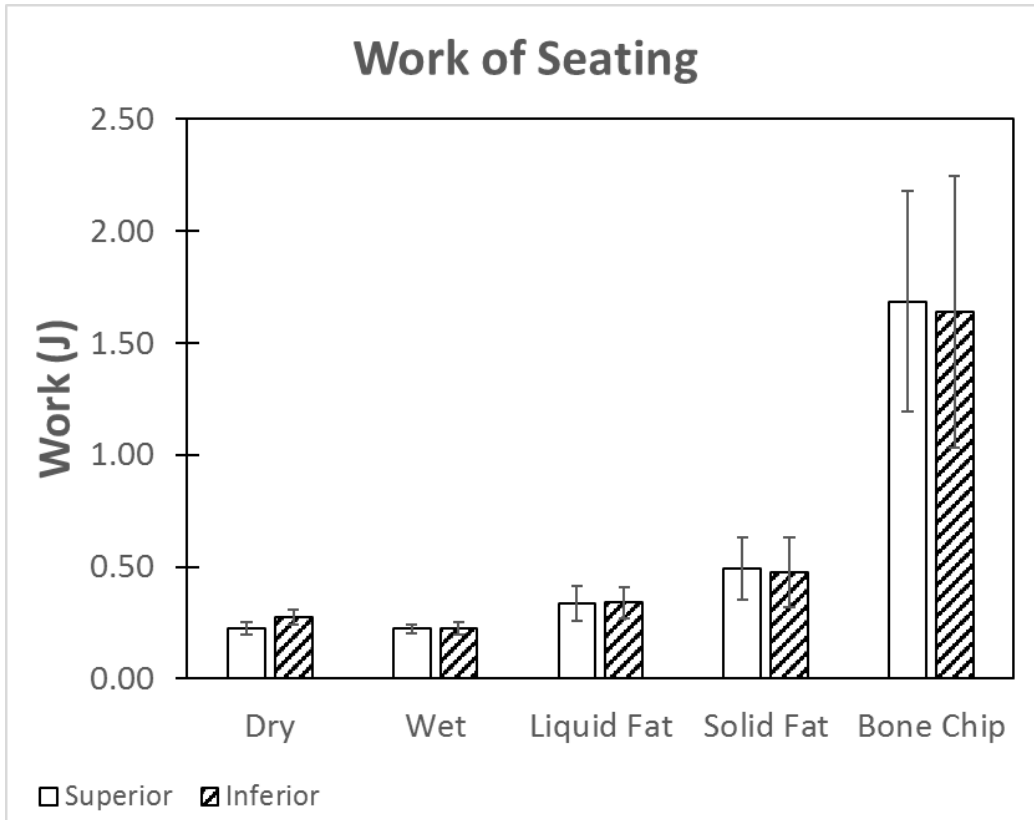
Fig. 29: Average work of seating per group showed the bone chip group had the greatest work of seating (P<0.05), the dry and wet groups recorded the lowest.

Pull-off load. The pull-off load after testing (see Fig. 30) shows the liquid fat and bone chip groups required significantly greater pull-off loads than the other groups (P<0.05). The remaining groups weren't different. For some of the liquid fat tapers, the pull-off load was as great as, or greater than the initial seating load.
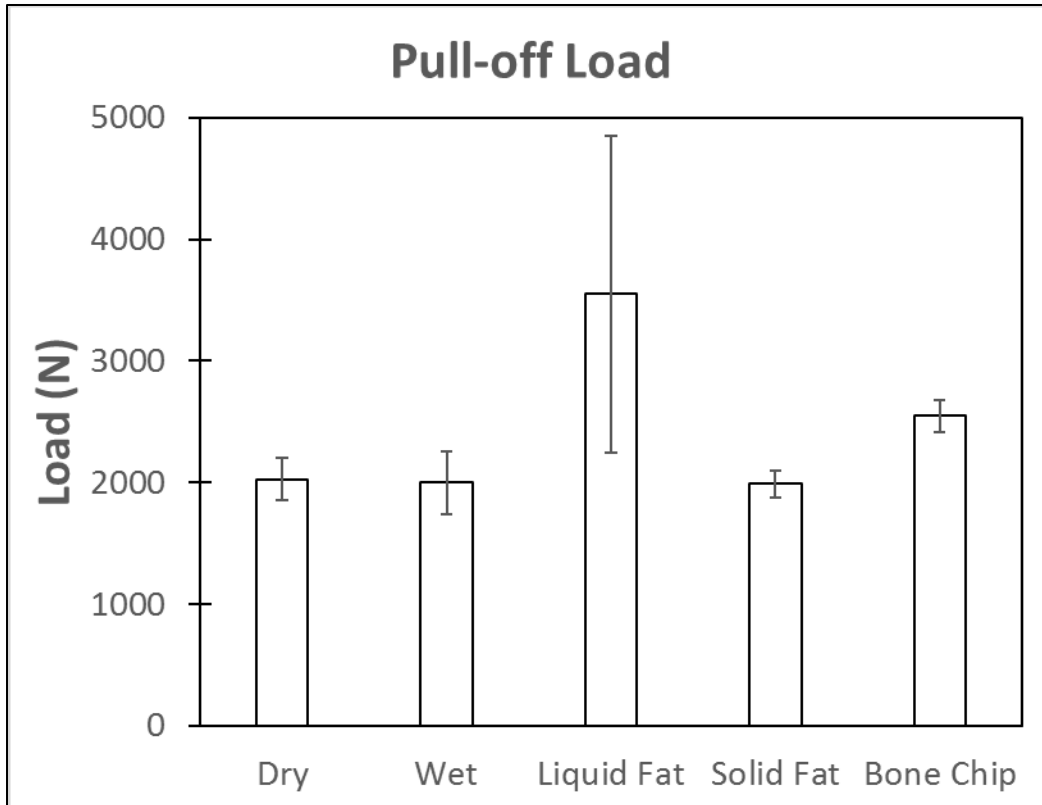
Fig. 30: The liquid fat group recorded a significantly greater average pull-off load than the remaining groups (P<0.05). In select instances the pull-off load of certain samples was a great, or greater than the seating load.

3.2 – Goal 2

ICFC Data Analysis

The analysis procedure for each ICFC sample will be examplified by the following Ti6Al4V/CoCrMo C taper sample. The wetted taper was seated to 2000 N at 35° off-axis and measured displacement using the two DVRT setup fixed to the stem targetting the head. **Seating and work of seating.** During loading, significant elastic bending displacements were captured and were presented along with the rigid motion in the raw data.
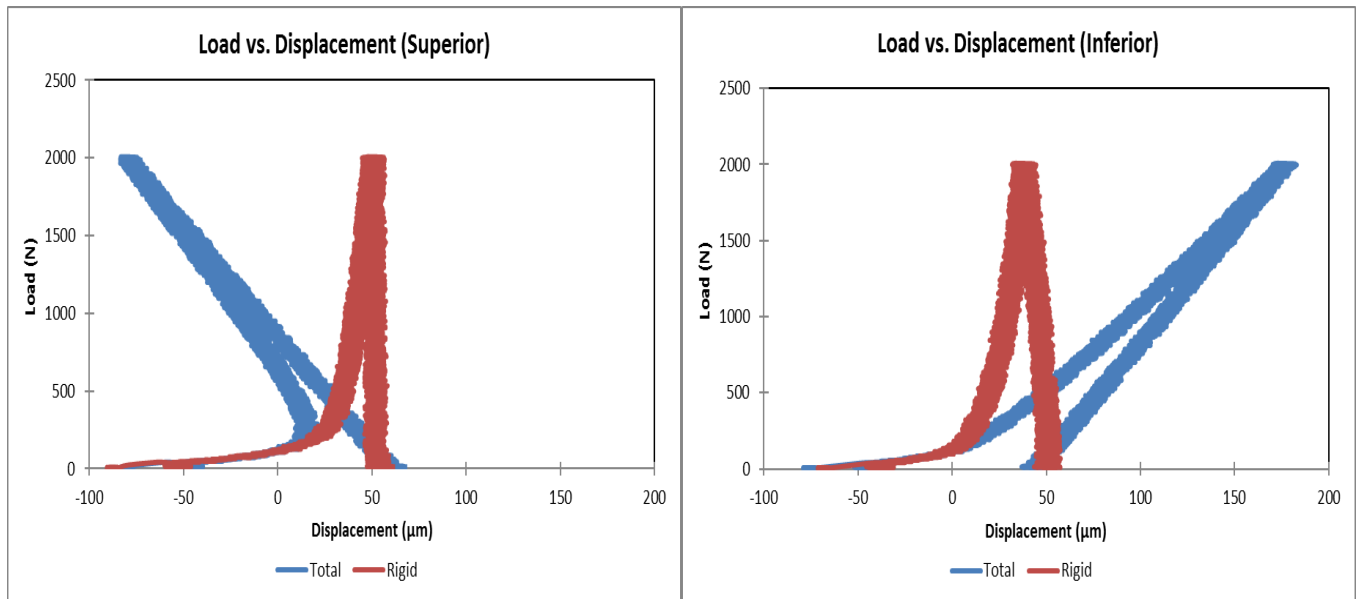
Fig. 31: Load-displacement plot highlighting total (blue) and rigid (red) displacement for both sensors (Ti64/CoCr C taper).

It can be seen (Fig. 31) that during loading, the total sensor-target displacement shows both elastic bending-like motion and rigid body seating. The blue plots (Fig. 34) present the total motion while the red plots show the rigid-only motion obtained by subtracting the load divided by the stiffness data from the total motion. Upon unloading after reaching 2000 N the head was seated approximately 50-55 µm onto the neck for each sensor. The displacement data was normalized at 100 N. Note removal of the elastic motion did not alter the final displacement point.

Work of seating was calculated using the area under the curve equation from the normalized load and displacement to unload of the rigid displacement data. It can be inferred by the total motion plots in Fig. 31 and the work of seating calculation that the elastic motion would greatly affect the work of seating calculation.

Static calibration. After the incremental cyclic tests, each individual test sample/sensor construct was calibrated with a series of static loads and then plotted. The slope of the linear

regression lines for each sensor were then input into the analysis program for the incremental

cyclic tests to determine true elastic-based motions (Fig. 32).
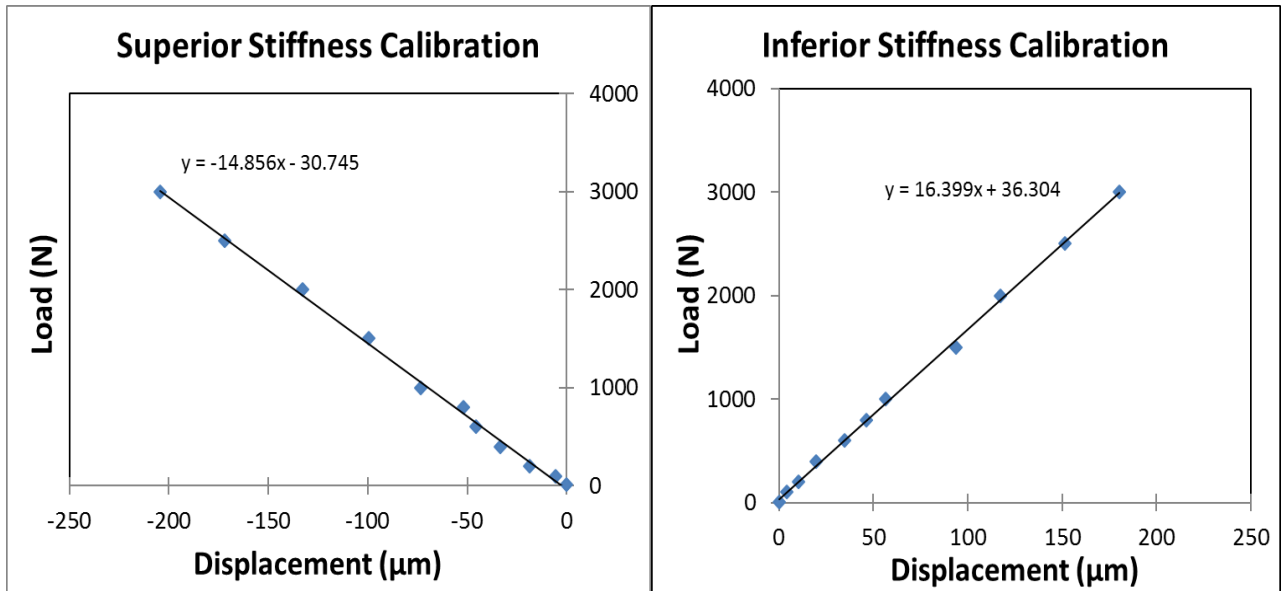
Fig. 32: Stiffness calibration (load vs. displacement) plot with linear regression used to determine the slope/stiffness of the construct (Ti64/CoCr C taper).

The stiffness of the construct is dependent upon parameters such as material (modulus),

coefficient of friction and surface roughness. Note the negative slope in the superior dis due to

the orientation of the sensors. With a load applied the sensor and target move opposite one

another leading to a more negative displacement due to bending.

Incremental cyclic fretting corrosion. There was a large amount of unique and specific

information that was obtained from the incremental cyclic test. A two second snapshot from the

LabView file was taken of the obtained data showing the sensor displacement, load and current

(Fig. 33).
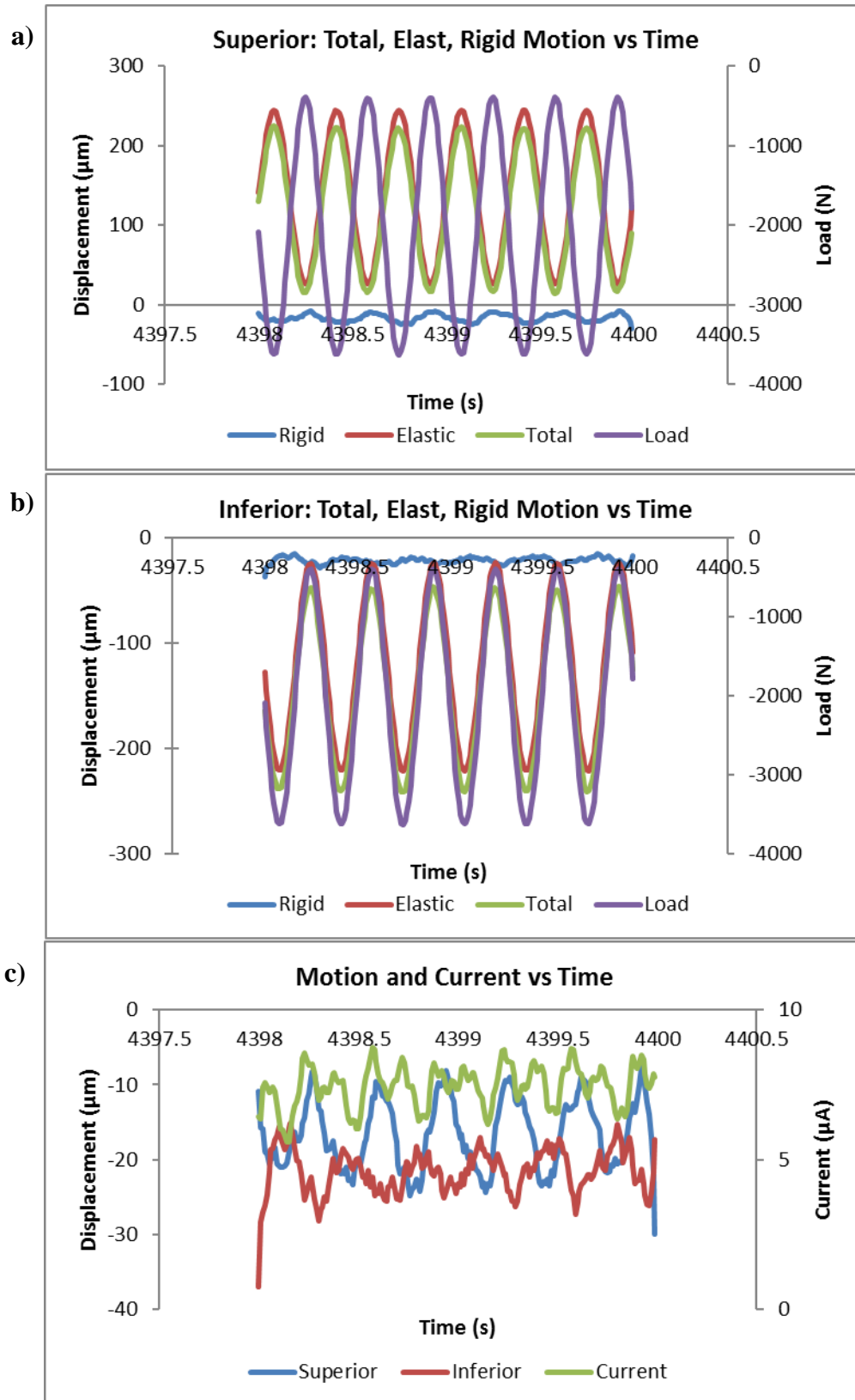
Fig. 33: Two second snapshot captured from cyclic testing (3600 N, Ti64/CoCr C taper). a & b) Show the total, elastic and rigid motion and load vs. time for the superior and inferior sensor. The load and rigid

displacement show an in-phase behavior. c) Shows the rigid motion of both sensors and current vs. time. The peak currents are achieved as the peak displacements are achieved. The current displays a biphasic behavior.

Fig. 33a & b show the total (green), elastic (red) and rigid (blue) motion and load (purple) vs. time for the superior and inferior sensors. Fig. 33c plots the current (green) and rigid motion for both sensors (superior – blue, inferior – red) vs. time. The plot shows the cyclic nature of all three components in-phase with one another meaning as the fretting motions arise the fretting currents also persist. The current is approximately 7 μA.

An example of the Wavematrix acquired data is plotted in Fig. 34, the average current vs. the load depicts the behavior of the current as a load was applied to the sample. The data was used to determine the onset load, the cyclic load in which the current deviates from the baseline, and the average current at 4000 N. Both parameters were used to assess the taper performance between the sample groups within a specific study.
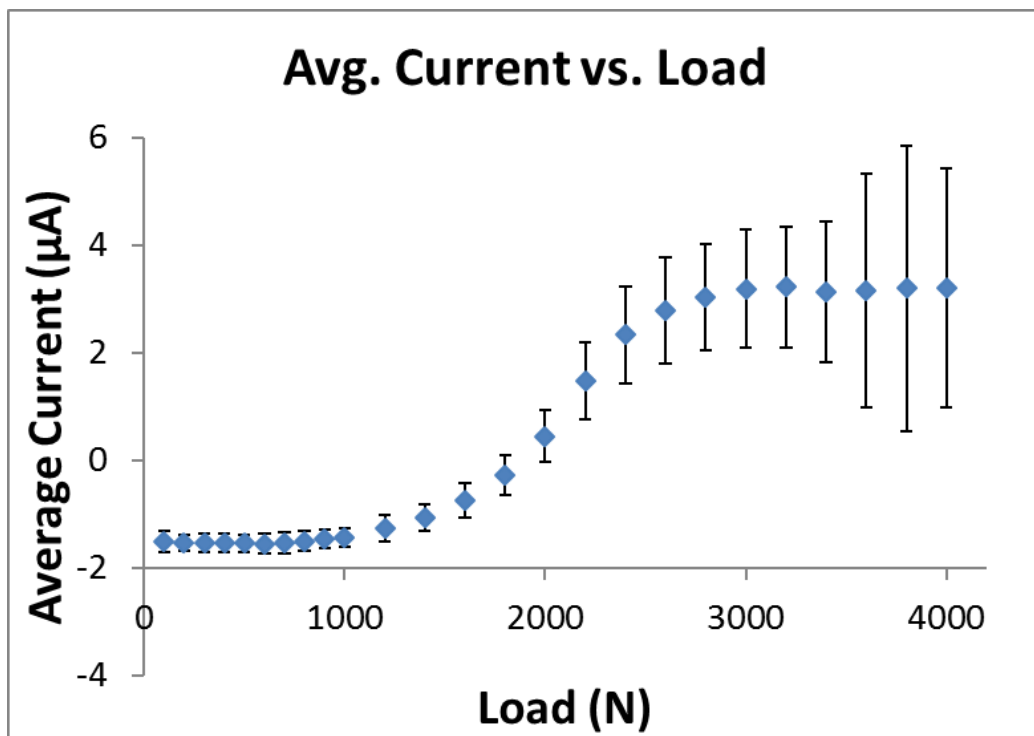
Fig. 34: Average current vs. load (Ti64/CoCr C taper). Error bars represent the root mean square of the current amplitude about the mean. The onset load is at 1200 N with an average current of approximately 3.5 μA at 4000 N.

Fretting motions. Micromotion recorded during loading was comprised of both elastic and rigid body motion. By calculating the stiffness then dividing it into the load one can calculate the instantaneous elastic-based displacements. The elastic motion is then subtracted from the total measured motion, the remaining motion will not be associated with elastic deformation and thus is the rigid body motion between sensor and target (Fig. 35).
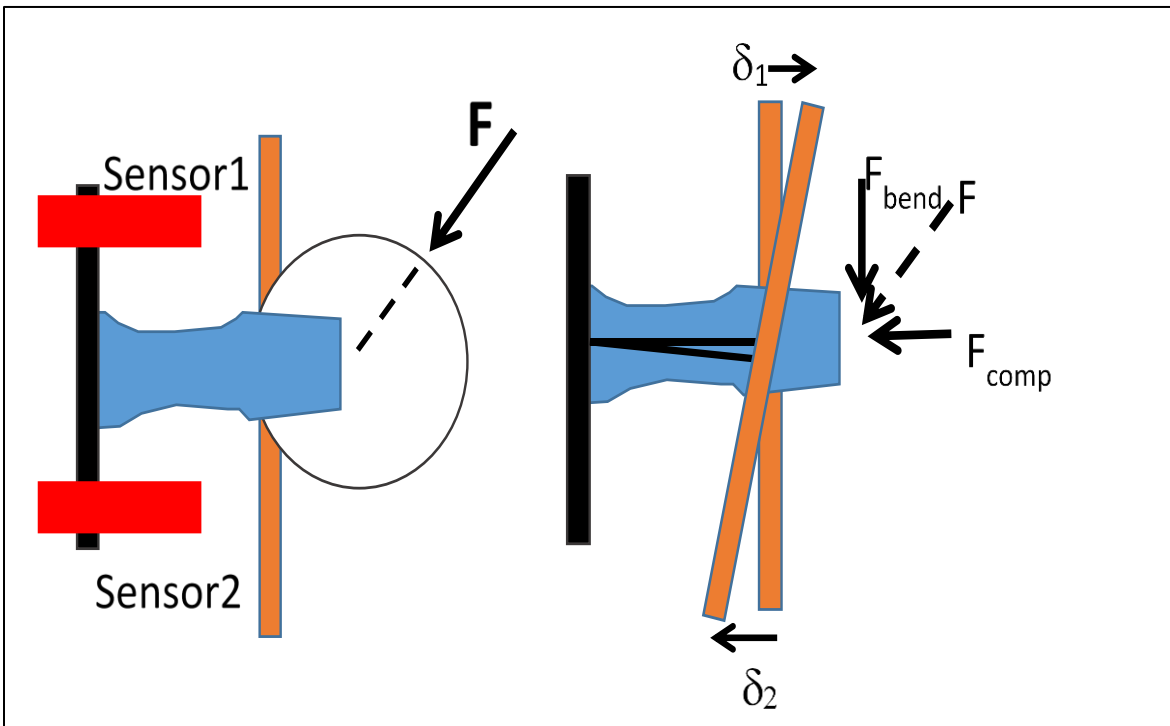
Fig. 35: Displacement schematic based on load orientation of 35° from the neck axis.

The following equation was used to determine the rigid motion,

$$\delta_{total} = \delta_{rigid} + \delta_{elastic} \text{ , and } \delta_{Rigid} = \delta_{Total} - \frac{F}{k_{elastic}} \text{ (Eqn. 12 \& 13)}$$

where F is the instantaneous load and $k_{elastic}$ is the elastic stiffness determined for each sensor. This approach, therefore, allows one to determine both the rigid body subsidence (i.e., the settling of the head on the neck over time), as well as the micromotion (the peak-to-peak cyclic

rigid-body motion in each cycle of loading). Negative subsidence implies further seating of the head onto the neck.

Analysis of micromotion and subsidence. The raw ICFC data file contained over 500,000 data points which were used to assess micromotion, subsidence and current vs. time and/or load.
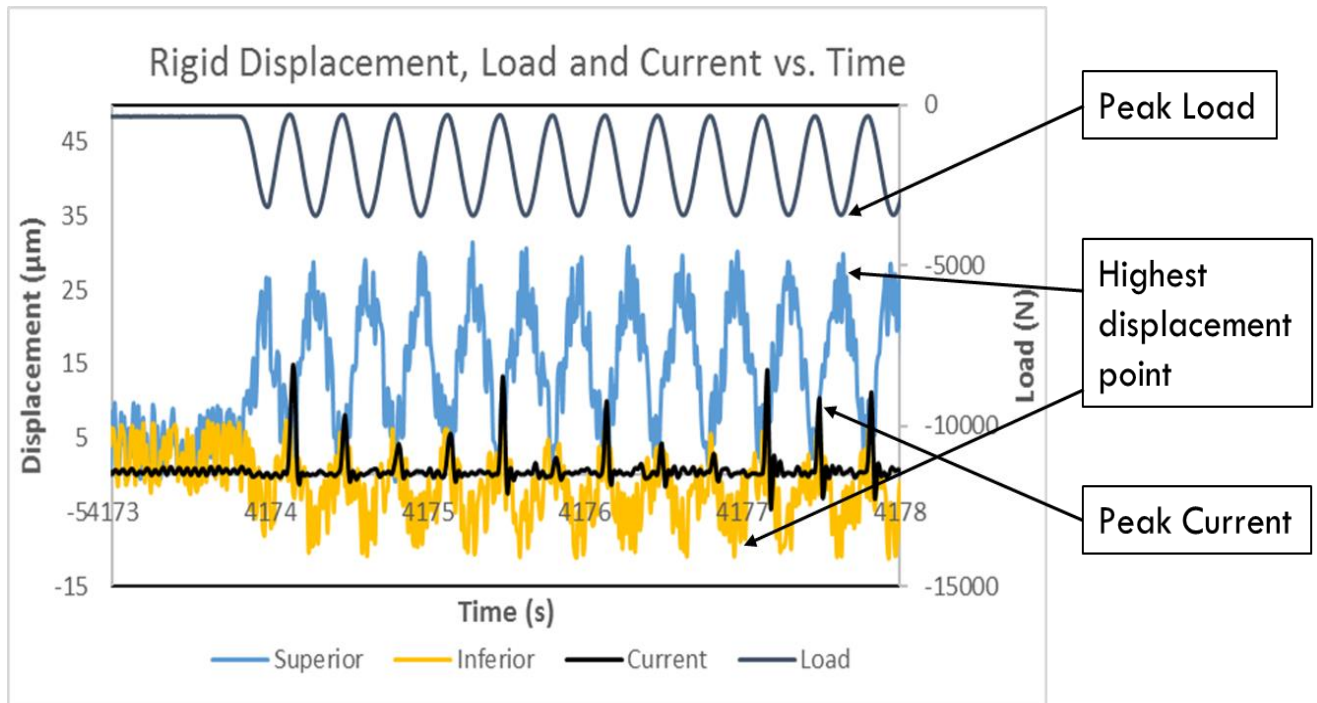
Fig. 36: Five second snap shot of raw ICFC data (Ti64/CoCr C taper).

The five second snap shot in Fig. 36 reiterates the cyclic behavior of the load, displacement (both superior and inferior sensors) and current vs. time, showing the in-phase relationship of the four components. The graph also shows without the presence of a cyclic load there is no fretting response in either the motions or current.
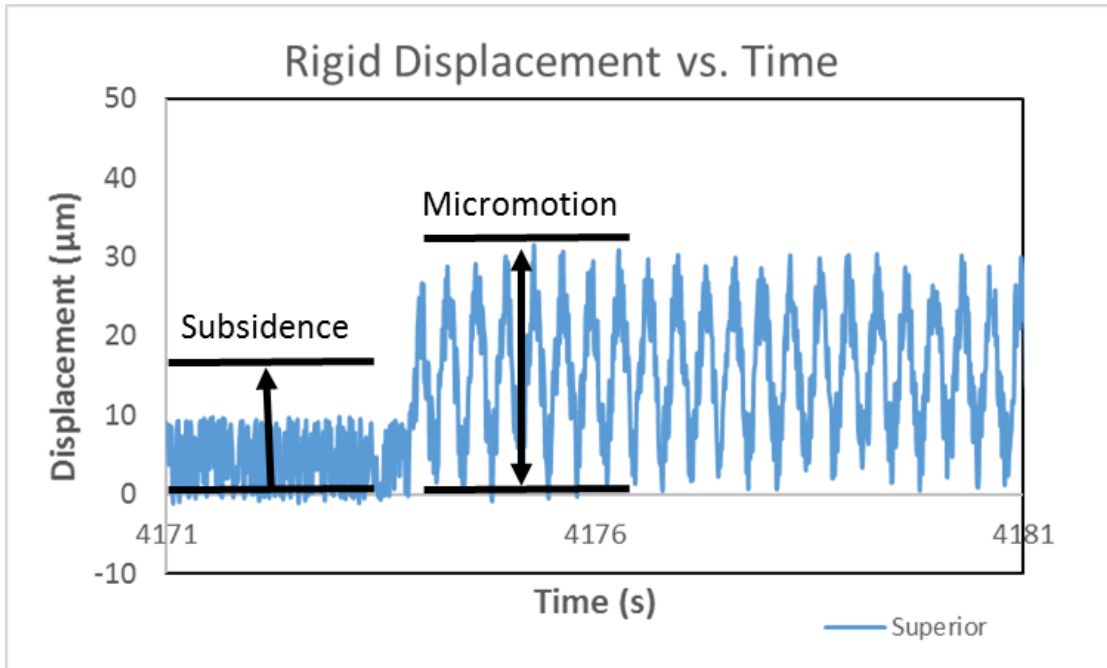
Fig. 37: Ten second snap shot highlighting micromotion and subsidence calculation of rigid ICFC data in superior sensor. Micromotion was defined as the average peak to valley amplitude of motion during a single cyclic load. Subsidence was permanent average movement away from the test starting position.

The micromotions were the average peak to peak amplitudes of motion during each cyclic load. The subsidence was calculated by taking the difference between the average displacements between cyclic loads over the course of cyclic testing (i.e. from one cyclic load to the next) (Fig. 37). Micromotion is not particularly sensitive to subsidence behavior due to the fact that is calculated by local peak to peak measurements.
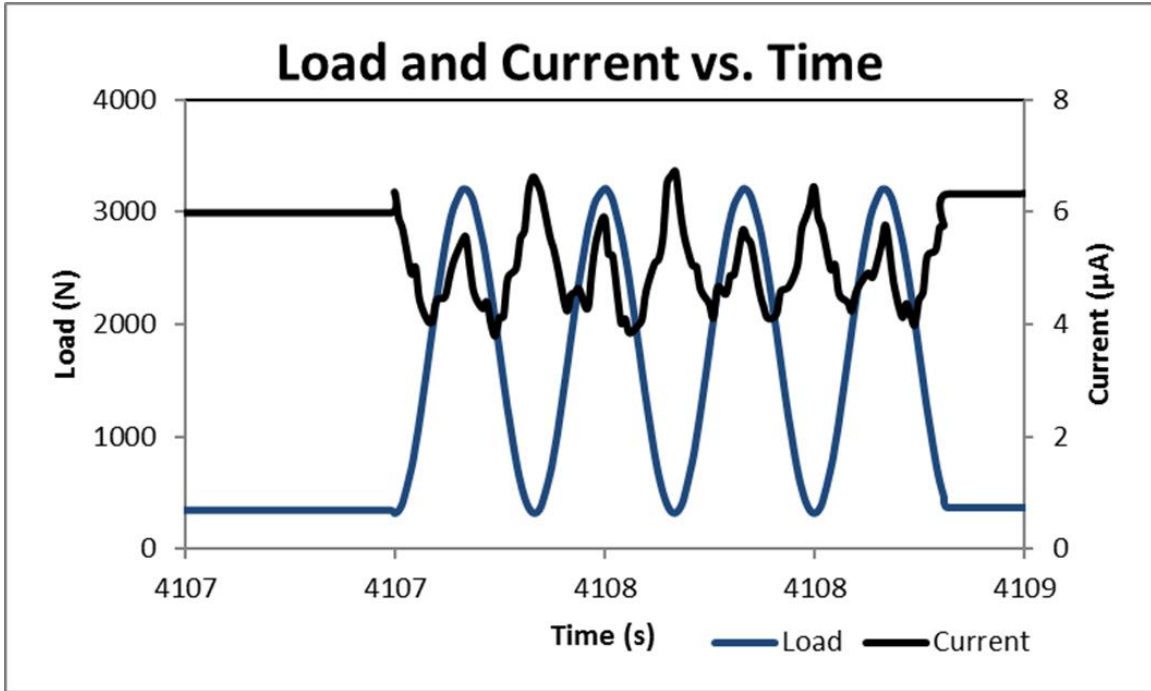
Fig. 38: The Load and Current vs. Time graph over two second interval. Note biphasic behavior in current as load is cycled.

The load and current vs. time graph (Fig. 38) shows the biphasic behavior of the sample as the cyclic load is applied. The data was used to determine the current vs. time shown in Fig. 39.
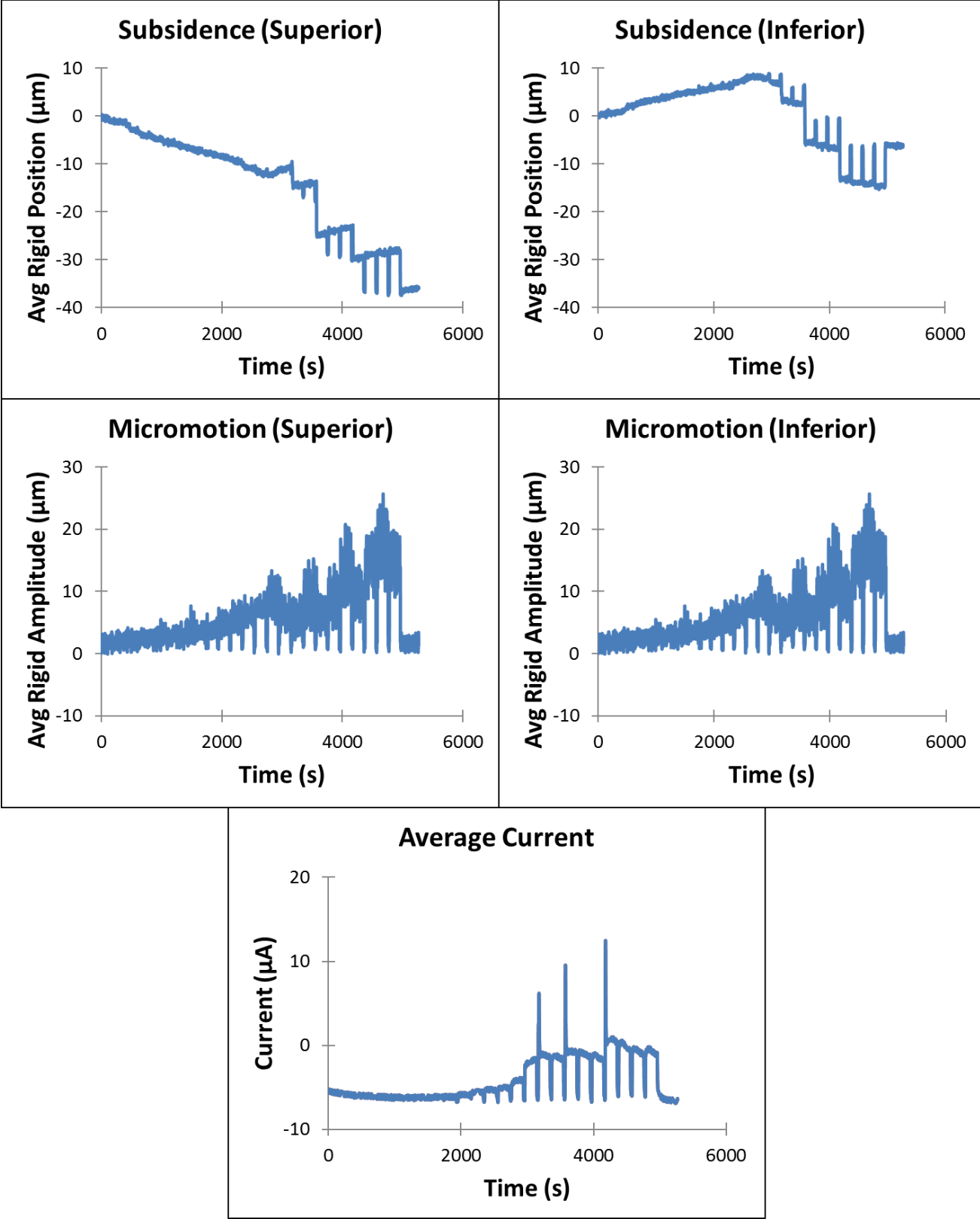
Fig. 39: Average rigid subsidence and micromotion vs. time for the superior and inferior sensors. b)
Current vs. time.

67

Further refinement of the raw data, shown in Fig. 39, shows the average rigid subsidence and micromotion vs. time over two second intervals throughout the test. Note the spikes seen in these graphs are the measured sensor positions during a pause in the cyclic load before commencing the next load cycle. The sudden step-wise jumps in the subsidence graphs indicate that at those time points the head began to subside due to cyclic loading. In this particular case these sudden jumps then correspond to jumps in the micromotion data for both sensors at the 3000, 3500, 4000 and 5000 s time marks. These jumps in the fretting motion can then be correlated to jumps in the fretting current vs. time. Thus, providing further evidence to support the relationship between fretting motions and fretting corrosion. The graphs were used to determine test assessment parameters such as the average total subsidence (final rigid position – initial) and micromotion at 4000 N per sample.

The compiled ICFC results per each study will reviewed in the subsections below.

3.2.1 – Load Magnitude ICFC

Seating. Seating load-displacement showed a linear increase in displacement with an increase in load. Displacements for the 4000 and 8000 N group were statistically greater than the 1000 and 2000 N ($P<0.05$), there was no difference between the 1000 and 2000 N groups (Fig. 40). The sample design as well as the sensor fixtures used in this study, detailed in Chapter 4.0.2, differed from those used in Section 3.1.1, which may be the reason for the lower seating displacement values reported.
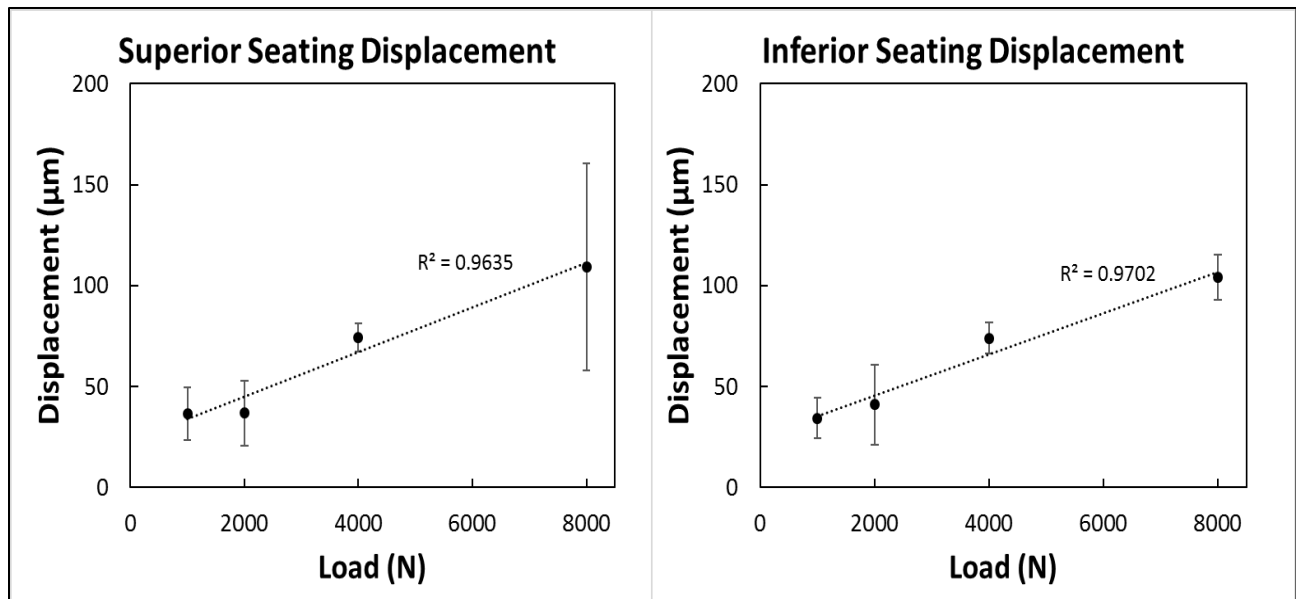
Fig. 40: Average seating displacement plots. The 8000 N group followed by the 4000 N recorded the greatest seating displacements compared to the remaining groups (P<0.05).

Work of seating increased parabolically with the increase in seating load; all groups were significantly different (Fig. 41) (P<0.05).
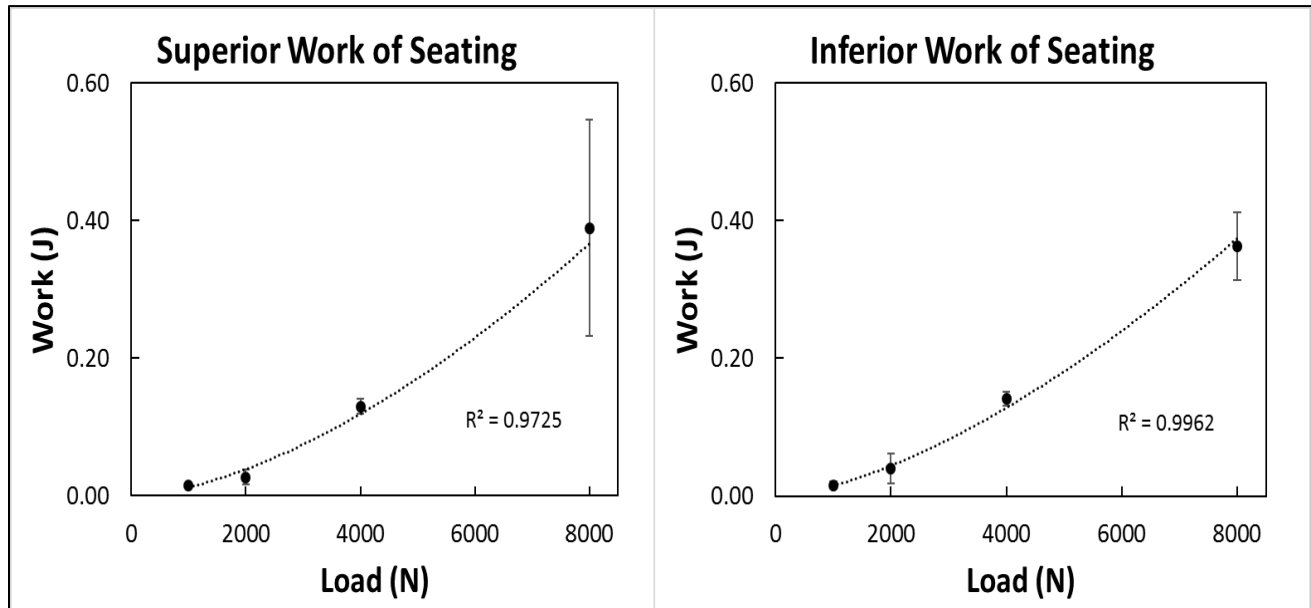
Fig. 41: Average work of seating plots. Each group was statically different from one another (P<0.05).

Cyclic testing.

All groups experienced micromotion and subsidence during cyclic loading. Negative subsidence indicated a further seating of the head onto the neck. Subsidence in the 1000 N group shows both the superior and inferior sensors indicated that as the cyclic load increased the head began to seat further on to the trunnion. However, due to the off-axis nature of the cyclic load, the head pivoted and rotated while seating causing uneven seating displacement between the two sensors. The 2000 N group shows similar behavior but the superior sensor, on average, had a positive motion while the inferior sensor exhibited further seating motion. The 4000 and 8000 N groups showed less overall subsidence, but there was still positive motion superiorly at 4000 N and little negative motion observed. The motion was less than 5 μm. Both 4000 N and 8000 N samples show statistically less inferior subsidence during testing than the 1000 N group (Fig. 42) ($P<0.05$).
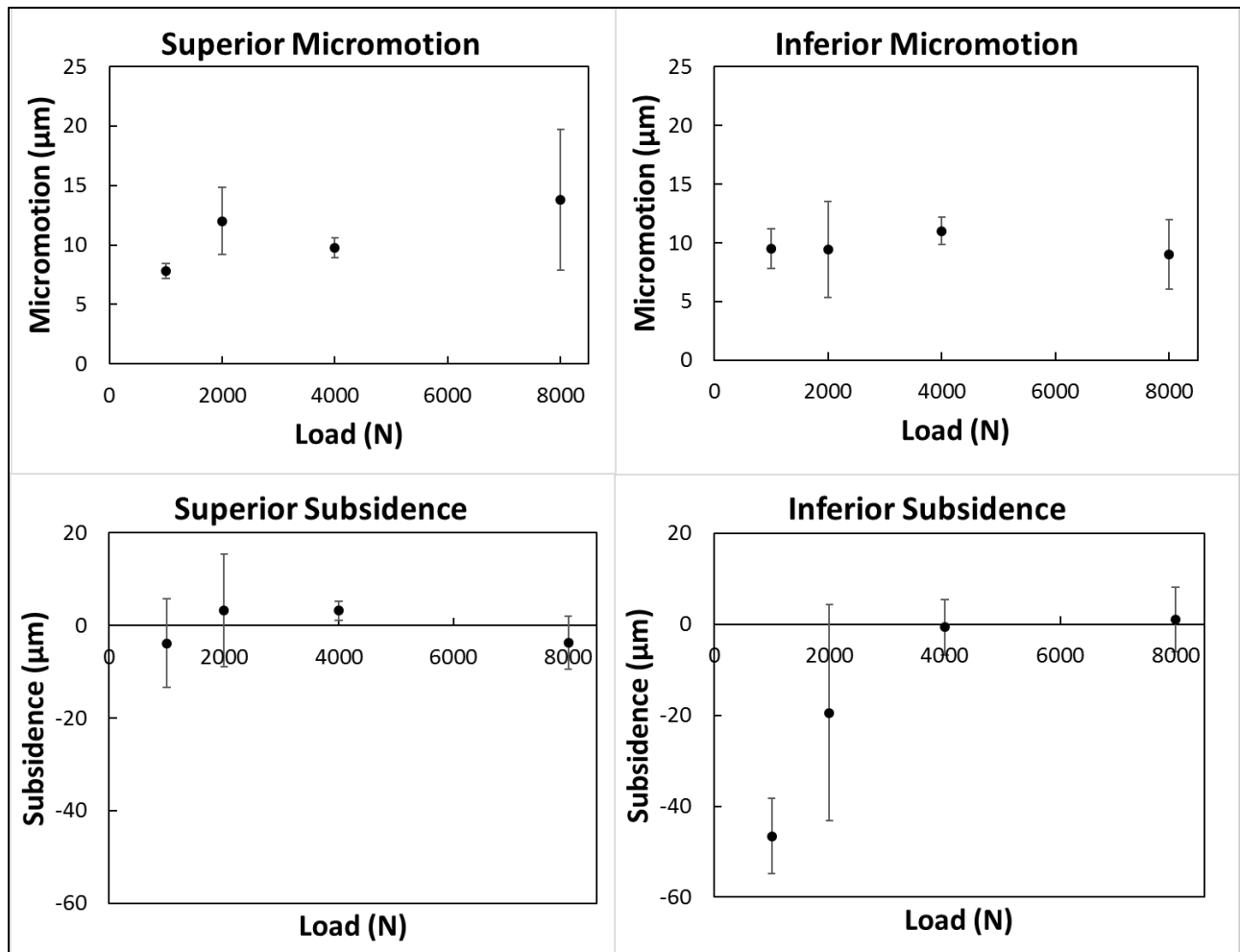
Fig. 42: Average micromotion and subsidence for the superior and inferior sensors. There was no difference in micromotion between the assembly load groups. However, the inferior sensor in the 1000 N group recorded more negative subsidence ($P<0.05$), the remaining groups were not different. The 4000 and 8000 N groups experienced little to no subsidence.

The onset load data, showed the 1000 N group required a statically lower cyclic load to initiate fretting corrosion. The remaining groups were not different (Fig. 43). The values indicate the initial taper stability of the 1000 N group was lower than the remaining groups allowing fretting corrosion to at lower cyclic loads. Importantly, for the 2000 N and above groups the onset load remained approximately constant at about 1200 N regardless of the seating loads applied. Importantly, this indicates that the onset cyclic loads for fretting corrosion cannot be further reduced with greater seating loads.

71
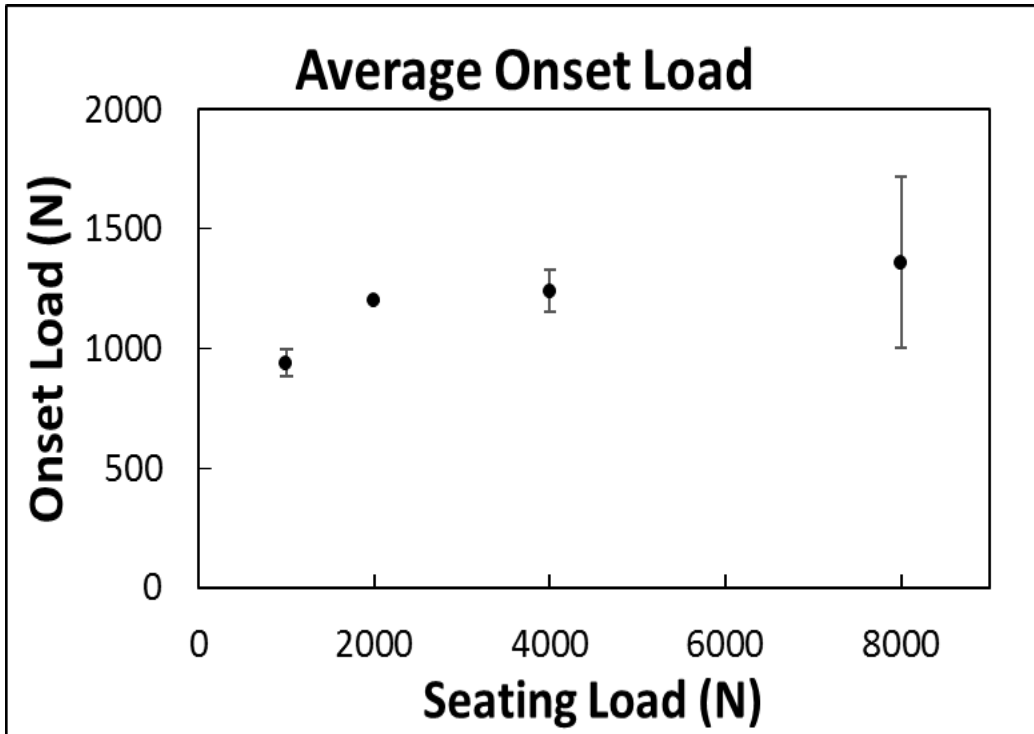
Fig. 43: Average current onset load. The 1000 N group was statistically lower than the other groups (P<0.05), the remaining groups were not different.

At the 4000 N cyclic load level the current was recorded in order to assess the total fretting corrosion due to cyclic motion. With an increase in seating load magnitude the current at 4000 N had a parabolic decrease, the 4000 and 8000 N groups had the lowest current values (Fig. 44) (P<0.05). Again, it is important to note that the fretting currents while reduced, were not eliminated even up to 8000 N seating load.
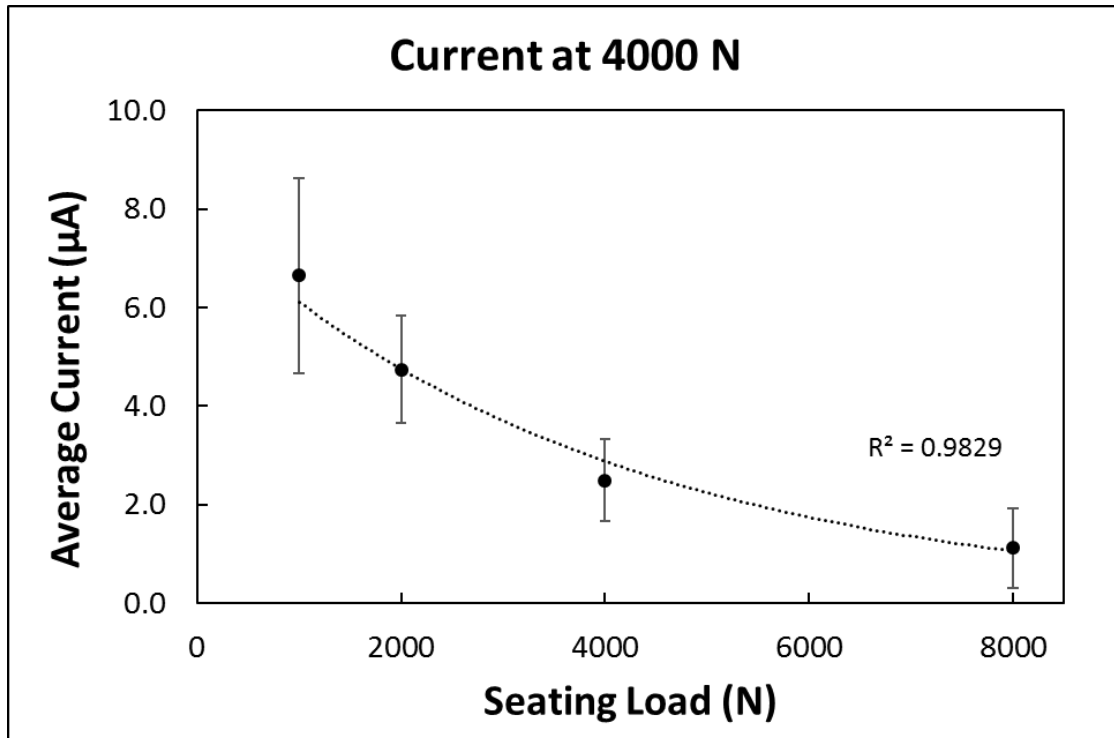
Fig. 44: Average current at 4000 N. The 4000 and 8000 N group were significantly lower than the other groups (P<0.05).

Post-test pull-off testing. Post cyclic testing, each sample was subjected to tensile loads. The reported average loads increased with an increase in seating load magnitude. Pull-off loads were statistically higher in the 4000 and 8000 N groups when compared to the 1000 N and 2000 N groups (Fig. 45) (P<0.05). It is interesting to note that the pull-off loads for the 1000 N and 2000 N assembly load groups were greater than those obtained from the immediate pull-off test done in Section 2.1. The cyclic fretting corrosion loading to 4000 N cyclic load increased the pull-off loads for these lower-seated cases, while for the 4000 N and 8000 N loads, there was little effect of cyclic loading on the pull-off loads measured.
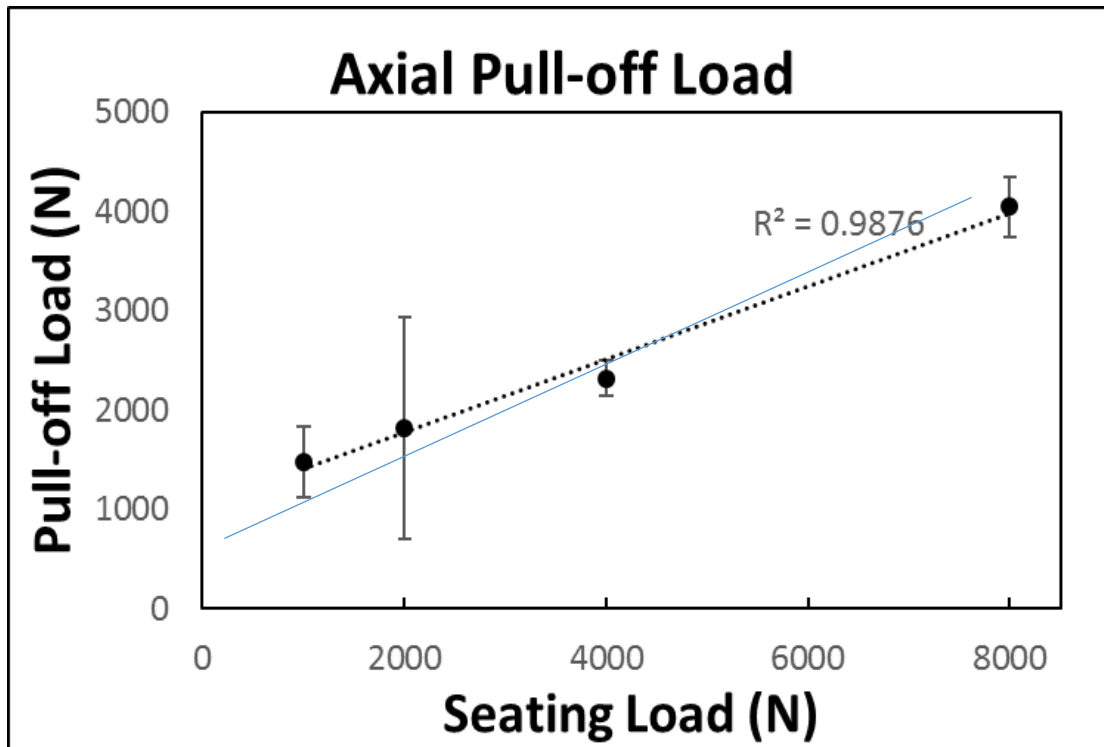
Fig. 45: Tensile pull-off loads per group. The 4000 and 8000 N groups recorded greater pull-off loads compared to the remaining groups (P<0.05). However, the 1000 and 2000 N groups recorded greater or equal pull-off load values compared to the initial assembly load.

3.2.2 – Load Orientation ICFC

The data reported is of the rigid body motion only.

Seating. The seating schematic in Fig. 46a-c illustrates the displacement behavior for each orientation group during seating. The seating load-displacement graph shows the 20° group had a statistically higher displacement on the inferior taper portion than the 0° group. No difference was calculated on the superior portion (Fig. 46d).
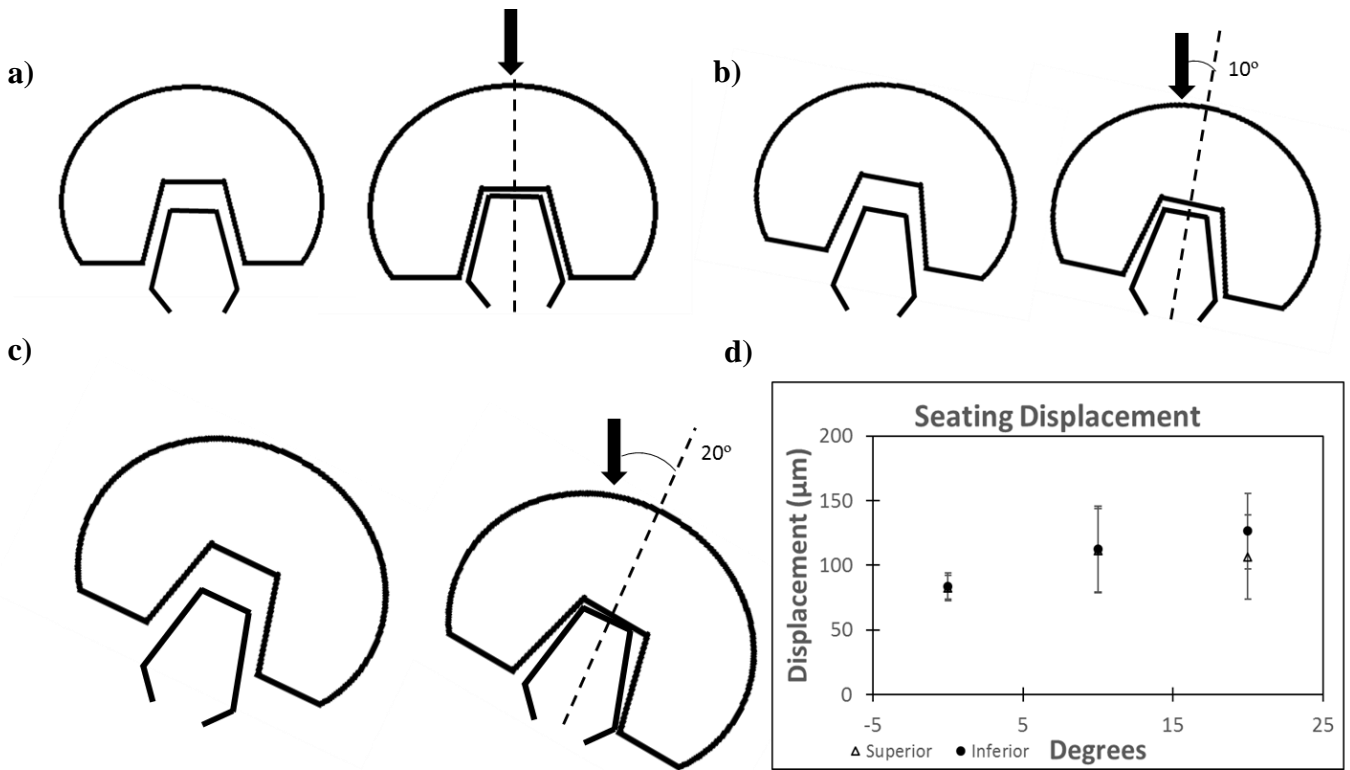
Fig. 46: Seating schematic for orientation groups (a) 0°, (b) 10° & (c) 20°. (d) Average Seating displacement graph for each group shows there was no statistical difference in the superior sensor displacements between the groups.

There was no difference in the work of seating between groups (Fig. 47). The data is similar to the previous study presented in Section 2.1 [65].
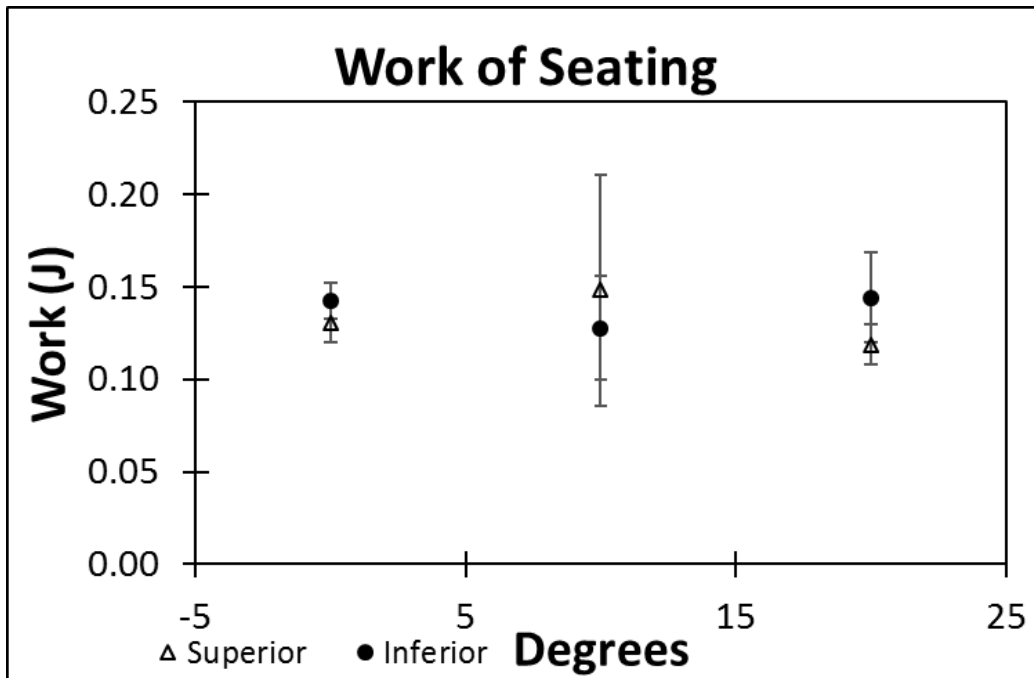
Fig. 47: Average work of seating per group (n=5). The groups were not statistically different (P>0.05).

Cyclic testing. Throughout cyclic testing up to 4000 N, each group experienced some level of micromotion and subsidence. For reference, negative subsidence indicates a further seating of the head after testing.

The 0° orientation group recorded higher micromotion values than the remaining off-axis groups (Fig. 48a). But despite the increase in micromotion there was no difference in subsidence between groups (Fig. 48b). The reported average subsidence values ranged from 3 to -3 µm. The data suggests an increase in seating load orientation reduced the inclination for fretting motions to arise at the junction.
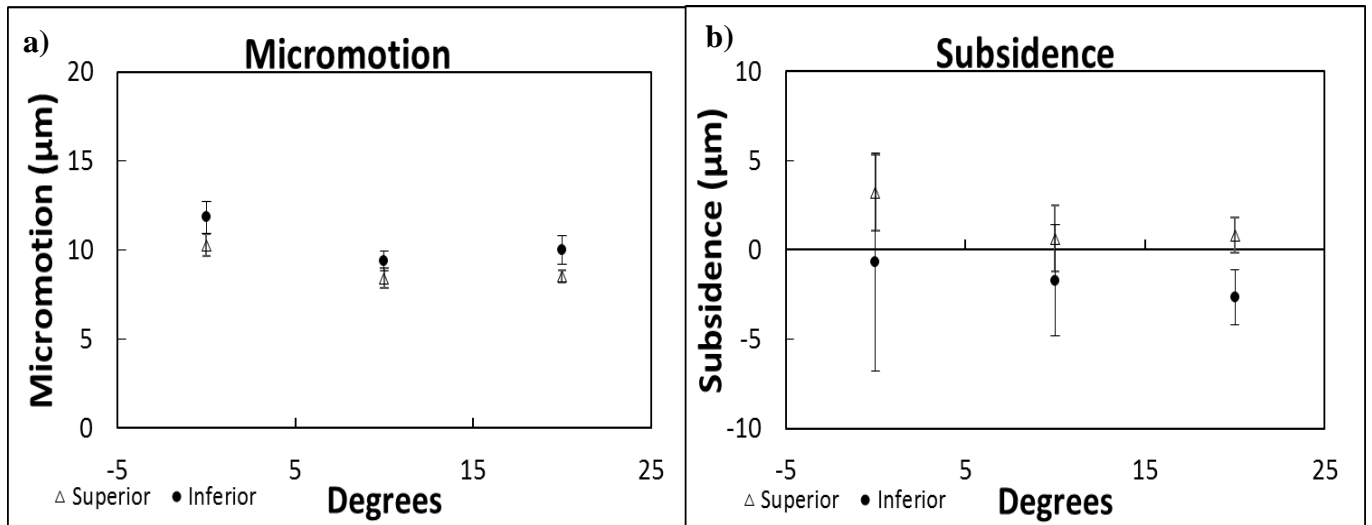
Fig. 48: Average (a) micromotion and (b) subsidence per group. The micromotion data showed the axially loaded group had higher micromotion than the off-axis groups (P<0.05), there was no difference in subsidence.

The electrochemical data collected during testing shows the 20° orientation group had a lower current onset load when compared to the remaining two orientation groups (P<0.05); however, there was no difference between the 0° and 10° group (Fig. 49a).
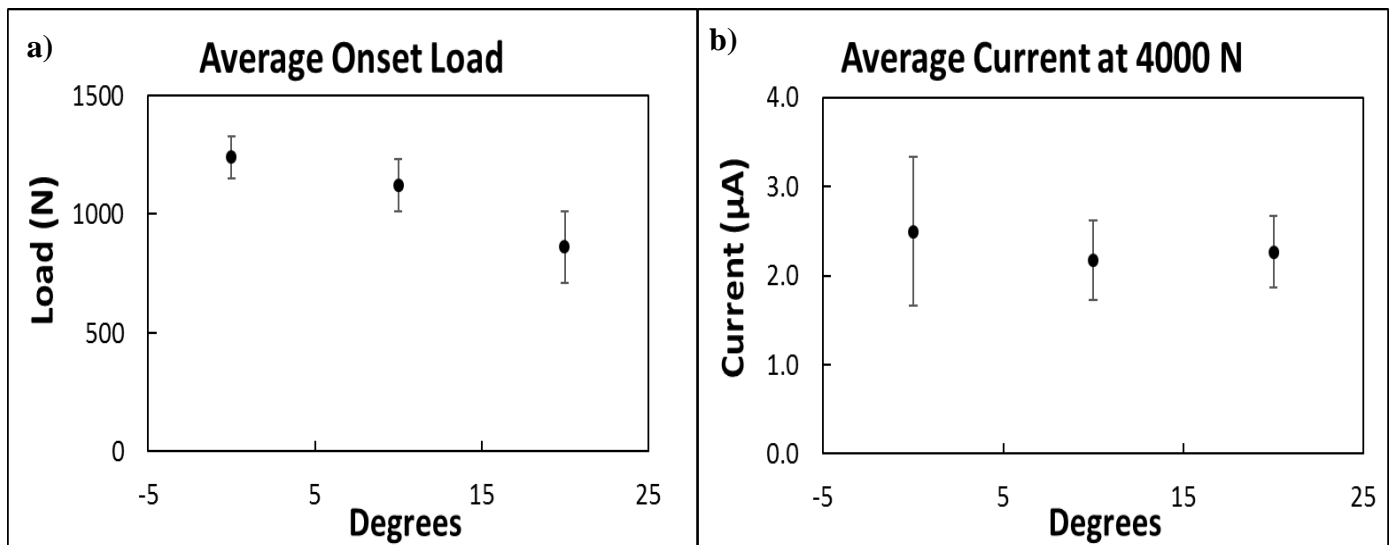
Fig. 49: Average (a) onset load and (b) current at 4000 N. The 20° group had a statistically lower onset load than the other groups (P<0.05), however there was no difference between the remaining groups. There was no difference between the average current at 4000 N.

There was no difference in current at the end of testing between the tested groups with values around 2.5 µA (Fig. 49b).

Post-test pull-off load. Post cyclic testing, each sample underwent pull-off load testing. The recorded loads show no statistical difference between the groups (Fig. 50).
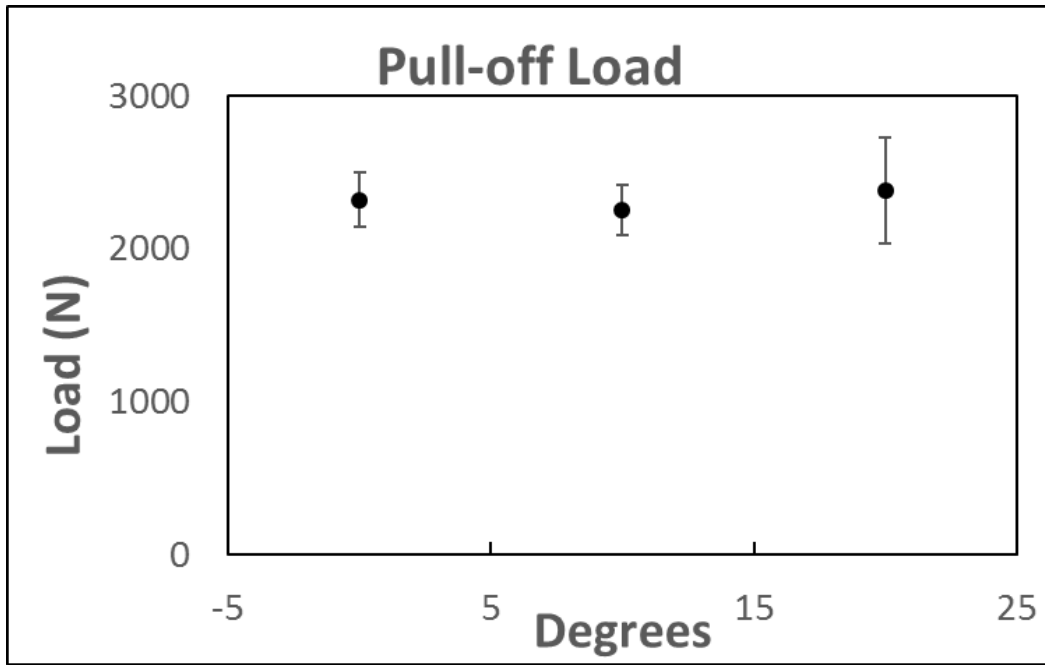
Fig. 50: Pull-off load per group after cyclic testing showed no difference between the groups.

All samples required about 2300 N of pull-off load to overcome the interlocking ability of the taper junction.

3.2.3 – Taper Contamination ICFC

Results reported in this section are comprised of rigid body motion data only.

Seating. The seating load-displacement behavior for the sample groups showed the control group as well as the liquid contamination groups had a statistically lower seating displacement compared to the solid contamination groups. The superior portion of the wet group had a statistically lower seating displacement compared to the control (Fig. 51) (P<0.05).
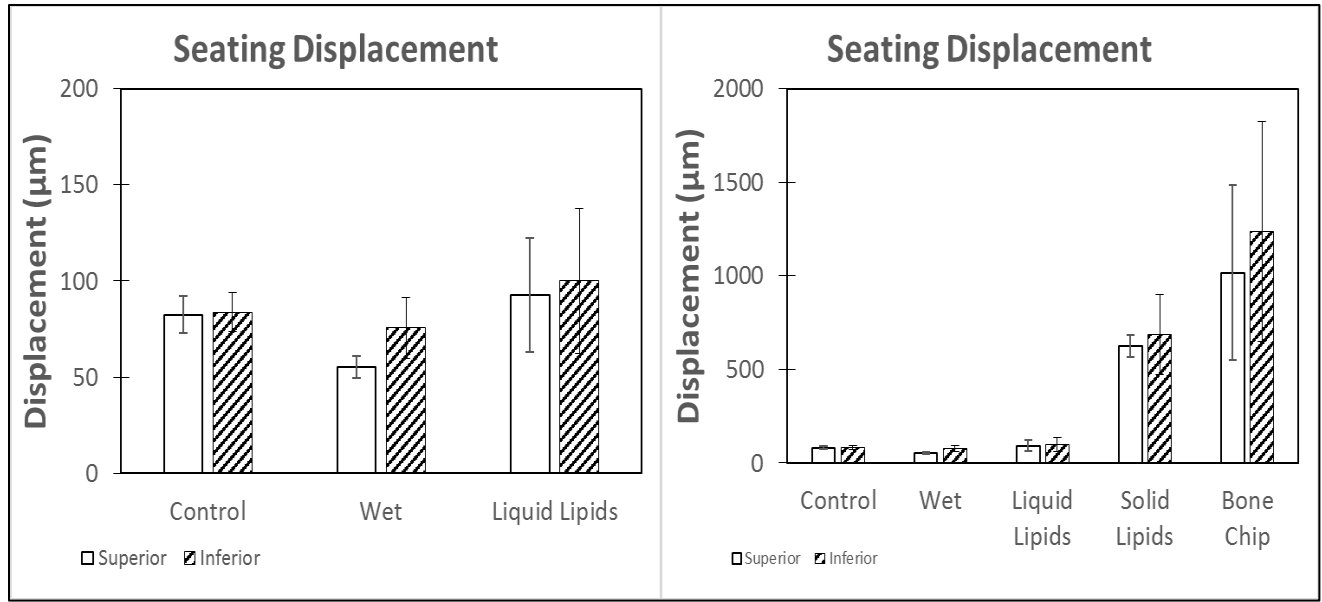
Fig. 51: Average seating displacement data per group (n=5) showed in the superior sensor the wet group had the lowest amount of seating compared to the remaining groups (P<0.05) The solid contaminants had the highest amount of seating.

Similarly, the work of seating for the wet group on the superior portion was lower than all other groups while work of seating for both sensors was highest in the solid contamination groups (Fig. 52) (P<0.05).
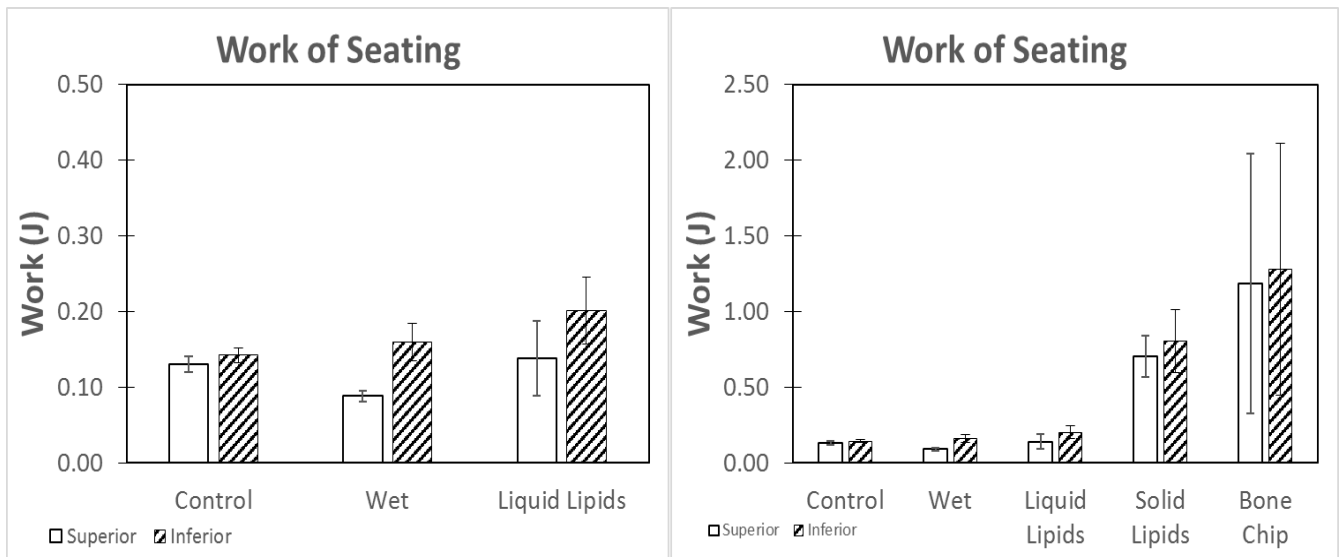
Fig. 52: Average work of seating per group (n=5). In the superior sensor the wet group had the lowest amount of work of seating compared to the remaining groups (P<0.05) The solid contaminants had the highest amount of work.

Cyclic testing. Fig. 53 summarizes the micromotion (Fig. 53a) and subsidence (Fig. 53b) for the different test groups.
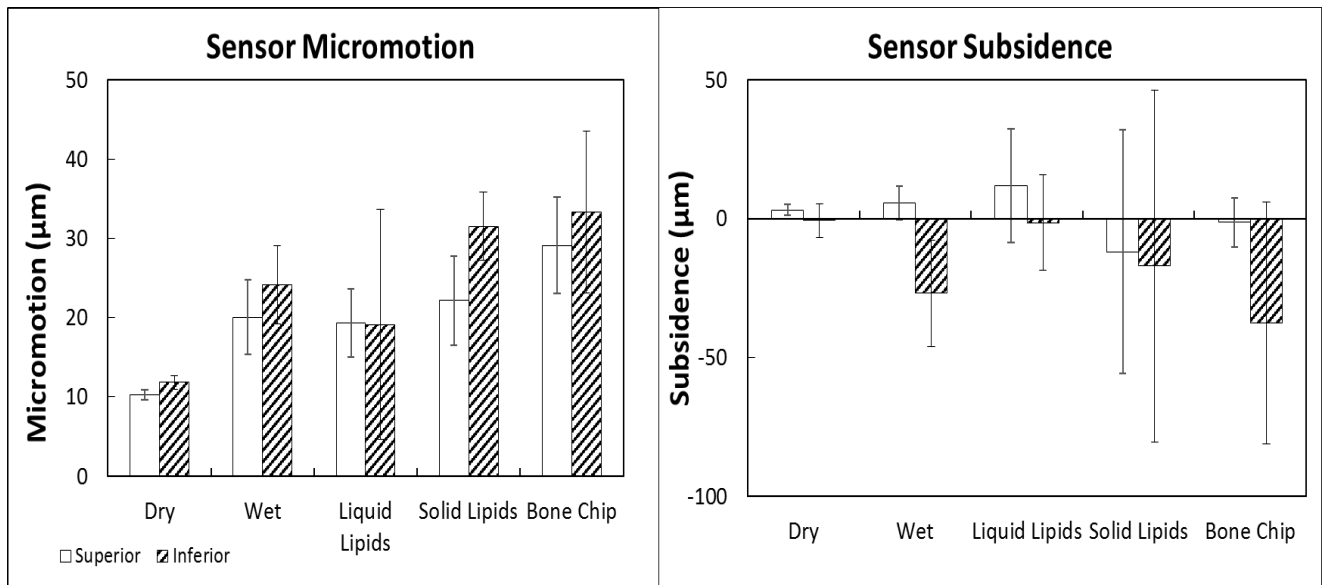
Fig. 53: (a) Average micromotion and (b) subsidence per group at 4000 N. The data shows the dry group had the lowest amount of micromotion at the end of testing ($P<0.05$)

During cyclic loading, all samples showed levels of micromotion and subsidence. However, the dry control group maintained lower levels of micromotion throughout testing ($P<0.05$), the other groups were not statistically different from one another. The inferior portion of the wet samples experience more negative subsidence, further seating of the head onto the neck, than the dry samples. The reported subsidence of the other groups was not different.
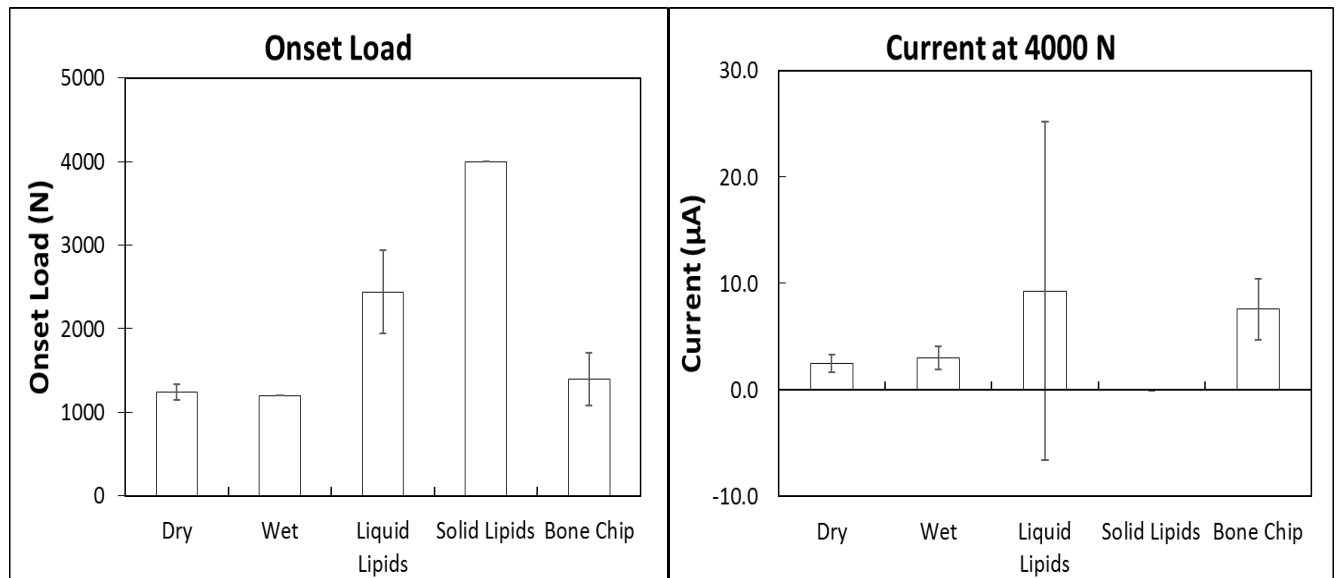
Fig. 54: Average (a) onset load and (b) current at 4000 N. These plots show the solid lipids group required a significantly larger load to commence current and had no current at the end of testing (P<0.05)

The onset load for fretting corrosion showed the two lipid groups required higher loads before the current deviated from the baseline (P<0.05). There was no difference between the remaining groups (Fig. 54a). The solid fat group had the lowest reported fretting currents at 4000 N opposite that of the bone chip group which had the highest currents on average (Fig. 54b) (P<0.05). The liquid fat had highly variable results as can be seen by the large standard deviation indicating that some currents were low and some were very high.

Pull-off testing. The pull-off loads captured after cyclic testing, shown in Fig. 55, show the wet group required the lowest amount of force to distract the head (P<0.05). The remaining groups were not different with an average approximate force of 2500 N. After cyclic testing the pull-off loads were not significantly different in the contaminated groups compared to the pull-off data reported in Section 3.1.2 (pre-ICFC). However, the control group needed approximately 300 N more pull-off force post ICFC (P < 0.05).
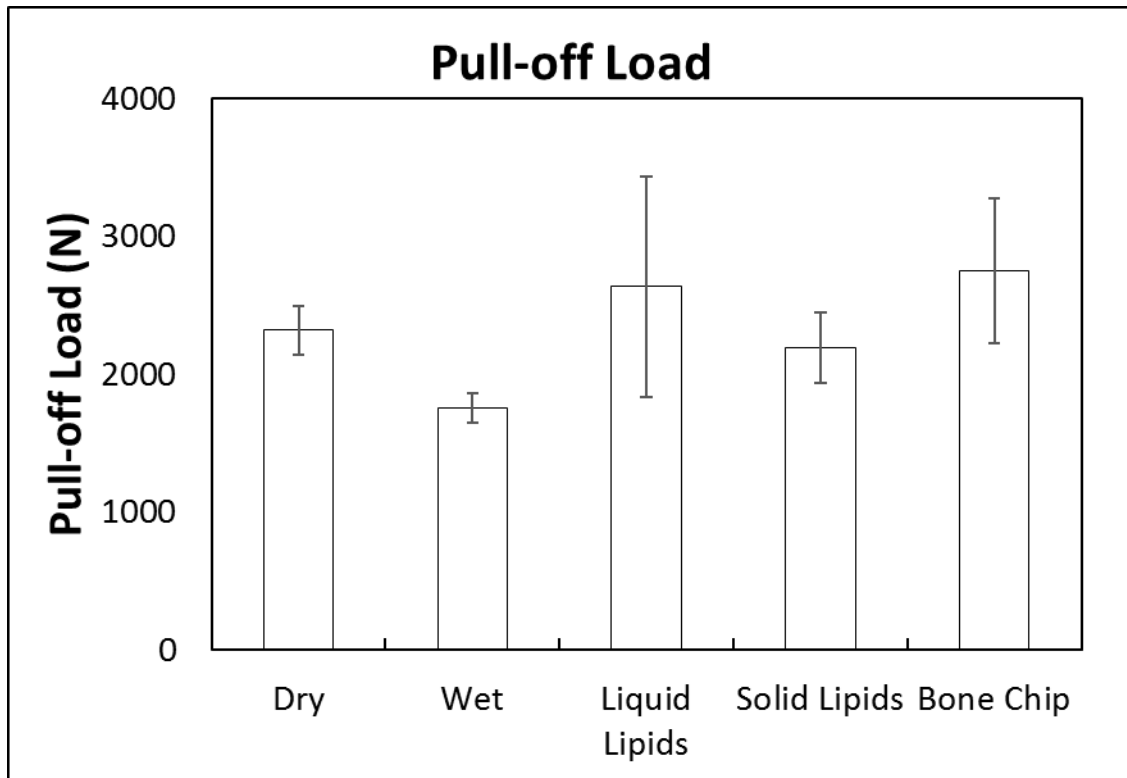
Fig. 55: Average pull-off force per group (n=5) showed the wet group required the lowest load to be pulled off (P < 0.05). The remaining groups were not different.

3.2.4 – Taper Design and Material Combination

Data reported below is exclusively rigid body motion unless stated otherwise.

Seating measurements and work of seating. During loading, significant elastic bending displacements were captured and were presented along with the rigid motion in the raw data.

The average seating measurements for each group were summarized in Fig. 56, with each group having an average seating displacements of about 40 to 60 µm. There were no statistical differences between the groups. There were rare instances in which the seating displacements in a single test were 20 to 30 µm different between the sensors indicating canting of the head on the neck during seating (not shown).
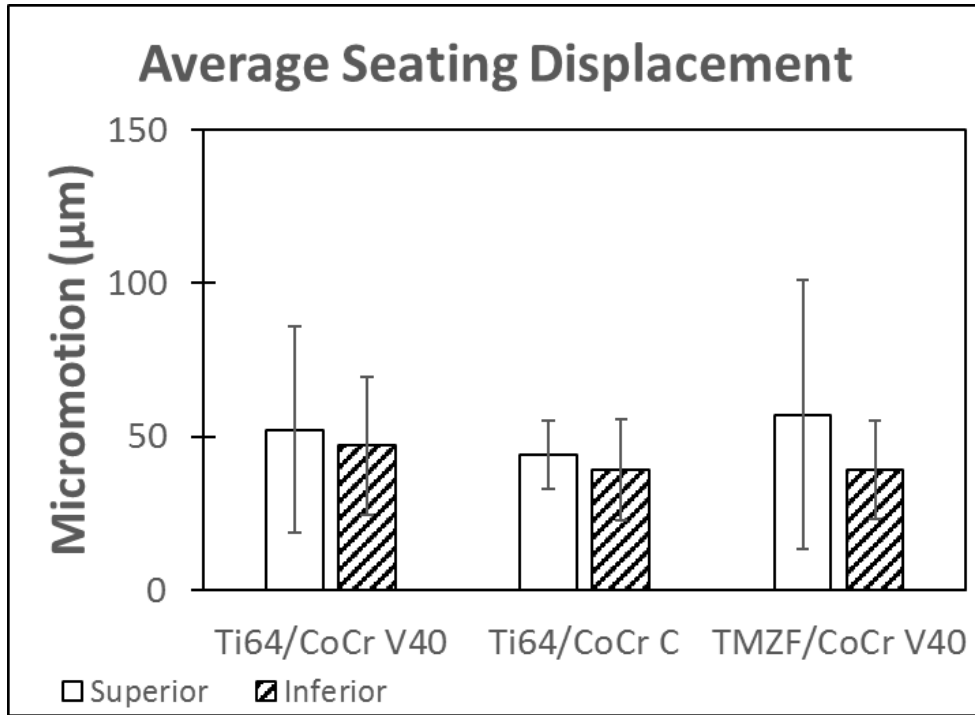
Fig. 56: Average seating displacement of three sample groups, no statistical difference.

The subsequent figure (Fig. 57) depicts the average work of seating for the superior and

inferior sensor for each group. The groups were not statistically different from one another.
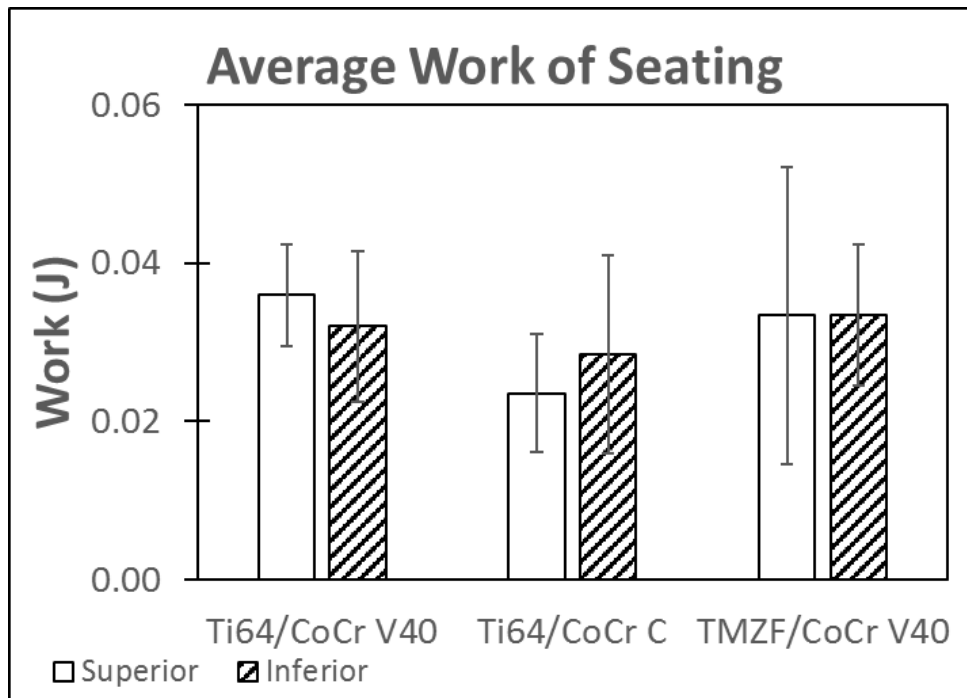
Fig. 57: Average work of seating of the three sample groups, no statistical difference.

The work of seating values mirror the seating displacement measured throughout testing, the lower the seating displacement the lower the work of seating.

Static calibrations and stiffness.

The average stiffness (k) of each group can be seen in Fig. 58. Data shows the superior sensor for group 2 (C taper for Ti/CoCrMo couple) had a statistically greater stiffness than that of groups 1 and 3 (i.e., V40 taper for Ti and TMZF alloys), (P<0.05). Groups 1 and 3 were not statistically different.
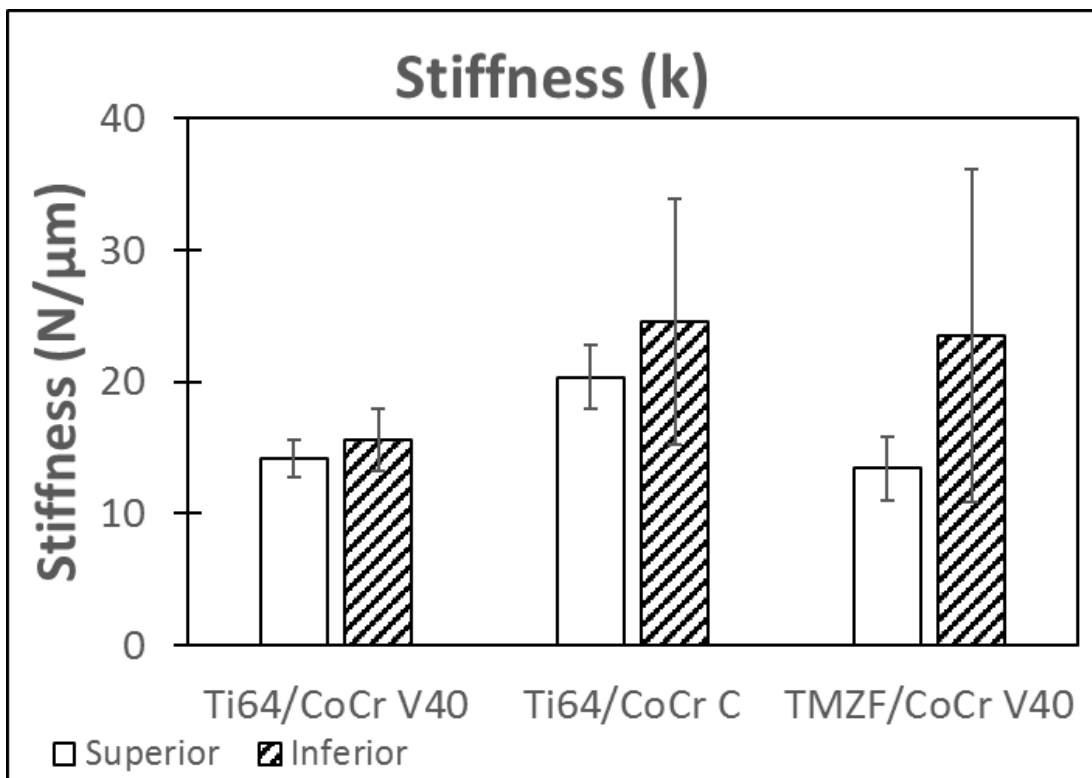
Fig. 58: Average stiffness per sample group. Superior sensor in the C taper group recorded significantly higher stiffness compared to the C taper (P<0.05).

Incremental cyclic loading. Electrochemical data from the incremental cyclic loading was summarized in Fig. 62 depicting the onset load and current at 4000 N (end of testing) for each group. The data from Fig. 59 was used to make assessments of the relative performance of the different implant taper geometries and material combinations.
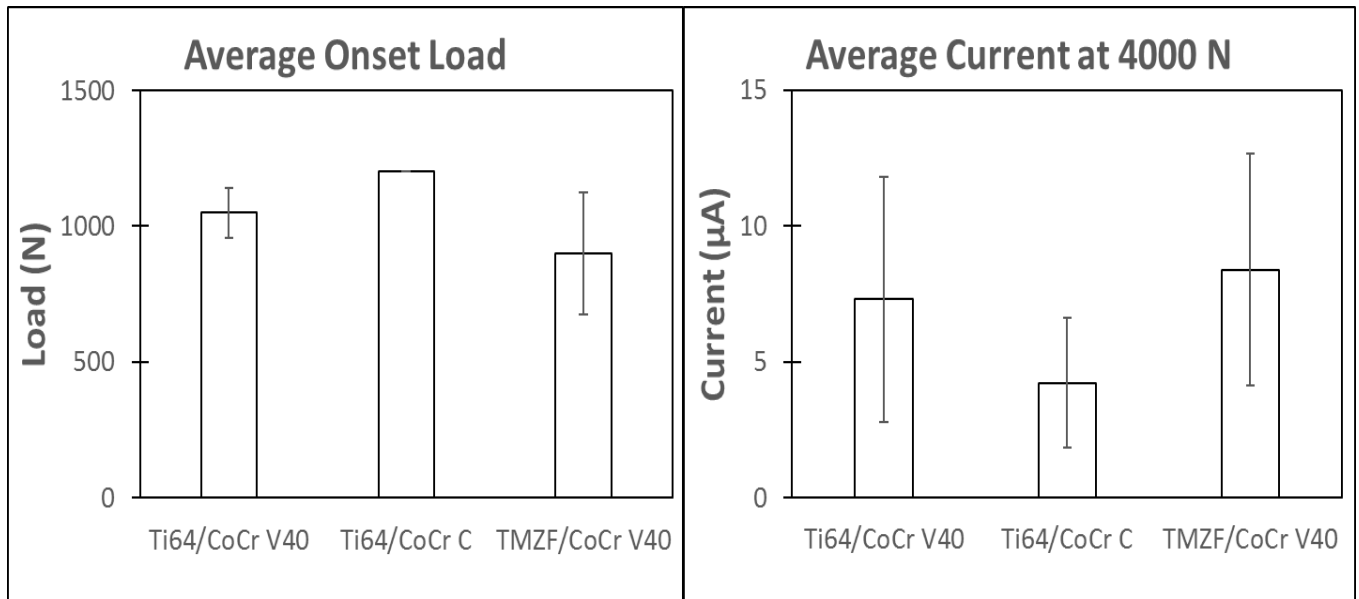
Fig. 59: Average onset load and current at the end of testing per group. The C taper was less susceptible to fretting corrosion (P<0.05).

A one-way ANOVA analysis of the onset load showed group 2 required a greater amount of force to initiate the MACC process (P<0.05). Groups 1 and 3, which share the same geometry but differ in material, are not different in terms of onset load. Current at the end of testing showed group 2 had a lower current on average compared to group 3 (P<0.05). The onset load for group 3 was lower than either the group 1 or group 2 conditions. This implies that it takes a lower load to induce fretting corrosion reactions in the C taper with TMZF alloy combination than the other two alloy-taper combinations.

Fretting motion. Fig. 60 plots the subsidence at the end of testing and micromotion amplitude at 4000 N, shown respectively. The superior sensor showed group 2 (C taper) was less vulnerable to micromotion than groups 1 and 3 (V40 tapers), which were not different from one another.
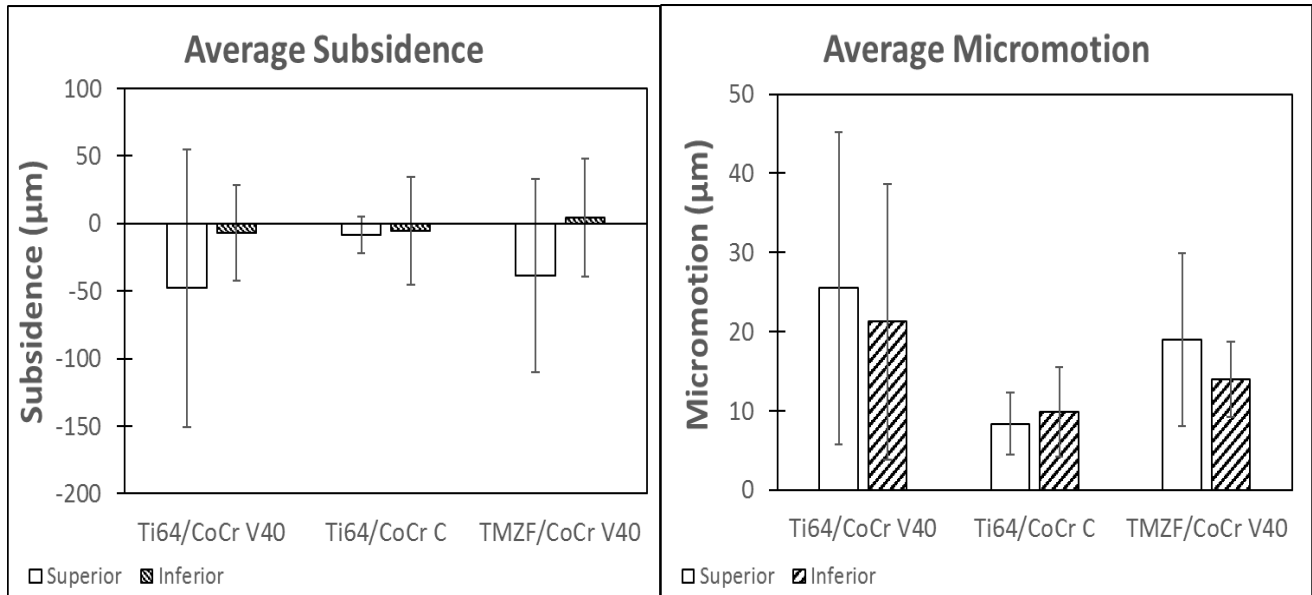
Fig. 60: Average subsidence per group with no statistical difference. Average micromotion showed the C taper was statistically lower than the V40 taper (P<0.05).

However, there was no statistical difference in subsidence between the different groups. All implants demonstrated some subsidence due to the cyclic loads of testing that generally resulted in greater seating of the head on the neck (negative value). The micromotions reported are measured at the sensor location, which is about 22 mm away from the neck axis.

3.2.5 – Impaction Assembly ICFC

Static calibrations. Post cyclic testing, each individual sample construct was calibrated by applying a series of static loads up to 3000 N and then plotting the load vs. displacement relationship (see Fig. 61).
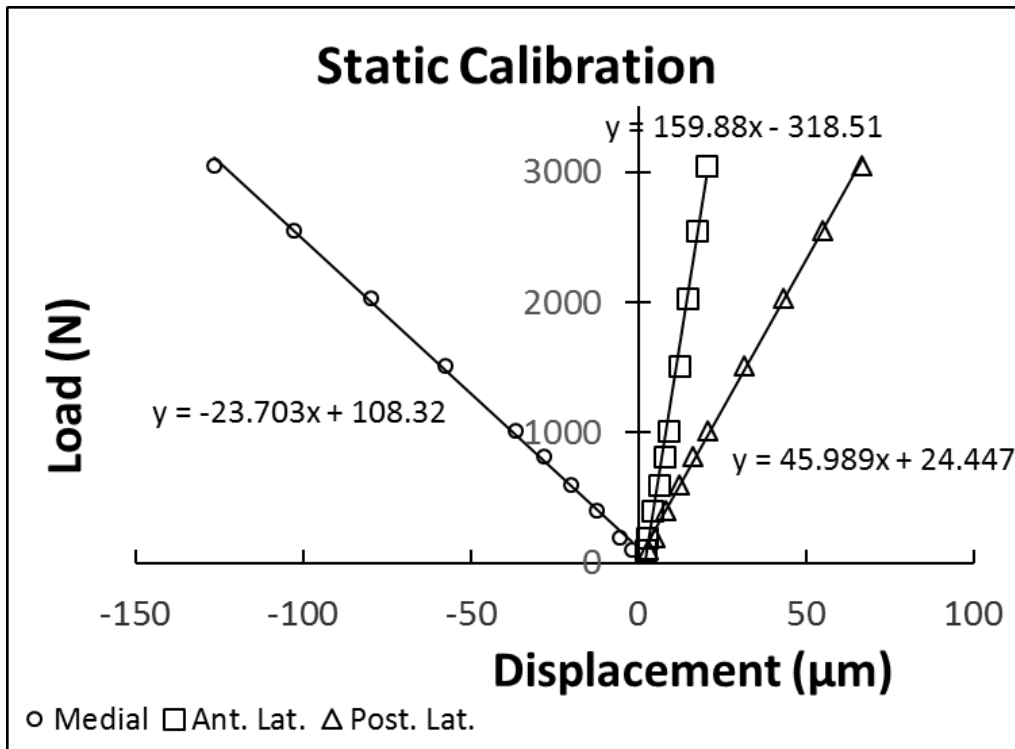
Fig. 61: Static calibration example (0.05 kN sample). Due to the compressive load and sensor configuration the medial sensor reports negative displacements while the lateral sensors report positive displacements. The slopes were used to calculate the elastic motion during testing.

The slope of the sensor load-displacement relationship was taken as the stiffness factor (k) for each sensor and then used to calculate the elastic-based motions. The compressive load applied during the static calibration caused the neck to elastically bend downward which due to sensor placement accounted for the medial sensors negative average stiffness versus the lateral sensors. Meaning as the load increased the head approached the neck in the medial direction while getting further in the lateral. The average stiffness data showed the impacted groups (6 and 14 kN) were more stiff in the posterior lateral region than the hand-assembled group (P<0.05) but were not different from one another (Fig. 62).
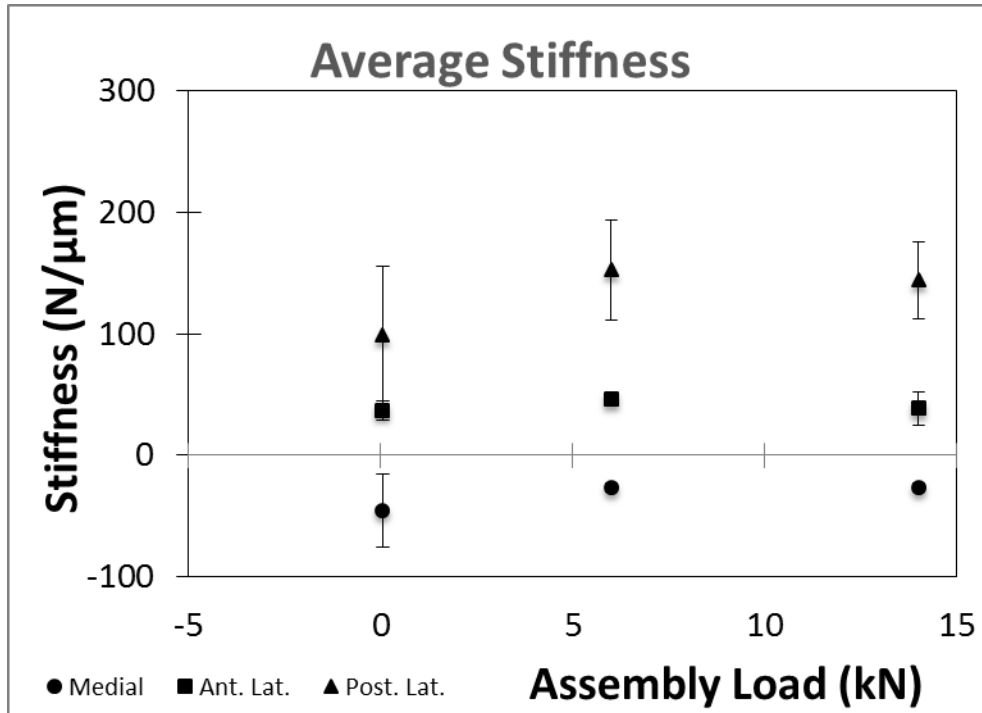
Fig. 62: Average stiffness (k) per assembly group. Stiffness in the 0.05 kN group was statistically lower than the impacted groups (P<0.05), the impacted groups were not different from one another.

Analysis of incremental testing. Data was analyzed as defined in the previous Incremental

Cyclic Fretting Corrosion section.

The average onset load per group increased as the impaction load increased (Fig. 63a).

Each group was statistically different from one another with the hand-assembled group having an

average onset load of 740 N followed by 1100 N and 1640 N for the 6 and 14 kN assembly load

groups respectively (P<0.05).

Despite the increase in average onset load with the increase in assembly load, the current

at the end of testing for the three groups on average was approximately 6 µA with no statistical

difference between the groups due to large variances in each sample group (Fig. 63b).

The data implies an increased impaction load leads to a more secure taper junction and

requires a larger cyclic load to induce micromotion and fretting corrosion. Yet despite inducing

fretting currents at different load points during testing each group exhibited fretting corrosion

currents of approximately equal amounts. This suggests a non-linear increase in fretting

corrosion from onset load to 4000 N.

However, it is important to note that even with a seating load of 14 kN, well above

clinically achievable loads, fretting currents were observed and the onset for those currents were

well within the physiological levels expected.
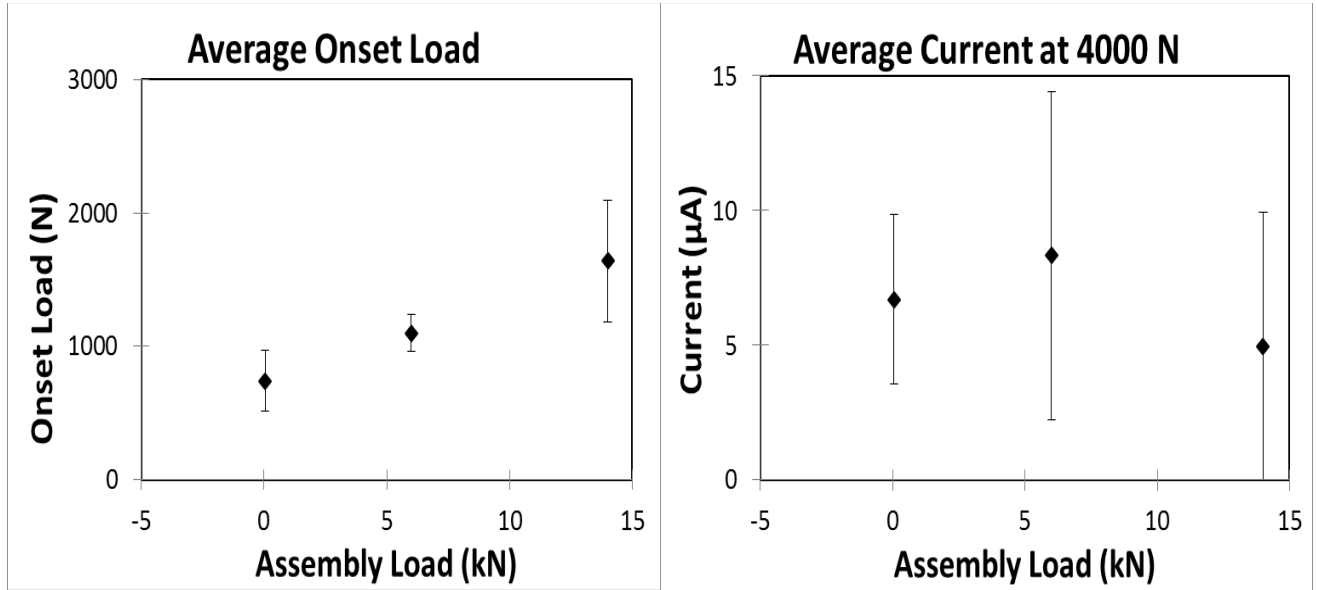
Fig. 63: Average (a) onset load and (b) current at 4000 N. The average onset load per group was statistically different from one another (P<0.05) but there was no difference in average current at 4000 N.

In terms of micromotion, as shown in Fig. 64 at 4000 N cyclic load the 14 kN samples

had less micromotion than the hand-assembled group (P<0.05). There was no significant

difference between the hand-assembled and 6 kN group or the two impacted groups. All samples

demonstrated levels of rigid-body micromotion and subsidence due to cyclic testing.
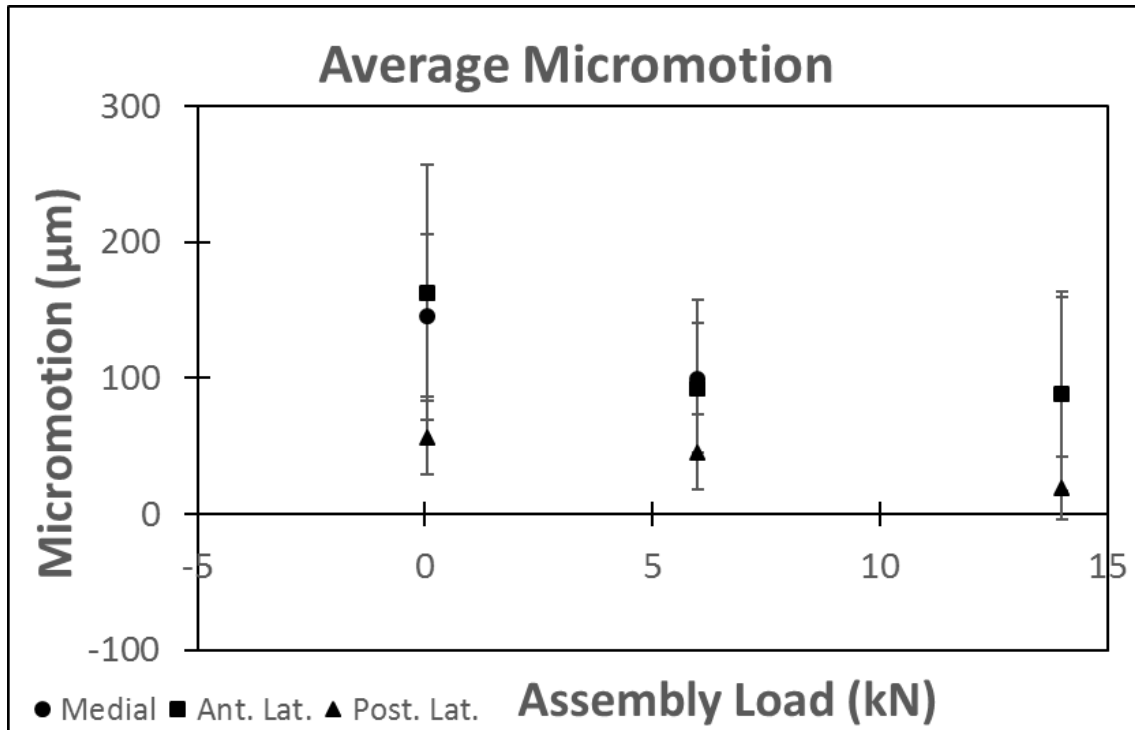
Fig. 64: Average micromotion per group. 14 kN reported statistically lower micromotion than hand-assembled group (P<0.05) but not the 6 kN group. There was no difference between the hand-assembled and 6 kN group.

Fig. 65 illustrates the average subsidence at the end of testing. The data shows the anterior lateral sensor in the hand-assembled group recorded more negative subsidence than the remaining group (P<0.05). The remaining test groups and sensors were not statistically different. The hand-assembled group seated further throughout testing presumably due to the low assembly load applied pre-cyclic loading contrary to the 14 kN assembly load group which amassed small amounts of subsidence throughout testing. The data also reveals an uneven average subsidence of the sensor due to cyclic loading which may indicate canting of the head on the neck. The 6 kN samples diverted from the assumed behavior and on average recorded positive subsidence, the dislodging and upward mobility of the head off the neck. This behavior may be due to the frictions of the junction being overcome by the external pressures applied during cyclic loading.
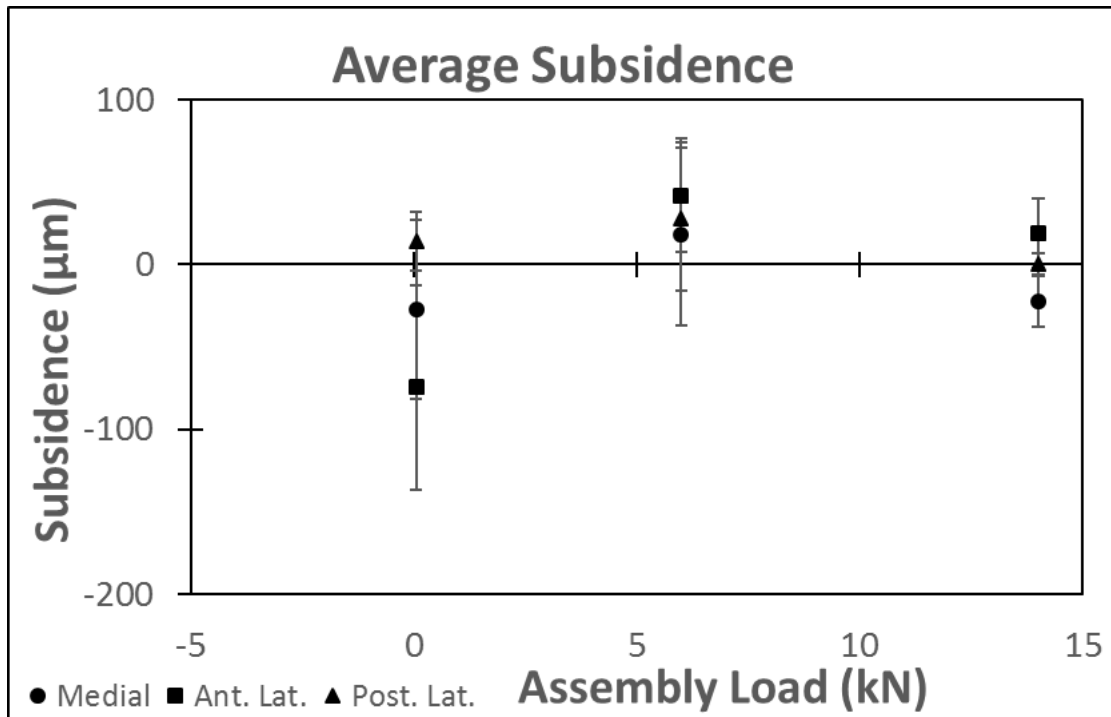
Fig. 65: Average subsidence per sample group. The anterior lateral sensor in the hand-assembled group recorded higher negative subsidence than the remaining groups (P<0.05). There was no statistical difference between the remaining sensors per group.

3.3 – Goal 3

The novel high-speed camera system provided large amounts of data. Analysis was systematically done in four major steps (exemplified using a non-compliant impacted sample).

3.3.1 – Load Rate and System Compliance Analysis and Results

Motion tracking. During impaction the camera was set to record up to 2 s of displacement data, approximately 16,000 frames. Both the motion of the head and neck were tracked using Motion Studio software (IDT Vision), which allowed a tracking square to be placed on a speckled point on both surfaces (Fig. 66).
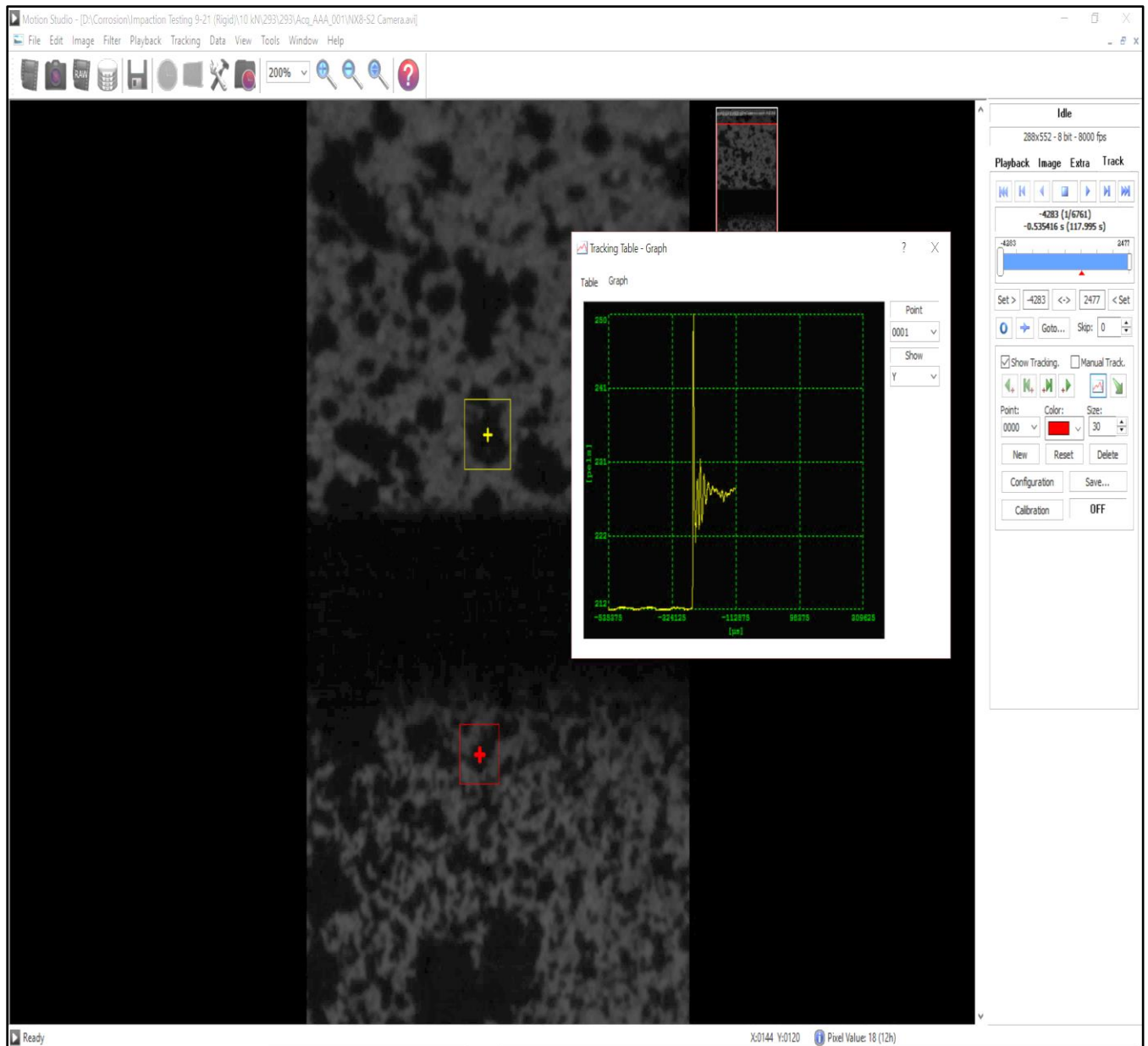
Fig. 66: High-speed camera video analysis tracking a point on the head (green) and neck (red). These points were used to determine relative motion of the head.

Displacement. The motion data was exported and the relative displacement was determined by subtracting the head motion by the neck motion. The data was then time synced and the peak load was aligned with the peak displacement in order to correctly calculate the load-displacement behavior (Fig. 67). Note the full displacement and load was achieved in less than 5 milliseconds.
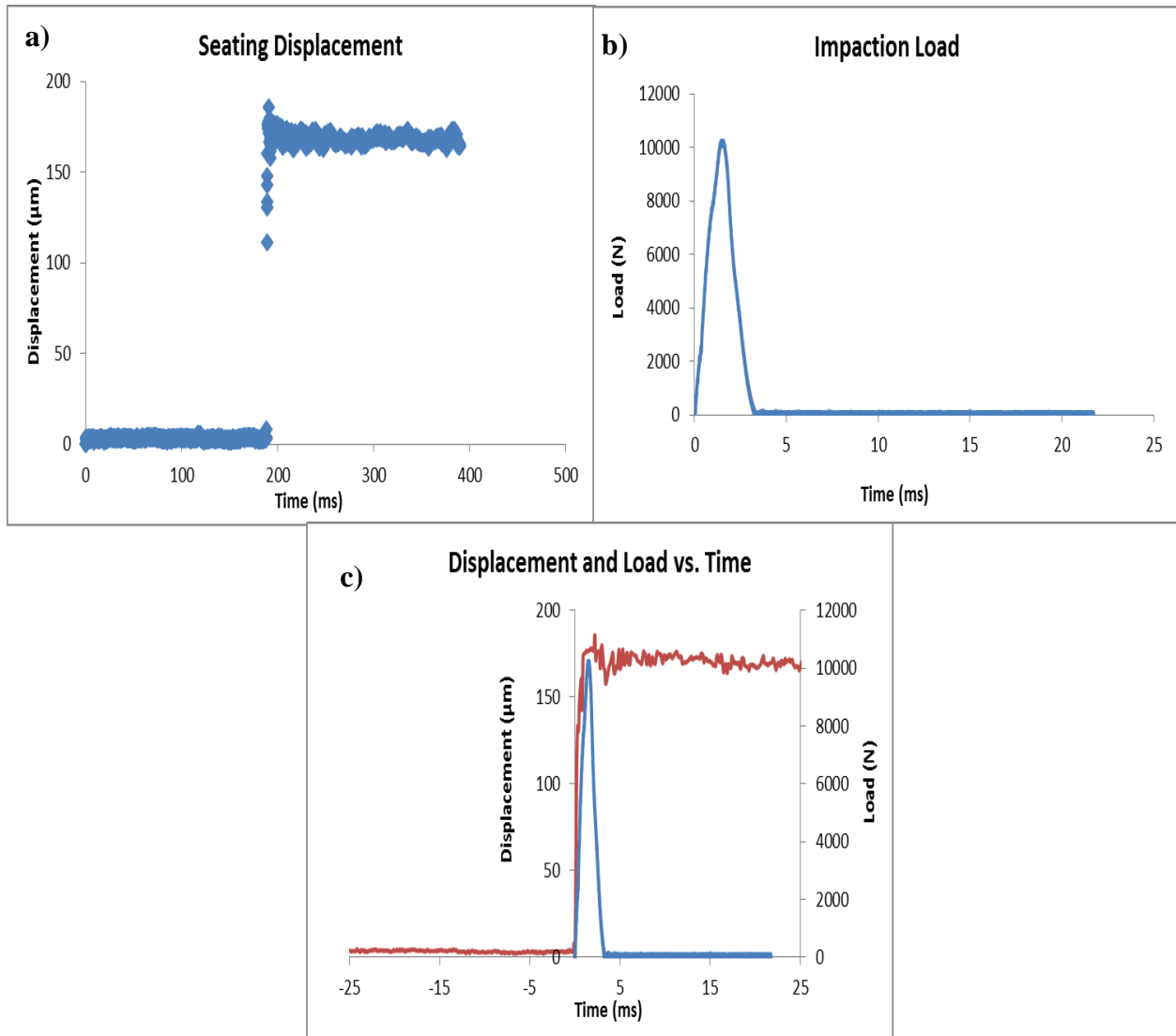
Fig. 67: Plots a and b show the offset in time between the camera recorded seating displacement and the impaction load applied by the impaction tower respectively. c) The displacement (red) and load (blue) data on a matching time synced plot. All motion which occurred pre-impaction were moved before the 0 s point.

Data interpolation. Despite recording at the maximum recording rate of the camera it was

determined that the displacement data was recorded a rate lesser than that of the load. Therefore,

the displacement data needed to be interpolated in order to analyze all the relevant data.

93
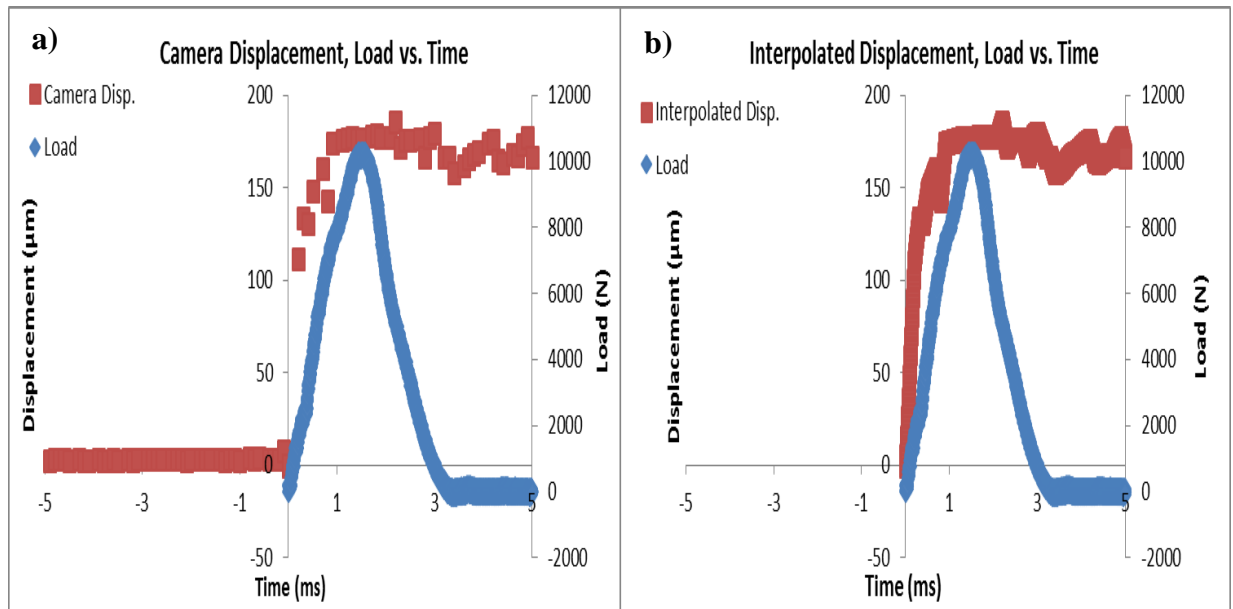
Fig. 68: a) Camera displacement, load vs. time and b) Interpolated displacement, load vs. time plots. The graphs show the missing displacement points over time show in plot a and the filled in points in plot b.

Fig. 68a shows a zoomed-in plot of the camera displacement and load vs. time, which highlights the fact that head motion occurs within about 1 ms of impaction and that there is a lack of displacement data in the initial period as the load increases. Fig 68b then shows the interpolated displacement and load vs. time, the newly interpolated points correspond with points of load (points from before the load was applied were removed).

Load-displacement. Lastly, the load vs. the interpolated data was plotted and used to determine the work of seating for each sample (Fig. 69). It can be seen that the seating load-displacement response has similarities to that seen in the quasistatic seating mechanics tests, But there is still significant noise and uncertainty present in the load-displacemennt plot.

94
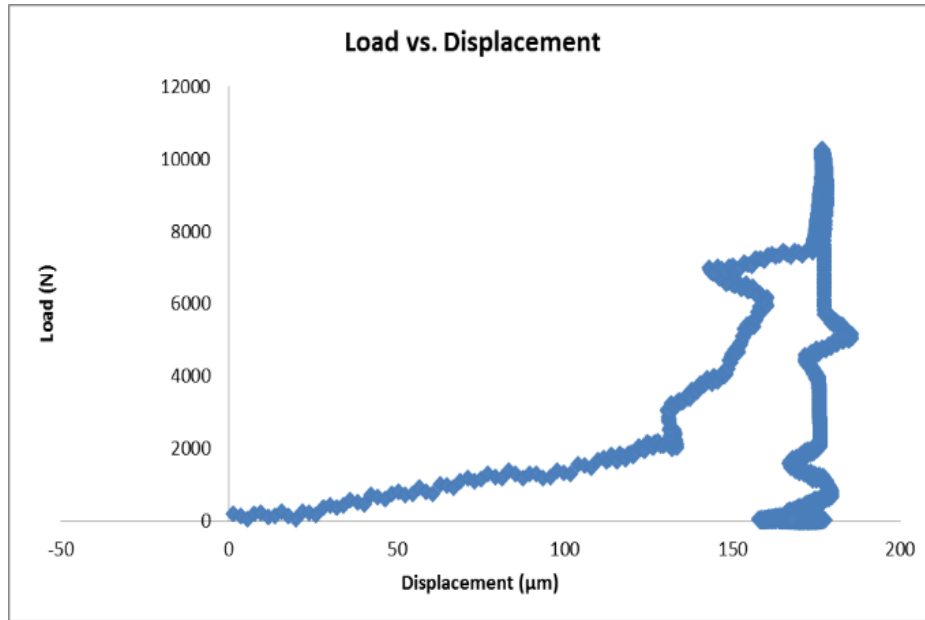
Fig. 69: Load vs. displacement plot with interpolated displacement data. The data was used to determine the work of seating per sample.

Seating displacement and work of seating. The average seating displacement of the non-compliant group showed the impacted group with an increased load rate yielded higher displacement compared to the static group ($P<0.05$) (Fig. 70a). Data from the compliant group showed less linearity and more variability as the load increased for the impacted samples (Fig. 70b). The seating displacement was not statistically greater in the complaint vs. non-complaint groups for the static sample groups.
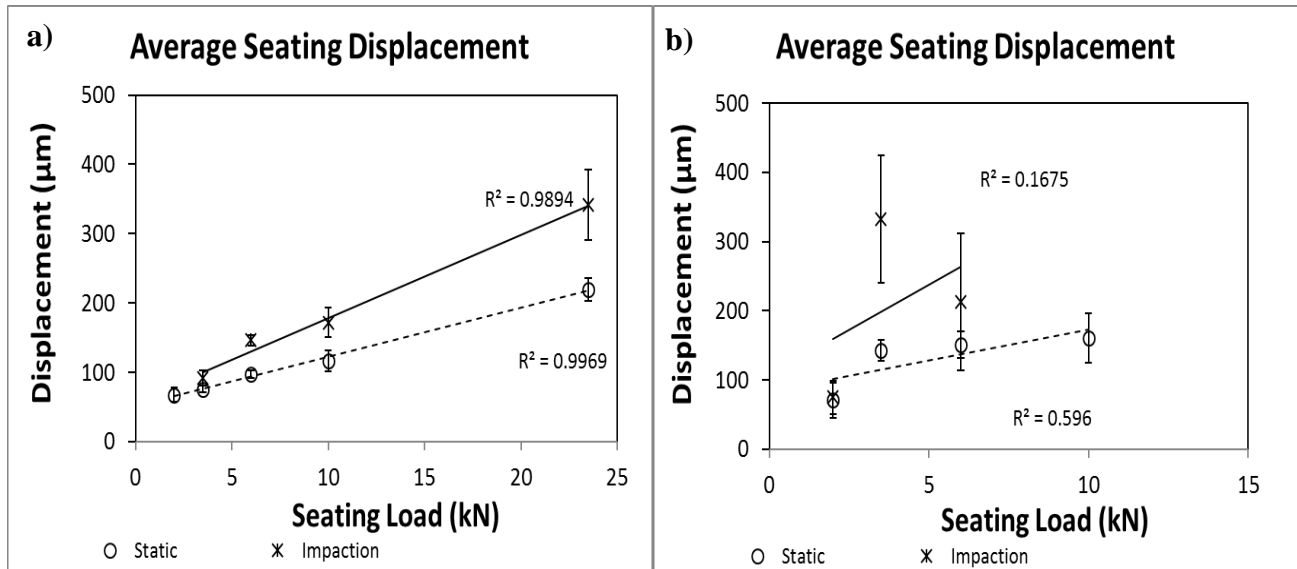
Fig. 70: Average seating displacement for static and impacted groups in the (a) non-compliant and (b) compliant setup. The impaction samples in the non-compliant setup were statistically different from the static (P<0.05). The impaction compliant data was extremely variable.

The work of seating showed no statistical difference between the non-compliant groups, the values increased parabolically as the load increased (P<0.05) (Fig. 71a). Again data for the compliant impaction groups showed high amounts of variability; the static samples increased parabolically (Fig. 71b). Comparatively there was no difference between the non-compliant and compliant sample groups in the static setup.
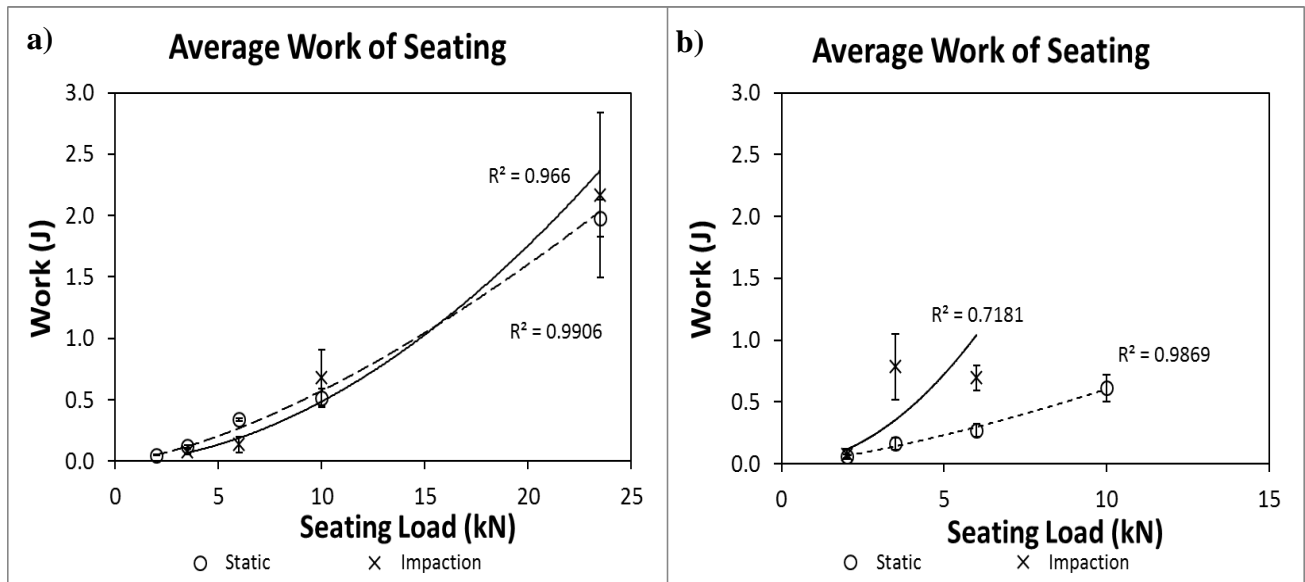
Fig. 71: Average work of seating for static and impacted groups in (a) non-compliant and (b) compliant setup. There was no difference between the non-compliant load rate samples. The impaction compliant samples showed a large amount of variability.

Taper stability. Taper stability was defined by the force necessary to overcome the locking ability of the taper (pull-off load) [46, 66]. The average pull-off load between the load rate and compliance groups showed no statistical difference in comparison (Fig. 72). The ratio of pull-off to seating loads for all cases ranged between 0.38 and 0.55.
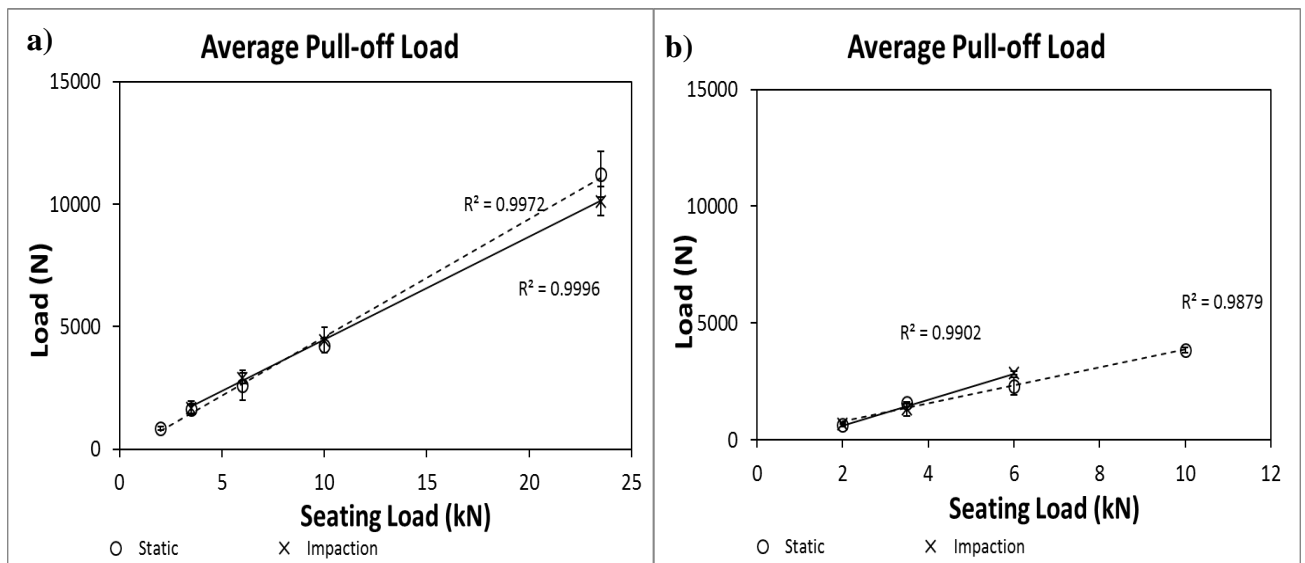
Fig. 72: Average pull-off load for the static and impaction groups in (a) non-compliant and (b) compliant setup. The groups were not statistically different regardless of the load rate or compliance setup.

97

Chapter 4 – Discussion

4.0.1 – Overall Discussion

In summary, the findings of this dissertation have contributed towards better understanding of taper mechanics, surgical assembly and design principles and their relationship with taper performance. Taper performance was defined as the amount of seating displacement, micromotion, subsidence, fretting corrosion current and pull-off load measured throughout different test procedures. The work presented also showed the influence of surgical assembly on seating mechanics and incremental cyclic fretting corrosion testing results. The taper contamination testing provided evidence which suggests applying a lipid like coating to the male portion of the trunnion may increase seating displacement, reduce fretting corrosion current and increase taper stability throughout testing.

Taper seating mechanics

While current surgical assembly practice remains unstandardized the testing done in the seating mechanics section identifies new and yet unreported effects of varied modular taper assembly on seating mechanics and taper stability. The new discoveries in the following subsections could influence taper assembly procedure and taper design components. In Goal 1, 12/14 head-neck taper junctions were subjected to various assembly loads at predetermined orientations. Seating mechanics was defined as the rigid load-displacement behavior as well as the work of seating during assembly. It was concluded that seating load magnitude has a direct correlation to seating displacement, work of seating and initial taper stability. As the seating load magnitude increased the measured seating displacement, work of seating and pull-off load increased. The seating response (load-displacement data) for each load group revealed a constant behavior which may be used in computer simulations as well as finite element analysis to predict

the seating displacement for such tapers when a known load is applied. The study also showed increasing the seating load orientation from 0° to 20° at a constant assembly load had no significant effect on seating displacement, work of seating and pull-off load. The results of testing in this section also support the mathematical models presented in the taper assembly section of the introduction.

Taper contamination testing done in subsection 2 introduced four likely contaminants, blood, liquid fat, solid fat and bone, to the modular junction during taper assembly. Clinically, as well as in literature, it is suggested that the taper be thoroughly cleaned of any solid or liquid contaminants in order to achieve the ideal taper assembly. However, testing showed the introduction of contaminants increased the seating displacement, work of seating and taper stability post seating. For example, liquid lipids about the male taper increased the average taper pull-off force by approximately 1500 N when compared to the control group.

ICFC testing

The following section looked to advance the understanding of taper assembly, design and material combination on fretting motions and current. The findings also adhere to mathematical models discussed in the fretting motion and corrosion sections of the background & significance chapter. Goal 2 presented the effects of load magnitude on 12/14 taper performance during incremental cyclic fretting corrosion and post-testing taper stability. Testing showed an increase in seating load magnitude led to increased taper stability which inherently reduced subsidence. Also revealing a correlation between subsidence and current at the end of testing. The increase in subsidence for the 1000 and 2000 N groups caused a large deviation from standard pull-off load values, increasing the pull-off load ratio considerably. A takeaway from this section was despite increasing the assembly load to 8000 N, fretting corrosion current was not eliminated.

Using similar testing methods, Goal 2.2 varied the seating load orientation from 0 to 20° clockwise away from the neck axis. During cyclic testing the samples were fixed at a 35° orientation. The results of testing showed an increased assembly load orientation led to a lower onset load. However, increasing the seating load orientation had no effect on the fretting corrosion currents at 4000 N or pull-off loads for these tapers.

Goal 2.3 delved further into the effects of contamination during ICFC testing. The findings provided evidence in favor of the use of lipids during assembly, contrary to that of clinical practice and literature. The introduction of lipids into the taper junction increased the onset load and reduced and in some instances eliminated fretting corrosion current during cyclic testing.

Within Goal 2.4 taper geometry and material combination were assessed using a novel benchtop test method which concurrently captured head-neck motion and electrochemical data. The results showed changes in the taper geometry of the materials caused a significant change in the stiffness of the construct. There were significant differences seen in the stiffness measured between the three groups with the Secure Fit with C Taper samples and LFIT Anatomic head (Ti-6Al-4V/CoCrMo) having the highest stiffness. Alterations in the taper geometry resulted in lower onset loads for the C tapers compared to the V40 taper. The Secure Fit group on average had lower current readings at the end of testing compared to the remaining groups. The data showed the novel test method has the capability to capture instantaneous measurements of motion and fretting corrosion currents and correlate those results to design parameters. Overall, the experimental test method is simple, quick and provides for a fast method to assess design and materials for susceptibility to fretting corrosion interactions. The results discussed in this section

are also bolstered by a retrieval analysis done by Higgs et al. [73]. In said study, both the C and V40 taper exhibited signs of fretting corrosion. However, 10% more of the V40 tapers exhibited higher levels of fretting damage. Fretting damage was rated on the Goldberg scare. Overall, taper size had no significant effect on fretting damage.

Lastly, Goal 2.5 specifies the effects of impaction assembly techniques on 12/14 taper junctions post-ICFC testing. The results indicated a larger stiffness as the load magnitude increased which lessened the overall micromotion and subsidence during testing. There was no significant effect on the current at 4000 N though there was an effect on onset load, suggesting the assembly load alters the fretting onset load but once corrosion is initiated it has the same affect. Cyclic loading data also presented the theory of elastic deformation within samples assembled at "excessive" load magnitudes which may lead to failed interlocking principles in the junction.

Goal 3 utilized a novel seating displacement measurement method. Load rate, load magnitude and system compliance were chosen to simulate clinical relevance. System compliance was used to simulate patient anatomy incorporating bone and tissue. Changes in load magnitude and load rate simulated surgical technique. The section presented evidence which stating load rate and system compliance had no significant effect on work of seating or taper stability. However, an increase in system compliance increased the overall input energy necessary to achieve the same impaction load in a non-compliant setup. These results are contrary to that of literature which state load rate and compliance would alter the loading mechanics of the taper junction.

Subsection 4.0.2 (following subsection) provided a visual analysis tool used to better understand the motions recorded about the taper interface during seating and incremental cyclic

testing. This tool allows for the depiction of uneven motions such as canting, toggling and positioning.

The results of the aforementioned studies have not only strengthened the link between taper mechanics, fretting behavior and taper performance but also challenge the literature which asserts the negative effects of taper contamination, compliance and load rate. The results discussed in this section highlight the negligible effects of certain contaminants, increased load rate and system compliance on seating mechanics and taper stability. However, the incorporation of lipids into the taper junction reduced the fretting response during ICFC testing and increased taper stability post seating.

Thus, the findings from this dissertation lead to questions for the need for standardization in manufacturing of taper geometry and surgical assembly. Should manufactures continue to create tapers with limited guidelines or should more stringent rules be in affect? Should surgeons be taught one standard method to assembling modular tapers which potentially introduces a lipid like substrate to the junction?

4.0.2 – Visual Basics Computational Analysis

Data collected during seating and ICFC testing presented unique data analysis opportunities such as the use of a Visual Basic program.

Programming Rationale:

Tested samples presented well over half a million data points which individually correspond with taper performance and/or seating mechanics over approximately a three hour testing time range. The assortment of displacement data consisted of microns of total motion which were then reduced further to rigid motion. Such minor amounts of movement are

extremely hard to register with the human eye. In order to better analyze and understand the

phenomena occurring during testing a visual analysis program within Visual Basic was created.

Program:

The program operated as follows:

1. Read in a comma separated values (*.csv) file from the computer directory which

   contained 23 rows of user specific information before displaying the numerical values for

   the X_Value (time), DVRT 1, DVRT 2, Load and Current data (Fig. 73). DVRT, load

   and current specific data was recorded in voltage. DVRT specific data was the total

   motion comprised of both elastic and rigid motion.

	A	B	C	D	E	F
1	LabVIEW Measurement					
2	Writer_Ve	2				
3	Reader_V	2				
4	Separator	Tab				
5	Decimal_S	.				
6	Multi_Hea	No				
7	X_Column	One				
8	Time_Pre	Absolute				
9	Operator	dpierre				
10	Date	########				
11	Time	17:34.6				
12	***End_of_Header***					
13						
14	Channels	4				
15	Samples	100	100	100	100	
16	Date	########	########	########	########	
17	Time	17:34.6	17:34.6	17:34.6	17:34.6	
18	Y_Unit_La	Volts	Volts	Volts	uA	
19	X_Dimens	Time	Time	Time	Time	
20	X0	0.00E+00	0.00E+00	0.00E+00	0.00E+00	
21	Delta_X	0.01	0.01	0.01	0.01	
22	***End_of_Header***					
23	X_Value	DVRT 1	DVRT 2	Load	Current (F	Comment
24	0	3.834664	3.630487	-0.01449	0.378248	
25	0.01	3.832117	3.639405	-0.01449	1.887647	
26	0.02	3.739163	3.562964	-0.00939	3.98287	
27	0.03	3.76463	3.564238	-0.01831	4.804148	
28	0.04	3.750623	3.556594	-0.01449	4.189697	
29	0.05	3.750623	3.566786	-0.02213	3.802177	
30	0.06	3.83721	3.657241	-0.01703	4.16556	

Fig. 73: *.csv file highlighting user specific information which was negated (row 1 to 23).

2. Stiffness calibration and micron/volt conversion values for each DVRT were manually
   input before the program was instructed to skip the beginning 23 lines of information and
   move directly to the numerical values.

3. The appropriate values were converted from voltage to displacement (µm), Load (N) and current (µA).

4. Each row was read into the program:

    a. Rigid displacement was calculated using **Eqn. 13** for each sensor.

    b. Work of seating was calculated using **Eqn. 11** for each sensor.

5. Unique visual diagrams were drawn. In box 1, the total and rigid motion of head and the loading behavior were drawn. A static image of the head was continuously displayed as a reference point compare the final displacement of the head versus the original positon. Box 2 and 3, plotted the load vs. displacement for both the superior and inferior sensors (Fig. 74).

6. The work of seating values (J) and elapsed time were displayed below Box 2 (Fig. 74, circled portion).
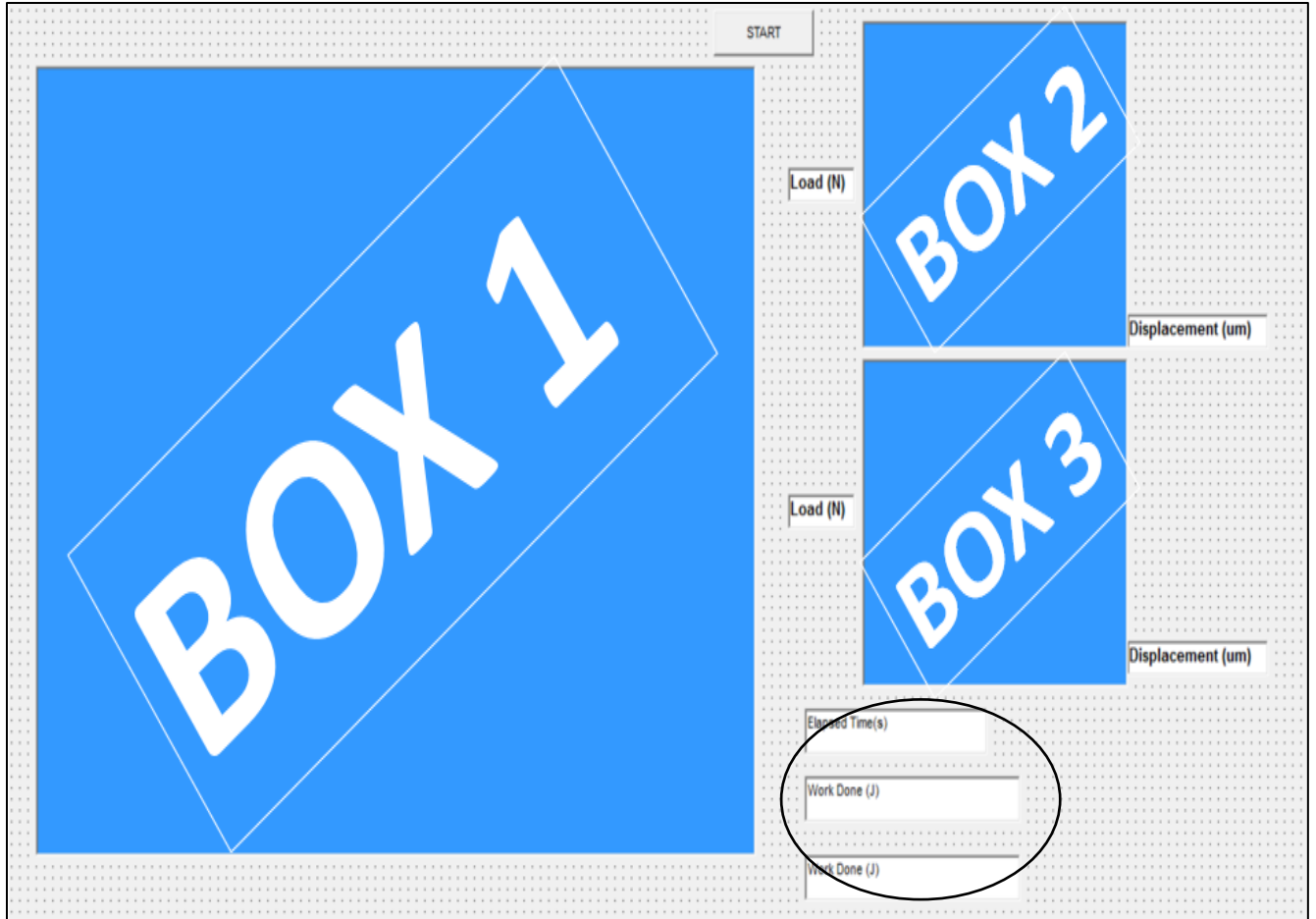
Fig. 74: Visual Basic program (pre-analysis).

7. Post analysis, the program displays visual representations of the amount of rigid motion which occurred during testing; this allows for a better understand of the head motion (Fig. 75).
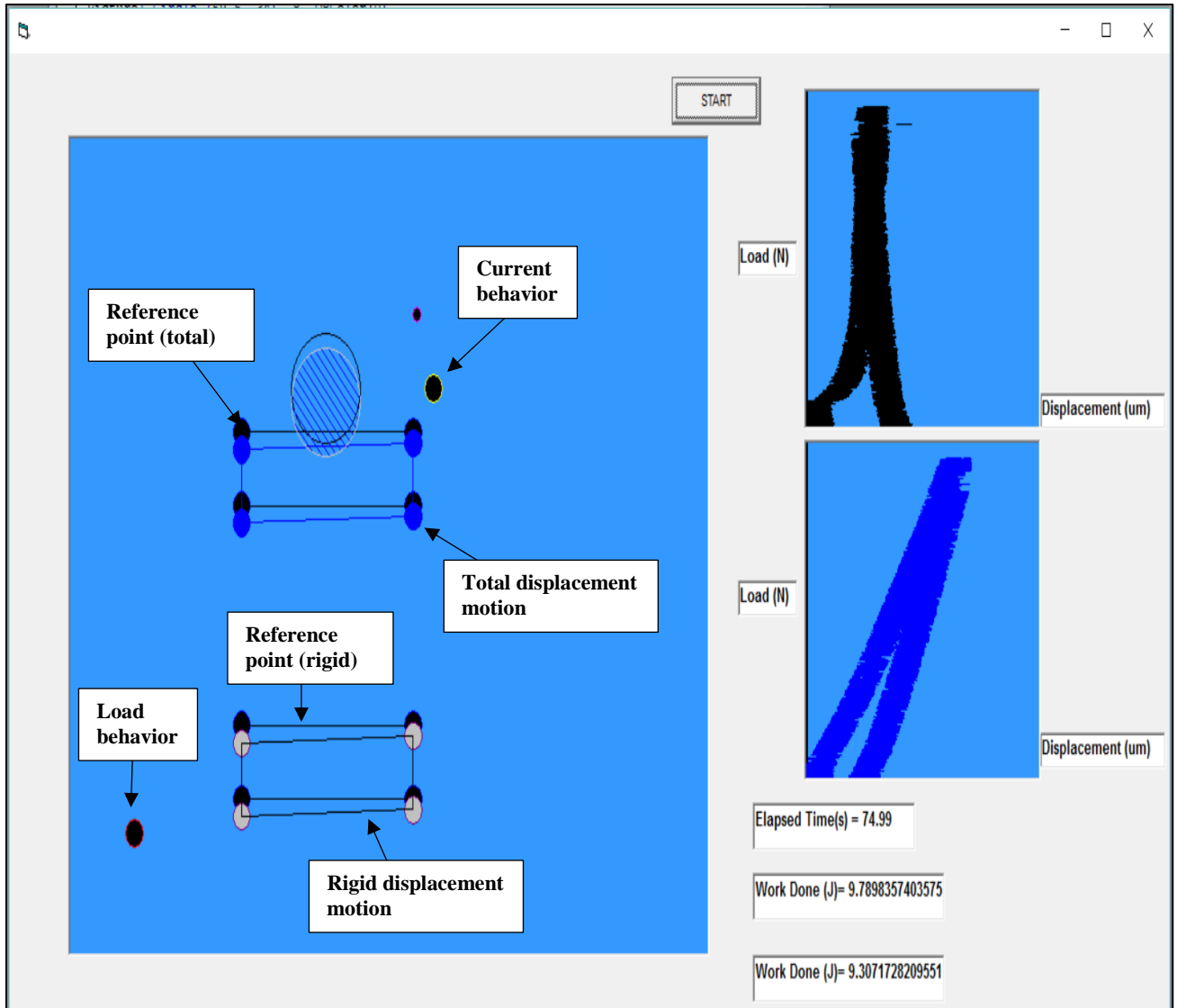
Fig. 75: Post-analysis visual basic program with highlighted information.

Conclusion:

Post-seating and incremental testing the Visual Basic program was used to highlight the rigid motions of the head during loading. Seating analysis has shown levels of disproportionate displacement as well as varied seating behavior such as slipping, pistoning, canting, etc. between the superior and inferior sensors which was not discernable during testing. Through the use of this program those motions were well-demonstrated and documented. The program was also able to convey micromotion and subsidence data from incremental cyclic testing. Small groups of

107

data, approximately 30 s to 1 min long, were read into the program to display the amount of subsidence one sensor recorded versus the other.

In all, the Visual Basic program provided a visual representation of the motions recorded during testing which were unable to be seen. This visual aid not only has the ability to calculate specific values such as the rigid displacement, work of seating, elapsed time, micromotion and subsidence but also serves as visual aid to the motions captured throughout testing.

4.1 – Goal 1

4.1.1 – Load Magnitude and Orientation

Seating load magnitude and orientation effects on seating mechanics and taper locking stability simulating surgical assembly were quantitatively studied.
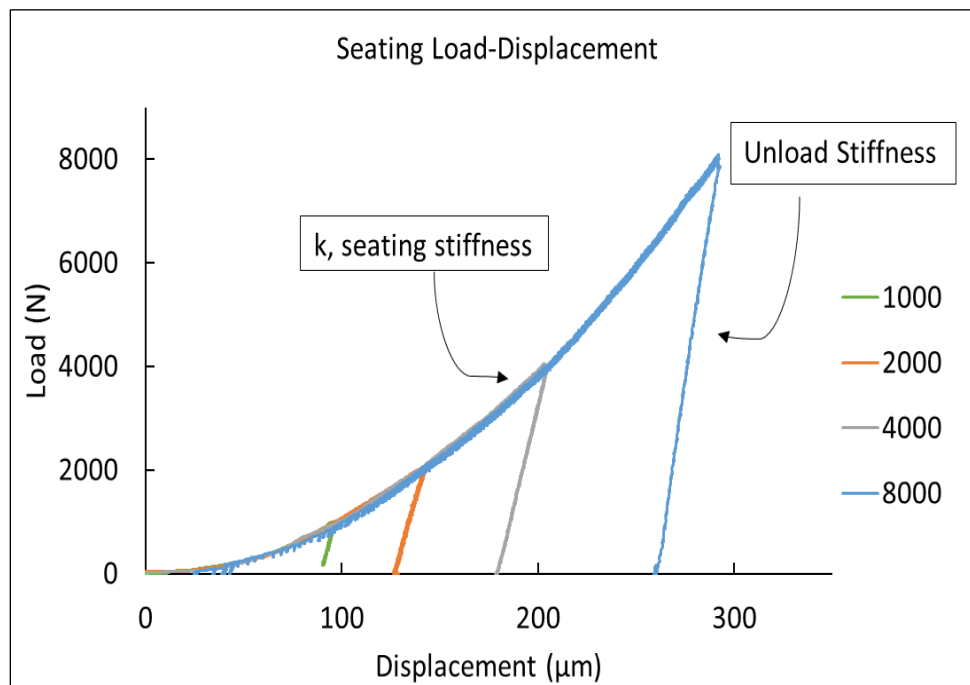
Fig. 76: Average seating load-displacement behavior of 12/14 Ti64/CoCr load magnitude samples.

The characteristic load-displacement behavior of the 12/14 Ti6Al4V/CoCrMo taper (Fig. 76) indicates a consistent load and unload stiffness during testing. The unload stiffness shows the

108

elastic-based deformation/compliance behavior. The seating stiffness, k, is dependent on taper design, coefficient of friction, material combinations and surface roughness. Despite the peak load the seating stiffness (k) is relatively similar across all seating loads. These seating load-displacement curves are unique to the design-material-surface topography combination used and may provide important information related to the locking interaction as a function of taper design and material factors. A theoretical algorithm may be developed which can determine seating displacement as a function of load applied when taper characteristics are known.

The relationship between seating load magnitude and seating load-displacement showed a similar response to previous studies [47, 60]. Pull-off load testing, a standard taper stability assessment method, also showed a linear response. Gilbert et al. describes a mathematical relationship between the initial seating load and the corresponding pull-off load where pull-off loads are approximately half the initial seating load depending of taper characteristics [9]. As the load increased displacement increased linearly but from 0 N to 1000 N there is no linearity. It can be inferred by Fig. 21 that a large amount of displacement occurs at lesser loads (< 1000 N).

Testing also showed seating load orientation up to 20° had no significant effect on seating displacement, work of seating or pull-off load. The average pull-off load plots appear to indicate that with increased mis-orientation beyond 20° the pull off load may decrease further.

There are limitations to this study. Each sample was placed directly under the load applicator but if a sample were to be placed off-axis the load applied to the sample could differ causing varied motions. Motion recorded during testing was only able to capture rocking and pistoning but foregoes twisting and off-axis rocking during loading due to sensor placement.

4.1.2 – Taper Contamination

The effects of contamination on the static seating and pull-off behavior of contaminated taper junctions simulating surgical scenarios were quantitatively studied in an instrumented seating and pull-off test. After quantitative measurement of seating, pull-off loads were captured to measure taper locking stability. The introduction of solid contaminants to the taper junction significantly altered the seating mechanics (seating load-displacement behavior and work of seating). Fig. 77a illustrates dry taper assembly, the head engages with the neck at a lower point and the superior and inferior portion seat equally. In Fig. 77b the head engages considerably higher due to the solid contaminant.
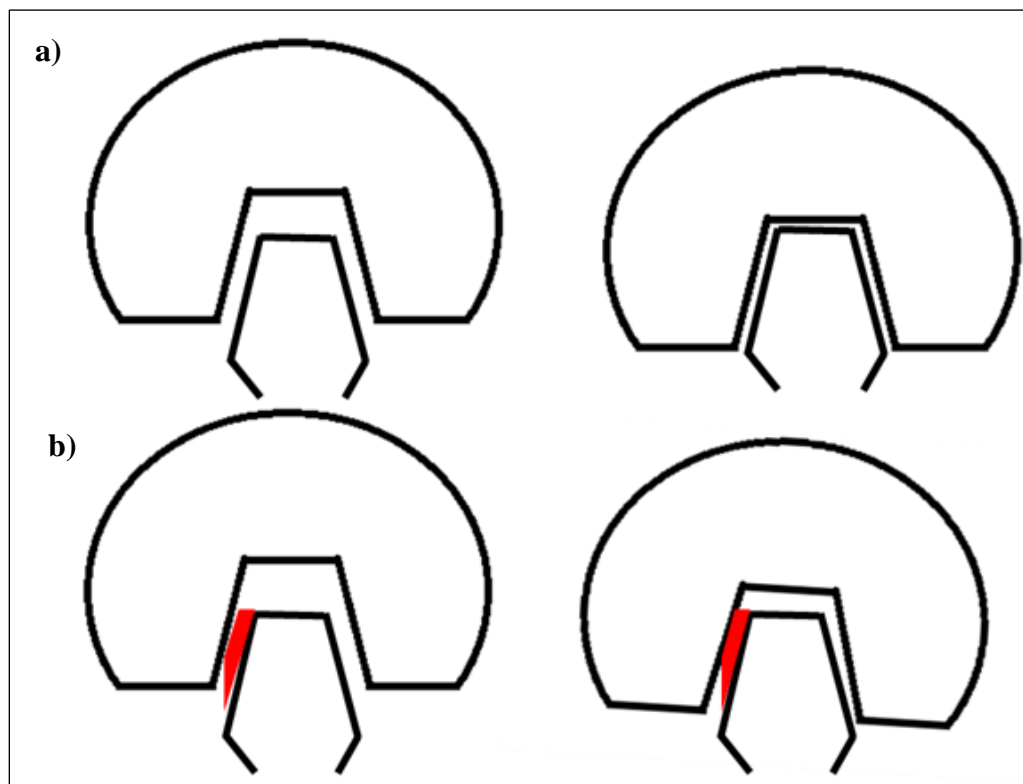
Fig. 77: Seating schematic of (a) dry assembled and (b) contaminated taper junction. The initial contact point of the trunnion is higher in the contaminated schematic. The contaminated junction also highlights uneven seating of the head, with higher seating displacement in the inferior compared to the superior (canted seating).

As the load is applied the non-contact sensors record larger displacements which are required to overcome the presence of the contaminant and reach the final seating displacement

point. The schematic also demonstrates the canting behavior caused by solid contaminants leading to varied seating between the superior and inferior sensors. The inferior sensor recorded 10-40 µm of greater seating displacement on average than the superior in the solid groups. The seating load-displacement behavior of a solid contaminant sample also captures a slipping phenomenon captured by both sensors at a low load level (Fig. 78). This slipping is the result of crushing and spreading of the solid contaminant into the constrained taper gap region. In the solid fat samples during slipping, there is a rendering of the solid fat into liquid which is then distributed about the taper gap. The slipping, caused by the contaminant, accounts for a large amount of the seating displacement captured during testing.
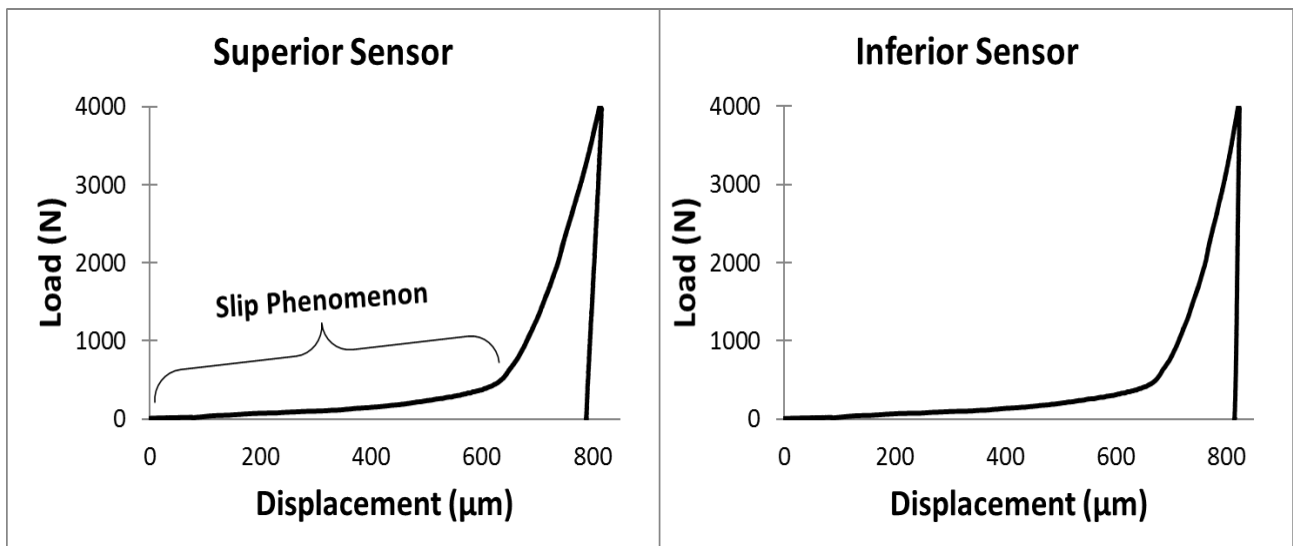
Fig. 78: Seating load-displacement graphs illustrating slip phenomenon in solid contaminant sample. Slipping accounted for a large amount of seating displacement.

After slipping the head-neck taper begins to engage and lock at the max load. After testing, the bone chip and solid fat contaminants were highly deformed and compressed in the taper gap region (see Fig. 79).
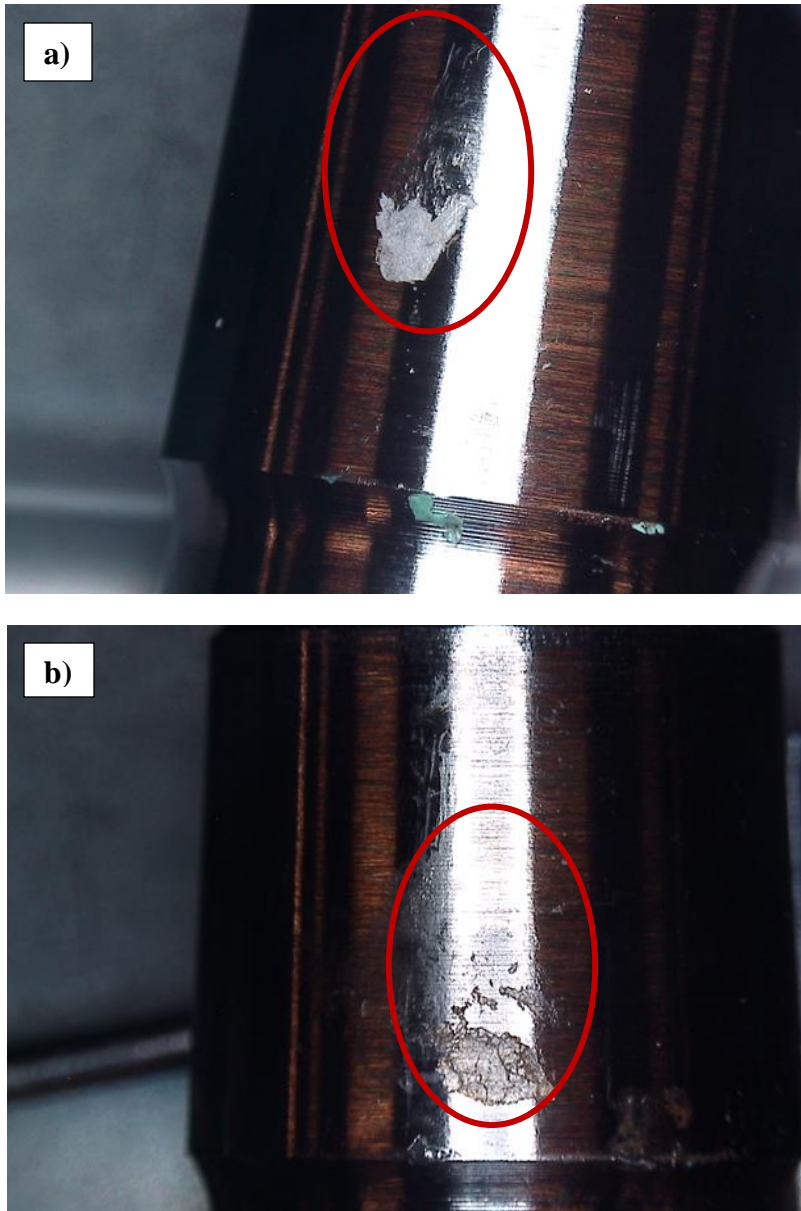
Fig. 79: Image of the deformed compressed a) bone chip and b) solid fat on the trunnion after testing (highlighted by the red circle).

Post seating, the pull-off loads were calculated and plotted in Fig. 30. Pull-off load values, used to assess the stability of the taper, are typically half the seating load depending on the taper geometry, coefficient of friction, etc. [9]. In this study, liquid fat samples on average recorded higher pull-off loads than three of the four remaining groups with an average pull-off load of ~3500 N. In some instances, the liquid fat samples recorded values greater than the initial seating load. These findings indicate liquid fat increased taper stability during testing. The exact

reasoning for this is not entirely understood but the liquid fat in the junction could have acted as a lubricant increasing the seating displacement versus the dry group leading to increased taper stability. The fat would then be squeezed out of the junction due to loading. The image in Fig. 80, shows the coagulated buildup of the liquid lipids at the bottom of the trunnion which led to the previous assumption.

Fig. 80: Coagulated ring buildup of liquid lipids about the base of the trunnion post testing. The image indicates a significant amount of the applied contaminant is squeezed out of the taper junction during seating.

Testing was completed on the same servohydraulic system using the same sensors but was still subject to certain limitations. The samples during axial loading could have toggled and/or rocked off-axis which would not be accurately read in the two sensor configuration. The exact dimensions of each contaminant was closely controlled but still may have had some variability which may have led to variability during testing.

4.2 – Goal 2

4.2.1 – Load Magnitude ICFC

The effects of seating load magnitude on incremental cyclic fretting corrosion and pull-off loads simulating surgical assembly and clinical use were quantitatively studied using micron-level displacement measuring methods. Such ICFC data may assist in better understanding the direct link between taper mechanics and fretting corrosion behavior as well as surgical factors associated with taper locking mechanics and performance.

Fretting corrosion, micromotion and subsidence of tapers were captured and used to determine how seating load magnitude affected taper locking stability and performance after cyclic testing. The data revealed, despite the consistency in micromotion between the groups that the lower seating load groups (1000 N and 2000 N) had increased subsidence post cyclic testing; meaning the heads were not fully seated during assembly and continued to move with increased cyclic loading. The larger error bars in the 1000 and 2000 N groups were due to some sample heads subsiding in one direction more versus the other, i.e. the head would toggle or cant and was not able to seat back down onto the neck under the load. Such variability speaks to the inconsistent behavior seen at lower seating loads. The plots below show the subsidence for a 4000 N sample compared to a 1000 N sample (Fig 81a & b, respectively). Subsidence values were taken at the time of unload after cyclic testing, at approximately 5300 s (circled portion in Fig. 81a).
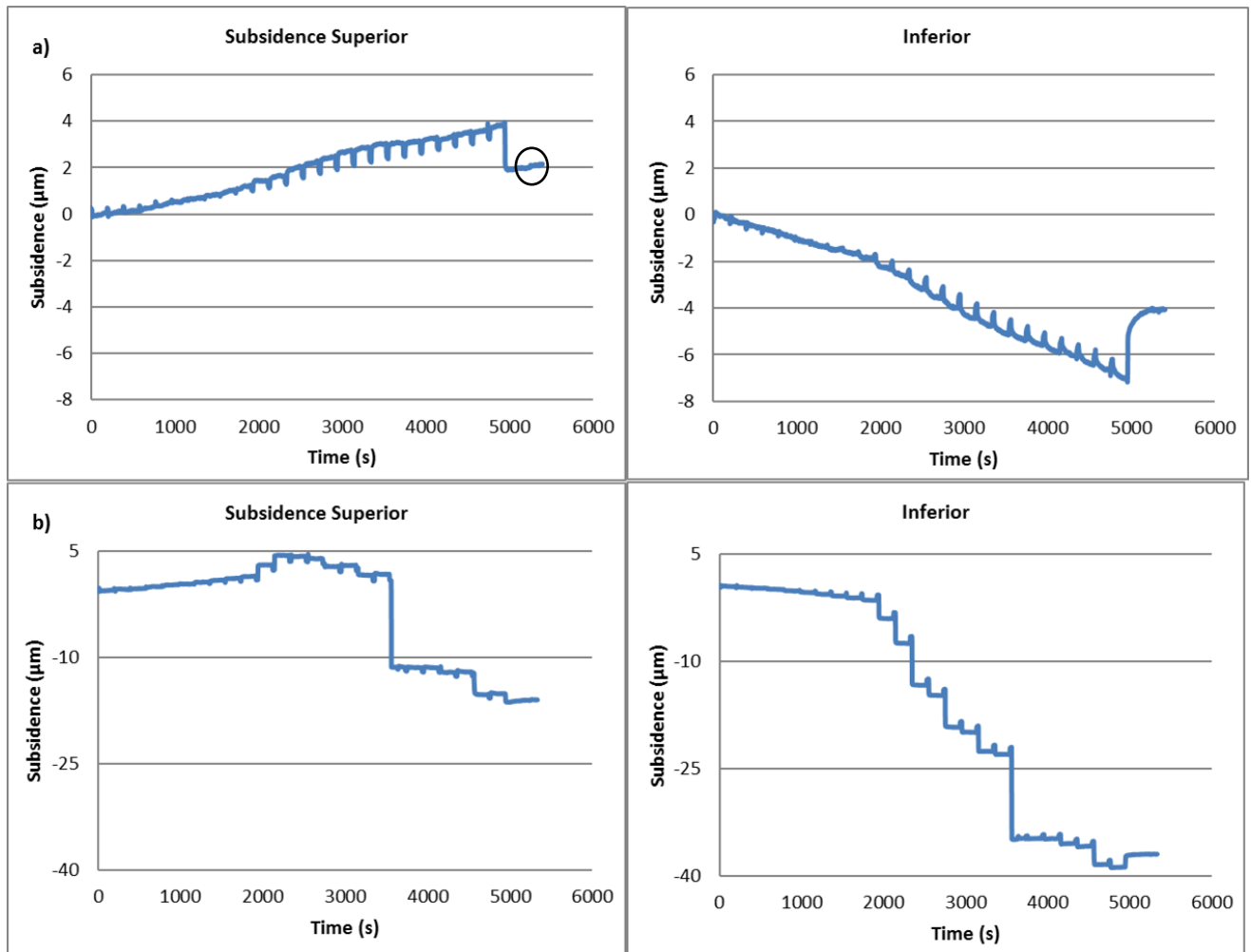
Fig. 81: Examples of superior and inferior subsidence for a) 4000 N and b) 1000 N sample. The 1000 N sample experiences much more negative subsidence in both sensors than the 4000 N sample. Circled portion highlights the final displacement point used to assess subsidence.

In Fig. 81a, the subsidence of the head shows minimal total subsidence of a few microns but also a slight typical rotation as the head is cyclically loaded. The superior portion had a positive subsidence meaning the head marginally separated from the neck; the inferior portion showed opposite behavior. Taken together, these show a rotation of the head on the trunnion. Fig. 81b shows subsidence for a 1000 N seated sample with somewhat similar behavior until ~1800 s (or 1000 N cyclic loading) when the head rotated more significantly before undergoing additional seating down onto the neck at about 3500 s (2800 N cyclic load).

Although there was variation in subsidence between the groups, only the 1000 N group had a statistically lower current onset load. Meaning there is a level of taper stability/interlock ability achieved with a seating load of 2000 N or more, but there is no further improvement in the onset load with seating load beyond 2000 N.

Highlighted as well by the data was the connection between assembly load, micromotion, and subsidence and current at 4000 N. The data suggests the current at the end of testing is dependent upon the initial assembly load. As the seating load increased the current at the 4000 N cyclic load decreased parabolically. Also suggesting that even with a seating force as high as 8000 N, significantly higher than average force used by surgeons, there is still the presence of fretting corrosion [74, 75].

There was no difference between the average onset loads for the 2000-8000 N groups, however, the currents at the end of testing were different. To better understand the corrosion process from onset to the end of testing the current was plotted versus the load. It was observed that throughout testing two characteristic current vs. load graphs were acquired. Fig. 82 depicts the two characteristic current graphs in two of 4000 N samples. Fig. 82a shows a somewhat continuous rise in current after the onset and Fig. 82b shows a rise then plateau then a continued rise again.
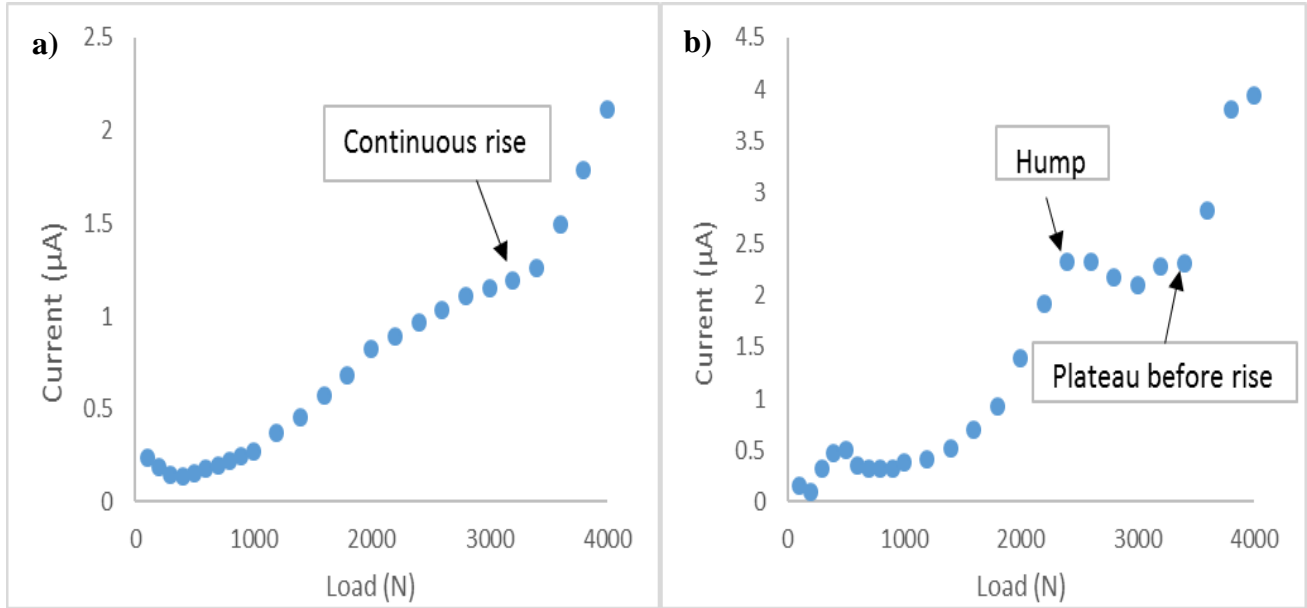
Fig. 82: The two characteristic current graphs of 4000 N samples noted in the text. a) Shows the continuous rise in current behavior, b) shows the rise, plateau then rise behavior of the current after the onset load.

These graphs show as the load increased the current begun to rise post-onset load until the end of testing. Using the same characteristic graph, the current vs. load for both a 2000 vs. 4000 N and 2000 vs. 8000 N sample are compared below.
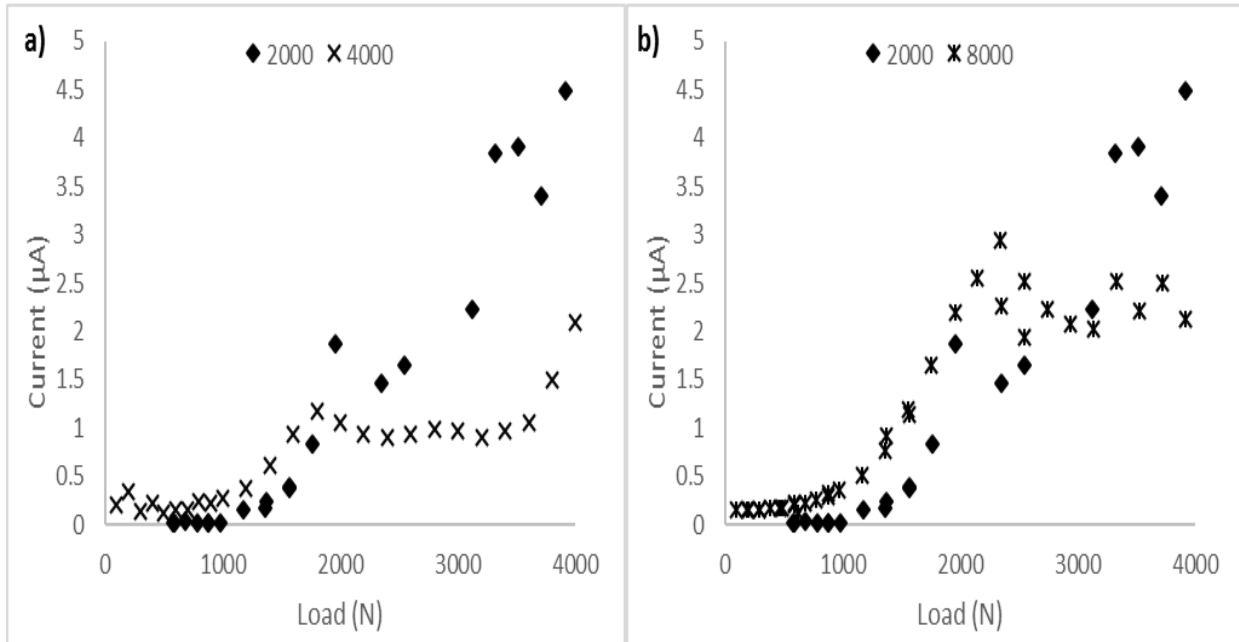
Fig. 83: Current vs. Load for a 2000, 4000 and 8000 N samples. Currents show the same characteristic behavior however the current at 4000 N are statically lower in the higher assembly load samples (4000 and 8000 N).

The comparison in Fig. 83a shows the two samples (2000 vs. 4000) have about the same onset but as the current for both samples rise, the 4000 N sample stops and begins to plateau while the 2000 N sample continues to rise. The onset load for the 2000 N sample is about 400-600 N more than the onset for the 4000 N sample shown. Similar behavior is noted in the 2000 vs. 8000 N samples seen in Fig. 83b, where a plateau in current is seen in the 8000 N seating sample and a lower onset load.

Post cyclic testing, each sample was tested for taper locking stability. Previously published studies support the claim that the typical pull-off load is approximately 40-50% of the initial seating load [60, 76, 77]. The pull-off loads acquired in Goal 1 Section 1 were approximately 44% of the initial load (refer to Fig. 23). In this study, the 1000 N group pull-off loads were on average 148% of the initial seating load magnitude. And the 2000 N group required 90% of the initial seating load to be disassembled. The remaining groups required about 50% of the initial seating load to be disassembled. This phenomenon can be attributed to the

subsidence which occurred during testing, seating the head further down the trunnion in the lower seating load groups.

4.2.2 – Load Orientation ICFC

In an effort to simulate surgical assembly, the effects of seating load orientation on seating displacement, incremental cyclic fretting corrosion and pull-off loads were quantitatively studied. Incremental cyclic fretting corrosion behavior and motion about the taper junction were captured and used to determine how seating load orientation affected taper stability.

As the seating load orientation increased up to a 20°, the average seating displacement behavior as well as the work of seating was not affected. Despite the lack of a change in seating mechanics, there was a decrease in micromotion throughout cyclic testing. Subsidence, though variable, was the same and not affected by changes in seating orientation.

Data from corrosion testing showed although seating orientation initially affected the current onset load there was no quantitative effects on the current at the end of testing. Meaning the 20° group began to corrode sooner than the remaining groups but over the time of testing the other groups began to corrode as much. Pull-off testing, done after cyclic testing, showed there was no statistical difference between the groups.

The overall results of testing suggest that seating load orientation up to 20° has no significant difference on the performance of the implant taper junction. Such ICFC plots may assist in better understanding the surgical factors associated with taper locking mechanics and performance.

Testing assumed that a typical surgeon would apply the same load on axis as off-axis during seating. Decreasing the seating load or the upper cyclic load could reveal a larger variability in performance between the groups.

119

4.2.3 – Taper Contamination ICFC

The effects of incremental cyclic fretting corrosion testing of contaminated head-neck taper junctions simulating surgical scenarios were quantitatively studied in an instrumented cyclic test method. Taper contaminants caused variations in seating load-displacement behavior, micromotion and subsidence as well as fretting corrosion behavior during cyclic loading. The information in this study can be used to better understand the role of contamination on fretting motions and subsequent fretting corrosion.

Subsidence data showed more negative subsidence on the superior portion of the solid contamination groups which could indicate that the contaminants required larger amounts of angled force to be negated. After being ground down, they no longer obstruct the seating motion and when overcome the head sat further down on that portion. The plots in Fig. 84 illustrate a significant change in both the subsidence and micromotion at about 4000 s in a bone chip sample. At approximately 2800 N the assumption can be made the load overcame the bone chip and upon continued cyclic loading the head seated further onto the neck increasing the subsidence and micromotion.
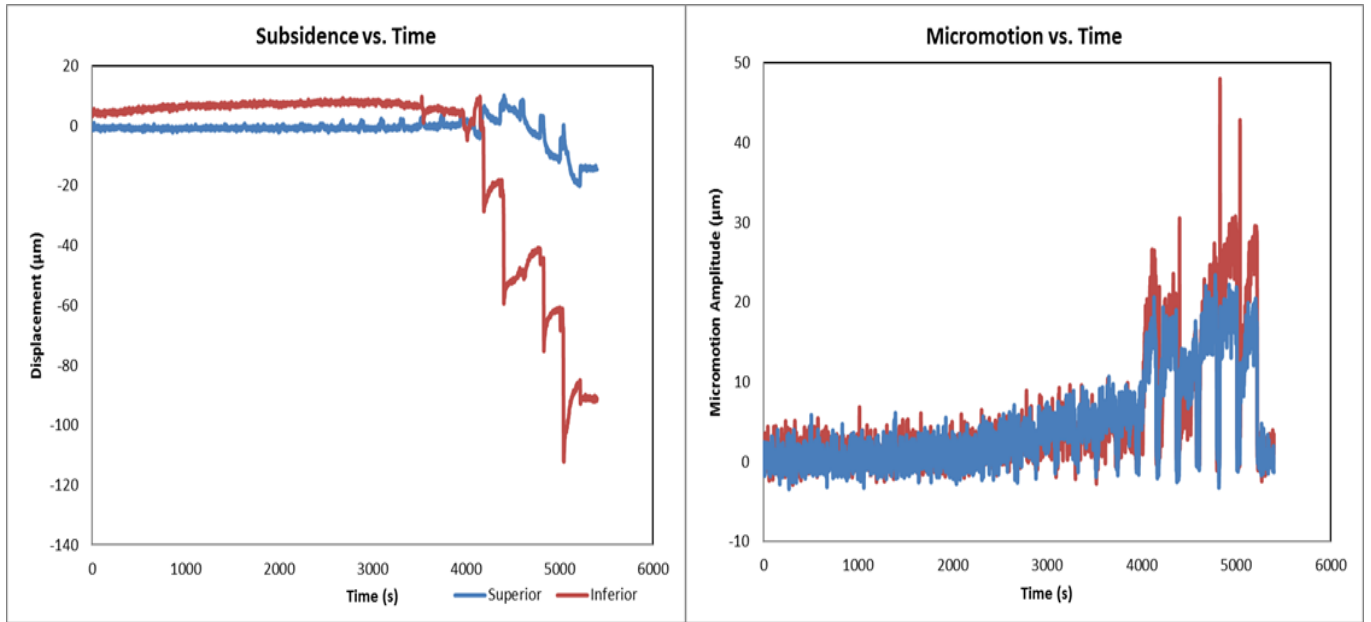
Fig. 84: Subsidence and micromotion vs. time of bone chip sample. The plots show the subsidence of the head onto the neck and corresponding micromotion for both sensors.

Fig. 85 illustrates the same behavior shown in the previous figure, where the solid lipid contaminant is overcome at about 3000 s which leads to a large subsidence and increase in micromotion.
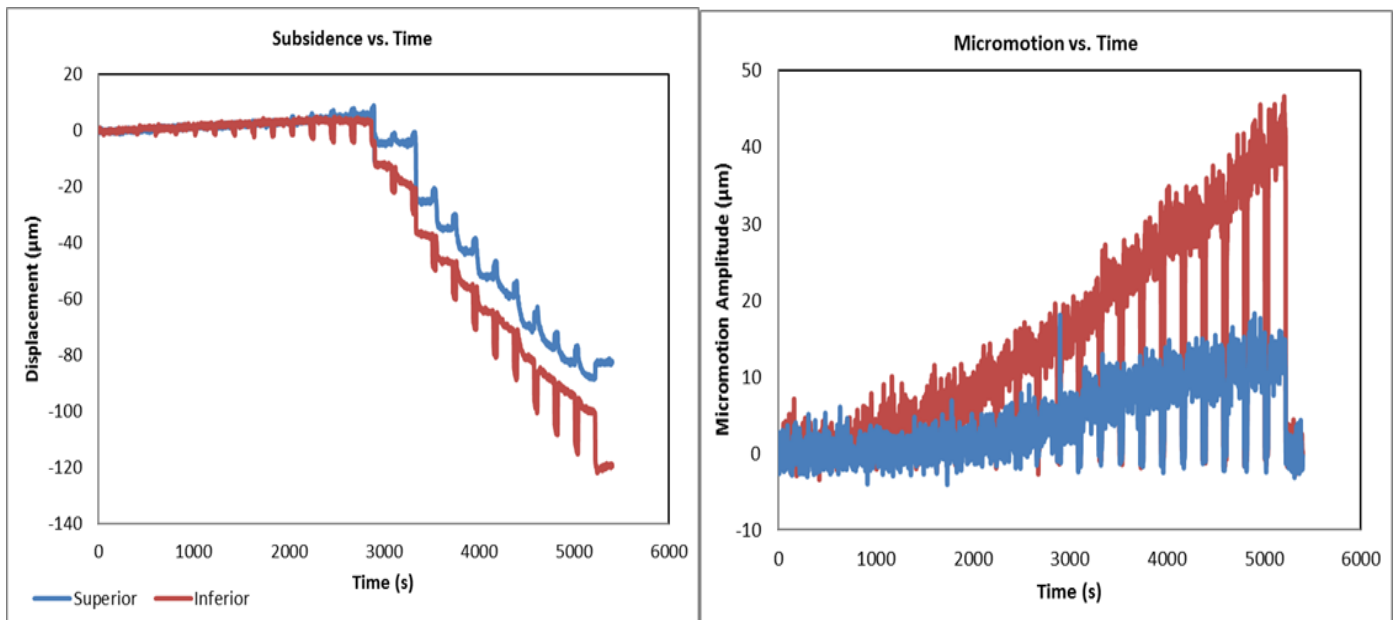
Fig. 85: Subsidence and micromotion vs. time of solid fat sample. The plots show the subsidence of the head onto the neck and corresponding micromotion for both sensors.

121

Yet despite the similarities in the two load-displacement plots throughout the course of testing, the solid lipids group displayed a unique phenomenon. As the micromotion and subsidence increase due to the contaminants, the current in the solid lipid group does not deviate from the baseline while the bone chip current rapidly rises with the increase in loud (Fig. 86).
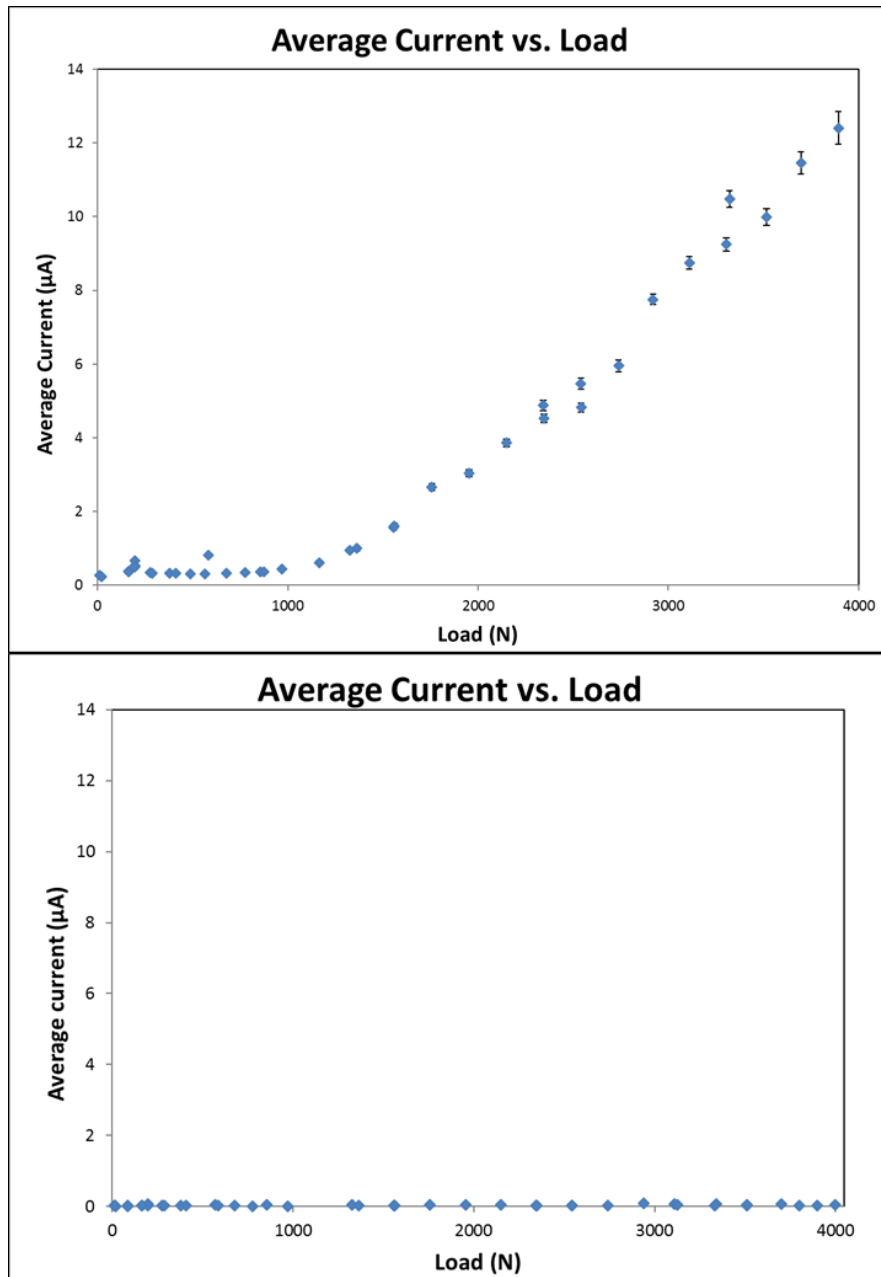
Fig. 86: Average current vs. load of the (a) bone chip and (b) solid lipid samples. The plots show the increase in average current throughout testing in the bone chip sample. However, there is no increase in the average current in the solid lipids sample.

Data from testing suggests the fat was overcome and extruded to the mouth of the junction creating a hydrophobic seal around the opening of the junction preventing the ingress of liquid which inhibited the fretting corrosion process. This can be seen in the image below (Fig. 87), where the fat created a seal of sorts around the base of the junction which altered the fretting corrosion response.
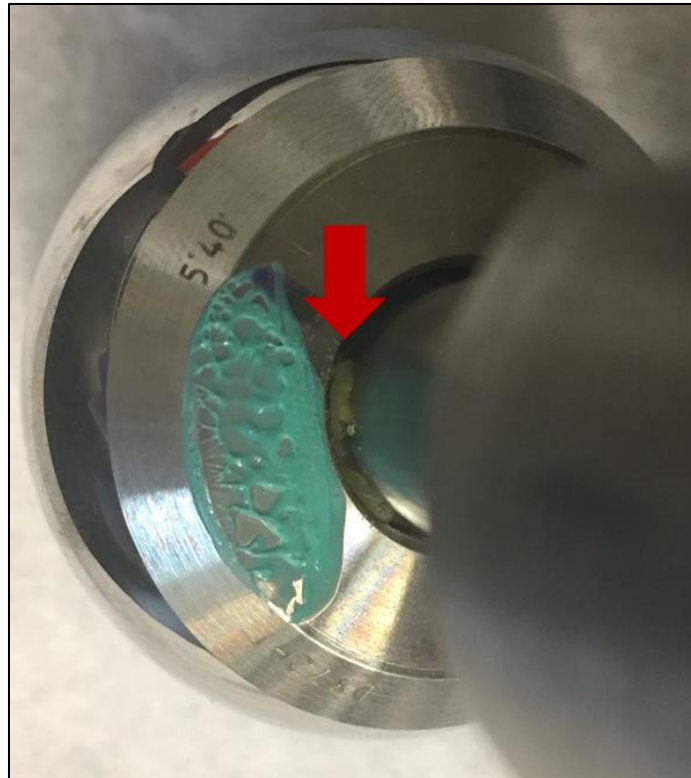
Fig. 87: Image shows the mouth of the head-neck taper where a ring of fat (indicated by the red arrow) has built up.

Testing was subject to a few limitations. Sensors were only able to capture up to 1 mm of displacement but during the seating of solid contaminant groups, the displacement exceeded the sensing range. To overcome the limitation, the samples were loaded from 0 to 1000 N, the sensors were then repositioned and the samples were loaded from 0 to 4000 N. Displacement was captured for both loading sequences (Fig. 88 a & b). Fig. 88c demonstrates how the two plots were combined, the displacement from the 0-4000 N seating test was shifted to align with

the end of the 0-1000 N test. The final seating displacement and work of seating could then be calculated.
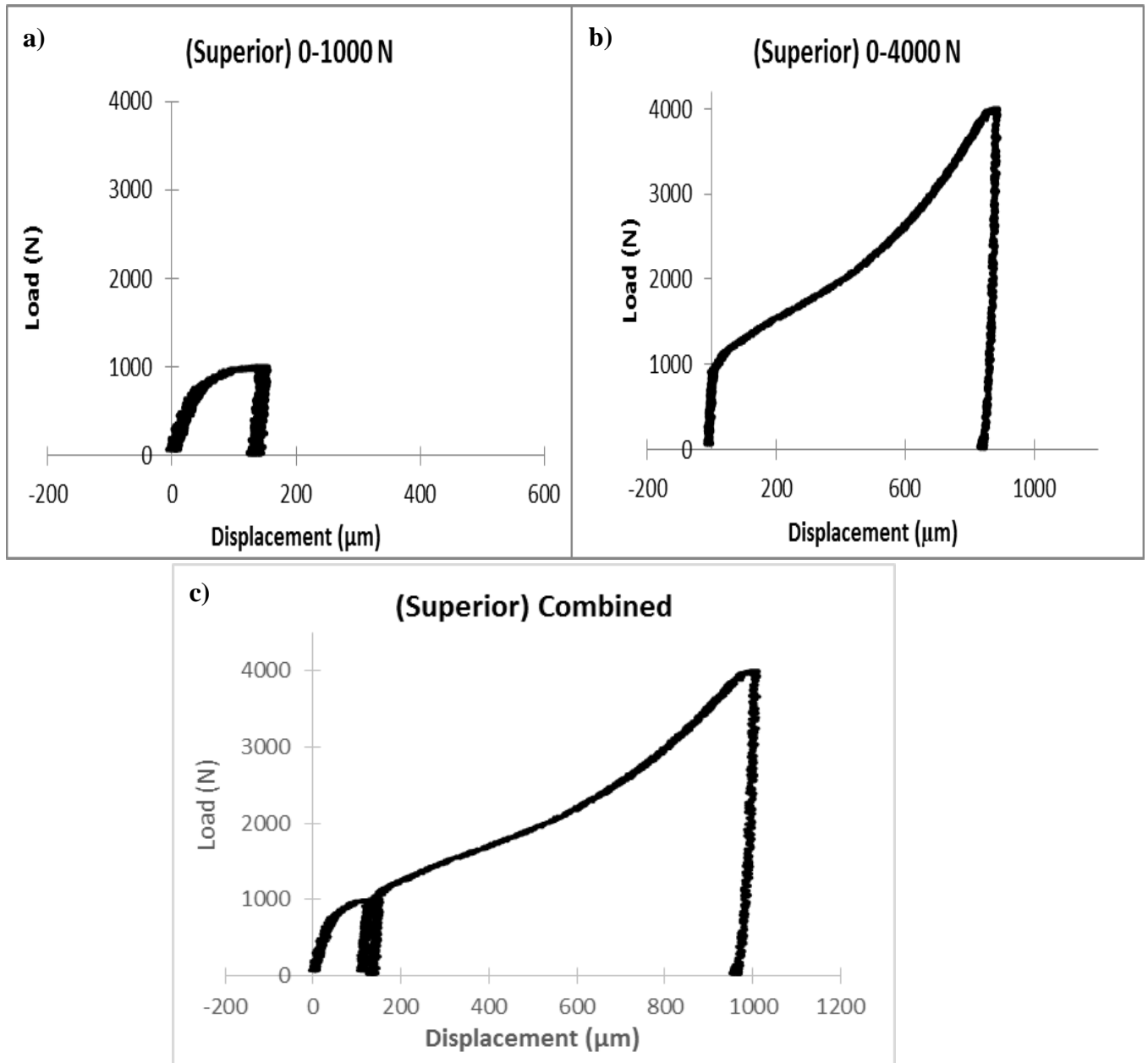
Fig. 88: a-c) Seating load-displacement graphs for a bone chip model. These graphs show a limitation in the working range of the sensors. Because of the limited range, seating had to be done in two separate load applications and merged together in an Excel file.

Positioning of the sensors also led to limitations. The sensors were able to capture positioning, toggling and rotation about one-axis but were not able to capture torsion which

124

could have been amplified due to the contaminants. Lastly, a weakness of this study was the large seating load (4000 N) was used to seat the tapers. It is likely a surgeon who induces significant contamination may also be likely to not seat the taper to as large a seating force as studied in this work. Additional work on contamination of poorly seated tapers may reveal more significant adverse effects on fretting corrosion of taper junctions than this high seating load case has.

4.2.4 – Taper Design and Material Combination

Literature indicates that the design and materials in modular taper junctions influence the overall performance of modular taper junctions [17, 78-80]. Goldberg et al. and Jauch et al. devised test methods, which were able to assess the effects of design elements and materials used in specific modular hip implants on the fretting corrosion behavior. Both reported the increase in failure mechanisms with an increase in load [8, 47]. In this study, the in vitro incremental cyclic fretting corrosion test method was used to compare the geometrical performance of C vs. V40 tapers as well as material design of Ti-6Al-4V vs. TMZF under incremental cyclic loading. This study demonstrated a combined measurement of micromotion and fretting corrosion of head-neck modular tapers in total hip replacements, where direct correlations between fretting motions (micromotion and subsidence) and fretting currents can be seen. This test method monitored seating of the taper, which is a beneficial approach to assessing the seating mechanics (load vs. displacement behavior).

The hypothesis of this study was taper geometry and material combination would affect the seating displacement, fretting motions (micromotion and subsidence) and fretting currents throughout ICFC testing. The data showed at the end of testing taper geometry affected the

125

stiffness of the construct, micromotion, onset load and current at 4000 N. Alloy combination did not have an effect on taper performance.

Geometrical taper comparison.

Comparatively between the three implant groups there were no statistical differences in seating displacement or work of seating. Seating showed examples of canting, where within certain instance there were recorded sensor displacement differences of 20 to 30 µm, throughout experimentation, favoring lower seating in inferior portion. This could prove taper geometry does not have a significant effect on the head displacement during seating or the associated work done. One would expect the taper geometry to play a crucial role in the head displacement and engagement of the head on the neck.

Data from the static calibrations show that the C Taper (G2) is a statistically stiffer than the V40 Tapers, thus geometry plays a role in the stiffness of a construct (P<0.05). Groups 1 and 3 were not different in terms of stiffness values recorded.

Geometry of the taper junction was also shown to have an effect on the onset load of the samples. The data recorded during incremental cyclic loading showed the C Taper (G2) had a higher onset load compared to the V40 Taper groups (G1 and G3) (P<0.05). Group 1 and 3 did not have different onset loads.

Outlined in Table 1 were the geometrical differences between the C and V40 taper with differences in conical taper diameter, engagement length and taper angle. Based on the results of testing and these differences one can assert that taper engagement length, conical taper diameter and taper angle play a role in taper mechanics and therefore taper performance.

126

Material comparison.

The two alloys tested, Ti-6Al-4V (G1) and TMZF (G3), were assessed and compared by the average onset load and average fretting corrosion current at 4000 N.

The average onset load and average current at 4000 N showed the two V40 taper groups performed similarly throughout cyclic testing and were not statistically different despite the change in material combination.

This study provides a new experimental test design which is a simple, reliable and innovative approach to evaluate the tribo-electrochemical behavior of taper design that can predict its ICFC performance. These tests are not meant for assessment of long-term performance but focus on quick assessment of design elements. Correlations of mechanical factors (e.g., stiffness, micromotion, subsidence) with fretting currents can be assessed with this test.

The conclusions from testing were also affirmed by Higgs et al. in a retrieval study where taper damage was assessed in samples which differed in taper geometry as well as material combination [73]. Higgs et al. reported no difference in the amount of damage in sample groups which consisted of the same material combination but noted an increase in the likelihood of damage when comparing V40 tapers to C tapers.

Weakness of the study. However, there were weaknesses in this study. For example, in seating, the initial placement of the head can cause the head to seat differently but the variability was overcome by comparing the rigid body position after seating the head to position at 100 N. This provided a consistent datum point for assessing the displacement. The seating load applied throughout this study was a 2000 N anatomical load which is not clinically relevant and therefore a weakness of the study. However, the methodology of seating displacement measurement is advantageous in understanding the seating mechanics of a particular taper junction.

Also, while fixing the sensors to the neck of the implant, the lack of rigidity of the fixture may lead to movement and variation in the recorded data in testing. The method of fastening the fixture to the porous coating of the implant with nylon screws works very well but has to be carefully placed to not touch the acrylic or silicone base which would also influence the resulting measurements when loaded.

Static calibration measurements should not have any significant subsidence present because the calibration was done post cyclic testing. However, the micromotion amplitude may be incorporated into these measurements. This has the effect of increasing the measured motion over and above the elastic-only motion. Thus, the stiffness parameters will be underestimates of the true sensor stiffness.

The magnitudes of micromotion at interface will likely be smaller than those recorded any distance away. In the future, using rigid-body mechanics methods, the motion at the sensors can be used to calculate the motions of any point on the affiliated rigid body system. To do this, the 2-D motion measured can be calculated from the combination of a translational vector – applied to all points of the body, plus a rotation about an axis normal to the plane occurring at one point in the body. All other points in the body can be determined by the translation, plus the motion resulting from the rotation and the radial distance between the point of rotation and the point of interest.

This is summarized in Fig. 89, which depicts two points A, B, move to A'B' which is made up of $\rho_{AA'}$ and $\omega\rho_{AB}$. That is, the motion of any point, B, can be found by translating that point the same amount as point A, and then rotating ($\omega\rho_{AB}$) to move B" to B' to find its final location. The distance between the two points and the difference in the two points motions are

used to find ρ_{AB} and ω, respectively. Once known, these parameters can be used to find how any point in the rigid body moves.
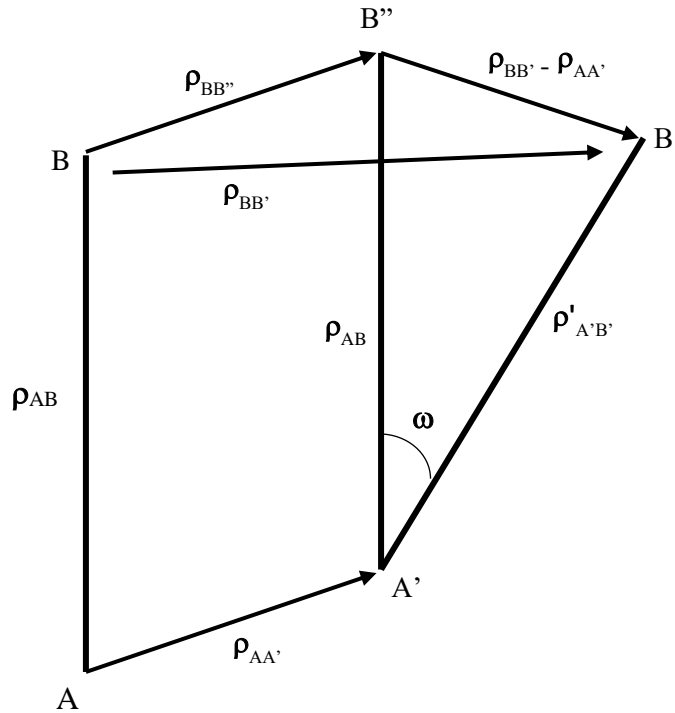
Fig. 89: 2-D translational vector relationship which could be used to determine the motion of a point in respect to a known position [81].

4.2.5 – Impaction Assembly ICFC

In this study the effects of impaction seating load on 12/14 Ti-6Al-4V/CoCrMo taper junctions were evaluated using an incremental cyclic fretting corrosion test method. Taper performance was quantified using micromotion and subsidence as well as fretting corrosion onset load and fretting corrosion currents recorded throughout testing.

The hypothesis of this study was an increased in taper assembly load would reduce fretting motions, therefore reducing fretting corrosion. This study showed there was a statistical

difference in stiffness, micromotion, subsidence and onset load between assembly load groups. The hand-assembled samples reported a lower stiffness than the impacted groups, the impacted groups were not different from one another. Similar results were seen in the average micromotion and subsidence data, the hand-assembled samples were reported larger micromotion and more negative subsidence than the impacted groups. The impacted groups were not statistically different. However, the average onset load increased as the assembly load increased (P<0.05).

The compiled results of testing show a larger onset load is a beneficial condition and signifies that a higher cyclic load is required to induce fretting corrosion at the taper junction. The average fretting current at 4000 N for a taper interface, also an indicator of fretting corrosion performance indicates that there is fretting corrosion damage taking place during testing.

The results of testing also indicated that impacting samples with higher impact loads increased taper locking thereby reducing micromotion between the non-impact group and 14 kN group. Impaction load magnitude also influenced the magnitude and orientation of subsidence, the non-impacted group demonstrated greater subsidence of the head onto the neck throughout testing while the impacted groups exhibited smaller subsidence and mostly positive movement on average. That is, for the 6 kN samples, the average subsidence was positive indicating that the heads moved up off of the taper.

Subsidence data for 6 kN and 14 kN impacted samples showed that the head begin to dislodge (move positively) during cyclic loading. This may signify that the cyclic loads, assisted by the locking pressures developed during seating synergistically combine to result in a pushing of the head off of the neck with cyclic loading in a ratcheting, elastic type of motion. That is, during seating, the impaction force results in the development of a pressure across the taper

interface and a friction stress along the interface. These two stresses remain present after assembly and represent the locking interaction. As cyclic loading occurred, and the onset load was surpassed, the combined stresses of loading and locking interact to cause the taper to move upward attempting to push the head off of the neck. The elastic deformation at the junction was then able to overcome the locking pressures which held the head fixed and allowed for slight upward displacement. Fig. 90 displays the onset load for a 14 kN sample as well as highlights the upward subsidence observed in each sensor. The onset of positive subsidence corresponds to the onset load where fretting currents develop, indicating the motion results in fretting currents.
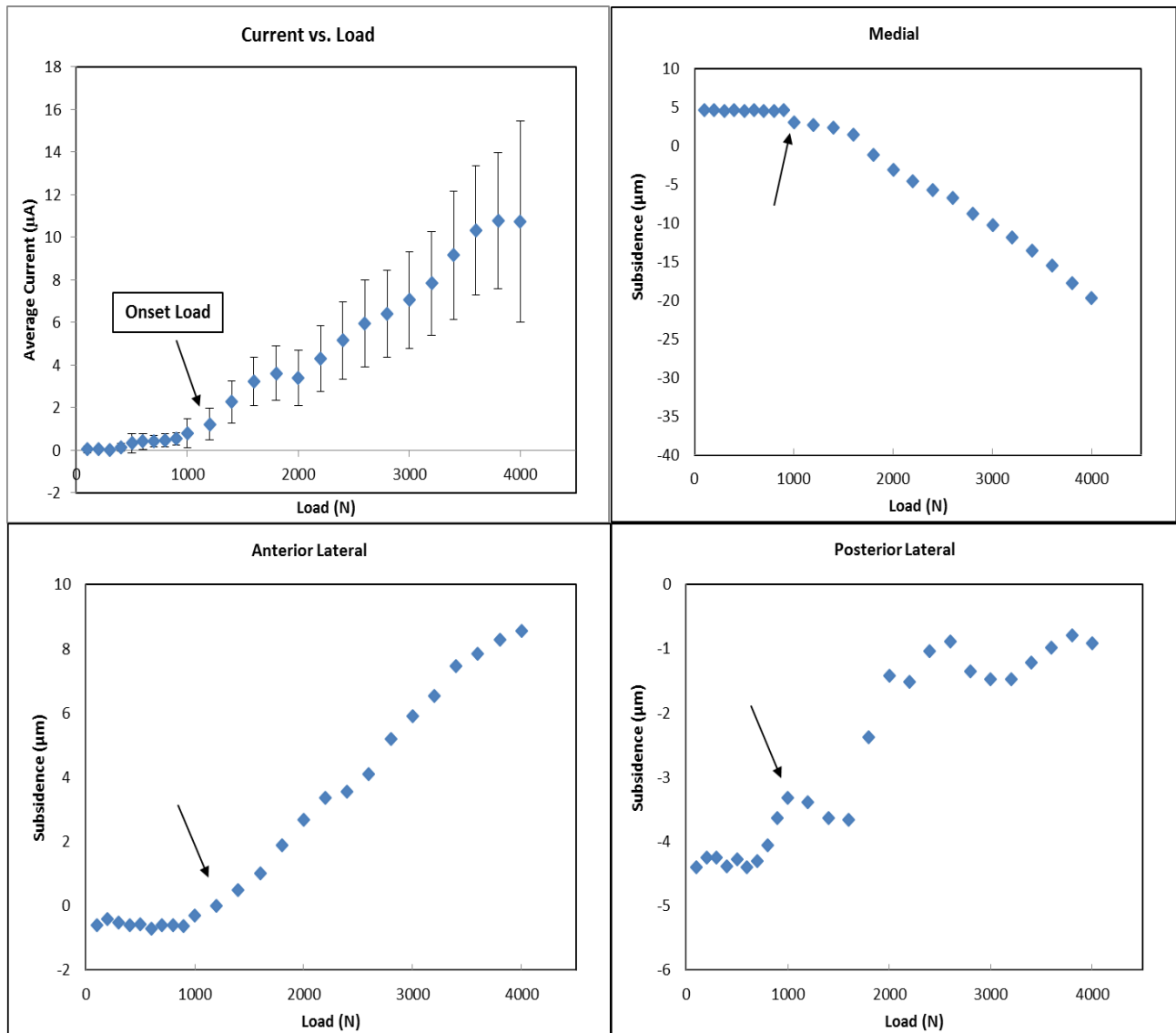
Fig. 90: Average Current vs. Load and Subsidence plots for 14 kN sample which displayed positive subsidence during cyclic loading (arrows highlight onset load).

Limitations present in the study were the inability to capture seating displacement during impaction due to sensitivity, durability and size of the sensors in the setup. Understanding the seating mechanics (load vs. displacement behavior) off the samples may have been insightful in analyzing their behavior during cyclic testing.

The seating method which impacted the femoral head three times and allowed the impactor to come to a complete rest before being reset may have altered taper performance. Large impaction forces may cause plastic damage to surface of the trunnion and abrade the oxide

132

film which will commence the corrosion process. These large impaction forces and subsequent rebound forces due to the impactor coming to a complete rest may also cause significant reaction forces which may lead to dislodging of the head. If the head were to dislodge prior to the next impaction or cyclic test, the head may improperly seat.

4.3 – Goal 3

4.3.1 – Load Rate and System Compliance

The purpose of this study was to assess variable surgical factors such as load magnitude, load rate and system compliance and the effects on seating behavior (displacement and work of seating) and taper stability. These variables were chosen to replicate and correlate to clinical scenarios with inconsistent factors such as surgical technique, strength and patient physiology. The compliant setup was modeled after cadaveric data collected by Stryker; rubber mats were used to simulate a patient's leg.

Researchers such as Heiny and Scholl et al. have established an identifiable relationship between seating load magnitude and immediate taper stability [10, 82, 83]. Based on an equation by Gilbert et al., the taper stability post-seating is approximately 50% of the initial seating load depending on taper characteristics [9]. Data from the current study affirms the conclusions and equation presented above. Taper stability for the static and impacted samples was approximately 45% of the seating load. As the seating load magnitude increased the seating displacement and pull-off increased linearly. The work of seating also parabolically increased, consistent with data from Pierre et al. [84].

The insignificance of load rate and compliance were also proven by this study. The load rate between static and impacted samples in the non-compliant setup differed by nearly a factor

of 10,000. Despite the tremendous increase, the work of seating and pull-off load for all non-compliant samples within the same load magnitude range were statistically similar. Comparison between the compliance setups was primarily done between the static sample groups because of the high amount of variability in the impacted groups. The data implies that compliance in this setup had no effect on the seating displacement, work of seating or pull-off load. Combining the two insights shows despite the setup and despite the assembly method if identical samples are loaded similarly in terms of orientation and load magnitude, taper stability will not be compromised. The system in Fig. 91 shows the impulse (ΔF) applied to a head and stem on a compliant substrate.
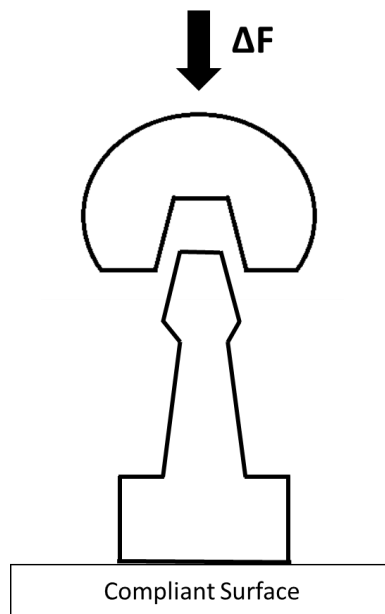
Fig. 91: Schematic showing the impulse (ΔF) applied to the system on a compliant substrate.

This system is governed by the equation

$$\int_0^t F * dt = \int m * dv \quad (\text{Eqn. } 14)$$

Where F is force, dt is the change in time, m is mass and dv is the change in velocity.

134

The system can be dynamically drawn as an impulse applied to the mass of the head (m_H) attached to the mass of the stem (m_S) by a spring constant of the head (k_H). There is also a spring constant for the stem and the substrate (k_S) due to compliance. The displacement of the head and stem can be defined by Δ and φ, respectively. And the displacement between the head and neck can be defined as δ (see Fig. 92).
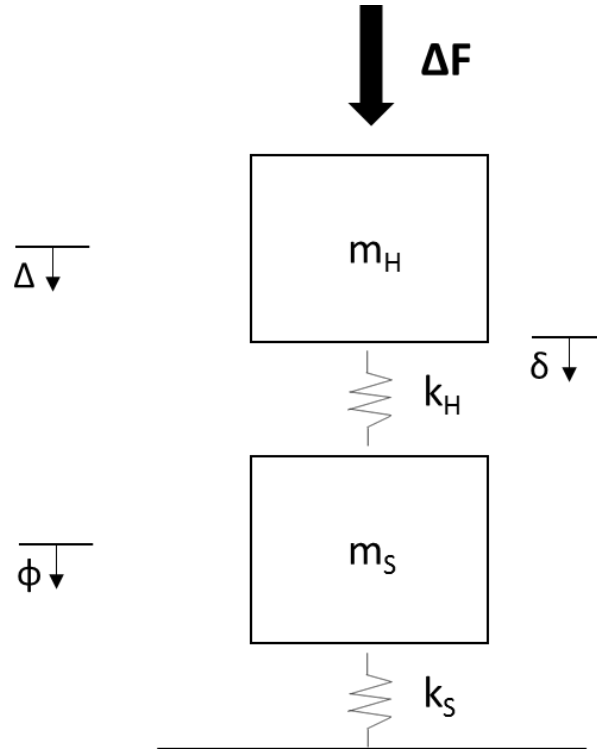
Fig. 92: Dynamic schematic of a compliant system where the variables are defined in the text above.

The equation for both the head and stem can be resolved as

$$m_H \frac{d^2\Delta}{dt^2} = \Delta F * k_H * \delta \quad \text{and} \quad m_S \frac{d^2\varphi}{dt^2} = \Delta F * k_S * -\delta \quad \text{(Eqn. 15 \& 16)}$$

These equations integrate the spring constants and displacement between the two systems into Newton's 2nd Law, F=m*a.

The resonance frequency, defined as an external force driving another system to move with a greater amplitude can be determined for head (ω_H) and stem (ω_S),

$$\omega = \sqrt{\frac{k}{m}} \qquad \text{(Eqn. 17)}$$

where in a head seated to 100 μm with a 4000 N force has a k of approximately 4E-7 N/m. The

k_S is approximately 10^3 N/m, as shown by the compliant load rate found during experimentation.

Based on the components, the mass of both systems are similar which can then be negated and

the remaining resonance equation is dependent upon the spring constant for either system. It can

then be determined that if $\omega_S \ll \omega_H$ then compliance does not matter, highlighted by Fig. 93

which shows the relationship between the motion of the head, the stem and the head onto the

stem.
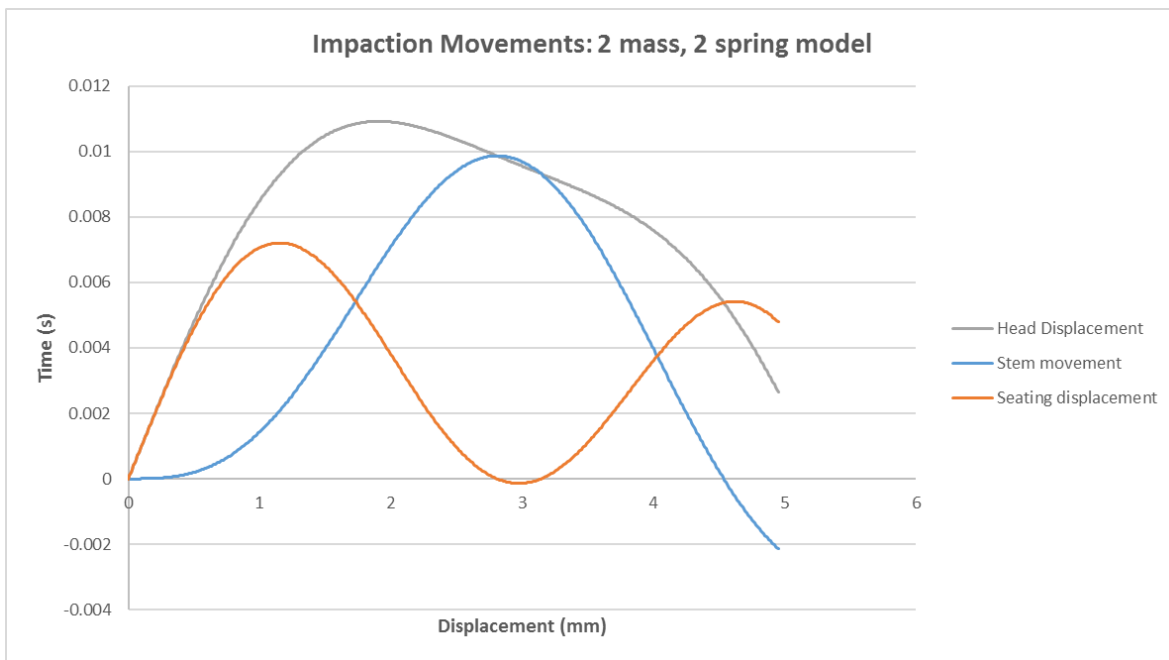
Fig. 93: Plot of the two mass systems and two springs as shown in Fig. 95 during an impulse in a displacement vs. time graph. The plots show as the impulse is applied over time full amount of seating displacement is achieve prior to the stem movement. This highlights that compliance is a non-essential factor during impaction.

Moving on, an observation noted during testing was the difference in energy necessary to

achieve the same impaction forces between the non-compliant and compliant setup. The

compliant group required approximately 42-50% more input energy than the non-compliant

group. Similar results in input energy were seen in cadaveric femoral studies where reasoning for the said effect was due to a damping effect caused by the excess biological material (bone and tissue) simulated by rubber in the presented study [85, 86].

The study was constrained by limitations in the high-speed camera system. The system was calibrated and verified using a non-contact eddy current DVRT and ARAMIS imaging system (Fig. 94a).
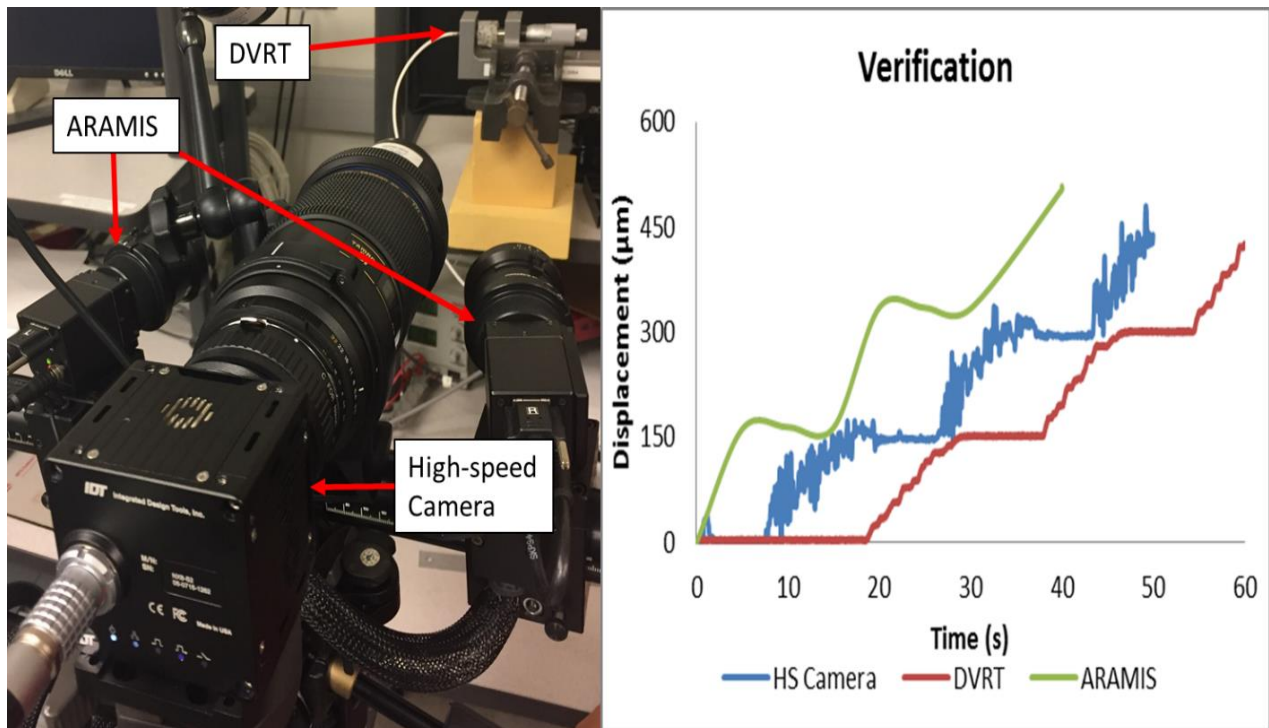
Fig. 94: (a) Three system verification. (b) Displacement vs. Time plot for three systems. The verification was done to assess the reliability of the high-speed camera versus systems that are more commonly used but weren't capable of capturing displacement in this study.

The three systems were fixed to a micrometer which displaced 100 µm every 5 s, each system output similar displacement data, a time sync was not applied (Fig. 94b). Though the verification process shows the displacement captured by the camera is correct, the displacement measured during non-compliant seating shows the seating displacements for the impacted samples were greater than the static counterparts. The displacement differences are unlikely because the work of seating is dependent on the load vs. displacement which did not show a

difference. The inconsistency in displacement data could have arisen in the motion tracking software which was dependent upon a fixed point on the head and neck which were not in the exact plane of focus (Fig. 95). The planes being out of focus could have led to increased displacement data during data analysis when in reality the sample is rocking to and away from the camera system.
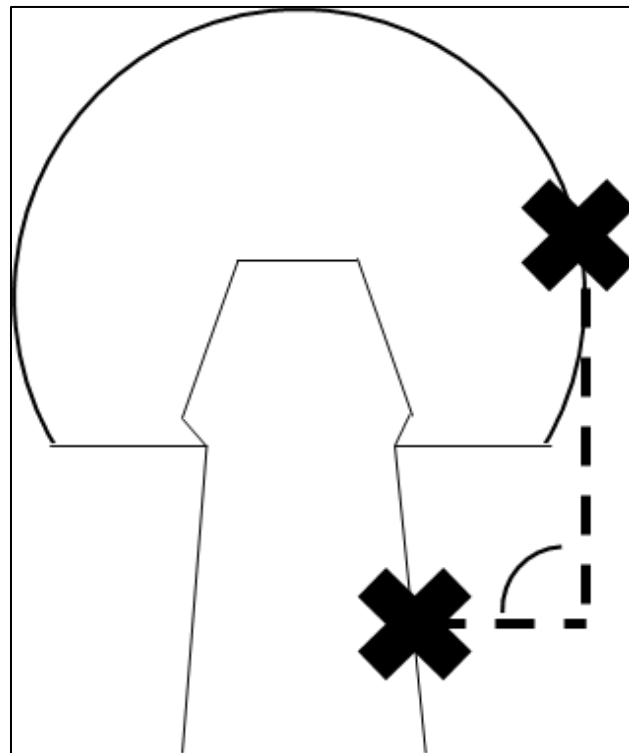
Fig. 95: Tracking point schematic of the camera on the system. The schematic shows the points on the head and the neck are not in the same focal plane which can lead to incorrect displacement data during testing.

Lastly, the camera system was limited by the resolution and its ability to limit the recording rate. The increase or decrease in resolution allowed the camera system to record less or more frames per second but decreasing the resolution decreased the field of view as well as the ability to track points during data analysis. This limitation became present during impaction loading which occurs in a matter of milliseconds. As previously shown the camera was not able to record all point during loading but the data was able to be interpolated.

138

4.4 – Limitation of Approach

Throughout the incremental cyclic fretting corrosion studies the testing fixtures evolved to a more refined, stable constructs reducing set test parameters and limitations such as sample prep time, materials used during testing and sample test dimensions. These refinements allowed each study to become more accurate and repeatable.

First Generation

The 1st generation design, shown in Fig. 96, was the initial sensor fixture used to fix the sensors to the superior and inferior portion of the stem targeting aluminum plates fixed to the head. The sensors were threaded to the fixture, which was held to the porous coating of the stem with nylon screws.

The design was limited in various aspects. To reduce vibration in the motion data the fixture needed to be isolated from all components aside from the stem which was difficult due to constraints in the size of the fixture and the rigidity of the sensor cables. The nylon screws used to fix the sensors to the stem were highly particular due to the porous coating; if the screws were overly tightened before testing the fixture could slowly move which would alter the sensed displacement throughout testing. Lastly, to quickly adjust the sensors one would have to adjust the entire fixture because the fixture moved as a monoblock system.

Fig. 96: 1st generation sensor fixture. Holds two eddy current sensors fixed to the stem targeting the head.

The potting apparatus consisted of a PVC pipe, acrylic bone cement and a polypropylene environmental chamber (Fig. 97). The bone cement required a minimum of four hours to cure while a protractor and clamp were used to hold the stem at a consistent orientation. The chamber required approximately 750 mL of PBS to submerge the taper. This construct did not allow for the reuse of any materials post testing which increased the cost of testing.

Fig. 97: 1st generation potting system and environmental chamber with sensors and target fixed to the implant.

Second Generation

The 2nd generation fixture was a three DVRT construct which fixed the sensors to the head targeting aluminum coins fixed to the stem (Fig. 98). The sensors were held in place using aluminum nuts which were tightened to hold the sensors in place. This design allowed for the sensor cables to be moved out the way during testing and allowed for the sensors to be independently adjusted. The sensors were securely fixed to the head by bolts which screwed into tapped holes at designated points on the head.

This design was significantly larger than 1st generation design in order to accommodate for the added sensor. The added area meant the environmental chamber needed to be larger, which increased the amount of PBS used for each test. Another drawback of the fixture was the need for the heads to be tapped to bolt the fixture in place. Chromium, an elemental component of the head, has a relatively high hardness coefficient making it difficult to machine without expensive equipment.
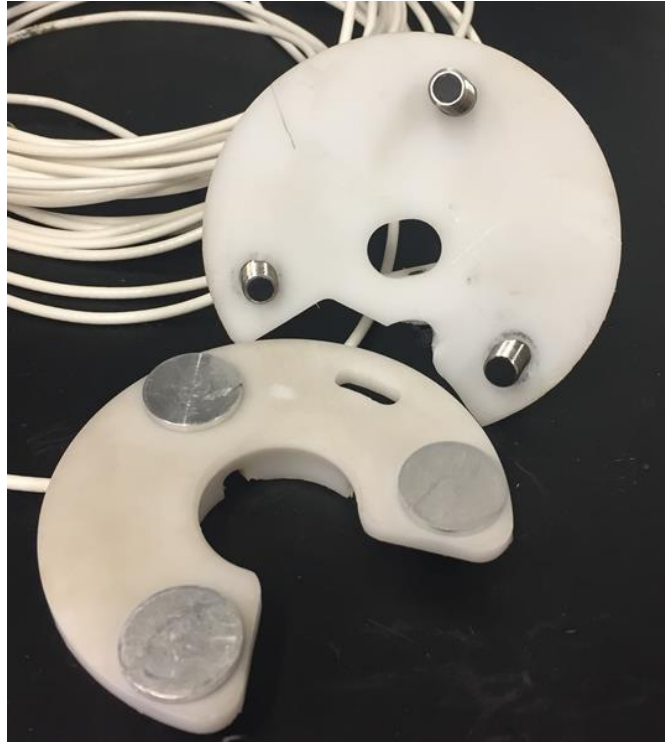
Fig. 98: 2nd generation sensor fixture. Holds three eddy current sensors fixed to the head targeting the stem.

The potting system consisted of stainless steel pot, non-conductive ceramic epoxy and a polypropylene environmental chamber (Fig. 99). Contrary to the previous design the metallic pot and plastic environmental chamber were reusable. However, the chamber required approximately 1.25 L of PBS to submerge the taper and the ceramic epoxy was relatively expensive. The epoxy also needed to be baked at high temperatures for 24 h to cure which significantly increased the preparation time between samples and cost of testing.
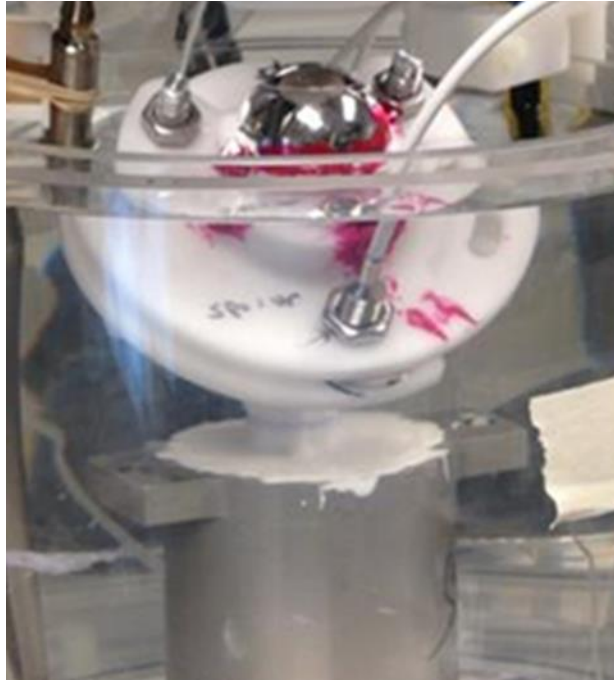
Fig. 99: 2nd generation potting construct and environmental chamber used during three sensor displacement measurement testing.

Third Generation

The 3rd generation and current design holds two eddy current sensors fixed to the superior and inferior portion of base of the head targeting an aluminum plate fixed to the stem (Fig. 100). The fixture was held firmly to the head using an epoxy. Unlike the previous designs, the sensor position as well as the aluminum target positon could be adjusted independently. This allowed for rapid adjustment of the measurement components without hassle.
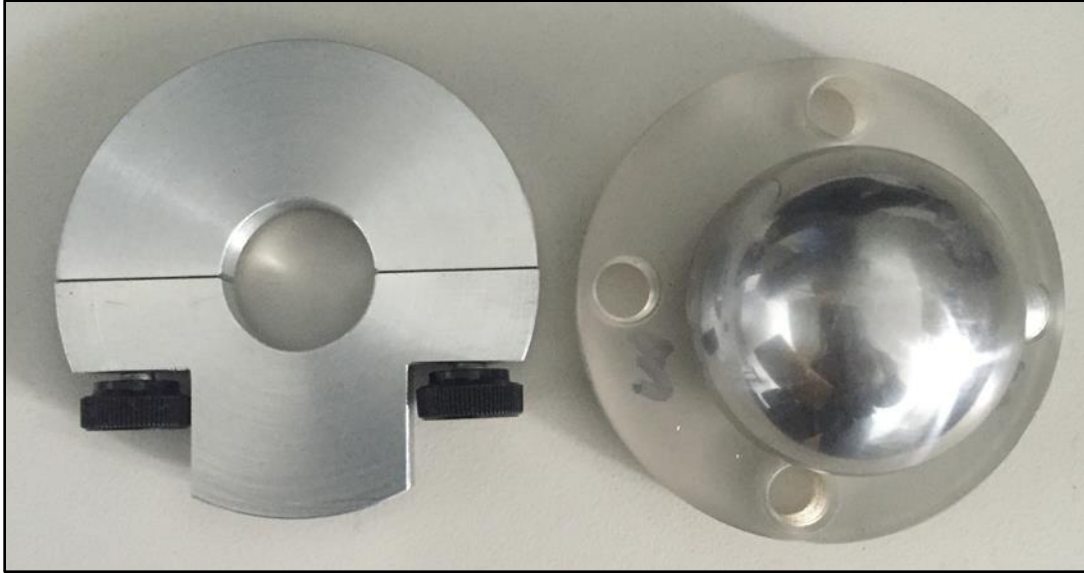
Fig. 100: 3rd generation sensor fixture. Holds two eddy current sensors fixed to the head targeting the stem.

Like the sensor fixture, the potting chamber and environmental chamber also changed to a more effective and efficient system (Fig. 101). The potting fixture held the sample in place using a threaded bolt which removed the need for costly or time consuming epoxies and the environmental chamber size was reduced due to the smaller fixture design. The chamber required approximately 450 mL to submerge the taper. All parts of the system expect the PBS were reusable.
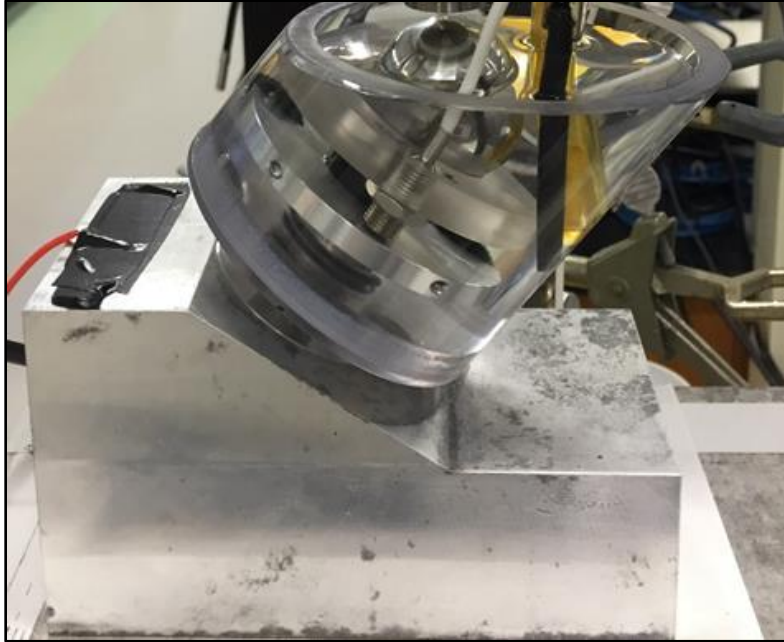
Fig. 101: 3rd generation potting fixture and environmental chamber.

Chapter 5 – Conclusion

5.0.1 – Overall Conclusion

The key findings from each subsection are presented below:

- Load magnitude has a significant effect on seating displacement, work of seating and taper stability. Load-displacement behavior in 12/14 tapers indicated a characteristic behavior in seating stiffness, which can be used in finite element analysis to predict seating displacement when a known load is applied.

- An increase in seating load magnitude altered taper performance and stability during ICFC testing. Increases in load magnitude increased taper stability which reduced subsidence during testing. The lower load groups experience large amounts of motion during testing due to the cyclic load increasing past the initial seating load.

- Lower seating load groups experienced larger amounts of fretting corrosion at the end of testing.

- Load orientation up to 20° had no significant effect on seating displacement, work of seating or taper stability. Changes in load orientation significantly alter the elastic motion recorded during seating.

- Load orientation up to 20° lowered the onset load during ICFC testing but had no effect on fretting corrosion currents or taper stability. However, the axially loaded group recorded larger micromotion values than the off-axis groups.

- Contamination load-displacement behavior showed the introduction of lipids to the taper junction increased seating displacement and taper stability. Solid contaminants caused the head to disproportionately seat during testing.

- ICFC testing of contaminated taper junctions reinforced the findings from the seating study. The introduction of lipids to the taper junction significantly altered the electrochemical results. The lipids group required larger loads to initiate fretting corrosion and in many causes corrosion was entirely mitigated.

- A short-term micromotion-fretting corrosion benchtop test method was developed to comparatively test taper performance in implants of different designs, materials and taper geometry.

- Taper geometry was shown to have an effect on taper construct stiffness which increased the onset load.

- 11/13 tapers recorded higher fretting corrosion currents than 12/14 tapers.

- Increase in impaction assembly load increased stiffness and reduced micromotion. The increase in load corresponded with an increase in onset load. Nonetheless, the increase in load did not affect the current at 4000 N.

- High impaction assembly loads may lead to elastic deformation at the trunnion which may lead to elastic rebound and positive subsidence of the head during cyclic loading.

- Load rate has no effect on seating displacement or taper stability.

- System compliance has no effect on seating displacement, work of seating or taper stability in static models.

- An increase in system compliance required larger input energies to achieve similar loads when compared to samples tested in a rigid non-compliant setup.

- Seating displacement may be captured and analyzed using a high-speed camera system.

- ICFC testing revealed two characteristic Current vs. Load behaviors, which seem to occur at random in one sample versus the other.

- A visual analysis tool can be used to analyze large data files and provide valuable insight into the motions recorded during testing. The tool has the ability to exemplify imperceptible microns of displacement and make them evident.

The overall key findings from each subsection can be combined to indicate the optimal implant and surgical assembly practice. A 12/14 Ti-6Al-4V/CoCrMo taper combination, with a lipid-like substrate coating applied to the trunnion, axially assembled at a load range of 4000-8000 N.

5.1 – Goal 1

5.1.1 – Load Magnitude and Orientation

In conclusion, the seating load magnitude has a direct correlation to seating displacement and initial taper stability. The greater the seating load magnitude the greater the seating displacement, work of seating and pull-off load. Seating load-displacement data revealed a trend

in seating mechanics as the load magnitude was increased which can be used to create an algorithm predicting seating displacement for an applied load.

The study also showed there was no significant effect on seating displacement, work of seating and pull-off load when the seating load orientation was increased from 0° to 20°.

5.1.2 – Taper Contamination

This study compared the influence of contamination (wet, lipids and bovine bone) at the taper junction on seating mechanics compared to control (dry) samples in 12/14 Ti6Al4V/CoCrMo trunnions. The introduction of contaminants significantly increased the measured seating displacement of the head on the neck as well as the work of seating. The solid contaminants (solid lipids and bone chip) recorded the greatest seating displacement and work of seating. Taper locking stability testing showed the introduction of liquid lipids significantly increased the pull-off load, approximately 89% of the seating load. Testing also showed solid contaminants may increase canted seating of the head (i.e. increased seating displacement of one portion of the head compared to the other).

5.2 – Goal 2

5.2.1 – Load Magnitude ICFC

In conclusion, the effects of seating load magnitude on incremental cyclic fretting corrosion behavior and pull-off loads in 12/14 tapers was explored. An increase in seating load magnitude increased taper stability and reduced subsidence. The correlation between subsidence and current at 4000 N cyclic loads was shown. As subsidence diminishes the current at 4000 N cyclic load decreased parabolically from 1000 to 8000 N. The increase in subsidence for the

149

1000 and 2000 N groups also caused a deviation from standard pull-off load values, increasing the pull-off load ratio considerably. Importantly, fretting corrosion onset loads were independent of seating loads above 2000 N and the fretting currents at 4000 N cyclic load did not go to zero for any of the seating loads investigated. This implies that while seating of the tapers is an important element in the overall performance of these modular tapers, it is not sufficient to eliminate fretting corrosion processes.

5.2.2 – Load Orientation ICFC

The presented data concluded increasing the seating angle up to 20° clockwise away from the neck axis lowered the load to initiate fretting corrosion. It also increased the seating displacements associated with seating, but had no effect on the fretting corrosion currents at 4000 N or pull-off loads for these tapers.

5.2.3 – Taper Contamination ICFC

In summary, the incorporation of contaminants to the head-neck taper junction not only led to increased seating displacement and work of seating but increased micromotion and subsidence during cyclic loading as well. Data from testing suggests the incorporation of lipids or a lipid-like substrate which accumulates about the mouth of the taper junction will increase the onset load and decrease the amount of corrosion at the end of testing. The incorporation of lipids also increased the pull-off load necessary to separate the head from the neck. There was no difference between the remaining groups.

5.2.4 – Taper Design and Material Combination

A short-term micromotion-fretting corrosion test method was developed that concurrently captures and correlates taper motions with currents. The combined measurement of motion and currents resulting from incremental cyclic loading were used to assess three different implant designs and compare the performance between taper geometry and alloy combination.

Testing showed taper geometry did have an effect on taper stiffness, micromotion, onset load and current at 4000 N, where the C taper outperformed the V40 taper. However, taper geometry and alloy combination did not have an effect on seating displacement, work of seating and subsidence.

The test developed has the capability to capture instantaneous measurements of motion and fretting corrosion currents and correlate those results to design parameters. Overall, the experimental test method is simple, quick and provides for a fast method to assess design and materials for susceptibility to fretting corrosion interactions. The test does not evaluate long-term performance, but could be modified to track corrosion and mechanics over long time periods.

5.2.5 – Impaction Assembly ICFC

The effects of impaction assembly load on Ti-6Al-4V/CoCr 12/14 tapers were assessed using incremental cyclic fretting corrosion testing, which simultaneously captured motion and fretting corrosion data during cyclic loading. The results indicate that increased impaction loads reduced micromotion and increased the onset load for fretting corrosion ($P<0.05$). The impaction load, however, increased the onset load, but did not have an effect on the fretting currents at 4000 N cyclic load indicating that increasing the impaction load may raise the cyclic loads needed to initiation fretting corrosion but once corrosion begins the magnitude of the fretting currents are the same. High impaction loads may result in high locking pressures due to elastic deformation which may lead to positive subsidence (dislodging of the head on the neck) during

cyclic loading indicating the possibility of loosening of the locking interaction with activities of daily living.

5.3 – Goal 3

5.3.1 – Load Rate and System Compliance

In conclusion, a novel seating displacement capture method which incorporated high-speed image analysis used during impaction and static loading was described. Load rate, load magnitude and system compliance were chosen to simulate clinical practice where load rate and magnitude differ between surgeon, surgery, patient positioning and implant. System compliance was used to simulate patient anatomy incorporating bone and tissue. This study also presented evidence which stated load rate and system compliance had no significant effect on work of seating or taper stability. However, it was shown that an increase in system compliance increased the overall input energy necessary to achieve the same impaction load in a non-compliant setup. With discovery of any novel method, this study dealt with certain limitations that were adequately overcome.

Chapter 6 – Future Work:

The results from each study presented in this dissertation identified factors which impacted the performance of the taper. However, using the diagram referred to in Fig. 1, these findings have provided more research topics and areas of study to be explored.

- Explore sticky-compliant interfaces: the effects of the neck taper microtopography (ridged vs. ground) on the fretting corrosion mechanics of the interface between TMZF and Ti-6Al-4V on CoCrMo. Machined ridges have been introduced into some trunnion surfaces, initially to reduce any localized stresses during assembly but the mechanics of surfaces during cyclic loading have yet to be characterized. The machined surfaces may play a larger role on taper fretting corrosion. The hypothesis being microtopography may have a direct correlation to neck taper fretting corrosion mechanics. The ridged design may decrease the locking mechanics of the two materials and under high load stress increase the wear mechanics due to the difference in modulus between the metals and lead to higher contamination about the junction. The wear of the metal over time would continue to lower the surface area and thus the contact points between to the two components, which would lead to more micromotion and corrosion. Testing could be fashioned in a pin-on-disk setup or couponed taper study. Fig. 102 displays potential surface geometries.
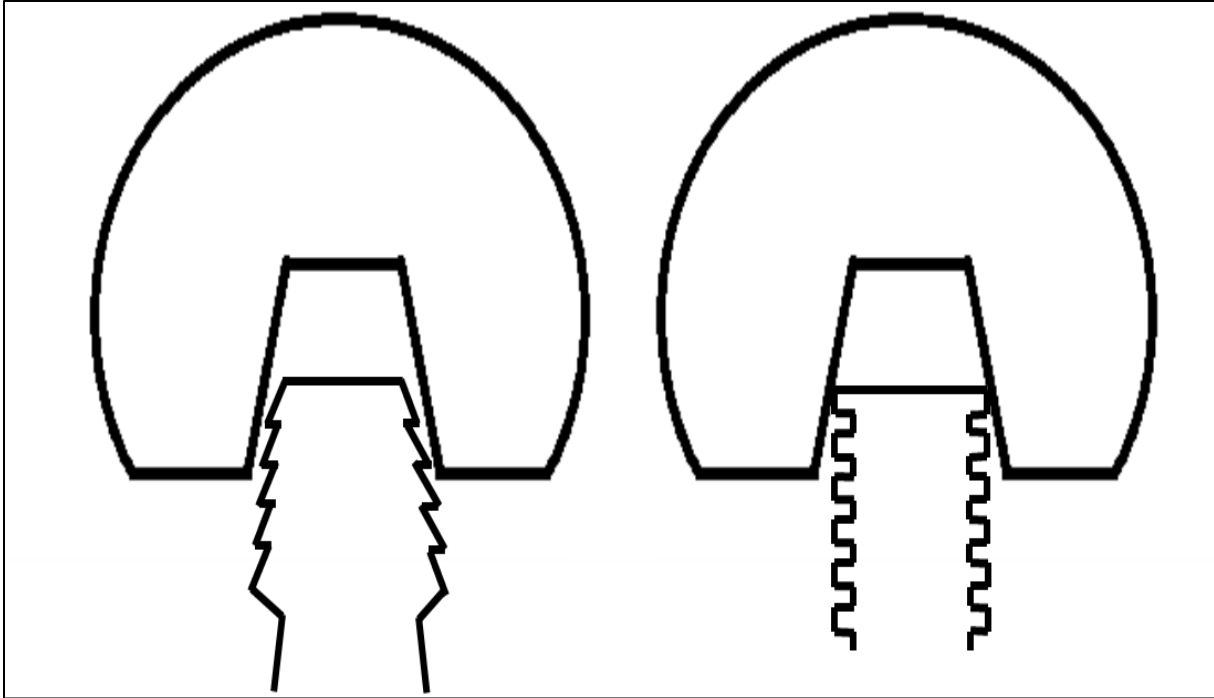
Fig. 102: Potential surface geometries in couponed taper setup which can be used to assess taper microtopography and the stick-slip compliance theory.

- In ICFC subsections 2 and 3 (Goal 2.3 and 2.4), the study used an ideal loading magnitude of 4000 N for off-axis and contaminated seating. The discussion sections indicate that though the load chosen constant between groups, clinically the load magnitude may be altered by the load orientation as well as contamination at the junction. Replicating the study but augmenting the initial seating magnitude may have a more clinically relevant impact on the seating mechanics as well as the taper performance during incremental cyclic fretting corrosion testing. The initial seating load would more than likely have an effect on the taper stability.

A more comprehensive understanding of the corrosive effects of cyclic motion in metal-on-metal modular implants. A systematic experiment where the current is not only collected outside of the implant (PBS solution surrounding implant) but also collected within the taper junction as well. A reference and counter electrode may be inserted in the taper junction by way of a 1 mm

154

hole drilled into the femoral head component. The taper junction would have to be wetted prior to seating in order to establish a liquid transport system in the beginning of testing. The purpose of this test would be identify any potential drop in current recorded outside of the taper and revise future test methods if so.

Chapter 7 – Appendix

Appendix I

Visual Basic Code used in Microsoft Excel to analyze ICFC data in 2 sensor configuration (green text is commented code):

```
Private Sub CommandButton1_Click()
Dim in1(6000) As Double
Dim in2(6000) As Double
Dim in3(6000) As Double
Dim in4(6000) As Double
Dim in5(6000) As Double

Close #1
gfile$ = Cells(1, 1) 'reads in file directory
k1 = Cells(2, 2) 'N/um 'reads in superior stiffness constant
k2 = Cells(3, 2) 'N/um 'reads in inferior stiffness constant
jstep = Cells(4, 2)
KDVRT1 = Cells(2, 5) 'reads in superior micron/voltage constant
KDVRT2 = Cells(3, 5) 'reads in superior micron/voltage constant

Sheet1.Cells.Clear
Cells(1, 1) = gfile$ 'file directory
Cells(2, 1) = "k1" 'writes in excel
Cells(3, 1) = "k2" 'writes in excel
Cells(4, 1) = "jstep" 'writes in excel
Cells(2, 2) = k1 'input value
Cells(3, 2) = k2
Cells(4, 2) = jstep
Cells(2, 4) = "KDVRT1" 'writes in excel
Cells(3, 4) = "KDVRT2"
Cells(2, 5) = KDVRT1 'input value
Cells(3, 5) = KDVRT2


Cells(9, 1) = "d1elast" 'writes in excel
Cells(9, 2) = "tavg"
Cells(9, 3) = "LDavg"
Cells(9, 4) = "DVRT1avg"
Cells(9, 5) = "DVRT2avg"
```

```
Cells(9, 6) = "DD1avg"
Cells(9, 7) = "DD2avg"
Cells(9, 8) = "Iavg"
Cells(9, 9) = "Damp1"
Cells(9, 10) = "Damp2"
Cells(9, 11) = "d2elast"

Cells(9, 13) = "Time" 'writes in excel
Cells(9, 14) = "DD1"
Cells(9, 15) = "DD2"
Cells(9, 16) = "load (N)"
Cells(9, 17) = "Delast 1"
Cells(9, 18) = "Delast 2"
Cells(9, 19) = "Dtot1"
Cells(9, 20) = "Dtot2"
Cells(9, 21) = "Current"
hfile$ = Sheet2.Cells(1, 1) + ".csv" 'reads data file, has to be *.csv

'write file name above data
'Cells(5, 1) = hfile$

Open gfile$ + hfile$ For Input As #1 'opens file in directory

'input the header
For i = 1 To 138 'skips the number of characters "138" before reading in data
Input #1, head$
Next i

k = 0 'set variables to 0
j = 0
l = 0

DVRT1init = 0#
DVRT2init = 0#

Do While Not EOF(1)

l = l + 1
j = j + 1

'setting all constants to 0
Iavg = 0#
tavg = 0
DVRT1avg = 0#
```

157

```
DVRT2avg = 0#
ldavg = 0#
D1max = -9999999 'setting max and min range
D1min = 9999999
D2max = -9999999
D2min = 9999999

For i = 0 To 199
Input #1, in1(i), in2(i), in3(i), in4(i), in5(i), in6 'time, DVRT 1, DVRT 2, Load, Current, Comment in
.csv file
If EOF(1) Then GoTo 9999
Next i

' 3 pt running averaging
in2(0) = (in2(1) + in2(0)) / 2 'DVRT 1 average
in2(1) = (in2(2) + in2(1) + in2(0)) / 3
in2(199) = (in2(198) + in2(199)) / 2
in2(198) = (in2(197) + in2(198) + in2(199)) / 3

in3(0) = (in3(1) + in3(0)) / 2 'DVRT 2 average
in3(1) = (in3(2) + in3(1) + in3(0)) / 3
in3(199) = (in3(198) + in3(199)) / 2
in3(198) = (in3(197) + in3(198) + in3(199)) / 3

' five pt running average

For i = 2 To 197
in2(i) = (in2(i - 2) + in2(i - 1) + in2(i) + in2(i + 1) + in2(i + 2)) / 5 'DVRT 1
in3(i) = (in3(i - 2) + in3(i - 1) + in3(i) + in3(i + 1) + in3(i + 2)) / 5 'DVRT 2
in5(i) = (in5(i - 2) + in5(i - 1) + in5(i) + in5(i + 1) + in5(i + 2)) / 5 'Load
Next i


For i = 0 To 199

'Average current
Iavg = Iavg + in5(i) / 200
tavg = tavg + in1(i) / 200
DVRT1avg = DVRT1avg + (in2(i) * KDVRT1) / 200 ' in um
DVRT2avg = DVRT2avg + (in3(i) * KDVRT2) / 200 ' in um
ldavg = ldavg + in4(i) * 500 / 200 ' in N

'Defining which is min and max
If in2(i) * KDVRT1 - in4(i) * 500 / k1 < D1min Then D1min = in2(i) * KDVRT1 - in4(i) * 500 / k1
```

```
If in2(i) * KDVRT1 - in4(i) * 500 / k1 > D1max Then D1max = in2(i) * KDVRT1 - in4(i) * 500 / k1
If in3(i) * KDVRT2 - in4(i) * 500 / k2 < D2min Then D2min = in3(i) * KDVRT2 - in4(i) * 500 / k2
If in3(i) * KDVRT2 - in4(i) * 500 / k2 > D2max Then D2max = in3(i) * KDVRT2 - in4(i) * 500 / k2

'Amplitude used to solve for the micromotion calculations
Damp1 = D1max - D1min
Damp2 = D2max - D2min




If j >= jstep Then 'inputs these values in the defined columns and rows
Cells(10 + i, 13 + k * 10) = in1(i)
Cells(10 + i, 14 + k * 10) = (in2(i) * KDVRT1 - DVRT1init) - in4(i) * 500 / k1
Cells(10 + i, 15 + k * 10) = (in3(i) * KDVRT2 - DVRT2init) - in4(i) * 500 / k2
Cells(10 + i, 16 + k * 10) = in4(i) * 500
Cells(10 + i, 17 + k * 10) = in4(i) * 500 / k1
Cells(10 + i, 18 + k * 10) = in4(i) * 500 / k2
Cells(10 + i, 19 + k * 10) = (in2(i) * KDVRT1 - DVRT1init)
Cells(10 + i, 20 + k * 10) = (in3(i) * KDVRT2 - DVRT2init)
Cells(10 + i, 21 + k * 10) = in5(i)

End If
' everything is in um and N

Next i

If l = 1 Then
DVRT1init = DVRT1avg
DVRT2init = DVRT2avg
End If

If j >= jstep Then
k = k + 1
j = 0
End If

'ideal deformation only motion for each point
Di1avg = ldavg / k1
Di2avg = ldavg / k2

' average rigid body motion for each point
DD1avg = (DVRT1avg - DVRT1init) - Di1avg
DD2avg = (DVRT2avg - DVRT2init) - Di2avg
```

```
'Prints the variables in defined columns
Cells(10 + l, 1) = Di1avg
Cells(10 + l, 2) = tavg
Cells(10 + l, 3) = ldavg
Cells(10 + l, 4) = (DVRT1avg - DVRT1init)
Cells(10 + l, 5) = (DVRT2avg - DVRT2init)
Cells(10 + l, 6) = DD1avg
Cells(10 + l, 7) = DD2avg
Cells(10 + l, 8) = Iavg
Cells(10 + l, 9) = Damp1
Cells(10 + l, 10) = Damp2
Cells(10 + l, 11) = Di2avg

Loop

9999 Close #1
'End program
End Sub
```

Appendix II

Visual Basic program used within excel to analyze ICFC data in 3 sensor configuration (green text = commented code):

```vb
Private Sub CommandButton1_Click()
Dim in1(6000) As Double
Dim in2(6000) As Double
Dim in3(6000) As Double
Dim in4(6000) As Double
Dim in5(6000) As Double

Close #1
gfile$ = Cells(1, 1)
k1 = Cells(2, 2) 'N/um
k2 = Cells(3, 2) 'N/um
k3 = Cells(4, 2) 'N/um
jstep = Cells(5, 2)
KDVRT = Cells(2, 5)

Sheet1.Cells.Clear
Cells(1, 1) = gfile$
Cells(2, 1) = "k1"
Cells(3, 1) = "k2"
Cells(4, 1) = "k3"
Cells(5, 1) = "jstep"
Cells(2, 2) = k1
Cells(3, 2) = k2
Cells(4, 2) = k3
Cells(5, 2) = jstep
Cells(2, 4) = "KDVRT"
Cells(2, 5) = KDVRT

Cells(9, 1) = "d1elast"
Cells(9, 2) = "tavg"
Cells(9, 3) = "LDavg"
Cells(9, 4) = "DVRT1avg"
Cells(9, 5) = "DVRT2avg"
Cells(9, 6) = "DVRT3avg"
Cells(9, 7) = "DD1avg"
Cells(9, 8) = "DD2avg"
Cells(9, 9) = "DD3avg"
Cells(9, 10) = "Damp1"
```

```vba
Cells(9, 11) = "Damp2"
Cells(9, 12) = "Damp3"
Cells(9, 13) = "d2elast"
Cells(9, 14) = "d3elast"

Cells(9, 16) = "Time"
Cells(9, 17) = "DD1"
Cells(9, 18) = "DD2"
Cells(9, 19) = "DD3"
Cells(9, 20) = "load (N)"
Cells(9, 21) = "Delast 1"
Cells(9, 22) = "Delast 2"
Cells(9, 23) = "Delast 3"
Cells(9, 24) = "Dtot1"
Cells(9, 25) = "Dtot2"
Cells(9, 26) = "Dtot3"

hfile$ = Sheet2.Cells(1, 1) + ".csv"

'write file name above data
'Cells(5, 1) = hfile$

Open gfile$ + hfile$ For Input As #1

'input the header
For i = 1 To 35
Input #1, head$
Next i

k = 0
j = 0
L = 0

DVRT1init = 0#
DVRT2init = 0#
DVRT3init = 0#

Do While Not EOF(1)

L = L + 1
j = j + 1

tavg = 0
DVRT1avg = 0#
```
162

```
DVRT2avg = 0#
DVRT3avg = 0#
ldavg = 0#
D1max = -9999999
D1min = 9999999
D2max = -9999999
D2min = 9999999
D3max = -9999999
D3min = 9999999

For i = 0 To 1499
Input #1, in1(i), in2(i), in3(i), in4(i), in5(i)
' time, ant. lat., post. lat., medial, force
If EOF(1) Then GoTo 99999
Next i

' Determine which is M, L1, L2 before proceeding
' 3 pt running averaging
in2(0) = (in2(1) + in2(0)) / 2
in2(1) = (in2(2) + in2(1) + in2(0)) / 3
in2(1499) = (in2(1498) + in2(1499)) / 2
in2(1498) = (in2(1497) + in2(1498) + in2(1499)) / 3

in3(0) = (in3(1) + in3(0)) / 2
in3(1) = (in3(2) + in3(1) + in3(0)) / 3
in3(1499) = (in3(1498) + in3(1499)) / 2
in3(1498) = (in3(1497) + in3(1498) + in3(1499)) / 3

in4(0) = (in4(1) + in4(0)) / 2
in4(1) = (in4(2) + in4(1) + in4(0)) / 3
in4(1499) = (in4(1498) + in4(1499)) / 2
in4(1498) = (in4(1497) + in4(1498) + in4(1499)) / 3

' five pt running average
For i = 2 To 1497
in2(i) = (in2(i - 2) + in2(i - 1) + in2(i) + in2(i + 1) + in2(i + 2)) / 5
in3(i) = (in3(i - 2) + in3(i - 1) + in3(i) + in3(i + 1) + in3(i + 2)) / 5
in4(i) = (in4(i - 2) + in4(i - 1) + in4(i) + in4(i + 1) + in4(i + 2)) / 5
Next i

'Print column headers
Cells(9, 16 + k * 12) = "Time"
Cells(9, 17 + k * 12) = "DD1"
Cells(9, 18 + k * 12) = "DD2"
```

```
Cells(9, 19 + k * 12) = "DD3"
Cells(9, 20 + k * 12) = "load (N)"
Cells(9, 21 + k * 12) = "Delast 1"
Cells(9, 22 + k * 12) = "Delast 2"
Cells(9, 23 + k * 12) = "Delast 3"
Cells(9, 24 + k * 12) = "Dtot1"
Cells(9, 25 + k * 12) = "Dtot2"
Cells(9, 26 + k * 12) = "Dtot3"


For i = 0 To 1499

' Average of data
tavg = tavg + in1(i) / 1500
DVRT1avg = DVRT1avg + (in2(i) * KDVRT) / 1500 ' in um
DVRT2avg = DVRT2avg + (in3(i) * KDVRT) / 1500 ' in um
DVRT3avg = DVRT3avg + (in4(i) * KDVRT) / 1500 ' in um
ldavg = ldavg + in5(i) * 1500 / 1500 ' in N


If in2(i) * KDVRT - in5(i) * 1500 / k1 < D1min Then D1min = in2(i) * KDVRT - in5(i) * 1500 / k1
If in2(i) * KDVRT - in5(i) * 1500 / k1 > D1max Then D1max = in2(i) * KDVRT - in5(i) * 1500 / k1
If in3(i) * KDVRT - in5(i) * 1500 / k2 < D2min Then D2min = in3(i) * KDVRT - in5(i) * 1500 / k2
If in3(i) * KDVRT - in5(i) * 1500 / k2 > D2max Then D2max = in3(i) * KDVRT - in5(i) * 1500 / k2
If in4(i) * KDVRT - in5(i) * 1500 / k3 < D3min Then D3min = in4(i) * KDVRT - in5(i) * 1500 / k3
If in4(i) * KDVRT - in5(i) * 1500 / k3 > D3max Then D3max = in4(i) * KDVRT - in5(i) * 1500 / k3


Damp1 = D1max - D1min
Damp2 = D2max - D2min
Damp3 = D3max - D3min

' everything is in um and N

Next i

If L = 1 Then
DVRT1init = DVRT1avg
DVRT2init = DVRT2avg
DVRT3init = DVRT3avg
End If

'ideal deformation only motion for each point
Di1avg = ldavg / k1
Di2avg = ldavg / k2
Di3avg = ldavg / k3
```

```
' average rigid body motion for each point
DD1avg = (DVRT1avg - DVRT1init) - Di1avg
DD2avg = (DVRT2avg - DVRT2init) - Di2avg
DD3avg = (DVRT3avg - DVRT3init) - Di3avg

Cells(10 + L, 1) = Di1avg ' elastic displacement 1
Cells(10 + L, 2) = tavg ' time
Cells(10 + L, 3) = ldavg ' load average
Cells(10 + L, 4) = (DVRT1avg - DVRT1init) ' subsidence 1
Cells(10 + L, 5) = (DVRT2avg - DVRT2init) ' subsidence 2
Cells(10 + L, 6) = (DVRT3avg - DVRT3init) ' subsidence 3
Cells(10 + L, 7) = DD1avg
Cells(10 + L, 8) = DD2avg
Cells(10 + L, 9) = DD3avg
Cells(10 + L, 10) = Damp1
Cells(10 + L, 11) = Damp2
Cells(10 + L, 12) = Damp3
Cells(10 + L, 13) = Di2avg
Cells(10 + L, 14) = Di3avg

Loop


99999 Close #1

End Sub
```

Appendix III

Visual Basic code for program defined in the Discussion Chapter (4.0.2) (green text = commented code).

```
Private Sub Command1_Click()
Dim in1 As Double
Dim in2 As Double
Dim in3 As Double
Dim in4 As Double
Dim in5 As Double
Dim x(10, 10) As Double

Open "C:\Users\David Pierre\Desktop\Seating\Group 1-sample3-seating1.csv" For Input As #1
K1 = -13.803 'Stiffness correction constant N/um
K2 = 27.826 'N/um

KDVRT1 = 90 ' um/volt, positive V is closer to DVRT
KDVRT2 = 93 ' um/V, negative V is closer to DVRT

'Begin drawing of the head in motion
Picture1.FillColor = QBColor(0)
Picture1.Circle (15, 95), 2, QBColor(13)

x(1, 1) = 50#
x(1, 2) = 50#
x(2, 1) = 60#
x(2, 2) = 60#
x(3, 1) = 50#
x(3, 2) = 65#
x(4, 1) = 45#
x(4, 2) = 55#

'input the header
For i = 1 To 138
Input #1, head$
Next i

mag = 20

k = 0
j = 0
l = 0
```

```
i = 0
DVRT1init = 0#
DVRT2init = 0#

'Scale and tick marks for Load vs Displacement graph (Box 2)
'Draw X axis.
Picture2.Line (0, 0)-(10, 0)
For xy = 0 To 9
Picture2.Line (xy, -1)-(xy, 1)
Next xy

'Draw Y axis
Picture2.Line (0, -20)-(0, 2100)
For xy = -19 To 2099
Picture2.Line (-0.1, xy)-(0.1, xy)
Next xy

'Box 3 LvD graph
'Draw X axis
Picture3.Line (0, 0)-(10, 0)
For xy = 0 To 9
Picture3.Line (xy, -1)-(xy, 1)
Next xy

'Draw Y axis
Picture3.Line (0, -20)-(0, 2100)
For xy = -19 To 2099
Picture3.Line (-0.1, xy)-(0.1, xy)
Next xy

'Calculating Work of seating
Fold = 0
Dold = 0
Work = 0
Fold1 = 0
Dold1 = 0
Work1 = 0

Do While i < 7500 'Depends on the elapsed time of testing

Input #1, in1, in2, in3, in4, in5, in6
i = i + 1
j = j + 1
l = 0
```

```
j = 0
Do While l < 75000
l = l + 1
j = j + 1
Loop

'Values for Work portion
XDVRT = in2 * KDVRT1
XDVRT20 = in3 * KDVRT2

XDVRT1 = in2 * KDVRT1
XDVRT2 = in3 * KDVRT2
LD = in4 * 500

If i = 1 Then

'Work portion
Xinit = XDVRT
X20init = XDVRT20

X1init = XDVRT1
X2init = XDVRT2
End If

'Work portion
XDVRT = XDVRT - Xinit
XDVRT20 = XDVRT20 - X20init

XDVRT1 = (XDVRT1 - X1init) / mag
XDVRT2 = (XDVRT2 - X2init) / mag

'Work portion
X10 = XDVRT
X20 = XDVRT20

X11 = XDVRT1
X21 = XDVRT2

'Work portion
XR = (X10 - (LD / K1))
XR20 = (X20 - (LD / K2))

XR1 = (X11 * mag - (LD / K1)) / mag
XR2 = (X21 * mag - (LD / K2)) / mag
```

168

```
If i > 2 Then
Picture1.Cls

'Draws total motion as visual representation of data
Picture1.FillStyle = 0
Picture1.FillColor = QBColor(0)
Picture1.Circle (15, 95 + LD / 500 * 10), 2, QBColor(12) ' load
Picture1.Circle (75 - XR2 * 4, 40 - in5 * 4), 1, QBColor(13) ' current
Picture1.Circle (75 - XR1 * 4, 50 - in5 * 4), 2, QBColor(14) ' current

'Total motion reference point (doesn't move)
Picture1.Circle (40, 50), 2, QBColor(9)
Picture1.Circle (40, 40), 2, QBColor(9)
Picture1.Circle (80, 50), 2, QBColor(9)
Picture1.Circle (80, 40), 2, QBColor(9)
Picture1.Line (40, 50)-(40, 40)
Picture1.Line (40, 40)-(80, 40)
Picture1.Line (80, 40)-(80, 50)
Picture1.Line (80, 50)-(40, 50)

'Total motion portion, top box (moving portion)
Picture1.FillStyle = 0
Picture1.FillColor = QBColor(0)
Picture1.Circle (40, 50 - X11), 2, QBColor(0)
Picture1.Circle (40, 40 - X11), 2, QBColor(0)
Picture1.Circle (80, 50 - X21), 2, QBColor(0)
Picture1.Circle (80, 40 - X21), 2, QBColor(0)
Picture1.Line (40, 50 - X11)-(40, 40 - X11)
Picture1.Line (40, 40 - X11)-(80, 40 - X21)
Picture1.Line (80, 40 - X21)-(80, 50 - X21)
Picture1.Line (80, 50 - X21)-(40, 50 - X11)

'Rigid motion portion (doesn't move)
Picture1.Circle (40, 90), 2, QBColor(9)
Picture1.Circle (40, 80), 2, QBColor(9)
Picture1.Circle (80, 90), 2, QBColor(9)
Picture1.Circle (80, 80), 2, QBColor(9)
Picture1.Line (40, 90)-(40, 80)
Picture1.Line (40, 80)-(80, 80)
Picture1.Line (80, 80)-(80, 90)
Picture1.Line (80, 90)-(40, 90)

'This is rigid motion, bottom box (moving portion)
```

```
Picture1.FillColor = QBColor(7)
Picture1.Circle (40, 90 - XR1), 2, QBColor(5)
Picture1.Circle (40, 80 - XR1), 2, QBColor(5)
Picture1.Circle (80, 90 - XR2), 2, QBColor(5)
Picture1.Circle (80, 80 - XR2), 2, QBColor(5)
Picture1.Line (40, 90 - XR1)-(40, 80 - XR1)
Picture1.Line (40, 80 - XR1)-(80, 80 - XR2)
Picture1.Line (80, 80 - XR2)-(80, 90 - XR2)
Picture1.Line (80, 90 - XR2)-(40, 90 - XR1)

End If

l = 0
Do While l < 7500
l = l + 1
Loop
Picture1.FillStyle = 0
Picture1.FillColor = QBColor(9)

Picture1.Circle (40, 50 - X11), 2, QBColor(9)
Picture1.Circle (40, 40 - X11), 2, QBColor(9)
Picture1.Circle (80, 50 - X21), 2, QBColor(9)
Picture1.Circle (80, 40 - X21), 2, QBColor(9)
Picture1.Line (40, 50 - X11)-(40, 40 - X11), QBColor(9)
Picture1.Line (40, 40 - X11)-(80, 40 - X21), QBColor(9)
Picture1.Line (80, 40 - X21)-(80, 50 - X21), QBColor(9)
Picture1.Line (80, 50 - X21)-(40, 50 - X11), QBColor(9)

'Head doesn't move
Picture1.FillStyle = vbFSTransparent
Picture1.Circle (59.6, 34), 8, QBColor(0)

'Head does move
Picture1.FillStyle = 4
Xhead = ((X11 + X21) / 2)
Picture1.Circle (59.6, 34 - Xhead), 8, QBColor(7) 'white circle
Picture1.Circle (0, 0), 0.1, QBColor(1) 'BEING USED TO MAKE SURE THE CIRCLE ABOVE DOESNT
DISAPPEAR!!!

If l = 1 Then
DVRT1init = DVRT1avg
DVRT2init = DVRT2avg
End If
```

```
If j >= jstep Then
k = k + 1
j = 0
End If
```

```
'ideal deformation only motion for each point
Di1avg = LDavg / K1
Di2avg = LDavg / K2
```

```
' average rigid body motion for each point
DD1avg = (DVRT1avg - DVRT1init) - Di1avg
DD2avg = (DVRT2avg - DVRT2init) - Di2avg
```

```
'Load vs Displacements graphs
Picture2.ForeColor = QBColor(0)
Picture3.ForeColor = QBColor(0)
graphx = -XR1
graphy = -LD
graphx1 = -XR2
   Picture2.Line (2 * graphx, graphy)-(2 * graphx + 1, graphy + 1)
   Picture3.Line (2 * graphx1, graphy)-(2 * graphx1 + 1, graphy + 1), QBColor(9)
```

```
'Work of seating/area under the curve equation
F = -LD
F1 = -LD
D = XR
D1 = XR20
Work = (((F + Fold) / 2) * (D - Dold) + Work) / 1000000 'converts from uJ to J
Work1 = (((F + Fold) / 2) * (D1 - Dold1) + Work1) / 1000000
Fold = F
Fold1 = F1
Dold = D
Dold1 = D1
```

```
Loop
```

```
'Elapsed Time
Text1.Text = "Elapsed Time(s) = " & in1
Text1.FontSize = 10
Text1.FontBold = True
```

```
'Work of superior
Text2.Text = "Work Done (J)= " & Work
Text2.FontSize = 10
```

```vb
Text2.FontBold = True

'Work of inferior
Text3.Text = "Work Done (J)= " & Work1
Text3.FontSize = 10
Text3.FontBold = True

Close #1


End Sub
```

References

1. Kurtz, S. and K. Ong, *Projections of primary and revision hip and knee arthoplasty in the United States from 2005 to 2030.* Journal of Bone and Joint Surgery, 2007. **89**(6): p. 780-785.

2. Shaw, G. and B. Nazario. *Hip and Knee Replacements on the Rise*. 2007 [cited 2015; Available from: http://www.webmd.com/arthritis/features/hip-knee-replacements-rise.

3. Urban, R.M., J.L. Gilbert, and J.J. Jacobs, *Corrosion of modular titanium alloy stems in cementless hip replacement*. ASTM Special Technical Publication 1471, ed. L.D. Zardiackas, M.J. Kraay, and H.L. Freese. 2006, West Conshohocken, PA: ASTM International.

4. Gilbert, J.L. and C.A. Buckley, *In-vivo corrosion of modular hip prosthesis components in mixed and similar metal combinations: The effect of crevice, stress, motion and alloy coupling.* Journal of Biomedical Materials Research, 1993. **27**(12): p. 1533-1544.

5. Gilbert, J.L. and J.J. Jacobs, *The Mechanical and Electrochemical Process Associated with Taper Fretting Crevice Corrosion: A Review.* Modularity of Orthopedic Implants, ASTM STP 1301, 1997: p. 45-59.

6. Gilbert, J.L., *Mechanically Assisted Corrosion of Metallic Biomaterials.* ASTM International Handbook, 2006. **13C**: p. 826-836.

7. Gilbert, J.L., *Electrochemical Behaviour of Metals in the Biological Milieu*, in *Comprehensive Biomaterials*. 2011, Elsevier Press.

8. Goldberg, J.R., et al., *Corrosion testing of modular hip implants.* Modularity of Orthopedic Implants, 1997. **1301**: p. 157-174.

9. Mali, S.A. and J.L. Gilbert, *Correlating Fretting Corrosion and Micromotions in Modular Tapers: Test Method Development and Assessment*, in *ASTM Special Technical Publication on Implant Modularity*, K. Greenwald, Lemons, Mihalko, Editor. 2015.

10. Rehmer, A., N.E. Bishop, and M.M. Morlock, *Influence of assembly procedure and material combination on the strength of the taper connection at the head-neck junction of modular hip endoprosthesis.* Clinical Biomechanics, 2012. **27**: p. 77-83.

11. Mroczkowski, M.L. and J.S. Hertzler, *Effect of impact assembly on the fretting corrosion of modular hip tapers.* Journal of Orthopedic Research, 2006. **24**(2): p. 271-79.

12. Haschke, H., S.Y. Jauch, and M.M. Morlock, *Assembly force and taper angle difference influence the relative motion of stem-neck interface of bi-modular hip protheses.* Journal of Engineering in Medicine, 2016. **230**(7): p. 690-99.

13. Frisch, N.B., J.R. Lynch, and R.F. Banglmaier, *The stability of dual-taper modular hip implants: a biomechanical analysis examining the effect of impact location on component stability.* Arthroplasty Today, 2016: p. 1-6.

14. Witt, F., et al., *Quantification of the Contact Area at the Head-Stem Taper Interface of Modular Hip Prostheses.* PLoS ONE, 2015. **10**(8).

15. Lavernia, C.J., et al., *The Effects of Blood and Fat on Morse Taper Disassembly Forces.* The American Journal of Orthopedics, 2009. **38**(4): p. 187-190.

16. Haschke, H., et al., *The Influence of Contamination and Assembly Load on the Micromotion at the Head-Stem Taper*. 2016, European Society of Biomechanics: Lyon, France.

17.   Goldberg, J.R., J.L. Gilbert, and J.J. Jacobs, *A multicenter retrieval study of the taper interfaces of modular hip protheses.* Clinical Orthopedic Related Research, 2002. **401**: p. 149-161.

18.   Urban, R.M., J.J. Jacobs, and J.L. Gilbert. *Corrosion of modular-body titanium alloy femoral stems for hip replacement.* in *Orthopedic Research Society*. 2005.

19.   Gilbert, J.L. and G.W. Kubacki, *Corrosion Causes Biology and Biology Causes Corrosion*, in *Oxidative Stress, Inflammation and the Corrosion of Metallic Biomaterials*, T. Dziubla and D.A. Butterfield, Editors. 2015, Elsevier Inc.

20.   Sato, N., *Basics of Corrosion Chemistry*, S.K. Sharma, Editor. 2012, Wiley-VCH Verlag GmbH & Co. p. 32.

21.   Hanawa, T., *In vivo metallic biomaterials and surface modification.* Material Science and Engineering: A, 1999. **267**(2): p. 260-66.

22.   Sawyer, P.N., *Dependence of thrombosis on the electrochemical characteristics of the blood vessel wall, blood cells and prosthetic materials.* Biblotheca Anatomica, 1969. **10**: p. 405-417.

23.   Sawyer, P.N., *The relationship between surface charge of the vascular interface and thrombosis.* Annals of the New York Academy of Sciences, 1983. **416**: p. 561-583.

24.   Swaminathan, V. and J.L. Gilbert, *Fretting corrosion of CoCrMo and Ti6Al4V interfaces.* Biomaterials, 2012. **33**: p. 5487-5503.

25.   Langton, D.J., *Early failure of metal-on-metal bearings in hip resurfacing and large-diameter total hip replacement. Journal of Bone and Joint Surgery*, 2010. **92B**(1): p. 39-46.

26.   Cooper, H.J. and V. Della, *Corrosion at the head-neck taper as a cause for adverse local tissue reactions after total hip arthroplasty.* Journal of Bone and Joint Surgery, 2012. **94**(18): p. 1655-1661.

27.   Cooper, J.H., MD, R.M. Urban, PhD, and R.L. Wixson, MD, *Adverse Local Tissue Reaction Arising from Corrosion at the Femoral Neck-Body Junction in a Dual-Taper Stem with a Cobalt-Chromium Modular Neck.* The Journal of Bone & Joint Surgery, 2013. **95**(10): p. 865-872.

28.   Cooper, H., *The Local Effects of Metal Corrosion in Total Hip Arthroplasty.* Orthopedic Clinics of North America, 2014. **45**(1): p. 9-18.

29.   Urban, R.M., J.J. Jacobs, and J.L. Gilbert, *Migration of corrosion products from modular hip prostheses. Particle microanalysis and histopathological findings.* Journal of Bone and Joint Surgery, 1994. **76A**: p. 1345-1359.

30.   Jacobs, J.J., R.M. Urban, and J.L. Gilbert, *Local and distant products from modularity.* Clinical Orthopedic and Related Research, 1995. **319**: p. 94-105.

31.   Svennson, O., *Formation of a fulminant soft tissue pseudotumor after uncemented hip arthoplasty.* Journal of Bone and Joint Surgery, 1998. **70A**: p. 1238-1242.

32.   Campbell, P. and E. Ebramzadeh, *Histological features of pseudotumors-like tissues from metal-on-metal hips.* Clinical Orthopedics and Related Research, 2010. **468**(9): p. 2321-2327.

33.   Grupp, T.M., *Modular titanium alloy neck adaptor failures in hip replacement-failure mode analysis and influence of implant materials.* BMC Musculoskeletal Disorders, 2010. **11**(3).

34.   Caicedo, M.S., R. Desai, and K. McAllister, *Souble and particulate Co-Cr-Mo alloy implant metals activate the inflammasome danger signaling pathway in human*

macrophages: A novel mechanism for implant debris reactivity. Journal of Orthopedic Research, 2009. **27**(7): p. 847-854.

35. Cooper, H.J., C.J. Della Valle, and J.J. Jacobs, *Biological implications of taper corrosion in total hip arthoplasty.* Seminars in Arthoplasty, 2010. **23**: p. 273-278.

36. Jones, D., et al., *Focal Osteolysis at the Junctions of a Modular Stainless Steel Femoral Intramedullary Nail. Journal of Bone and Joint Surgery*Journal of Bone and Joint Surgery, 2001. **83A**(4): p. 537-548.

37. Gilbert, J.L., J.J. Jacobs, and C.A. Buckley, *Intergranular corrosion fatigue failure of Co-Cr femoral stems: A failure analysis of two implants.* Journal of Bone and Joint Surgery, 1994. **76**: p. 110-115.

38. Cook, S.D. and R.L. Barrack, *Corrosion and wear at the modular interface of uncemented femoral stems.* Journal of Bone and Joint Surgery, 1994. **76**: p. 68-72.

39. Collier, J.P., et al., *Corrosion at the interface of cobalt alloy heads on titanium-alloy stems.* Clinical Orthopedic Related Research, 1991. **271**: p. 305-312.

40. Collier, J.P., et al., *Corrosion between the components of modular femoral hip prostheses.* Journal of Bone and Joint Surgery, 1992. **74**(4): p. 511-517.

41. Lieberman, J.A.Y.R. and C.M. Rimnac, *An analysis of the head-neck taper interface in retrieved hip prostheses.* Clinical Orthopedic Related Research, 1994. **300**: p. 162-167.

42. Gilbert, J.L., *Direct in vivo inflammatory cell-induced corrosion of CoCrMo alloy orthopedic implant surfaces.* Journal of Biomedical Materials Research Part A, 2015. **103**(1): p. 211-223.

43. Kubacki, G. and J.L. Gilbert. *Electrocautery induced damage to Ti-6Al-4V and CoCrMo alloy surfaces in vivo and in vitro: an additional damage source to inflammatory cell induced corrosion.* in *International Society for Technology in Arthroplasty.* 2016. Boston, MA.

44. Shareef, N. and D. Levine, *Effect of manufacturing tolerances on the micromotion at the morse taper interface in modular hip implants using the finite element technique.* Biomaterials, 1996. **17**(6): p. 623-630.

45. Chu, Y.H., J.J. Elias, and G.N. Duda, *Stress and micromotion in the taper lock joint of a segmental bone replacement prosthesis.* Journal of Biomechanics, 2000. **33**(9): p. 1175-1179.

46. S.Y., J., et al., *Influence of material coupling and assembly condition on the magnitude of micromotion at the stem-neck interface of a modular hip endoprosthesis.* Journal of Biomechanics, 2011. **44**: p. 1747-1751.

47. Jauch, S.Y., G. Huber, and M.M. Morlock, *Micromotions at the taper interface between stem and neck adapter of a bimodular hip prosthesis during activities of daily living.* Journal of Orthopedic Research, 2013. **31**: p. 1165-1171.

48. Rehmer, A., *Influence of assembly procedure and material combination on the strength of the taper connection at the head–neck junction of modular hip endoprostheses.* Clinical Biomechanics, 2012. **37**(1): p. 77-83.

49. Goldberg, J.R. and J.L. Gilbert, *In vitro corrosion testing of modular hip tapers.* Journal of Biomedical Materials Research: Part B-Applied Biomaterials, 2003. **64B**: p. 78-93.

50. Chistofollni, L. and E. Varini, *In-vitro method for assessing femoral implant-bone micromotions in resurfacing hip implants under different loading conditons.* Proceedings of Institute of Mechanical Engineers. Part H, Journal of Engineering in Medicine, 2007. **221**(8): p. 943-950.

51.   Gilbert, J.L. and C.A. Buckley, *Mechanical-electrochemical interactions during in-vitro fretting corrosion tests of modular taper connections*, in *Total Hip Revision Surgery*, G. J.O., R. A.G., and C. J.J., Editors. 1994, Raven Press: New York. p. 41-50.

52.   Gilbert, J.L., M. Mehta, and B. Pinder, *Fretting Crevice Corrosion of Stainless Steel Stem–CoCr Femoral Head Connections: Comparisons of Materials, Initial Moisture, and Offset Length.* Journal of Biomedical Materials Research Part B: Applied Biomaterials, 2009. **88**(1): p. 162-173.

53.   Higgs, G.B. and J.A. Hanzlik, *Is increased modularity associated with increased fretting and corrosion damage in metal-on-metal total hip arthroplasty devices?: a retrieval study.* Journal of Arthroplasty, 2013. **28**(8): p. 2-6.

54.   Munir, S., W.L. Walter, and W.R. Walsh, *Variations in the trunnion surface topography between different commercially available hip replacement stems.* Journal of Orthopedic Research, 2015. **33**(1): p. 98-105.

55.   Kao, Y.Y., C.N. Koch, and T.M. Wright, *Flexural rigidity, taper angle, and contact length affect fretting of the femoral stem trunnion in total hip arthroplasty.* Journal of Arthroplasty, 2016. **31**(9 Suppl): p. 254-8.

56.   Mistry, J.B., M. Chughtai, and M.A. Mont, *Trunnionosis in total hip arthroplasty: a review.* J Orthrop Traumatol, 2016. **17**(1): p. 1-6.

57.   Porter, D., et al., *Modern trunnions are more flexible: a mechanical analysis of THA taper designs.* Clin Orthop Relat Res, 2014. **472**(12): p. 3963-70.

58.   Weisse, B. and C. Affolter, *Influence of contaminants in the stem-ball interface on the static fracture load of ceramic hip joint ball heads.* Proc Inst Mech Eng H, 2008. **222**(5): p. 829-35.

59.   Pierre, D. and J.L. Gilbert. *Incremental Cyclic Fretting Corrosion and Micromotion Test of Hip Implant Head-Neck Tapers*. in *Society for Biomaterials*. 2014. Denver, Co.

60.   Pennock, A.T., *Morse-Type Tapers: Factors That May Influence Taper Strength During Total Hip Arthroplasty.* The Journal of Arthroplasty, 2002. **17**(6): p. 773-778.

61.   Jauch, S.Y. and A.W. Miles, *Does the surface finish, the taper angle difference and the assembly force effect the taper strength between stem and ball head of a modular hip implant?*, in *ORS*. 2014, Orthopedic Research Society: Lousianna.

62.   Palmer, R.M. and L. Scholl, *Effect of contamination on torque testing of the taper junction in total hip arthroplasty.* American Association of Hip and Knee Surgeons, 2015. **55**.

63.   Panagiotidou, A., T.E. Cobb, and G.W. Blunn. *Effect of Impact Assembly on the Interface Deformation and Fretting Corrosion of Modular Hip Tapers: An In Vitro Study*. in *AAOS*. 2015. Las Vegas, Nevada: American Academy of Orthopaedic Surgeons.

64.   Panagiotidou, A., *Enhanced wear and corrosion in modular tapers in total hip replacement is associated with the contact area and surface topography.* Journal of Orthopaedic Research, 2013. **31**(12): p. 2032-2039.

65.   Pierre, D. and J.L. Gilbert, *Effects of Seating Load Magnitude and Load Orientation on Seating Mechanics in Modular Taper Junctions*. 2016: International Society of Arthroplasty.

66.   Scholl, L. and D. Pierre, *Influence of Surgical Variables on Initial Taper Stability*. 2016: International Society of Arthroplasty.

67.   Hirakawa, K., et al., *Mechanisms of failure of total hip replacements: lessons learned from retrieval studies.* Clinical Orthopaedics and Related Research, 2004. **420**(10).

68. Dyrkacz, R.M.R., et al., *Finite element analysis of the head–neck taper interface of modular hip prostheses.* Tribology International, 2015.

69. Malik, A., A. Maheshwari, and L.D. Dorr, *Impingement with total hip replacement.* The Journal of Bone & Joint Surgery—American Volume, 2007. **89**(8): p. 1832-1842.

70. Padgett, D.E., et al., *Influence of total hip design on dislocation: a computer model and clinical analysis.* Clinical Orthopaedics and Related Research, 2006. **447**: p. 48-52.

71. Barrack, R.L., et al., *Stem design and dislocation after revision total hip arthroplasty: clinical results and computer modeling.* Journal of Arthroplasty, 2001. **16**: p. 8-12.

72. F04, C., *Standard Practice for Surface Preparation and Marking of Metallic Surgical Implants.* ASTM, 2013. **F86**(13).

73. Higgs, G.B., S. Kurtz, and J.L. Gilbert, *Does Taper Size Have an Effect on Taper Damage in Retrieved Metal-on-Polyethylene Total Hip Devices?* The Journal of Arthroplasty, 2016. **31**: p. 277-81.

74. Heiney, J.P., S. Battula, and G.A. Vrabec, *Impact magnitudes applied by surgeons and their importance when applying the femoral head onto the Morse taper for total hip arthroplasty.* Arch Orthop Trauma Surg, 2009. **129**(6): p. 793-796.

75. Lavernia, C.J., L. Baerga, and R.A. Hernandez. *Head trunnion assembly in total hip replacement - intraoperative technique.* in *Orthopedic Research Society.* 2016.

76. Mali, S.A. and J.L. Gilbert, *Correlating fretting corrosion and micromotions in modular tapers: Test method development and assessment.* ASTM Special Technical Publication, 2015. **STP 1591**: p. 259-282.

77. Schmidig, G., et al., *Evaluation of Variability in head impaction forces Among Multiple orthopaedic surgeons.* 2015: ORS.

78. Lewis, G., *Geometric element analysis of fretting in a model of a modular femoral component of a hip implant.* Biomedical Materials and Engineering, 2004. **14**: p. 43-51.

79. Hol, P.J., A. Molster, and N.R. Gjerdet, *Should the galvanic combination of titanium and stainless steel surgical implants be avoided?* Injury, 2008. **39**: p. 161-169.

80. Hallab, N.J., et al., *Differences in the fretting corrosion of metal-metal and ceramic-metal modular junctions of total hip replacements.* Journal of Orthopedic Research, 2004. **22**: p. 250-259.

81. Point, T. *2D Transformation.* 2016 [cited 2016 11/22/2016].

82. Heiny, J.P., S. Battula, and G.A. Vrabec, *Impaction magnitudes applied by surgeons and their importance when applying the femoral head onto the morse taper for total hip arthroplasty.* Archives of Orthopedic Trauma Surgery, 2009. **129**(6): p. 793-796.

83. Scholl, L., G. Schmidig, and A. Faizan, *Evaluation of surgical impaction technique and how it affects locking strength of the head-stem taper junction.* Journal of Engineering in Medicine, 2016. **32**(9): p. 968-73.

84. Pierre, D., J.L. Gilbert, and V. Swaminathan, *Effects of Seating Load Magnitude and Load Orientation on Seating Mechanics in Modular Taper Junctions*, in *International Society of Orthopedics.* 2016: Boston, MA.

85. Burgers, T., et al., *Time-dependent fixation and implantation forces for a femoral knee component - an in vitro study.* Medical Engineering & Physics, 2010. **32**(9): p. 968-73.

86. Maharaj, G.R. and R.D. Jamison, *Intraoperative Impact: Characterization and laboratory simulation on composite hip protheses*, in *ASTM STP 1178.* 1993, American Society for Testing and Materials: Philadelphia, PA. p. 98-108.

Curriculum Vitae

Education:
Syracuse University, Syracuse, NY
Doctor of Philosophy in Bioengineering   December 2016

Worcester Polytechnic Institute, Worcester, MA
Bachelor of Science in Biomedical Engineering, May 2012
Bachelor of Science in Mechanical Engineering, May 2012

Experience:
Clemson University, Clemson, SC
February 2017-Present
  Postdoctoral Appointment
- Assist in starting up and developing new lab
- Lab manager
- Assist in surgical research with spinal fixtures
- Formulate intellectual property

Syracuse University, Syracuse, NY   August 2012-January 2017
  Lab Researcher/Teaching Assistant
- Electrochemical and biomechanical testing of various modular tapers
- Collaborative research with industry and academia
- Teach recitation courses for Engineering Materials, Properties and Processing; Introduction to Engineering

Stryker Corporation, Mahwah, NJ   June 2014-August 2016
  Advanced Technology Group
- Assess variable seating conditions in metal-on-metal modular orthopedic implants
- Provide in depth reports
- Create sustainable data analysis templates and codes

Prospect Hill Academy Charter School, Cambridge, MA   April 2016-June 2016
  Engineering Teacher/Substitute Teacher
- Create curriculum and lesson plans for elective course
- Mentor high school students and discuss STEM field placement

Worcester Polytechnic Institute, Worcester, MA   January 2010-May 2011
  Lab Technician
- Cardiovascular experimentation
- Co-lab manager

Project Experience:
Ph.D. Research   August 2012-December 2016

To systematically assess the effects of material combination and design, surgical assembly factors (i.e. load magnitude, load rate, load orientation and contamination) and taper geometry on the seating mechanics, pull-off load and overall performance of modular tapers in commercial total joint replacements. Each study delves into an important aspect of surgical taper assembly and manufacturing using innovative test methods to assess the performance of each test sample in practical simulations.

Languages: Fluent- Haitian Creole & Spanish; Conversational in French
Computers: Microsoft Office, Java, MatLab, Solid Works, LabView, MathCAD, Bluehill Wavematrix, Visual Basic
Lab: Servohydraulic and screwdriven test frame, Droptower, Non-contact eddy current sensors, Digital microscope, Scanning Electron Microscopy, Differential Scanning Microscopy, Tensile testing, Static testing, Dynamic motion testing
Awards: Business Plan and Innovation Competition Award Recipient, AGEP Fellow

Conference Publications:
1) Pierre, D., Swaminathan, V., Scholl, L., TenHuisen, K., Gilbert, J.L. **Incremental Cyclic Fretting Corrosion and Micromotion Test of Hip Implant Head-Neck Tapers**. *Society for Biomaterials*. 2014. Denver, Co.
2) Pierre, D., Swaminathan, V., Scholl, L., TenHuisen, K., Gilbert, J.L. **Effects of Impaction Assembly Forces on Micromotion and Electrochemical Performance of Taper Junctions.** *Orthopedic Research Society.* 2015.
3) Pierre, D., Swaminathan, V., Scholl, L., TenHuisen, K., Gilbert, J.L. **Effects of Impaction Assembly Forces on Micromotion and Electrochemical Performance of Taper Junctions.** *American Society of the International Association for Testing and Materials.* 2015.
4) Pierre, D., Swaminathan, V., Scholl, L., TenHuisen, K., Gilbert, J.L. **Effects of Seating Load Magnitude and Load Orientation on Seating Mechanics in Modular Taper Junctions.** *International Society of Arthroplasty.* 2016.
5) Pierre, D., Swaminathan, V., Scholl, L., TenHuisen, K., Gilbert, J.L. **Influence of Surgical Variables on Initial Taper Stability.** *International Society of Arthroplasty.* 2016.
6) Pierre, D., Swaminathan, V., Scholl, L., TenHuisen, K., Gilbert, J.L. **Effects of Seating Load Magnitude on Incremental Cyclic Fretting Corrosion in 12/14 Modular Taper Junctions.** *Orthopedic Research Society.* 2017.
7) Pierre, D., Swaminathan, V., Scholl, L., TenHuisen, K., Gilbert, J.L. **Effects of Seating Load Orientation on Incremental Cyclic Fretting Corrosion in 12/14 Modular Taper Junctions.** *Orthopedic Research Society.* 2017.

Journal Publications:
1) Pierre, D., Swaminathan, V., Scholl, L., TenHuisen, K., Gilbert, J.L. **Incremental Cyclic Fretting Corrosion and Micromotion Test of Hip Implant Head-Neck Tapers**. *Journal of Arthroplasty (In Process)*
2) Pierre, D., Swaminathan, V., Scholl, L., TenHuisen, K., Gilbert, J.L. **Effects of Impaction Assembly Forces on Micromotion and Electrochemical Performance of Taper Junctions.** *Journal of Arthroplasty. (In Process)*

3) Pierre, D., Swaminathan, V., Scholl, L., TenHuisen, K., Gilbert, J.L. **Effects of Seating Load Magnitude and Load Orientation on Seating Mechanics in Modular Taper Junctions.** *Journal of Orthopaedic Research (In Process)*

4) Scholl, L., Pierre, D., Swaminathan, V., Scholl, L., Gilbert, J.L., TenHuisen, K. **Effect of Substrate Compliance on Total Hip Modular Taper Seating Stability.** *Journal of Engineering of Medicine: Part H (In Review)*

5) Pierre, D., Swaminathan, V., Scholl, L., TenHuisen, K., Gilbert, J.L. **Effects of Seating Load Magnitude on Incremental Cyclic Fretting Corrosion in 12/14 Modular Taper Junctions.** *Journal of Orthopaedic Research (In Process)*

6) Pierre, D., Swaminathan, V., Scholl, L., TenHuisen, K., Gilbert, J.L. **Effects of Seating Load Orientation on Incremental Cyclic Fretting Corrosion in 12/14 Modular Taper Junctions.** *Journal of Orthopaedic Research (In Process)*

7) Pierre, D., Swaminathan, V., Scholl, L., TenHuisen, K., Gilbert, J.L. **Effects of Taper Junction Contamination on Seating Mechanics and Pull-off Loads in 12/14 Tapers.** *Clinical Biomechanics (In Process)*

8) Pierre, D., Swaminathan, V., Scholl, L., TenHuisen, K., Gilbert, J.L. **Effects of Taper Junction Contamination on Incremental Cyclic Fretting Corrosion and Pull-off Loads in Modular 12/14 Tapers.** *Clinical Biomechanics (In Process)*